PROPAGATION AND REFLECTION OF PULSE WAVE IN FLEXIBLE TUBES AND RELATION TO WALL PROPERTIES

A thesis submitted for the degree of Doctor of Philosophy

by

Ye Li

Brunel Institute for Bioengineering

Brunel University

December 2011

Abstract

The wall properties of the arteries play an important role in cardiovascular function. Stiffness of large artery is predictive of cardiovascular events. To understand the function of the cardiovascular system, special attention should be paid to the understanding of pulse wave propagation, because pulse waves carry information of the cardiovascular function, and provide information which can be useful for the prevention and diagnosis of diseases. This thesis presents a series of *in vitro* experimental studies of wave propagation, wave reflection and determination of mechanical properties of flexible vessels.

In this thesis, several studies have been included: 1) applied and compared foot-to-foot, PU-loop and *ln*DU-loop methods for determination of wave speed in flexible tubes and calf aortas; 2) investigated the variation of local wave speed determined by PU-loop with proximity to the reflection site; 3) investigated using wave intensity analysis (WIA) as the analytical technique to determine the reflection coefficient; 4) developed a new technique which based on one-point simultaneous measurements of diameter and velocity to determine the mechanical properties of flexible tubes and calf aortas.

In the first study, it is found wave speeds determined by PU-loop and *ln*DU-loop methods are very similar, and smaller than those determined by foot-to-foot method. The timing of arrival time of reflected wave based on diameter and velocity technique highly agreed with the corresponding timing based on pressure and velocity technique. The shapes of forward and backward non-invasive wave intensities based on diameter and velocity are very similar with the corresponding shapes based on pressure and velocity. Although the density term is not part of the equation, the *ln*DU-loop method for determining local wave speed is sensitive to the fluid density.

In the second study, it is found wave speed measured by PU-loop is varied with proximity to the reflection site. The closer the measurement site to the reflection site, the greater the effect upon measured wave speed; a positive reflection caused an increase in measured wave speed; a negative reflection caused a

decrease in measured wave speed. Correction iteration process was also considered to correct the affected measured wave speed.

In the third study, it is found, reflection coefficient determined by pressure, square roots of wave intensity and wave energy are very close, but they are different from reflection coefficient determined by wave intensity and wave energy. Due to wave dissipation, the closer the measurement site to the reflection site, the greater is the value of the local reflection coefficient. The local reflection coefficient near the reflection site determined by wave intensity and wave energy are very close to the theoretical value of reflection coefficient.

In the last study I found that distensibility determined by the new technique which utilising *ln*DU-loop is in agreement with that determined from the pressure and area which obtained from tensile test in flexible tubes; distensibility determined by the new technique is similar to those determined in the static and dynamic distensibility tests in calf aortas; Young's modulus determined by the new technique are in agreement with that those determined by tensile tests in both flexible tubes and calf aortas.

In conclusion, wave speed determined by PU-loop and *ln*DU-loop methods are very similar, the new technique *ln*DU-loop provides an integrated noninvasive system for studying wave propagation; wave speed determined by PU-loop is affected by the reflection, the closer the measurement site to the reflection site, the greater the change in measured wave speed; WIA could be used to determine local reflection coefficient when the measurement site is close to the reflection site; the new technique using measurements of diameter and velocity at one point for determination of mechanical properties of arterial wall could potentially be non-invasive and hence may have advantage in the clinical setting.

Contents

List of Tables

List of Figures

Acknowledgement

I would like to acknowledge and thank the following people who supported and helped me during my PhD study.

First, I would like to thank Dr Ashraf Khir for his excellent supervision of my PhD research. I really appreciate his valuable comments, constant support and guidance, and encouragement to complete my research work and the thesis.

I would also like to thank Dr Quan Long, my second supervisor, for full of advice and support; and Professor Kim Parker of Imperial College, for the precious advice and pleasant discussions during my PhD research.

My thanks also go to everyone in Brunel Institute for Bioengineering, for being so welcoming and friendly; especially thanks to Jenny, Caroline, Larry and Roger, for all their support.

Special thanks are due to my friends, Alessandra Borlotti, Gianpaolo Bruti Francesco Clavica, Hao Gao, Yi Li, Karnal Patel, Marcel Swalen, Ning Wang for their support.

Finally, I dedicate this PhD thesis to the most important people in my life, my parents and my husband zhefeng, for their constant support and encouragement throughout my PhD.

Chapter 1
Background Information

1.1 Introduction

Research interest in the cardiovascular system is as old as recorded history. Galen (129 -217 AD) is known as the first to discover that arteries carried blood. William Harvey (1578-1657) is the physician most commonly known as the first person who describes the circulatory system. Although others described components of the circulatory system before Harvey's time, his description was the most complete, but did not explain the exchange of blood between arteries and veins away from the heart.

When time comes to now, cardiovascular system attracts more and more attention. Recently, most countries face high and increasing rates of cardiovascular disease. According to the report of the World Health Organisation, cardiovascular diseases are the number one cause of death globally. Worldwide, 17.3 million people died of cardiovascular diseases, particularly heart attacks and stroke, every year. This number represents 30% of all global deaths. Of these deaths, an estimated 7.3 million were due to coronary heart disease and 6.2 million were due to stroke. This is predicted to reach nearly 23.6 million deaths from cardiovascular diseases, mainly from heart disease and stroke annually by 2030. These are projected to remain the single leading causes of death (World Health Organisation, 2011). In UK, cardiovascular disease is the biggest cause of death now (Alleyne, 2011). Cardiovascular diseases cause more than one in three of all deaths in the UK, accounting for more than 191,000 deaths each year at an estimated cost of £30 billion to the economy. Additionally, there are nearly 2.7 million people living with heart disease in the UK (British Heart Foundation, 2011).

1.2 Background

The aorta acts as both a conduit and an elastic buffering chamber. As an elastic chamber, the elasticity of the aorta works to modulate pulsatile flow in heart to a steady flow in peripheral vessels. In 1733, Hales (Hales, 1733) published his observations which showed that aorta expands to contain a large fraction of the stroke volume. Hales proposed that the aorta works as an elastic chamber which expands with blood during the heart's contraction and discharges blood through the peripheral resistance by elastic recoil while the heart refills. An analogy was made with early fire-engine pump, which smoothes a pump's pulsatile flow of water. In 1899, Frank used this analogy to propose the well-known Windkessel theory. The researches on the elasticity of the aorta are enormous.

1.2.1 Arteries

Arteries transport blood from the heart to the organs in the body. The anatomy of the artery (**Figure 1.1a**) is broken down into the lumen, tunica intima, tunica media, and the tunica externa (Milnor, 1982). The lumen is the empty center of the artery, which blood flows through. The inner layer of the artery is the tunica intima and it is the closest to the lumen; consisting of endothelium, a basement membrane, and internal elastic lamina containing a simple squamous epithelium lining. The complete cardiovascular system has a continuous layer on the inner surface of endothelial cells. This endothelial lining of the blood vessel is usually the only layer to come into contact with the blood. The middle layer, generally the thickest layer, is the tunica media; the circularly arrangements around the lumen are elastic fibres and smooth muscle fibres. It is the abundant elastic fibres that cause arteries to have a high compliance. This high compliance means that the walls stretch or expand easily to the reaction of small pressure increases without tearing. The tunica externa is the outermost layer made up of elastic and collagen fibres.

Figure 1.1b show an artery with a plaque. The formation of plaques occurs in a sequential way. First, cholesterol-rich lipids (fat) permeate the epithelium and are located within the wall of a blood vessel. Then, abnormal smooth muscle cells move to the location of the plaque which is developing, causing a bulge which narrows the lumen of the artery. A connective tissue cap is followed to

form (scar tissue) over the developing plaque. Eventually the plaque becomes hardened by participation of calcium salts. The plaque protrudes into the lumen of the artery, thus diminishing blood flow in the artery.

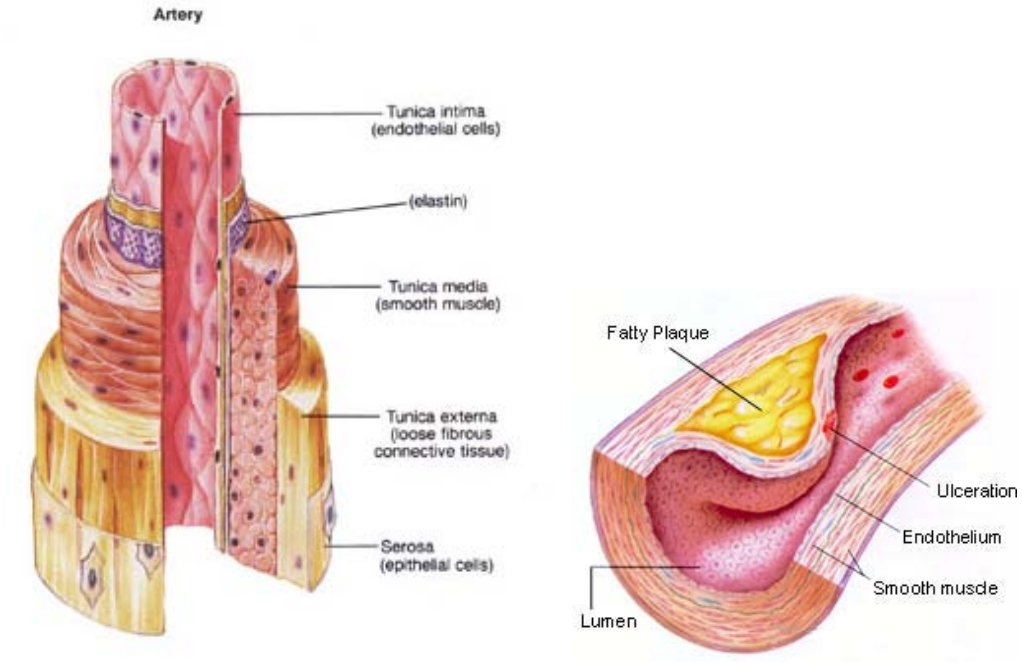

(a) (b)

Figure 1.1: (a) Arterial Anatomy (Taken from Fox, 1992). (b) Artery with plaque inside (Taken from http://www.biosbcc.net/doohan/sample/htm/vessels.htm).

Arteries are able to expand and contract because they contain elastic layers made up of two fibrous proteins: elastin and collagen. In the unstretched structure of an artery, collagen fibres are normally kinked and are not directly stressed, so the behaviour of the tissue is due mostly to the compliant elastin fibres. At higher pressures, the elastic modulus of collagen fibres, are about 1000 times greater than that of elastin. The collagen fibres are straightened and begin to become directly stressed, and the arterial wall gets stiffer, **Figure 1.2 (**Nichols and O'Rourke, 2005). Therefore, the elastic properties of arterial walls are non-linear. According to Tardy et al. (Tardy et al., 1991), viscoelastic effects are small within the physiological ranges of pressures.

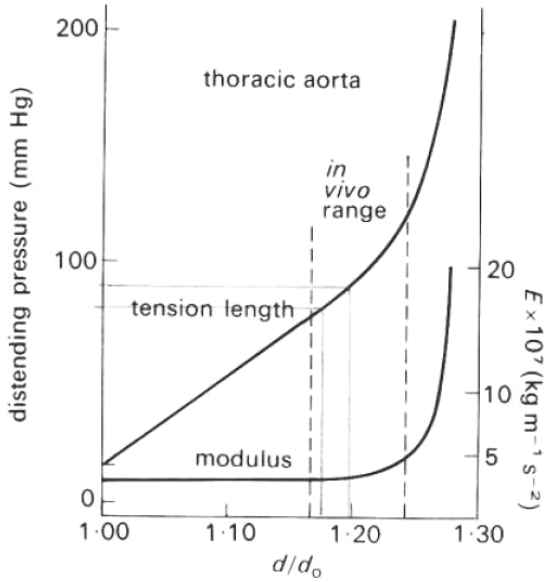

Figure 1.2: Pressure versus diameter (d) for a segment of artery of fixed length (d_0 is the unstretched diameter). This is the typical non-linear behaviour of a systemic artery. The normal *in vivo* range is highlighted by the two vertical dashed lines. The figure also shows the Young's modulus (E) relating circumferential stress to circumferential strain, which increase dramatically for distending pressures greater than their normal physiological range (Taken from Nichols and O'Rourke, 2005).

Arterial mechanical properties describe the characteristics that make up the tissue. The major mechanical properties include compliance, distensibility, radius, wall thickness, wave speed, and Young's modulus. Below in **Table 1.1** arterial information are shown.

Table 1.1 Approximate number of each type of arteries with the approximate lumen calibre (D), wall thickness (h), total cross-sectional area (A_T), and percentage of the total blood volume (V) contained in each type of arteries. (Gregg, 1966)

Vessel	Aorta	Arteries	Arterioles	Capillaries
Number	1	10^2	10^7	10^{10}
D (mm)	25	4	0.03	0.008
h (mm)	2	1	0.02	0.001
A_T (cm^2)	5	20	400	4500
V (%)	2	8	1	5

For the arterial wall, the range of Young's modulus is 0.2-0.8 MPa, which can be converted to 200 - 800 kPa. Young's modulus is a proportion between the strain and the stress, stated by Hooke's Law.

The mechanical characteristics of blood vessels are mainly determined by both passive and active tissue components. The most significant passive components are the fibrous connective tissues: elastin and collagen. Glycosaminoglycan- rich ground substance also is present in the walls of arteries, and the water and ion-binding potential of this material could alter wall mechanics, either directly or indirectly, by altering the behavior of the vascular muscle. However, the significance of these effects remains to be determined. Endothelial cells, nervous tissue, and fibroblasts also are present. Histologically these factors appear to represent a small percentage portion of vessel wall volume. Measurements of rat tail artery show that the endothelium represents less than 3% of the cross-sectional area that exist in capillary walls, exhibits negligible inherent mechanical stiffness. The quantity and mechanical characteristics of nervous tissue and fibroblasts in arteries are unknown (Dobrin, 1978).

1.2.2 Arterial stiffness

Artery stiffness is a predictor of both cardiovascular events, and of all cause mortality, such as hypertension, diabetes, or renal disease. Blacher et al. (1999a) demonstrated in a 710 hypertensive subjects study, that higher cardiovascular risk was related with increased wave speed (a measure of arterial stiffness). A similar study carried out by Laurent et al. (2001) stated the same trends in a study of 1,980 hypertensive patients, with arterial stiffness being associated with both cardiovascular and all cause mortality. The study of end-stage renal disease patients confirmed that arterial stiffness as measured by wave speed (Blacher et al., 1999b) and by aortic pressure augmentation index (London et al., 2001) was associated with cardiovascular events and outcomes. A correlation between arterial stiffness and cardiovascular diseases was also shown in diabetes patients (Stamler et al., 1993). More generally, in the elderly population, aged above 70 years, Meaume et al. (2001) proved arterial stiffness as a predictor of all-cause and cardiovascular death.

The importance of arterial stiffness is not limited to several populations or disease groups. Mattace-Raso et al. (2006) showed that in their 2,835 subjects' study, in apparently healthy people, arterial stiffness remains an independent predictor of coronary heart disease and stroke. Increased arterial stiffness is specifically a risk factor of cardiovascular conditions and diseases (Arnett et al., 1994) including: aging (Avolio et al., 1983; Gillensen et al., 1995; Salomaa et al., 1995), hypertension (Avolio et al., 1985; Dzau and Safar, 1988; Heintz, 1993), diabetes (Liu and Fung, 1992), atherosclerosis (Dart et al., 1991), coronary heart disease (Boutouyrie et al., 2002), smoking (Liu and Fung, 1993; Stefanadis et al., 1997) and stroke (Laurent et al., 2003). Generally, the evidence supports the use of arterial stiffness as a diagnostic tool in the clinical setting (Laurent et al., 2006; Mackenzie et al., 2002; Nichols, 2005; O'Rourke et al., 2002). The clinical importance of arterial stiffness in treatment and prevention of cardiovascular disease was highlighted by the inclusion of wave speed, a measure of arterial stiffness, in the European Society of Hypertension guideline for the treatment of hypertension (Mancia et al., 2007).

In large arteries, increased arterial stiffness decreases the elastic capacity of these arteries, is investigated in older people (Avolio et al., 1983; McEniery et al., 2005). The central aortic pressure is directly increased due to the increase of arterial stiffness. The increased pressures increase the left ventricular load and cardiovascular events later (Mitchell and Pfeffer, 1999). The increased stiffness also increases the reflection of pressure wave, which has an additive effect to systolic pressure. The knowledge of the artery stiffness will enable a good understanding of treatment and prevention of cardiovascular diseases.

1.3 Motivation for research

From the clinical background discussed above, it is clear that wave speed is an important measure of the arterial stiffness. Despite the fact that wave speed was studied extensively, most of the techniques which determine wave speed rely on the measurements of the pressure in most cases. Most of the pressure measurements are invasive, and the noninvasive measurements of pressure are less accurate than the invasive measurements. It is difficult to apply the techniques of determining wave speed into the routine examinations. Furthermore, wave speed is related to the mechanical properties of the arterial

wall, changes in such properties will affect wave speed. Similarly wave speed could be used to reflect the mechanical properties of the arterial wall. Increased stiffness of large elastic arteries represents an early risk factor for cardiovascular diseases (Arnett et al., 1994; Hodes et al., 1995). Specifically, increased aortic stiffness is associated with aging (Avolio et al., 1983; Gillensen et al., 1995; Salomaa et al., 1995), hypertension (Dzau and Safar 1988, Heintz, 1993), diabetes (Liu and Fung, 1992; Salomaa et al., 1995), hyperlipidemia (Lehmann et al., 1992), atherosclerosis (Dart et al., 1991), heart failure (Khan et al., 1999) and other conditions. Therefore, the assessment of aortic mechanical properties is particularly important in understanding the mechanism of cardiovascular disease, and if this assessment is carried out noninvasively, it would be advantageous.

In previous work, the PU-loop method for determining wave speed has been validated *in vitro* (Khir and Parker, 2002) and *in vivo* (Khir et al., 2004) with the foot-to-foot method and has been used to determine the wave speed in the ascending aorta of patients with cardiovascular disease (Khir et al., 2001a). However, the PU-loop method relies on a period during which only a unidirectional wave is present, for example, the early part of the systolic upstroke in the aorta. This restriction makes the PU-loop method unsuitable for determination of wave speed in the coronary arteries, because coronary arteries are subject to influence from the aortic and microcirculatory ends (Sun et al., 2000). In other words, the PU-loop method for determination of wave speed might be influenced by the reflection in the short segment. Investigation on this phenomenon and improve this method would be useful for the clinical application of this method.

Quantification of wave reflection in the arterial system is important because it is responsible for the altered contour and amplitude of pressure waveform as it travels towards the periphery. The analysis of reflections at discontinuity in 1D has been discussed by Caro et al. (1978). The pulse wave is partially reflected at the discontinuity and returned to the inlet of the mother tube and the transmitted wave continues to travel downstream in the daughter tubes. To truly quantify the magnitude of wave reflection, both the pressure and flow wave should be recorded simultaneously at the same site. This allows for the separation of the measured pressure and velocity waveform into their forward

and backward component, as first demonstrated by Westerhof et al. (1972). Wave Intensity Analysis (WIA) was introduced in 1990 by Parker and Jones (Parker and Jones, 1990). WIA is a relatively new one-dimensional time-domain based method for the analysis of arterial waves that was based on the method of characteristics. This approach has advantages in a clinical setting as it is a time domain analysis which can be easily related to physiological events. Therefore, to investigate the WIA used to determine the value of the local reflection coefficient is important in understanding and managing the cardiovascular disease.

1.4 Literature review

The most important aspect of the development and progression of cardiovascular diseases is the role of hemodynamics. Hemodynamics consists of the properties of flow of blood; these properties are pressure, flow and resistance of circulated blood. These properties are important to the judgment of the cardiovascular system. The following literature review will examine a variety of techniques that have been developed to quantify these properties and will discuss the important findings of the published data.

1.4.1 Wave propagation

A wave is a disturbance that propagates in space and time. Waves propagate in arteries as a result of the balance between the inertial force of the blood and the restoring force of the walls (since blood is relatively incompressible, the contribution for fluid compressibility is usually neglected in the arterial wave analysis). For example, heart contraction generates a forward travelling wave (or series of wavefronts) that propagates distally through the aorta to the rest of the circulation. Such a wave will propagate unchanging in a uniform tube containing an inviscid fluid, but discountinities in terms of the cross sectional area or elasticity of the tube will give rise to a reflection, this is discussed in more detail in subsequent sections. Wave propagation in arteries has been studied extensively, these work were carried out in the frequency domain through impedance approach and in the time domain through wave intensity analysis (WIA).

1.4.2 Wave propagation in frequency domain: Impedance analysis

Previous works on wave propagation were mostly done in the frequency domain through impedance analysis using Fourier transform, in which the complex propagation coefficient that varies with frequency was used to describe both wave speed and attenuation (McDonald et al., 1968a; Taylor, 1959).

The first appropriate mathematical model of pulse wave propagation was proposed by a Swiss mathematician, Leonhard Euler (1707-1783) in 1775 (Euler, 1775). He derived the partial differential equations expressing the conservation of mass and momentum of an inviscid fluid; these equations are the foundation for all one-dimensional models of blood flow in arteries. But, clearly, he did not recognise the wave-like nature of the blood flow and was not able to find a solution for his equations. In 1955 Womersley solved these non–linear equations of flow for an elastic artery and generated linearised forms of these equations which could be solved using Fourier analysis (Womersley, 1955). McDonald was an early person who proposed using harmonic analysis in arterial hemodynamic (McDonald, 1955). In 1960 McDonald measured pressure and velocity simultaneously at several locations in the aorta, the femoral and saphenous arteries. He observed that the magnitude of the pressure wave increases and its upstroke becomes steeper, but the magnitude and upstroke of the flow wave diminishes as measurements are taken more distally (Nichols and O'Rourke, 2005). Taylor expanded these studies by developing an analytical model of the entire vascular system and suggested that the transmission of the pressure pulse was quite influenced by reflections (Taylor, 1966). More recently, Westerhof and colleagues (Westerhof et al., 1972) broaden the impedance approach to allow the separation of the pressure and flow waveforms into forward and backward components. Investigation into the effects and extent of wave reflections became a popular subject over the following years.

Impedance-based analysis has greatly improved the understanding of arterial hemodynamics. However, like all other techniques, impedance analysis has several limitations: although Fourier analysis can be applied to a waveform of any shape; it assumes that the system is linear, for example, waves interact additively. Also, although Fourier transform identifies the amplitude and phases

of the various frequencies that contribute to a time series, it cannot provide information on their localisation within a time series. Fourier analysis may not be suitable to be used to study non-periodic or transient flow. Impedance technique therefore assumes both linearity and periodicity; both questionable assumptions in the cardiovascular system. Varying aspects of the cardiovascular system including the geometry of the blood vessels and the structure of the wall are now known to modulate wave travel (Koh et al., 1998; Wang et al., 2004). It is reported that at any point in which the mechanical properties of arterial wall change, a wave will be partially reflected (Avolio, 1992). Most researchers had assumed previously that reflections from the periphery had a more significant effect than those in the aorta. However Wetterer (Wetterer, 1956) studied the pressure and flow waves in the ascending aorta and explained that as the pressure pulse is maintained to a high level but the flow decreases rapidly in late systole the aortic reflections clearly affect the contour of the pressure waveform. He also concluded that the reflected wave is the summation of reflection that has arisen from both the heart and the periphery. Remington (Remington and O'Brien, 1970) confirmed Wetterer's findings; however these studies were all concerned with the measured pressure and flow waves. Numerous efforts were made to separate the pressure and flow waves into their forward and backward components. In 1972, Westerhof first introduced the separation of pressure and flow into their forward and backward waves. Westerhof dedicated his time to studying the amount of reflection in the arterial system. He found that while the larger arteries contribute a small, fixed amount to the intensity of reflection, the peripheral contribution is higher but variable amount.

1.4.3 Wave propagation in time domain

1.4.3.1 Wave speed

Wave speed (c) is the speed by which disturbance travels along the medium, and it is well accepted as one of the key parameters describing wave propagation in arteries (Nichols and O'Rourke, 2005). Wave speed depends chiefly upon the local properties of the arterial wall (Bergel, 1961a) and widely used clinically to determine arterial stiffness (Asmar et al., 1995). Further, wave speed increases with aging (Avolio et al., 1985) and has been associated with

cardiovascular diseases such as atherosclerosis and arteriosclerosis (Blacher et al., 1999a).

Wave speed in an artery depends on the cross sectional area and elastic characteristics of vessel and density of blood, through the Bramwell-Hill equation,

$$c = \sqrt{\frac{1}{\rho D_s}} \tag{1.1}$$

Where vessel distensibility (D_s) is inversely proportional to the square of the wave speed. It is for this reason that wave speed is now commonly used by clinicians as an indicator of cardiovascular disease and arterial stiffeness. A decrease in distensibility due to stiffening of the arteries leads to an increase in wave speed (Avolio, 1992).

Young's modulus (E) is a measure of the rigidity of a vessel and in 1878 Moens and Korteweg both independently defined the wave speed equation for thin walled tubes with homogenous elastic properties.

$$c = \sqrt{\frac{Eh}{\rho D}} \tag{1.2}$$

Where h is the wall thickness and D is the internal diameter of the vessel. This equation assumes that wall thickness is small compared to the vessel diameter. From this equation, it is seen that wave speed is related to the square root of the Young's modulus of elasticity. Therefore measuring pulse wave velocity leads to an estimate of the stiffness of the tube. Higher wave speed corresponds to higher arterial stiffness.

There are various existing methods which evaluate wave speed over years. Westerhof et al. (Westerhof et al., 1972) suggested that the ratio of magnitudes of pressure to flow velocity, the characteristic impedance, can be used to determine wave speed. They argued that at the higher harmonics the effect of reflected sinusoidal wave-trains will be negligible, and the characteristic impedance indicates wave speed (Newman and Greenwald, 1980).

The most commonly method is known as the foot-to-foot method. This method involves the simultaneous measurement of either pressure or velocity at two sites as known distance apart (L) and determining the time delay between the two measurements (Δt), so the wave speed

$$c = \frac{L}{\Delta t} \tag{1.3}$$

This method has been used extensively. **Figure 1.3** shows an example of the technique which takes the simultaneous pressure measurement from carotid artery to femoral artery (Laurent et al., 2006). Other investigators have applied this method to several sites along the rising limb of the pressure waveform (Frank, 1905) and found that wave speed measured at these different points was not changed significantly. Despite the choosing of the reference point to be the major limitation, wave speed determined by this method is an averaged wave speed. The wave speed calculated using this method provides only an average value because the physical properties of the arterial length is not constant, over the distances routinely used to measure wave speed using transit time methods. The recent Arteriograph method determines wave speed from the pressure waveform measured at the brachial artery with an occluding cuff (Horvath et al., 2010). Also by its nature, this method provides average estimation of wave speed over a length of the arterial tree.

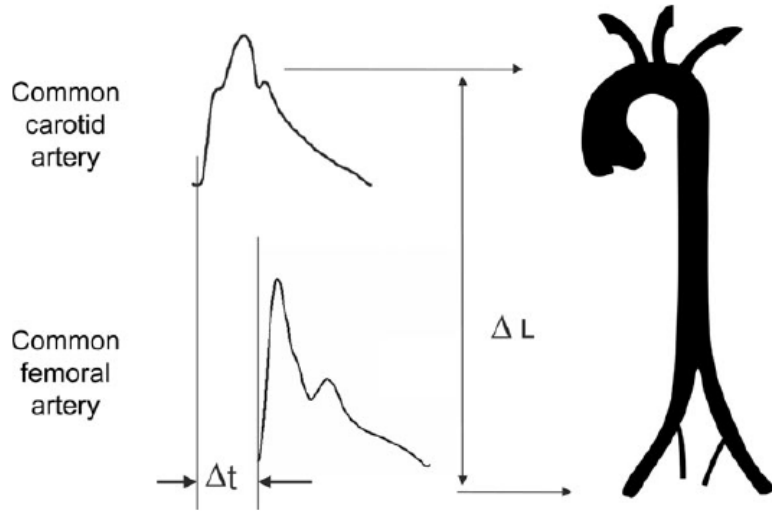

Figure 1.3: The foot-to-foot technique involves measuring the transmission time that it takes for a wave to travel from one site to another. If the distance (L) is known then wave speed can be calculated. A reference point on the waveform is required which is the foot of the pressure wave in this example. In this example the first site is the common carotid artery and the other site is the common femoral artery (Taken from Laurent et al., 2006).

Khir et al. (2001a) used the water hammer equation, introduced the PU-loop method, argued that in the absence of reflections the relationship between pressure and velocity should be linear and the slope of the initial linear portion of the loop is related to wave speed. PU-loop method has the advantage of measuring local wave speed. This method has been compared with the foot-to-foot method *in vivo* (Khir et al., 2004) and wave speed calculated using the PU-loop was found to be lower than those calculated using the foot-to-foot method. This was not a surprising finding as wave speed increases in more distal arteries and the foot-to-foot method represents a weighted average of all the intervening segments (Latham, 1985). To deal with reflections, Davies et al. (2006a) introduced the sum of the squares technique for determining wave speed in shorter arterial segments. The application of the above methods requires simultaneous measurements of pressure and velocity at the same site. This requirement may not be practical in the clinical setting, due to the invasive nature of collecting reliable pressure measurements.

Due to the inconvenience of acquiring invasive pressure measurement, noninvasive determination of wave speed has attracted several researchers. Harada (2002) presented an on-line one-point measurement method to determine wave speed noninvasively; the principle of the method is to derive wave speed from the stiffness parameter of the artery. They measured the diameter change of the carotid artery, calibrated the maximal and minimal values of the diameter waveform using systolic and diastolic blood pressure measured with a cuff-type monometer at the upper arm then substituted the calibrated diameter waveform for the pressure waveform. Hence, the ‘stiffness parameter’ can be obtained simultaneously. The ‘stiffness parameter’ is an index to diagnose sclerotic degrees of the carotid artery. Under the stable physiological condition, there is an exponential relation between intravascular pressure and diameter, substitute the natural logarithm of systolic-diastolic pressure ratio and the arterial wall extensibility for intravascular pressure and diameter. Then, the relation will be linear, and the straight slope is the stiffness parameter (Arterial stiffness index, 2012). The stiffness parameter is considered to be independent of pressure. Wave speed calculated from the ‘stiffness parameter’ is a direct method which uses only the knowledge of the elastic property of the artery. Also, Meinders et al. (2001) introduced a multiple M-line

system to assess local pulse wave velocity, which was determined as the ratio of the temporal and spatial gradient of adjacent distension velocity waveforms that were determined simultaneously along a short arterial segment length is set by the characteristics of the ultrasound probe and does not vary over measurements. Further, Rabben et al. (2004) presented a method for estimating wave speed from ultrasound measurements; the flow-area loop method, in which wave speed is estimated as the ratio between the change in flow to the change in cross-sectional area during the reflection-free period of the cardiac cycle.

Another study by Feng and Khir (2010) has developed a novel technique using the noninvasive measurements of velocity and vessel diameter for the determination of wave speed (*ln*DU-loop). The authors demonstrated that the relationship between diameter and velocity is linear in the absence of reflection and the slope of the loop is linear in the early part of the cycle when only forward waves are present. Recently, Alastruey (2011) developed a new method; D^2P-loop, which estimate wave speed from simultaneous pressure and diameter measurements in late diastole. This method has only been tested using a Voigt-type viscoelastic model of the arterial wall.

1.4.3.2 Wave reflection

Up to this point we have largely neglected one of the most important features of the arterial system - the complexity of the arterial tree with its numerous bifurcations and anastomoses. These anatomical variations in the arteries mean that the waves propagate along them are continuously altering to the new conditions that they encounter.

Any discontinuity in the properties of the artery will cause the wavefronts to produce reflected and transmitted waves according to the type of discontinuity. There are many types of discontinuities in the arterial system; such as changes in cross-sectional area, local changes in the elastic properties of the arterial wall, bifurcations, and so on.

It has now been recognised that arterial stiffness contributes to increased aortic systolic pressure and pulse pressure and is an important indicator of cardiovascular events. (Benetos et al., 1997; Mitchell et al., 1997a; Mitchell et

al., 2008). Timing and magnitude of the reflected wave contribute strongly to systolic and pulse pressure.

It has been long recognised that the pressure and flow waves generated during ventricular systole are partially reflected from the vasculature and these reflections make a significant contribution to ventricular afterload and overall hemodynamics (Brin and Yin, 1984; O'Rourke and Kelly, 1993; Duan and Zamir, 1995; Koh et al., 1998; Penny et al., 2008). Moreover, accurate quantification of the value of wave reflection is important in view of the increasing use of indices based on this measurement in the management of clinical conditions such as hypertension. The value of wave reflection from a given reflection site can be quantified by calculation of a local reflection coefficient (Latham et al., 1985; Greenwald et al., 1990; Khir and Parker, 2002; Segers et al., 2006).

The conservation of mass and energy at a discontinuity in an elastic vessel require that an incident wave with a pressure change ΔP must generate a reflected wave with pressure change δP that is given by a reflection coefficient R= δP/ ΔP. This definition is familiar from many branches of wave mechanics when it is remembered that pressure has the units of energy per unit volume (Franklin et al., 2010). The value of the reflection coefficient depends upon the area and wave speed upstream and downstream of the discontinuity. Westerhof et al. (1972) demonstrated that the pressure wave can effectively be separated into a forward and backward component provided that aorta pressure and flow are known. This wave separation analysis is considered as a gold standard method to assess wave reflection (Milnor, 1982; Westerhof et al., 2004; Nichols and O'Rourke, 2005).

The arrival time of reflected wave (Trw) to the ascending aorta is another parameter that is of clinical and physiological importance. For example, the arrival time of reflected wave has been used to diagnose ventricular hypertrophy and cardiac failure (Koh et al., 1998). Earlier arrival of reflected compression waves suggests higher wave speed and causes an increase in pressure, which is thought to increase left ventricle (LV) afterload (O'Rourke, 1982). This increase may augment LV oxygen demands in order to maintain cardiac output (Kelly et al., 1992). Mitchell et al. (2004) found the distance to the 'effective' reflection site where the reflected wave appears to originate, also

known as the effective length of the arterial tree (Sipkema and Westerhof, 1975), to decrease with age.

In clinical practice, waveform analysis is often used to study wave reflection, with different coexisting approaches to assess 'landmarks' on the waveform which are indicative for return of the reflected wave. Waveform analysis resulted in identification of the shoulder or inflection point as landmark points, derivate forward and reflected pressure and the determination of the augmentation index to help to understand the contribution of reflections to systolic pressure and pulse pressure. Augmentation index (AIx), expressing the ratio of the 'augmented pressure', is a measure of the degree to which the peak of a measured pressure wave is over and above the peak of the incident pressure wave due to the addition of the reflected pressure wave. AIx is a measure of the compliance and structure of vessels distal to the site of measurement. AIx attributed to the reflected wave, to the pulse pressure (Kelly et al., 1989a; O'Rourke et al., 2003).

AIx is basically a quantification of Murgo's wave classification scheme (Murgo, 1980). Murgo suggested that time of the inflection point on the upstroke of the pressure waveform represented arrival time of reflected wave. An attractive feature of AIx is the fact that its assessment requires measurement of the pressure wave morphology only. The major drawback of AIx is that it is a composite measure depending on the magnitude of wave reflection, but also on the timing of wave reflection (Segers et al., 2007).

AIx is dependent on the transit time of the reflected wave and the time of arrival of the reflected wave during the pressure pulse. AIx is sensitive to heart rate. A slower heart rate will cause the peak of the reflected wave to occur relatively earlier in systole, which will lead a increase in the AIx. Conversely, a faster heart rate will cause the reflected wave arriving relatively later in systole that will decrease the AIx. In the recent Anglo-Cardiff Collaborative Trial (McEniery et al., 2005), it is shown that AIx increased with age, AIx might be a more sensitive marker of arterial stiffening and risk in younger individuals but aortic PWV is likely to be a better measure in older individuals.

Since the direct measurement of ascending aortic blood pressure waveforms is invasive, non-invasive methods of derivation of similar data by applanation tonometry have been developed (Davis, 1985; Gravlee et al., 1989; Cameron

and Dart, 1994; Chen et al., 1997). In Kelly's work (1989b), applanation tonometer was used to measure the carotid pressure waveform. Then, the carotid waveforms were analysed to measure the shoulder and peak of the waves to calculate the AIx. Arteiral applanation tonometry is a technique that allows continuous and non-invasive registration of the arterial pressure waveform, the clinical use of the tonometry had its breakthrough only in the 1990's (Matthys and Verdonck, 2002), proved its usefulness in several arterial compliance and hypertension studies (Boutouyrie et al., 2000; London et al., 1996). This technique is applicable to superficial, large arteries such as the carotid, radial and femoral arteries. Although non-invasive assessment of waveforms in arteries close to the central aorta give acceptable estimates of central aortic waveform characteristics, carotid (Cameron and Dart, 1994) and subclavian (Aakhus et al., 1993), the radial artery is often proposed as the preferred site for applanation tonometry because it is well supported by bony tissue making optical applanation theoretically easier to achieve. However, the waveform contour in the radial artery is substantially different from that in the ascending aorta and requires further work before adequately approximating the central aortic waveform shape (Chen et al., 1997).In order to derive the central aortic pulse waveform from a peripheral pulse waveform, a valid transfer function based on Fourier analysis have been promoted for this purpose. The transfer function analysis requires a good transfer function model for the peripheral-aortic path consisting of vessels of elastic and bifurcated (Chen et al., 1997; Segers et al., 2000), which induce damping and reflections and result in a peripheral pulse waveform very much different from an aortic pulse waveform.

Parker and Jones (1990) introduced Wave Intensity Analysis (WIA), a time domain technique, which allows for the separation of the forward and backward pressure, velocity waveforms and wave intensities (dI_{PU}). WIA thus can be used for the determination of the arrival time of reflected wave, and has been applied to different sites in the cardiovascular system; aorta (Koh et al., 1998), coronary arteries (Sun et al., 2000) and left ventricular (Wang et al., 2005). WIA has been shown to accurately estimate arrival time of reflected wave *in vitro* (Khir and Parker, 2002) and *in vivo* (Khir and Parker, 2005). However, both the inflection point on pressure waveform and WIA methods require a reliable measurement of local pressure.

In Khir and Parker's work (2002), reflection coefficient is calculated as the ratio of changes in pressure related to the forward and backward waves; with the remaining approaches, using WIA, reflection coefficient is directly obtained from the wave magnitude, which can be quantified by peak wave intensity (Jones et al., 1992; Jones et al., 2002; Bleasdale et al., 2003; Fujimoto et al., 2004; Khir and Parker, 2005; Penny et al., 2008; Smolich et al., 2008) or the wave area (Davies et al., 2006b). Thus, reflection coefficient has been calculated from the ratio of the cumulative intensities of backward and forward waves (Hollander et al., 2001; Hobson et al., 2007). Mynard et al. (2008) calculated and compared the reflection coefficient with wave intensity method in a non-linear computer model of a single vessel with various degrees of elastic non-linearity, determined by wave speed and pulse amplitude, and a terminal admittance to produce reflections. Their results showed that under linear flow conditions, reflection coefficient calculated from the pressure is equivalent to the square-root of reflection coefficients calculated from the wave intensity and wave area. However, for non-linear flow, significant errors related to the degree of elastic non-linearity arise in reflection coefficients calculated from the wave intensity and wave energy, but reflection coefficient calculated from the pressure is unaffected by the degree of non-linearity and thus concluded it is more accurate. Segers et al. (2007) compared the wave separation analysis with the waveform analysis for the timing and magnitude of the reflected wave, and they concluded that analysis of pressure wave reflection is optimally based on the measurement of pressure and flow, rather than on waveform analysis alone. At the same time, that simultaneous measurement of pressure and flow might not always be feasible in a clinical context.

1.4.4 Wave intensity analysis

In 1988 Parker et al. (Parker et al., 1988) described a new one-dimensional time domain based method for the analysis of arterial waves that was based on the method of characteristics. Unlike impedance analysis the method of characteristics does not assume either linearity or periodicity (Parker and Jones, 1990).

Fundamentally wave intensity analysis (WIA) views any wave as being composed of small incremental waves or wavefronts and that the intensity of a

wave is a measure of energy flux density (i.e. power) carried by the wave. Wave intensity is defined as the product of the change of pressure and velocity, and a change in pressure and velocity is always associated with a ‘wave’. The magnitude of wave intensity is calculated by multiplying the change in pressure by the change in velocity.

$$dI = dPdU \tag{1.4}$$

Further analytical and derivated details are described in chapter 2. With knowledge of wave speed, the net wave intensity can be separated into forward components arising from the heart and backward components originating from the circulation (Parker and Jones, 1990). This approach has advantages in a clinical setting as it is a time domain analysis which can be easily related to physiological events. Using terminology derived from gas dynamics waves are considered to be either ‘compression’ waves (associated with an increase in pressure) or 'expansion' waves (associated with a decrease in pressure). The value of WIA also could be used for the assessment of dynamic ventricular-arterial interaction (Ramsey and Sugawara, 1997). Knowledge of amplitude and timing of forward compression and expansion wave intensities as well as backward wave intensity benefits understanding of contribution of wave energy ejected by ventricle and reflected by peripheral arteries (Jones et al., 1992; 1994). The accurate prediction of timing of compression and expansion wave and backward wave is of clinical significance for understanding of cardiac-arteries interaction.

WIA has led to the discovery that reflected (compression) waves are not the only factors that influence the shape of the waveforms. WIA has revealed that late in systole the reduction in rate of contraction of the LV generates a forward travelling expansion wave (FEW) that contributes to closure of the aortic valve (Parker et al., 1988; Parker and Jones, 1990). If linearity of the system is assumed then WIA, like impedance analysis, can be used to separate pressure and flow into forward and backward components using the water hammer equation. Under uniform conditions the water hammer equation enables one to estimate the pressure dependent wave speed of a wavelet when travel is unidirectional.

The method of characteristics is arguably more flexible than impedance analysis; nevertheless it does assume that the 1-D theory is valid: pressure and velocity will vary along the system but will have a uniform value at each cross-sectional area and that speed of propagation of the wave (wave speed) is greater that the velocity of blood flow.

1.4.5 Non-invasive wave intensity

A major limitation to the initial use of wave intensity as a measure of ventricular and vascular function in an everyday clinical setting was that invasive measurement of pressure and flow recordings were needed. In 2000, Sugawara and colleagues studied the relationship between intravascular pressure and diameter-change of the carotid artery. Their research showed that during diastole, the pressure-diameter relationship was slightly non-linear; however during systole, when wave intensity is well defined in the carotid artery the waveforms are in fact very similar (Sugawara et al., 2000). After this discovery, a new non-invasive real-time measurement system of wave intensity was developed (Harada et al., 2000). In their work, diameter changes can be measured accurately using an echo-wall tracking system, which is installed into an ultrasound system and arterial diameter changes can be used as a surrogate for pressure changes. The blood flow velocity along the vessel can then be measured using range-gated color Doppler signals. Both diameter change and velocity measurements along with the ECG are fed into a personal computer that displays all information in real time. Blood pressure is taken using a cuff manometer at the upper arm; this information is also fed into the personal computer. The systolic and diastolic blood pressures are used to convert diameter change into pressure and wave intensity can be calculated.

Another study by Feng and Khir (2010) involved the development of an algorithm to separate wave intensity into its forward and backward directions using measured diameter of a flexible tube’s wall with measured velocity. This group also found that the results determined using measured diameter were almost identical to those calculated using measured pressure and velocity in the traditional wave intensity way.

1.4.6 Wave and reservoir theory

In 1733 a smoothing mechanism called the Windkessel effect (**Figure 1.4**) was first described by Hales with an air chamber (or Windkessel in German) model. Frank put Hales' idea into mathematical form in 1899 (Frank, 1899) in which it is assumed that all pressure changes in the arteries occur simultaneously and hence without accounting for pulse wave propagation. However, as a zero-dimensional model, Windkessel is incompatible with wave transmission and in practice it can not satisfactorily predict the sharp of upstroke or the shoulder often observed on the aortic pressure waveform. For this reason, the impedance based approaches had been developed by Womersley (1955). Wang et al. in 2004 presented the equal magnitude, self cancelling forward and backward waves drawn from one-dimensional wave theory to explain why after the closure of the aortic valve, the aortic flow stops immediately but the corresponding aortic pressure remains high and decreases slowly rather than zero flow outcome the proximal to distal pressure gradient be required to be zero. Wang et al. (Wang et al., 2003) proposed a combined approach between the Windkessel model and the wave model, termed the wave-reservoir model. This model takes account of the distensibility of the aorta, and attributes the quasi-exponential decline in diastolic pressure to this, but also incorporates wave transmission in systole. This attractive, contentious proposal, remains to be studied further in depth. Davies et al. (Davies et al., 2007) have argued that neglect of the radial expansion of the aorta and large elastic arteries in systole may lead to misleading results using simple wave analysis and that subtraction of this 'reservoir pressure' should be performed before undertaking wave separation.

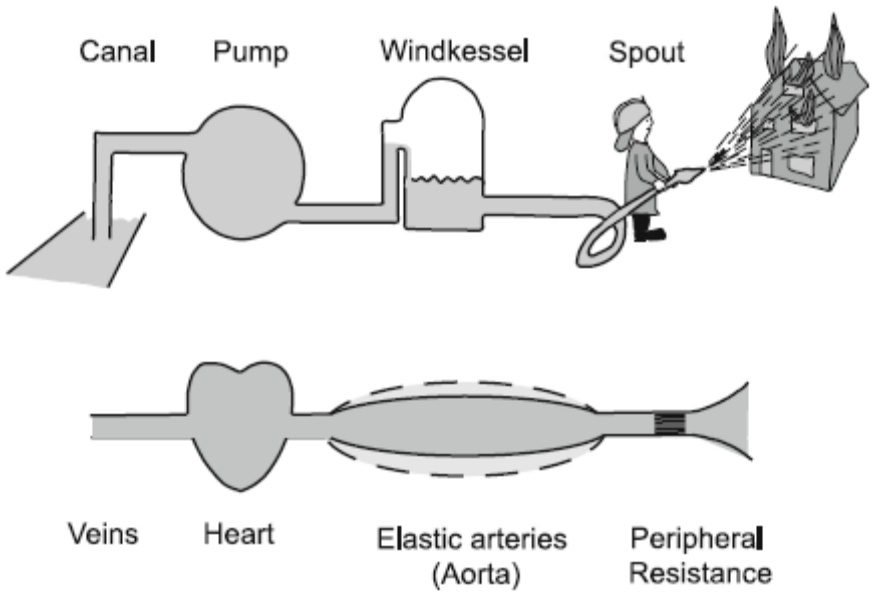

Figure 1.4: The concept of the Windkessel. The air reservoir is the actual Windkessel, and the large arteries act as the Windkessel. The combination of Compliance, together with aortic valves and peripheral resistance, results in a rather constant peripheral flow (Taken from Westerhof et al., 2009).

1.4.7 Mechanical properties of arteries

Elasticity of arteries reflects the ability of an artery to expand and recoil with cardiac pulsation and relaxation (Arnett et al., 1994). In sedentary humans, the compliance of the large-sized arteries in the thoracic region (central circulation) decreases with aging (Avolio et al., 1985; Arnett et al., 1994; Tanaka et al., 1998). Large artery's distensibility is important for circulatory efficiency. It reduces impedance to systolic ejection and cardiac work, slows wave speed, and benefits coronary perfusion during diastole. Conversely, arterial stiffening (as with aging, atherosclerosis, hypertension and heart failure) is functionally disadvantageous, particularly in the presence of cardiac dysfunction, high blood pressure, or coronary artery disease. The chronic effects of aging and disease on resting distensibility, attributed generally to structural changes in the arterial wall, have attracted increasing clinical interest in recent years (Avolio et al., 1983; Dart et al., 1991; Cameron et al., 1995; Gatzka et al., 1998). Distensibility can be measured by relating luminal diameter and transmural pressure or by pulse wave velocity (wave speed) to which it is inversely related (Avolio et al., 1983). Goodfellow et al. (Goodfellow et al., 1996) and Ramsey et

al. (Ramsey et al., 1995) have shown, for example, the distensibility measured by wave speed is acutely increased during a hyperemia-induced increase in flow in normal subjects but not in patients with heart failure or diabetes where flow-related endothelium-mediated vasodilatation is impaired.

Several methods have been applied to determine the mechanical properties of arteries. Bergel (1961a, b) developed an apparatus to determine the pressure-radius relationship of arterial specimens *in vitro*, both static and dynamic behavior were measured.

In animal assessment of the mechanical properties of the arterial wall is done by increasing the pressure inside the vessel and measuring the change in radius (or in volume). The change in volume divided by the change in pressure represents the slope (or arterial compliance) of the pressure-volume relationship and is used as a quantitative index describing the elasticity of the system (Levy, 1996). Several *in vivo* models of the arterial circulation have been described to determine arterial compliance in animal and humans (O'Rourke, 1982; Milnor, 1982; Safar and Simon, 1986; Safar and London, 1987; Westerhof and Huisman, 1987). The classic 'Windkessel' model assumes the arteries as a system of interconnected tubes with fluid storage capacity. Fluid is pumped at one end in a pulsatile type (ventricular ejection) whereas outflow at the other end is approximately steady.

In the last ten years, the group of Holzapfel have published several works of layer-specific data (Schulze-Bauer et al., 2002, 2003; Holzapfel et al., 2004; Sommer et al., 2008) with a variety of vessels on the behavior of human vessels, which probably are the most comprehensive studies due to the complexity of the layer separation and the difficulty in obtaining samples. From the results it is shown that aged arteries experience a more sudden stiffening in both layers than young ones. For the media, this may be related to fatigue induced fracture of elastic laminae; for the adventitia, it might be a consequence of increased cross-linking among collagen fibers, derived from remodeling process.

There is also lots of research about non-invasive assessment of arterial mechanical properties. Ultrasound can be used to measure arterial mechanical properties (distensibility and compliance), but its use is focused on the larger and more approachable arteries. Hence this technique has been used mainly on the brachial, femoral, carotid arteries and the abdominal aorta (Hayoz et al.,

1992; Bank et al., 1999; Hoeks et al., 1999). By using ultrasound, several images of the vessel wall are obtained in each cardiac cycle, and the maximum and minimum cross-sectional areas of the vessel are calculated by wall tracking and computerized edge-finding software (Mackenzie et al., 2002). Problems with the use of ultrasound to assess mechanical properties of arteries include the limited resolution, which can make the detection of small changes in vessel diameter (area) difficult. The technique also relies heavily on the ability of the operator to image the walls of the vessel being studied accurately, and there have been some concerns about the reproducibility of the technique, although with an experienced operator this problem can be improved. McVeigh et al. (McVeigh et al., 2002) wrote a review evaluated the mechanical arterial properties from clinical, experimental and therapeutic aspects. They compared the methods used to estimate the mechanical properties of arteries, shown in **Table 1.2**.

Table 1.2 Methods used to estimate the mechanical properties of arteries.

Note: BP, blood pressure; TTE, trans-thoracic echocardiography; TEE, trans-esophageal echocardiography; ET, echo tracking; IVUS, intravascular ultrasound (McVeigh et al., 2002)

Methods	Advantages	Limitations	Information
Direct			
Angiography	Evaluation of different aortic segments	Expensive, invasive, limited clinical application	Regional wall properties
Magnetic resonance imaging	Non-invasive, not limited by acoustic window, can examine multiple arterial segments	Claustrophobia, expensive, limited availability, remote site of BP measurement	Regional wall properties
TTE/TEE	TTE non-invasive, reasonable availability	Expensive, TTE limited by acoustic window, operator-dependent technique, TEE invasive, remote site of BP measurement	Regional wall properties
Transcutaneous ET/IVUS techniques	Transcutaneous technique is non-invasive; both techniques reproducible	Operator dependent, IVUS invasive, remote site of BP measurement with ET, clinical research application	Local wall properties
Indirect			
Fourier analysis of pressure and flow waveforms	Reference technique, pulsatile and steady-state information	Expensive, invasive, limited to the research arena	Total arterial impedance and local properties
Stroke-volume to pulse-pressure ratio	Non-invasive, reasonable availability	Non-invasive estimate of stroke volume required, brachial BP measurement	Total arterial compliance
Pulse-wave velocity	Non-invasive, reproducible, potential for wider clinical application	Limited to aorta, errors estimating path length and waveform distortion with pulse propagation	Segmental arterial stiffness
Pulse-contour analysis	Non-invasive, reproducible, potential for wider clinical application	Non-invasive measurement of stroke volume, assumed model of the arterial system	Compliance estimates derived from Windkessel modelling

Arterial Testing

Arterial testing was performed in order to obtain an understanding of the mechanical properties of the arterial wall. In this section, some of the most relevant and cited work developed by multiple groups that had led to the understanding of the properties of the arterial tissue.

In 1922, Bramwell and Hill carried out an experiment to measure the velocity of a pressure wave in an excised human carotid artery (Bramwell and Hill, 1922). A representation of the setup they used is shown in **Figure 1.5**.

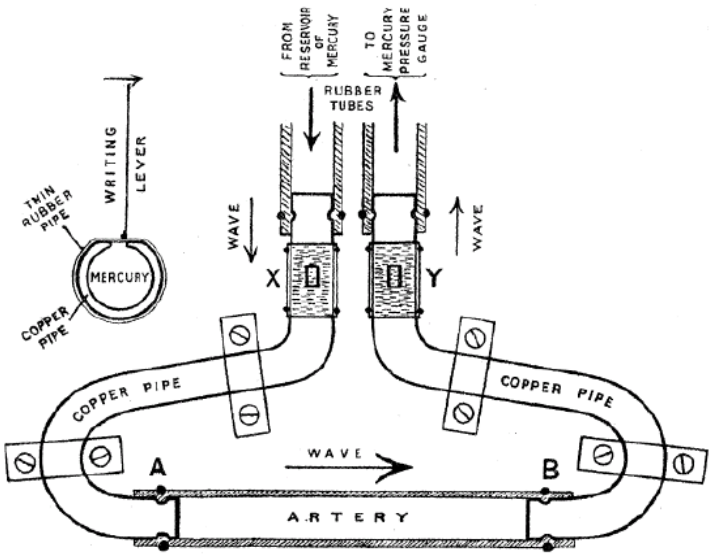

Figure 1.5: Schematic diagram of the experiment done by Bramwell and Hill in 1922 to measure the pulse wave velocity (Taken from Bramwell and Hill, 1922).

In the experiment they fixed the carotid artery between two copper tubes. Then, the entire system was filled with mercury in order to slow down the pressure wave to have better accuracy in the measurements. The travel time of the pressure wave was measured using fine bamboo levers attached to a membrane placed in a window at each end of the copper tubes. With this experiment they were able to show that the speed of propagation increased with pressure. They noted that the speed remained relatively constant up to 80 mmHg and then increased significantly with pressure. Similar findings were calculated by Bramwell and Hill from a study by Roy and Brown in 1880 where they characterized the change in diameter of arterioles with pressure.

Bergel in 1961 published two studies in which he described the static and dynamic elastic properties of the arterial wall. In these studies he used the local arterial stiffness approach, measured the changes of diameter as a function of pressure in different positions of the arterial tree (thoracic aorta, abdominal aorta, femoral and carotid arteries). In the static study he reported the incremental modulus for the circumferential direction, which he showed in a previous work to be 1.5 times stiffer than the longitudinal modulus. The dynamic study of the arterial properties was done using a similar method to measure the changes in diameter and a sinusoidal pressure by means of a mechanical piston. This study showed that there was little change in the incremental modulus with frequency; the different segments showed different behaviors with frequency.

Patel and Vaishnav investigated the relation between forces acting on a blood vessel and the resulting deformation (Patel and Vaishnav, 1972). They developed the applicability of three polynomial expressions for the strain energy density function for the orthotropic incompressible, aortic tissue.

Fung and co-workers developed a biaxial testing machine for soft tissues and published work with rabbit skin in 1974 (Lanir and Fung, 1974). This allowed studying the anisotropic properties of soft tissues. Using a similar setup, Debes and Fung later on studied pulmonary arteries of dogs (Debes and Fung, 1995). In this setup, arterial rings were cut open and the tissue was prepared in a trampoline-like way, using threads allowing for the straining of the tissue in two directions: longitudinal and circumferential. This work also focused in the “zero stress state”, which is achieved when the rings are cut open and the artery springs open. This “zero stress state” was calculated from the opening angle. Some of the results from the biaxial testing showed that within the physiological deformation, the strain-stress relationships were slightly nonlinear, and anisotropic. In this study the stress-strain relationship in the longitudinal direction suggested that the artery was stiffer along this axis compared to the circumferential one. This differs from what Bergel and others had observed with the local stiffness approach. The differences might be explained by the zero stress state compared to the *in situ* shape used in Bergel’s experiments.

Arteries are ono-linearly elastic, becoming stiffer as they are distended, typically by a factor of 100 between mean pressures of 60 and 180 mmHg (Nichols and

O'Rourke, 2005). The importance of the composite nature of the artery wall in providing the essential elastic non-linearity was clearly shown in a classic study proposed by Roach and Burton (1957). In their study, the individual mechanical roles of elastin and collagen were studied. They found that the initial stiffness (tension) of the arterial wall represented the elasticity of the elastin, while the much stiffer collagen fibres remain folded, and the much higher stiffness at high strains represented the contribution of fully tensed collagen fibres.

In 1984 Dobrin and Canfield published a work on common carotid arteries of dog in which they also studied the contributions of elastin and collagen to the overall properties of the arterial wall. The study suggested that elastin undertakes a portion of the distending load in both the longitudinal and the circumferential directions. Histological evidence of the distribution of the elastic lamellae in the aorta (Wolinsky and Glagov, 1964; Wolinsky and Glagov, 1967) supports these findings.

A multiaxial testing machine was developed by the group led by Kassab in 2003 (Guo and Kassab, 2003). This machine allowed the study of the coronary arterial tissue in its physiological shape. They observed that the hysteresis loop from the twist (torque) testing was very small, meaning that the viscoelasticity feature of the shear modulus in the epicardial coronary arteries was small.

Other studies have focused on studying the properties of decellularized arteries (Roy et al., 2005), and the effect of cryopreservation on the arterial wall strength (Venlatasubramanian et al., 2006). Several groups have studied the effect of temperature on arterial tissue. Tsatsaris studied the distensibility and mechanical properties of the aorta (Tsatsaris, 2005). Guinea et al. studied the thermo-mechanical behavior of human carotid arteries (Guinea et al., 2005).

1.5 Aims and objectives of the study

By the motivation in this chapter and of the literature reviews, the aim of this thesis therefore is to increase the understanding of wave propagation, and methods for determining and comparing wave speed. Also, the aim of this thesis is to introduce a non-invasive technique for determining the mechanical properties of the arterial wall.

The objectives of this thesis are:

1) To experimentally apply and compare different methods for the determination

of wave speed and arrival time of reflected wave in flexible tubes.

2) To investigate the effect of proximity to a reflection site on wave speed determined by PU-loop.

3) To investigate using wave intensity analysis to determine the local reflection coefficient.

4) To introduce a new non-invasive technique which use measurements of the diameter and velocity at one point to determine the mechanical properties of the flexible tubes and animal arteries noninvasively.

1.6 Thesis outline

The work undertaken in this thesis in order to achieve the above mentioned aims and objectives has been structured according to the following outline:

- Chapter 2: This chapter is entitled ‘Methodology’. This chapter contains a detailed explanation of the mathematical formulation for all the theories used throughout this thesis. Also the basic experimental set up, the measuring equipment used for the experiments, the calibration techniques and the reproducibility of the recorded signals are all described in this chapter.
- Chapter 3: This chapter is entitled ‘Experimental comparison of methods for determination of local wave speed. This chapter compares the foot-to-foot, PU-loop, and *ln*DU-loop methods to determine the wave speed in flexible tubes; compares the PU-loop and *ln*DU-loop methods to determine the arrival time of reflected wave, the separation of wave and wave intensity. Effect of fluid density on wave speed determined by *ln*DU-loop is also considered in this chapter.
- Chapter 4: This chapter is entitled ‘Variation of wave speed determined by PU-loop with proximity to reflection sites’. This chapter investigates the wave speed determined by PU-loop affected by the reflection. An algorithm to correct the measured wave speed which is affected by the reflection, is also considered and discussed in this chapter.
- Chapter 5: This chapter is entitled ‘Using wave intensity analysis to determine the local reflection coefficients’. This chapter examines whether wave intensity analysis can be used to determine the local reflection coefficient.

- Chapter 6: This chapter is entitled '*In-vitro* non-invasive determination of mechanical properties of flexible vessels'. An algorithm developed based on the one point measurements of diameter and velocity to determine mechanical properties of flexible tubes and calf aortas. The non-invasive determination of wave speed is also validated with calf aortas in this chapter.
- Chapter 7: This chapter is entitled 'Conclusions and future work'. This chapter contains general discussions, all the conclusions summarized from chapter 3 to chapter 6 and future works.

Chapter 2
Methodology

2.1 Theoretical analysis

2.1.1 Introduction

In 1775 Euler introduced a one-dimensional model to describe blood flow in arteries, and wrote the fundamental non-linear equations that are still widely used in fluid dynamics today. Euler's one-dimensional equations of motion for fluid (Euler, 1775) are complex, hyperbolic partial differential equations that remained unsolved until Riemann introduced the method of characteristics in 1860 (Riemann, 1860). The work of Riemann prepared the way for the development of wave intensity analysis (WIA). WIA, based on the solution of the Euler's mathematical model and equations using the method of characteristics, made it possible to consider the arterial waves as infinitesimal wavefronts or wavelets (Parker and Jones, 1990).

Figure 2.1 show a one-dimensional tube of length l, circular cross-sectional area A(x,t), with uniform properties around the circumference. Area A is allowed to change in time t, because the deformability of the arterial wall is a key characteristic of the performance of the system. Then the problem can be described in one spatial dimension, and this assumption is suitable for the large conduit arteries whose thickness is small compared to their diameter.

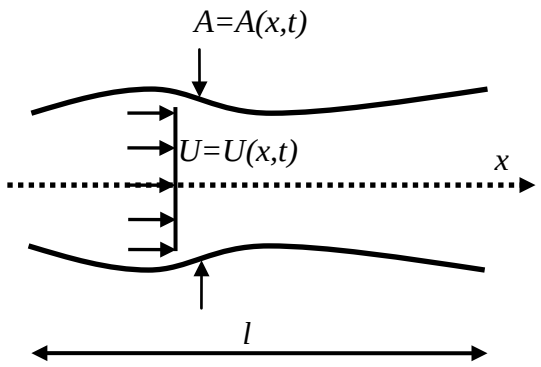

Figure 2.1: Layout of a one-dimensional compliant vessel.

There are two assumptions to be made when one-dimensional flow equations are applied in the circulation. The reasons and suitability of these two assumptions are discussed as follows:

1) The validation of one-dimensional model:

If the flow in arteries were assumed as one-dimensional, the measured pressure and flow can be expressed as the function of distance and time, that is P = P(x,t) and Q = Q(x,t). It has been reported that under normal conditions velocity distribution in the arteries tends to be axisymmetrical in straight, branchless segments (Schultz et al., 1969). It is also been stated that axial flow is dominant in the aortic arch (Pedley, 1980). Lighthill stated that arterial radius expands and contracts by up to 10% in thoracic aorta of its undisturbed value, resulting in radial motions negligible small compared with the longitudinal motion, which suggests that the one-dimensional theory is quite a reasonable approach and accurate enough to analyse blood flow in the arterial system (Lighthill, 1978).

2) Blood is treated as an incompressible fluid:

Pedley suggested that the blood can be approximately treated as incompressible liquid (Pedley, 1980). Lighthill also stated that the compressibility of the blood is negligibly small compared to the large distensibility of the arterial wall (Lighthill, 1978).

2.1.2 Governing equations

Blood flow in the arterial system follows the laws of conservation for mass and momentum.

Mass law: The continuity equation expresses the conservation law by equating a net flux over a surface with a loss or gain of mass or volume within the surface. Mass can neither be created nor destroyed thus an equal quantity of incompressible fluid flowing into a system must flow out.

$$A_t + U(A)_x = 0 \tag{2.1}$$

Where A is the cross-sectional area, t is time, U is spatially averaged velocity and x is the axial distance along the tube.

Momentum law: As momentum is 'mass in motion' Newton's second law:

Force = mass x acceleration can be reworked to become Force = rate of change of momentum, which is equal to the resultant acting on the body.

$$U_t + UU_x + \frac{P_x}{\rho} = 0 \tag{2.2}$$

Where P is the spatially averaged pressure.

Blood vessels are assumed to be impermeable elastic tubes where the effects of viscous dissipation are insignificant and the properties are believed to be uniform and constant. As the cross-sectional area of the tubes differs during systole and diastole as a result of the change in pressure and the elastic properties of the wall, the values depend on the instantaneous pressure only (Parker et al., 1990). Therefore, the cross-sectional area can be described as a function of pressure, which itself is a function of distance and time. Equation (2.3) describes the tube law which is the relationship between transmural pressure and cross sectional area.

$$A = A(P(x,t)) \tag{2.3}$$

The values can then be expressed as the rate of change of the cross-sectional area (A) at time (t) and distance (x)

$$A_t = \frac{dA}{dP}P_t \quad \text{and} \quad A_x = \frac{dA}{dP}P_x \tag{2.4}$$

Substitution of equation (2.4) into the continuity equation (2.1), can be expressed as an ordinary differential equation in terms of pressure and velocity

$$\frac{dA}{dP}P_t + \frac{dA}{dP}UP_x + AU_x = 0 \tag{2.5}$$

Which when divided by a measure of the segment's compliance dA/dP and rearranged:

$$P_t + UP_x + \frac{A}{dA/dP}U_x = 0 \tag{2.6}$$

The distensibility of the arterial vessel wall, D, can be defined as the relevant change of the cross sectional area per change of the pressure compared to the initial area:

$$D = \frac{1}{A}\frac{dA}{dP} \tag{2.7}$$

Equation (2.6) is a first order hyperbolic partial differential equation, which can be solved using the method of characteristics, using the characteristic directions U ± c (Riemann 1860). U is the flow speed and the waves propagate with a wave speed of c. Equations (2.2) and (2.6) can be written in matrix form:

$$\omega t + \Omega\omega x = \Phi \tag{2.8}$$

Where $\omega = \begin{pmatrix} P \\ U \end{pmatrix}$ and $\Omega = \begin{pmatrix} U & \frac{1}{D} \\ \frac{1}{\rho} & U \end{pmatrix}$

These equations are hyperbolic and amenable to solution by the method of characteristics.

The eigenvalue, λ, of the matrix Ω, are solutions of the characteristic polynomial

$$\left|\Omega - \lambda I\right| = 0 \tag{2.9}$$

Where I is the identity matrix and the eigenvalue depicts speed of propagation

$$\Omega = \begin{bmatrix} (U-\lambda) & \frac{1}{D} \\ \frac{1}{\rho} & (U-\lambda) \end{bmatrix} = (U-\lambda)^2 = \frac{1}{\rho D} \tag{2.10}$$

If define the left term of equation (2.10) as c^2,

$$c^2 = \frac{1}{\rho D} \tag{2.11}$$

and also, $c^2 = (U-\lambda)^2$ (2.12)

Therefore the eigenvalue of the matrix Ω:

$$\lambda_{\pm} = U \pm c \tag{2.13}$$

The physical meaning of the term c is the local wave speed. In equation (2.13), the positive sign, '+' indicates the forward direction and the negative sign '-' indicates the backward direction. Usually in the arterial system, the forward direction indicates the wave is running from ventricle to the peripheral arteries and the backward direction means that the wave is running from the peripheral arteries to the ventricle.

The method of characteristics relies on the observation that the waves run in the space-time plane along the characteristics direction, which are

$$\frac{dx}{dt} = U \pm c \tag{2.14}$$

Along the characteristic directions of the partial differential equations (2.8) can be reduced to ordinary differential equations

$$\frac{dU}{dt} \pm \frac{1}{\rho c}\frac{dP}{dt} = 0 \tag{2.15}$$

If wave speed is a function of local pressure, these equations can be written in Riemann function terms, R represents Riemann invariants in the forward (+) and backward (-) directions.

$$R_{\pm} = U \pm \int_{p_0}^{p} \frac{dP}{\rho c} \tag{2.16}$$

Where, P_0 is initial pressure. The differential form of equation (2.16) can be written as:

$$dR_{\pm} = dU \pm \frac{dP}{\rho c} = 0 \tag{2.17}$$

2.1.3 The water hammer equation

Rewriting equation (2.17) along the characteristic directions gives the water hammer equation:

$$dP_{\pm} = \pm \rho c dU_{\pm} \tag{2.18}$$

Under uniform conditions the water hammer equation enables one to estimate the pressure dependent wave speed of a wavelet when travel is unidirectional.

2.1.4 Wave separation and wave intensity

All measured pressure and velocity values are derived from a forward and backward wavefront that intersect at a precise time and plane. If we assume that the changes in pressure and velocity are the linear summation of increments of pressure and velocity in forward and backward directions, then:

$$dP = dP_+ + dP_- \tag{2.19}$$

$$dU = dU_+ + dU_- \tag{2.20}$$

The water hammer equation (2.18) can be used to separate the changes of measured pressure and velocity into forward and backward components.

$$dP_\pm = \frac{1}{2}(dP \pm \rho c dU) \tag{2.21}$$

$$dU_\pm = \frac{1}{2}(dU \pm dP/\rho c) \tag{2.22}$$

The forward and backward pressure and velocity waveforms can then be calculated by integration.

$$P_+ = \sum_{t=0}^{T} dP_+ + P_0\,,\ P_- = \sum_{t=0}^{T} dP_- \tag{2.23}$$

$$U_+ = \sum_{t=0}^{T} dU_+ + U_0\,, U_- = \sum_{t=0}^{T} dU_- \tag{2.24}$$

Where P_0, U_0 are initial integration constants taken as diastolic values, P_0 is the diastolic pressure, U_0 is the integration constant, taken to be zero, and t is time.

Wave intensity, dI=dPdU, is the flux of energy carried by the waves per unit area, having units of W/m^2. Also, dI can be separated into forward wave intensity, $dI_+=dP_+dU_+$, and backward wave intensity, $dI_-=dP_-dU_-$, which can be obtained from measurement of P and U, and knowledge of wave speed:

$$dI_\pm = \pm\frac{1}{4\rho c}(dP \pm \rho c dU)^2 \tag{2.25}$$

Equation (2.25) shows that forward wave intensity is always positive and backward wave intensity is always negative.

Furthermore, the forward and backward wave energy can be obtained by integration of $dI_\pm$ with respect to time,

$$I_\pm = \int_0^T dI_\pm dt \tag{2.26}$$

2.1.5 Wave speed determined by PU-loop

The separation of pressure and wave intensity requires knowledge of wave speed. The water hammer equation can be used to determine the wave speed only if waves passing by the measurement site are running in one direction. Therefore, plotting the measured pressure against the measured velocity over the cycle, a PU-loop obtained (**Figure 2.2**). Its slope during the very early part of the cycle, when waves are most probably running only in the forward direction, equals ρc.

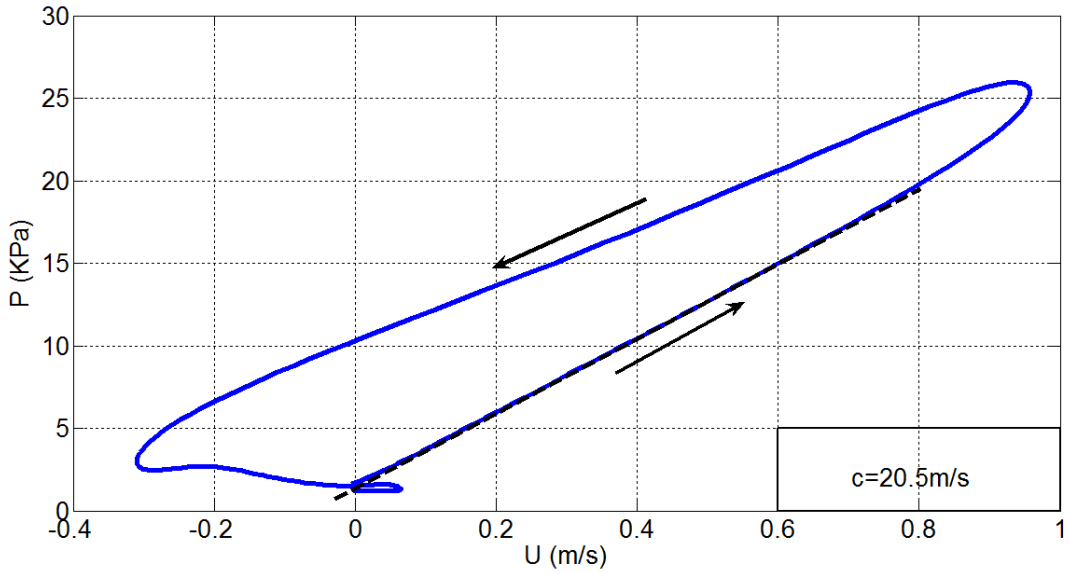

Figure 2.2: An example of a PU-loop in a 10 mm diameter, 1 mm thickness, 1 m long silicone tube. The measurement was taken at 25 cm away from the inlet of the tube. A pulse is generated at the inlet of the tube using a piston pump. During early part only forward wave generated from the pulse are present. The dashed line showed the linear part of the PU-loop. The slope of the dashed line can be used to calculate the wave speed. Arrows indicate the direction of the loop. Wave speed is 20.5 m/s in this case.

2.1.6 Non-invasive determination of wave intensity using diameter and velocity

A major limitation to the initial use of wave intensity as a measure of ventricular and vascular function in an every day clinical setting was that invasive pressure and flow recordings were needed. Non-invasive wave intensity determined by the diameter and flow would benefit the clinical routine exam.

Assume a circular initial cross section of a vessel with an area

$$A = \pi \frac{D^2}{4} \tag{2.27}$$

And the change in the cross-sectional area

$$dA = \frac{\pi}{2} D dD \tag{2.28}$$

Therefore, dividing (2.28) by (2.27)

$$\frac{dA}{A} = \frac{2dD}{D} \tag{2.29}$$

It is well established that wave speed is a function of distensibility of tube wall (Pedley, 1980)

$$c^2 = \frac{1}{\rho D} = \frac{AdP}{\rho dA} \tag{2.30}$$

Rearranging equation (2.30) gives

$$dP = \rho c^2 \frac{dA}{A} \tag{2.31}$$

The change in pressure, dP, can be considered as the linear summation of the change in pressure in the forward and backward direction, see equation (2.19). It is reasonable to assume that change in diameter, dD, to be considered as the linear summation of diameter changes due to changes in the forward and backward pressure changes,

$$dD = dD_+ + dD_- \tag{2.32}$$

Substituting equation (2.31) into the water hammer equation (2.18), gives

$$dD_\pm = \pm \frac{D}{2c} dU_\pm \quad \text{or} \quad dU_\pm = \pm \frac{2c}{D} dD_\pm \tag{2.33}$$

If we assume the change in the velocity waveform, dU, is the result of the algebraic summation of the changes in the forward and backward directions, see equation (2.20).

Substitution $dU_\pm$ from equation (2.33) into (2.20) gives

$$dU = \frac{2c}{D} dD_+ + (-\frac{2c}{D} dD_-) \tag{2.34}$$

The change in diameter resulting from the change in pressure in the forward and backward directions can be obtained by multiplying (2.32) by (2c/D), adding and subtracting (2.34), and rearranging given

$$dD_{\pm} = \frac{1}{2}(dD \pm \frac{D}{2c} dU) \tag{2.35}$$

To determine the change in diameter in the forward and backward directions we substitute (2.33) into (2.32),

$$dD = \frac{D}{2c} dU_{+} + (-\frac{D}{2c} dU_{-}) \tag{2.36}$$

The velocity differences in the forward and backward directions can be similarly determined,

$$dU_{\pm} = \frac{1}{2}(dU \pm \frac{2c}{D} dD) \tag{2.37}$$

If consider that dD/D which is the incremental hoop stress equals d*ln*D, rewrite equation (2.33), (2.35) and (2.37) as

$$c = \pm \frac{1}{2} \frac{dU_{\pm}}{d \ln D_{\pm}} \tag{2.38}$$

Equation (2.38) provides an expression of wave speed using measurements of diameter and velocity. Note that this equation does not include a density term, unlike PU-loop.

$$dD_{\pm} = \pm \frac{1}{2}(d \ln D \pm \frac{1}{2c} dU) \tag{2.39}$$

$$dU_{\pm} = \pm \frac{1}{2}(dU \pm 2c d \ln D) \tag{2.40}$$

The forward and backward diameter and velocity can be obtained by summation of changes in diameter and velocity in the forward and backward directions.

$$D_{+} = \sum_{t=0}^{T} dD_{+} + D_0 , \quad D_{-} = \sum_{t=0}^{T} dD_{-} \tag{2.41}$$

$$U_{+} = \sum_{t=0}^{T} dU_{+} + U_0 , \; U_{-} = \sum_{t=0}^{T} dU_{-} \tag{2.42}$$

Where D_0 is the undisturbed diameter of the vessel, U_0 equal to zero.

Traditionally, wave intensity is determined by the change of pressure and velocity. To distinguish wave intensity determined by the pressure and velocity from that by the diameter and velocity, we use the terms, dI_{PU} and dI_{DU}, respectively.

dI_{DU} can be established by multiplying the change of diameter by the changes of velocity,

$$dI_{DU} = dDdU \tag{2.43}$$

Similar to dI_{PU}, dI_{DU} can also be separated into the forward and backward directions, dI_{DU+} is wave intensity in the forward direction and dI_{DU-} is wave intensity in the backward direction.

$$dI_{DU\pm} = \pm\frac{1}{2}(d\ln D \pm \frac{1}{2c}dU)^2 \tag{2.44}$$

2.1.7 Non-invasive determination of wave speed: *ln*DU-loop

The separation of diameter, velocity and dI_{DU} waveforms also requires knowledge of wave speed. We hypothesized that in the absence of reflected wave, *ln*D and U are related linearly with the slope of ½(dU/d*ln*D) based on the relationship of the change of diameter and velocity shown in equation (2.38). A typical *ln*DU-loop is shown in **Figure 2.3**. *ln*DU-loop shows that the relationship of diameter and velocity in the beginning of *ln*DU-loop is linear due to the absence of reflected wave. Therefore, the slope of linear part of *ln*DU-loop during the beginning, when the reflection wave has not arrived, can be used to determine wave speed by the slope. The wave speed expressed in terms of diameter and velocity, see equation (2.38).

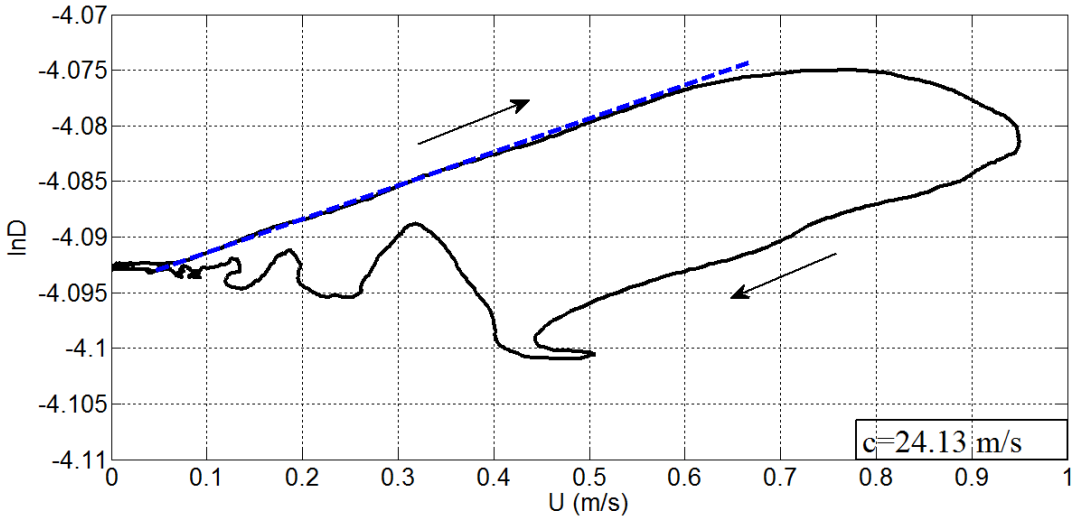

Figure 2.3: An example of *ln*DU-loop in a 16.7 mm diameter, 1.5 mm thickness, 1 m long rubber tube. The measurement was taken at 25 cm away from the inlet of the tube. A pulse is generated at the inlet of the tube using a piston pump. During early part only forward wave generated from the pulse are present. The dashed line showed the linear part of the *ln*DU-loop. The slope of the dashed line can be used to calculate the wave speed. Arrows indicate the direction of the loop. Wave speed is 24.13 m/s in this case.

2.1.8 Wave reflection

It has been long recognised that the pressure and flow waves generated during ventricular systole are partially reflected from the vasculature and that these reflections make a significant contribution to ventricular afterload and overall hemodynamics (Brin and Yin, 1984; O'Rourke and Kelly, 1993; Duan and Zamir, 1995; Koh et al., 1998; Penny et al., 2008).

a. Wave classification

There are four categories of waves: forward and backward (reflected) compression and expansion waves. Direction is expressed in relation to the normal principal direction of blood from the heart and by convention forward wave travel is positive. Compression waves are associated with an increase in pressure and diameter, cause acceleration if running in the forward and deceleration if running in the backward direction. Expansion waves are associated with a decrease in pressure and diameter, causes acceleration if

running the backward and deceleration if running in the forward direction, see **Table 2.1**.

Table 2.1 Wave classification

Wave nature	Wave effect	
	Forward (+)	Backward (-)
Compression	dP>0	dP>0
	dD>0	dD>0
	dU>0	dU<0
Expansion	dP<0	dP<0
	dD<0	dD<0
	dU<0	dU>0

b. The type of reflection sites

In this thesis, wave propagation was investigated in single long tubes. Generally, reflection sites in single long tubes can be positive or negative.

The value of the reflection coefficient R depends upon the area A and wave speed c upstream 0 and downstream 1 of the discontinuity. For arteries where the velocity is generally much lower than the wave speed the equation for R is valid

$$R_t = \frac{\frac{A_0}{c_0} - \frac{A_1}{c_1}}{\frac{A_0}{c_0} + \frac{A_1}{c_1}} \tag{2.45}$$

The types of reflection sites can be classified as following:

Positive reflection sites: 0<R<1;

Negative reflection sites: -1<R<0;

No reflection: R=0;

Close end: R=1;

Open end: R=-1.

2.2 Methods of experimental work

This section will discuss the experimental procedures, instrumentation, calibration methods and analytical tools that were adopted in this thesis. The general experimental setup is shown in **Figure 2.4**. Specific experimental setups will be separately described in detail in the relevant chapters.

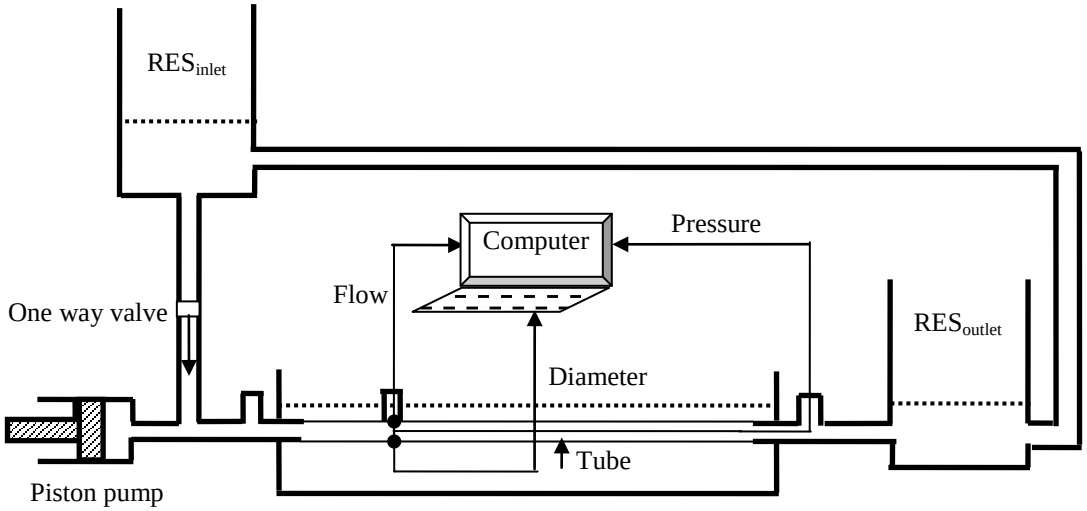

Figure 2.4: A schematic of general experiment setup. RES$_{inlet}$ and RES$_{outlet}$ are the inlet and outlet reservoirs which provided the initial pressure to the system, and kept the tube free of air. Pressure and flow were measured using transducer tipped catheters, and ultrasonic flow meter and probes, respectively. Diameter was measured using a pair of ultrasound crystals. All elements of the experiment are placed on the horizontal plane so that the heights of the inlet and outlet reservoirs were equal.

2.2.1 Instrumentation and measurements

a. Pump

A piston pump was used during most parts of this thesis (**Figure 2.5**). The piston pump is producing an approximately semi-sinusoidal single pulse wave with the piston moving forward from the bottom to the top dead centre. The cylinder of the pump is of 5 cm in diameter and the stroke of the piston is 2 cm; giving a displaced volume of approximately 40ml. A 15 Watts graphite brushes DC motor (Maxon 110937, A-max, sachseln, Switzerland) is used to drive the pump. The motor used a constant DC power supply. The characteristics of this

motor reveal that speed of motor will reduce when the load increase for a fixed voltage of power supply.

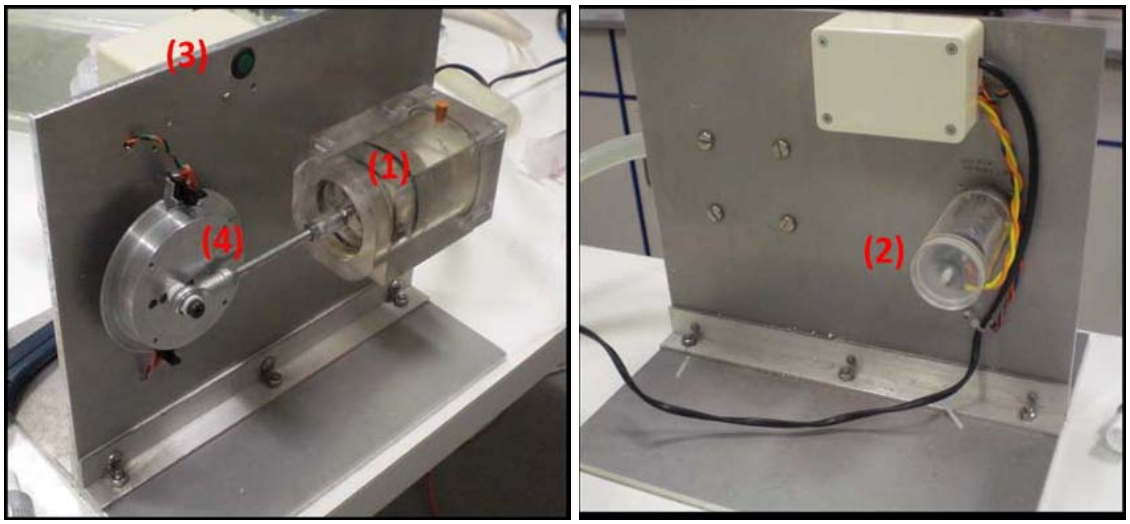

Figure 2.5: Details of the pump: 1. piston; 2. DC motor; 3. switch; 4. rod crank system to transform the rotating motion of the DC motor into assail motion of the piston.

The pressure pulse generated by the piston pump is single pulse. Single pulse is similar to the first pulse of the cycling pulses. The starting point of these pulses is from zero or the initial pressure. The second and followed pulses in the cycling generated pulsed are affected by the previous pulse, the starting point of these pulses is the initial pressure add the end pressure of the previous pulse.The duration of single pulse will be longer than the cycling generation of pressure waves.

b. Tubes

There were three different types of tubes used in the experimental works, silicone, rubber and latex tubes. In each type of the tubes, there were different diameters, wall thicknesses to meet the different experimental conditions. Different experimental setups have been used in this thesis and will be described in the relevant chapters.

c. Reservoirs

The inlet and outlet reservoirs were interconnected, and the height of the fluid in the reservoirs was adjusted to 10cm above the longitudinal axis of the tube; producing an initial hydrostatic pressure of 1 kPa. It is noticed that although the transmural pressure for the different-sized tubes will vary, this variation was

ignored as it was not significant and its effect was expected to be minimal. The experimental tubes were connected to the reservoirs using rigid polyurethane tubing. A one-way valve was placed between the outlet of reservoir and the inlet of each tube, as shown in **Figure 2.4**, to prevent any portion of the displaced volume flowing directly into the reservoir.

d. Pressure measuring equipment

Pressure was measured with 8F transducer-tipped pressure catheters (Millar Instruments Inc., Houston, Texas, USA). The frequency response of the Millar catheter according to manufacturer specifications is: DC to 1000Hz (-3dB), minimum (PCU2000), the transducer sensitivity is 5μV/V/mmHg. Pressure data was acquired at 500 Hz with Sonolab (Sonometrics Corporation, London, Ontario, Canada) and later processed in Matlab (The Mathworks, Natick, MA, USA).

e. Flow measuring equipment

Flow was measured with ultrasonic flow probes (Transonic, Ithaca, NY, USA). Different probe sizes have been used according to the different setups, including: 8, 10, 12, 16, 20, 24 and 28 mm. The smaller probe (8 mm) operate according to the principle of V-beam illumination, with one pair of transducers on the same side of the vessel transmitting alternately in upstream and downstream directions, while larger probes (10-28 mm) operate according to the principle of X-beam illumination, with two pairs of transducers on opposites sides of the vessel transmit alternately in upstream and downstream directions (Probe Validation), as shown in **Figure 2.6**. The probes were attached to transonic flow meters (T206 model and HT323 model). The sampling rate of Transonic flow probes, according to manufacturer instructions, ranges from 3.6 MHz (smallest probes, 8 mm) to 1.2 MHz (Largest probes, 28 mm) allowing full resolution of pulsatile flow (Frequency Response). The absolute accuracy of the flow probe is ±15% of the measurements, which could reach relative accuracy level (±2%) with calibration. The recorded flow data were filtered by the Savitzky-Golay filter written in matlab.

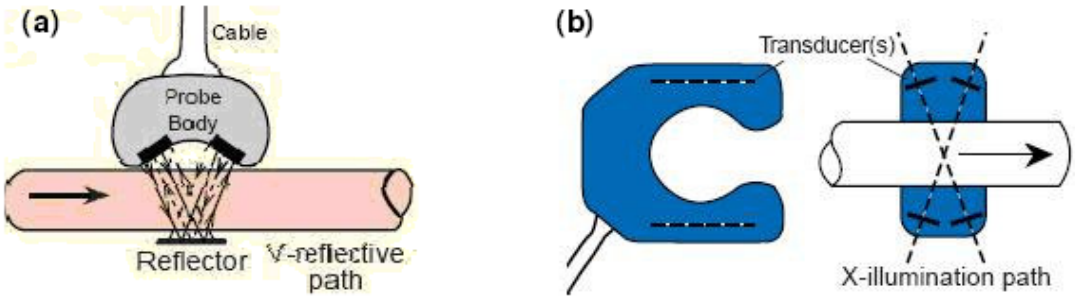

Figure 2.6: Transonic flow probes with V-shape (a) and X-shape (b) pattern of ultrasonic illumination (Taken from Probe Validation).

e. Diameter measuring equipment

Outer diameter was measured by a pair of ultrasound sonomicrometer crystals (Sonometrics, Ontario, Canada). Different sizes of crystals were used according to the different setups, including 1mm and 2 mm. The minimum value of the crystal measurement is up to 0.024 mm. The small paired sound transducer (commonly called “crystals”) made from piezo-electric ceramic material can both transmit and receive sound energy. Typically, these transducers operate at ultra-sound frequencies (1 MHz and higher). To perform a single distance measurement, one crystal will transmit a burst of ultrasound, and a second crystal will receive this ultrasound signal. A specialized digital circuitry continuously measures the distance between the transducers throughout the cycle allowing diameter changes to be measured while the wave is propagating. Data from the crystals was obtained by an external ultrasound transceiver unit which is connected with the computer, recorded using Sonolab (Sonometrics system software). **Figure 2.7** is a diagram that shows how the crystals enable the calculation of diameter changes.

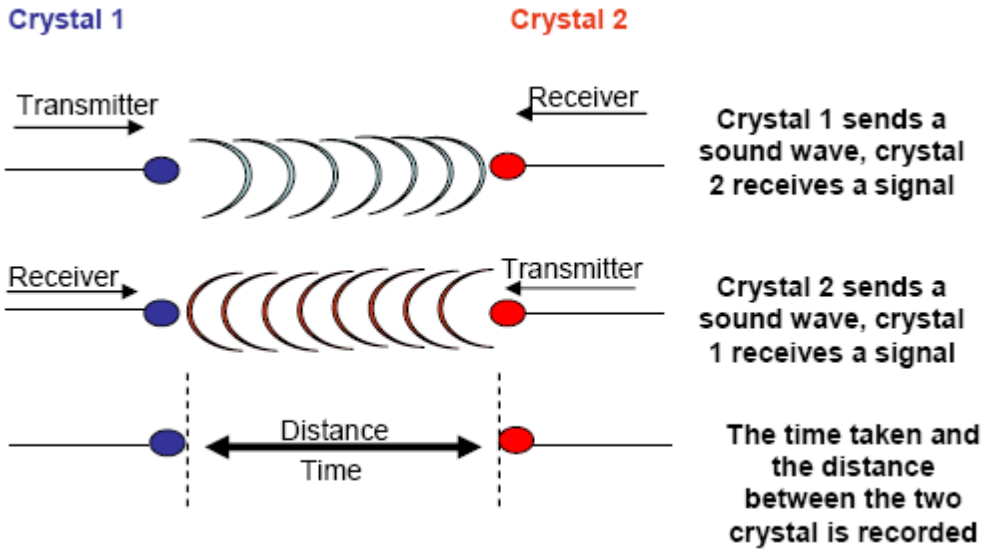

Figure 2.7: A diagram shows how the ultrasound crystals enable the calculation of diameter changes by acting as both transmitters and receivers (Taken from Page, 2009).

2.2.2 Calibrations

a. Pressure calibrations

Pressure calibrations were performed with the method of the column of water. Pressure in voltage was recorded advancing the pressure catheter in the water-column is steps of 10 cm up to a height of either 100 cm or 180 cm, depending on the range of pressures expected during the individual experiments. The pressure due to the water-column was converted into kilo Pascal. Pressure in counts and pressure in Pa were plotted and the equation of the regression line relating these values was used to convert the pressure measured in volts into kilo Pascal. Conversion lines from volts to kilo Pascal for the Millar tip catheter is shown as examples in **Figure 2.8**.

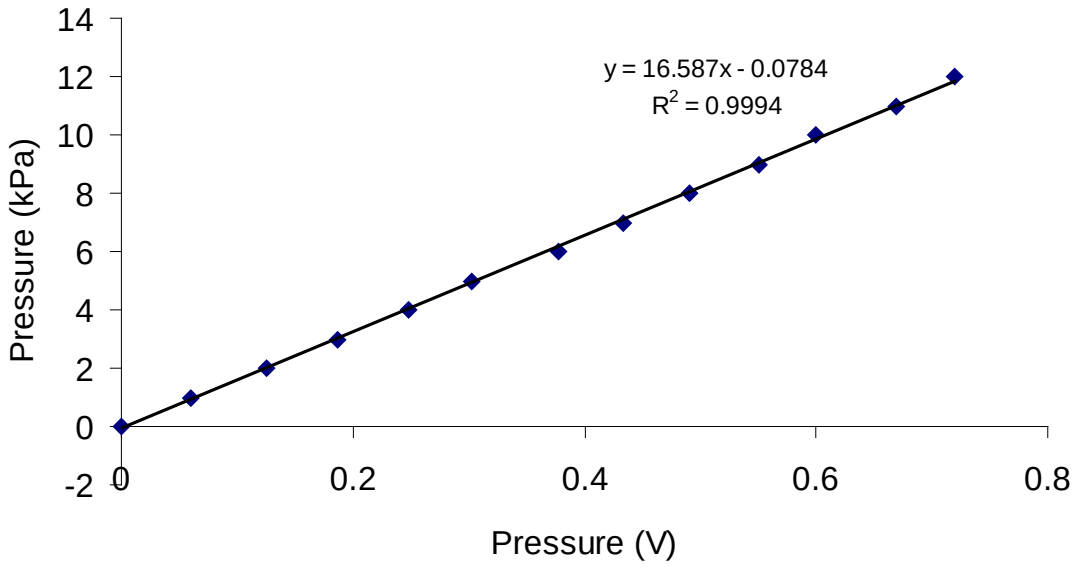

Figure 2.8: Calibration for pressure using water-column method. The equation of regression line is used to conversion the pressure into kilo Pascal.

b. Flow calibrations

Transonic flow probes are pre-calibrated by the manufacturer and conversion values are provided to different probe sizes. Probes with diameter > 6 mm are calibrated in latex. Since the experimental setups in this thesis involve tubing of different materials (latex, silicone and rubber), manufacturer calibration values were used only in the case of measurements in latex tubes, but calibrations were repeated for probes of different sizes in silicone and rubber tubes.

For the calibration procedure, a continuous flow pump was used to generate flow. Once constant flow in the system was ensured, flow was regulated by means of a tap valve in order to generate different flow-rates. Flow was measured with the probes of interest fitted around the tube, which was merged in a water tank. At the same time, output flow was also collected for 30 seconds with a measuring cylinder.

Measured flow in l/min was plotted versus flow in volts measured by the flow probe being calibrated and conversion lines were thus obtained. Examples of conversion lines from volts to l/min for different probe sizes (8 mm, 10 mm, 12 mm, and 24 mm) are shown in **Figure 2.9**.

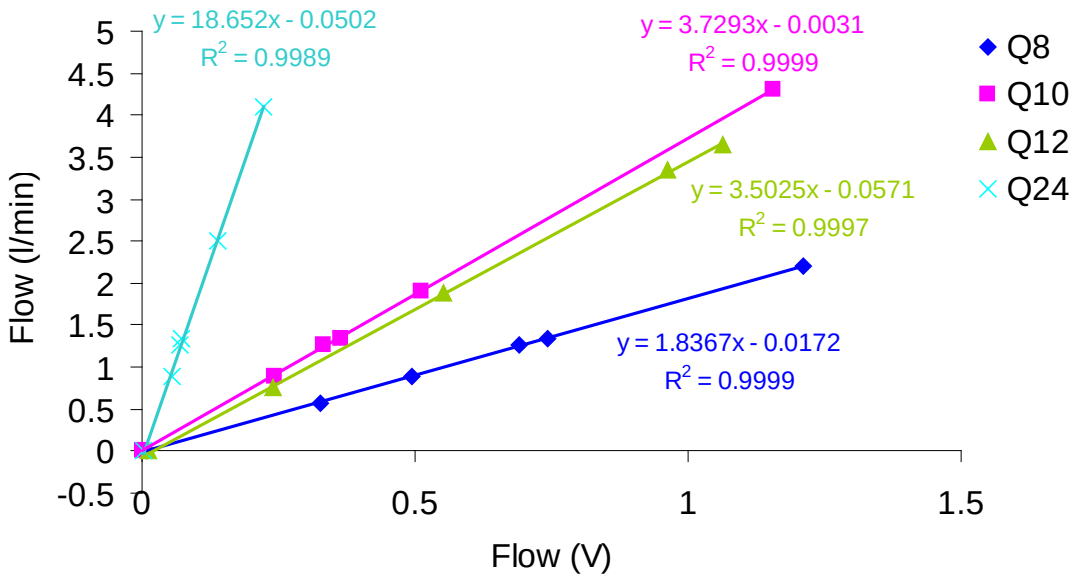

Figure 2.9: Conversion lines for flow measured by different flow probes: 8 mm (Q8), 10 mm (Q10), 12 mm (Q12) and 24 mm (Q24).

c. Crystal calibration

The crystal calibrations were carried out to obtain the accuracy of the measurement of diameter changes. During the calibration, one of the crystals was fixed on a fixed scale on the ruler (0-150 mm, accuracy: ±1 mm); the other crystal was moving from 5 mm away from the first crystal to further, the distance moving in each step is 5 mm. The performances were carried out under water, and each measurement was recorded for 10 seconds. **Figure 2.10** shows the distance measured by the crystals versus distance measured by ruler.

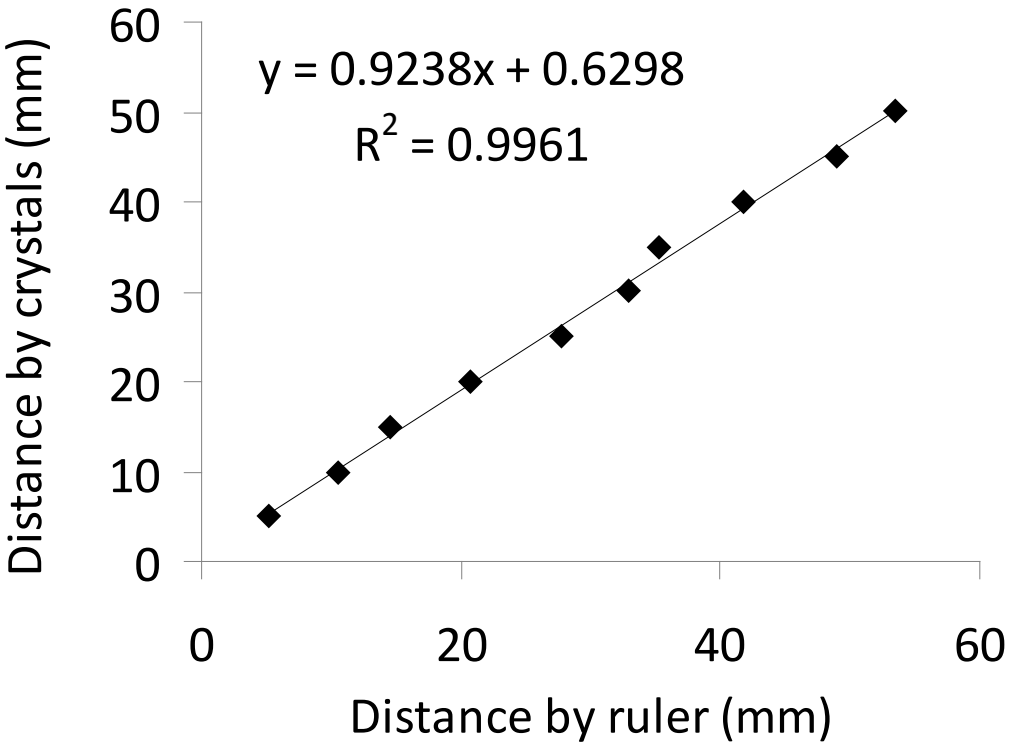

Figure 2.10: Calibration for diameter change. The regression line is used to convert the distance measured by crystals to real distance.

2.2.3 Mechanical test

The mechanical properties of tube wall and animal aorta wall (Young's modulus) were determined from the mechanical test (tensile test) after the wave propagation measurements finished.

The tensile test was performed on an Instron tensile test machine (model 5542, Norwood, MA, USA) for two types: longitude test (tube) and radial test (biological tissues).

The Instron tensile test machine (model 5542) is a single column, table-top load frames, designed for relatively low-force laboratory and quality control testing application (**Figure 2.11**). It could test the tension, compression and reverse stress, is also capable of limited cyclic testing. The limit of load cell of the machine is 100 N, the speed of the test is 0.05-1000 mm/min.

(a) (b) (c)

Figure 2.11: (a) Instron tensile test machine, (b) Grips for long sample test, (c) Grips for ring sample test.

2.2.4 Reproducibility

In order to ensure the reproducibility of the data, pressure measurements at sites of 0.3 m away from the inlet of the tube were repeated 10 times, shown in **Figure 2.12**. These ten recordings were compared and it was shown that the data is highly reproducible.

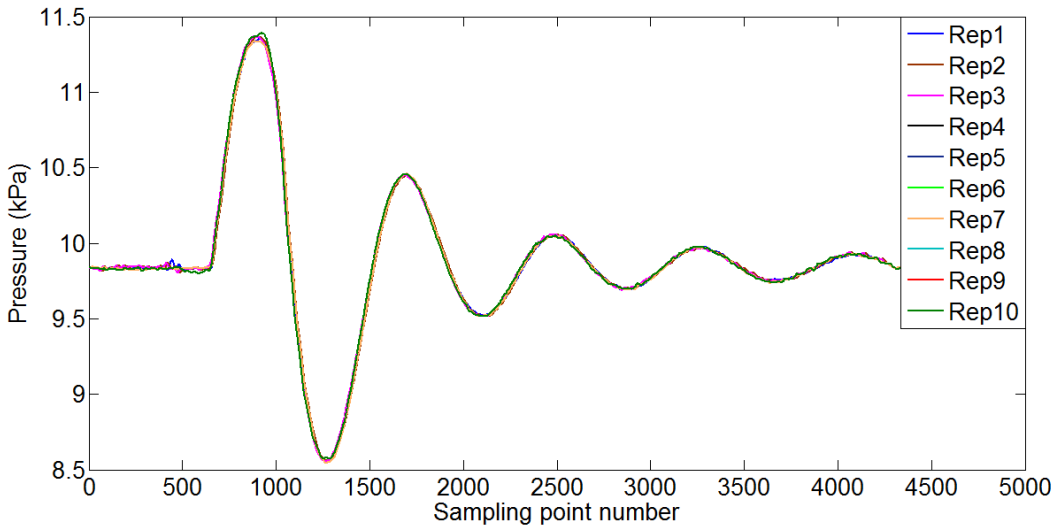

Figure 2.12: Comparison of ten repeated measurements of the pressure at 30 cm away from the inlet. The waveforms superimpose one another, giving confidence of the reproducibility of the piston pump.

Chapter 3
Experimental Comparison of Methods for the Determination of Wave Speed*

3.1 Introduction

Wave speed is the speed by which disturbance travels along the medium, and it is well accepted as one of the key parameters describing wave propagation in arteries (Nichols and O'Rourke, 2005). Wave speed depends chiefly upon the local properties of the arterial wall (Bergel, 1961a) and widely used clinically to determine arterial stiffness (Asmar et al., 1995). Further, wave speed increases with aging (Avolio et al., 1983) and has been associated with cardiovascular diseases such as atherosclerosis and arteriosclerosis (Blacher et al., 1999a).

Several methods have been proposed to estimate wave speed. The most widely used technique for measuring wave speed is the foot-to-foot method, which depends upon the transit time of the pressure wave and the distance between two sites of pressure measurement (Latham et al., 1985). By the nature of this method, it provides an average estimation of wave speed over a length of the segment.

---

* Partly published in: **Li Y, Khir AW**. Experimental validation of non-invasive and fluid density independent methods for the determination of local wave speed and arrival time of reflected wave, *Journal of Biomechanics* 44(7): 1393-1399. 2011.

Westerhof et al. (1972) suggested that the ratio of magnitudes of pressure to flow velocity, the characteristic impedance, can be used to determine wave speed. They argued that for the higher harmonics the effect of reflected sinusoidal wave-trains will be negligible, and the characteristic impedance indicates wave speed. This was later validated experimentally by Newman (Newman et al., 1986). Khir et al. (2001a) introduced the PU-loop method, which used the water hammer equation to calculate the local wave speed. The technique suggested that in the absence of reflections the relationship between pressure and velocity should be linear and the slope of the initial linear portion of the loop is related to wave speed. To deal with reflections, Davies et al. (2006a) introduced the sum of the squares technique for determining wave speed in shorter arterial segments. The application of the above methods requires simultaneous measurements of pressure and velocity at the same site. This requirement may not be practical in the clinical setting, due to the invasive nature of collecting reliable pressure measurements.

The arrival time of reflected wave to the ascending aorta is another parameter that is of clinical and physiological importance. The timing and amplitude of reflected waves may influence cardiac function (Kirkpatrick et al., 1991). Several methods have been proposed for the determination of the arrival time of reflected wave. Murgo et al. (1980) suggested that time of the infection point on the upstroke of the pressure waveform represented the arrival time of reflected wave. Parker and Jones (1990) introduced Wave Intensity Analysis (WIA), which is a time domain technique, considers changes in pressure and velocity at any points to be the result of interaction between forward and backward travelling waves carrying energy. WIA thus can be used for the determination of the arrival time of reflected wave.

Feng and Khir (2010) have developed novel techniques using the non-invasive measurements of velocity and the vessel diameter for the determination of wave speed and the arrival time of reflected wave. The authors demonstrated that the relationship between *ln*D and U is linear in the absence of reflections and the slope of the *ln*DU-loop is linear in the early part of the cycle when only forward waves are present. It is worth noting that this method is independent of the fluid density. Using diameter, velocity and wave speed, the authors also introduced a technique for the separation of the forward and backward diameter, velocity

waveforms and non-invasive wave intensities, which can also be used to estimate the arrival time of reflected wave.

Given the variety of different methods and the lack of comparisons between them, the aim of this chapter is therefore to experimentally compare the relative accuracy of the foot-to-foot, PU-loop and *ln*DU-loop methods for measuring wave speed, compare the *ln*DU-loop and non-invasive wave intensity methods for estimating the arrival time of reflected wave in flexible tubes as compared with the PU-loop and wave intensity methods.

*ln*DU-loop is a relatively new technique used to determine wave speed. Due to no density term exist in the equation of *ln*DU-loop to determine wave speed, it is necessary to test the sensitivity of *ln*DU-loop to the fluid density for determining wave speed; the effect of speed of piston pumping on *ln*DU-loop of determination of wave speed will also be investigated. A discussion of these parameters on the wave propagation will be presented at the end of this chapter.

3.2 Materials and Methods

In this chapter, C determined using the foot-to-foot method is referred as ($C_{foot\text{-}to\text{-}foot}$), that determined using the *ln*DU-loop method as (C_{DU}) and that determined using the PU-loop method as (C_{PU}). Also, it is referred that T_{rw} determined using dI_{DU} as (T_{rwDU}) and that determined using dI_{PU} as (T_{rwPU}). Further, subscripts of (+) and (-) indicate the forward and backward direction respectively. The derivation of the methods used to calculate $C_{foot\text{-}to\text{-}foot}$, C_{DU}, C_{PU}, T_{rwDU} and T_{rwPU} have been described in chapter 2, Section 2.1.4 - 2.1.7, but the equations used by each method are compared in **Table 3.1**.

Table 3.1 The expressions of P, U and D, U based techniques for the determination of wave speed (C), the separation of waves and wave intensity.

	P, U based equations	D, U based equations
Wave speed	$c = \pm\frac{1}{\rho}\frac{dP_{\pm}}{dU_{\pm}}$	$c = \pm\frac{1}{2}\frac{dU_{\pm}}{d\ln D_{\pm}}$
Forward and backward changes in P and D Forward and backward P and D waveforms	$dP_{\pm} = \pm\frac{1}{2}(dP \pm \rho c dU)$ $P_{\pm} = \sum_{t=0}^{t} dP_{\pm} + P_0$	$dD_{\pm} = \pm\frac{1}{2}(d\ln D \pm \frac{1}{2c}dU)$ $D_{\pm} = \sum_{t=0}^{t} dD_{\pm} + D_0$
Forward and backward changes in U Forward and backward U waveforms	$dU_{\pm} = \pm\frac{1}{2}(\frac{dP}{\rho c} \pm dU)$ $U_{\pm} = \sum_{t=0}^{t} dU_{\pm}$	$dU_{\pm} = \pm\frac{1}{2}(dU \pm 2cd\ln D)$ $U_{\pm} = \sum_{t=0}^{t} dU_{\pm}$
Forward and backward Wave Intensity	$dI_{PU\pm} = \pm\frac{1}{4\rho c}(dP \pm \rho c dU)^2$	$dI_{DU\pm} = \pm\frac{c}{2}(d\ln D \pm \frac{1}{2c}dU)^2$

Determination of wave speed using foot-to-foot method

Foot-to-foot method involves the simultaneous measurement of either pressure or velocity at two sites at a known distance apart (L) and determining the time delay between the two measurements (Δt), so the wave speed

$$c = \frac{L}{\Delta t} \tag{3.1}$$

To calculate the wave speed by the foot-to-foot method, the identification of the foot of the wave is very important. 'Tangent Intersection' method (Latham, 1988) is always used to determine the start of the pressure pulse. Due to the lack of the ECG signal, in this study, the foot of the pressure pulse is determined as the start point of the sharp upstroke of the pressure pulse by eye.

3.2.1 Experimental setup

The general experimental setup (**Figure 2.4)** introduced in Chapter 2 is used for this work.

Tubes: Flexible tubes of different materials and sizes were used in this study, dimensions are given in **Table 3.2**. The mechanical properties of each tube were uniform along its 1m length. The tubes were fully immersed in a tank and all experiments were carried out in the horizontal position.

Fluids: Experiments were carried out for three fluids with different densities, water (1000 kg/m^3), 50% and 75% glycerin-water solution (1126.3 kg/m^3 and 1194.9 kg/m^3).

Measurements: Simultaneous waveforms of pressure (P), outer diameter (D_0) and flow (Q), from which D and U were determined, were measured sequentially at three different sites, 25cm, 50cm and 75cm away from the inlet of each tube. One pressure catheter was placed at the end of the tube in order to measure the pressure waveform allowing to calculate the wave speed by the foot-to-foot method. P and Q were measured using 6F tipped catheter pressure transducer (Millar Instruments, Texas, USA) and ultrasonic flow probe (Transonic System, Inc, NY, USA), respectively. D_o was measured using paired ultrasonic crystals (Sonometrics Corporation, Ontario, Canada). All data were sampled at 500Hz using Sonolab (Sonometrics Corporation) and analysed using Matlab (The Mathworks, MA, USA).

The measurements of wall thickness were carried out with digital calliper

(manufacturer: toolzone, range: 0-150 mm, accuracy: ±0.02 mm. The tubes used in this work are flexible tubes, and thus would be compressed by the claws of the calliper and result in an underestimation of the wall thickness of the tubes. The improved way used in this work to measure the wall thickness of soft materials is therefore to put the soft material between two pieces of hard materials, measure the distances between the outer layer of the two hard pieces at several locations, minus the thickness of the two hard pieces, the wall thickness of the soft material will be obtained.

Table 3.2 Materials and dimensions of the tubes used in the experiments. Also shown are the average wave speeds measured in each tube with water (ρ = 1000 kg/m^3).

Material	Internal diameter (D_{in}) (mm)	Wall thickness (h) (mm)	C_{DU} m/s	C_{PU} m/s	$C_{foot\text{-}to\text{-}foot}$ m/s
Silicone	8	1	22.3±1.5	22.0±1.0	22.4±0.6
		2	26.7±2.8	28.7±2.0	29.8±1.2
		3	33.5±3.3	32.0±3.0	35.1±1.4
	10	1	20.0±5.3	20.2±4.9	20.8±0.6
		2	25.3±1.5	24.3±1.2	26.0±0.9
		3	29.9±3.3	30.2±3.5	30.2±0.3
	16	2.4	22.4±2.8	21.9±3.0	22.3±1.1
		3	25.1±4.5	23.1±3.2	23.3±0.5
Rubber	16.7	1.5	23.9±5.0	24.2±4.0	24.3±0.3
	20.6	1.5	20.7±6.2	20.9±6.1	20.7±0.4
Latex	8.5	0.1	5.2±0.5	5.4±0.8	6.0±0.4
	24.2	0.27	3.1±0.9	2.9±0.8	3.1±0.3
	32.3	0.27	2.6±0.7	2.6±0.7	2.7±0.2

3.2.2 Analysis

Because tubes used in this work were with a range of diameter (D) and wall thickness (h), a normalization parameter, h/D was used, to compare C_{DU} in different tubes. Trw was determined as the sampling point indicating time of the onset of the backward pressure (P_-), velocity (U_-), diameter (D_-), and backward intensities dI_{PU-} or dI_{DU-}. Regression and paired t-test analyses were performed to identify the correlation between C_{PU} and C_{DU}, and between Trw_{DU} and Trw_{PU} to indicate the relative accuracy of the new compared to the established techniques. Data are presented as mean±SD and values of $p<0.05$ were considered significant. The Bland-Altman technique (Bland and Altman, 1986) was also used to establish the agreement between P, U and D, U based techniques, and the acceptable range for the mean difference was taken as ±2SD.

3.3 Results

3.3.1 Local wave speed

Figure 3.1 shows P, U and D waveforms and the corresponding PU-loop and *ln*DU-loop measured at 50 cm away from the inlet of a rubber tube. The initial portion of the *ln*DU-loop is clearly linear and the slope corresponds to C_{DU} of 24.13 m/s. C_{PU} measured at the same site is 24.58 m/s, and the difference between the results of both methods is 0.45 m/s (~ 2%), which is very small considering the level of experimental noise .

The regression line and Student's t-test show that values of C_{DU} and C_{PU} in all of the tubes, locations and fluid densities highly correlated (R^2=0.99, $p< 0.005$), **Figure 3.2a**.

The agreement of wave speed determined by the *ln*DU-loop and PU-loop methods is also assessed using Bland-Altman method. The results show that mean of difference between these two methods is 0.28 m/s, which indicated that wave speed determined by PU-loop is slightly above that determined by *ln*DU-loop. The difference between C_{DU} and C_{PU} is within the acceptable range of mean±2SD (0.28±2.04 m/s), **Figure 3.2b**.

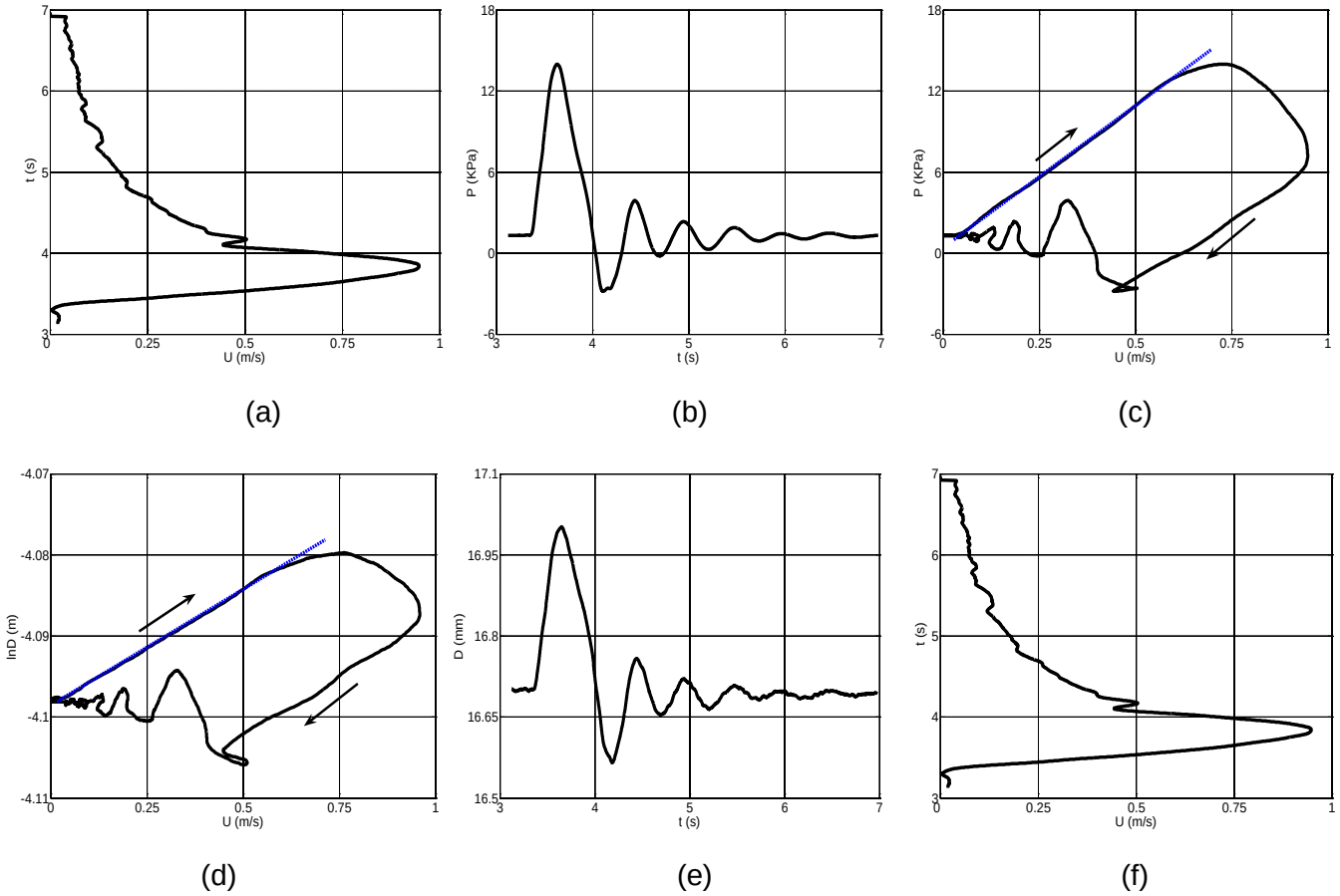

Figure 3.1: The pressure (b), diameter (e) and velocity (a, f) waveforms measured at 50 cm away from the inlet of 1m length rubber tube. Tube size is 16.7 mm in diameter (unloaded) and 1.5 mm in wall thickness. The PU-loop is shown in (c) and *ln*DU-loop is shown in (d) indicating wave speed of 24.58 m/s and 24.13m/s respectively. The dashed line indicates the initial linear portion of the each loop, and the arrows show the direction of the loop.

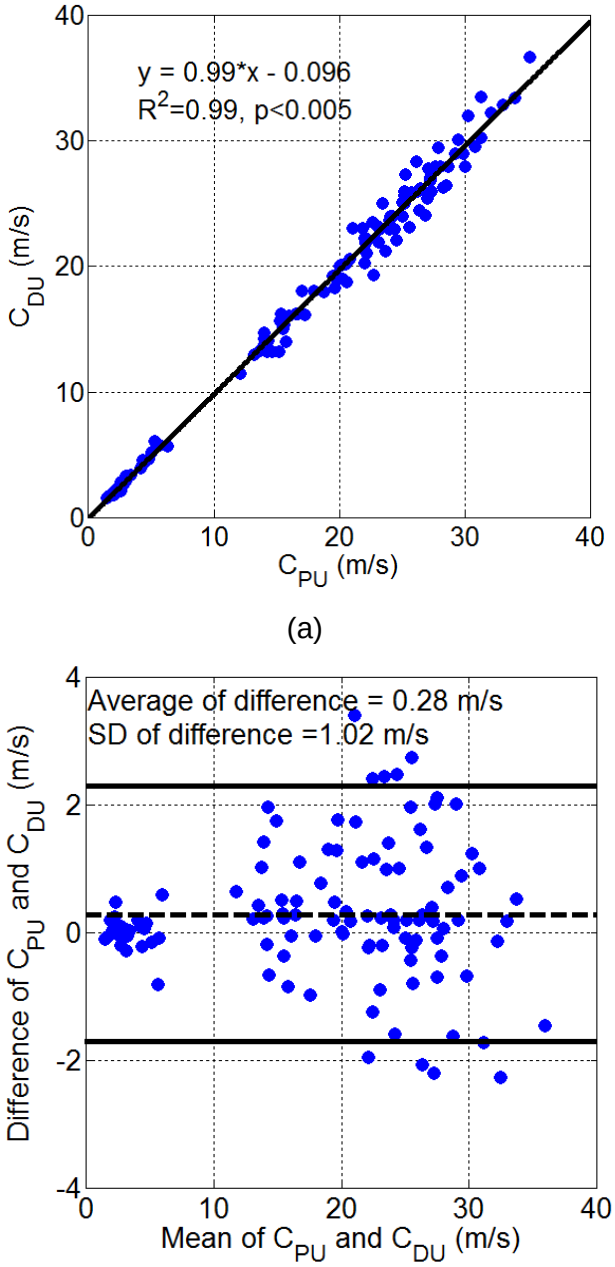

Figure 3.2: (a) Correlation of wave speed determined by *ln*DU-loop and PU-loop. The correlation coefficient R^2=0.99, p<0.005. (b) The agreement between wave speed determined by the *ln*DU-loop and PU-loop is assessed by Bland-Altman method. The middle horizontal line (dashed) indicates the mean of difference of wave speed determined by the two methods. The upper and lower horizontal lines (solid) indicate twice the standard deviation (2SD). Note that most of the data points fell within ±2SD range, and the zero line fell within the acceptable confidence limits of the average, indicating no statistically significant difference between C_{DU} and C_{PU}.

3.3.2 Regional wave speed

Figure 3.3 shows the results of wave speed determined by foot-to-foot methods with different fluids in flexible tubes.

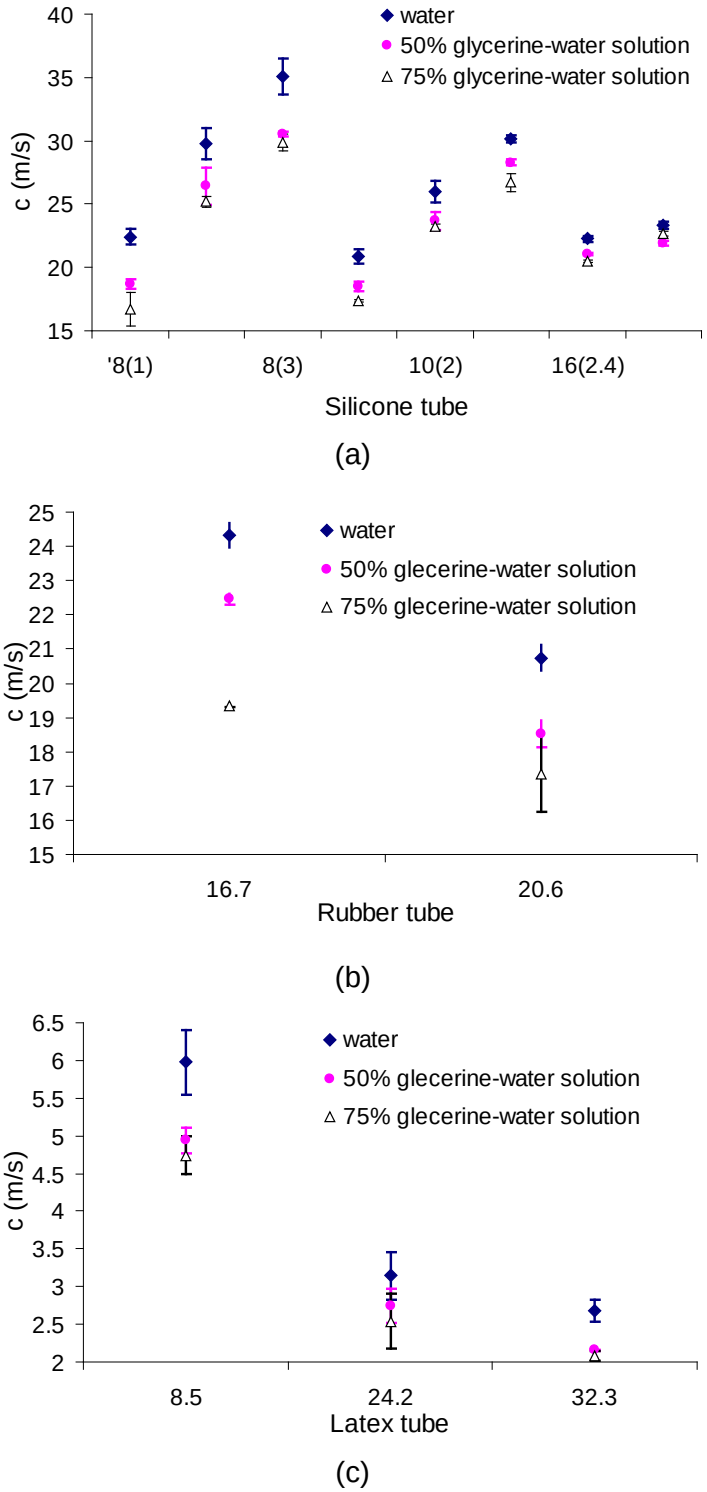

Figure 3.3: Wave speeds determined by foot-to-foot method with different fluids in silicone (a), rubber (b) and latex (c) tubes. The data points and the error bars show the mean±SD.

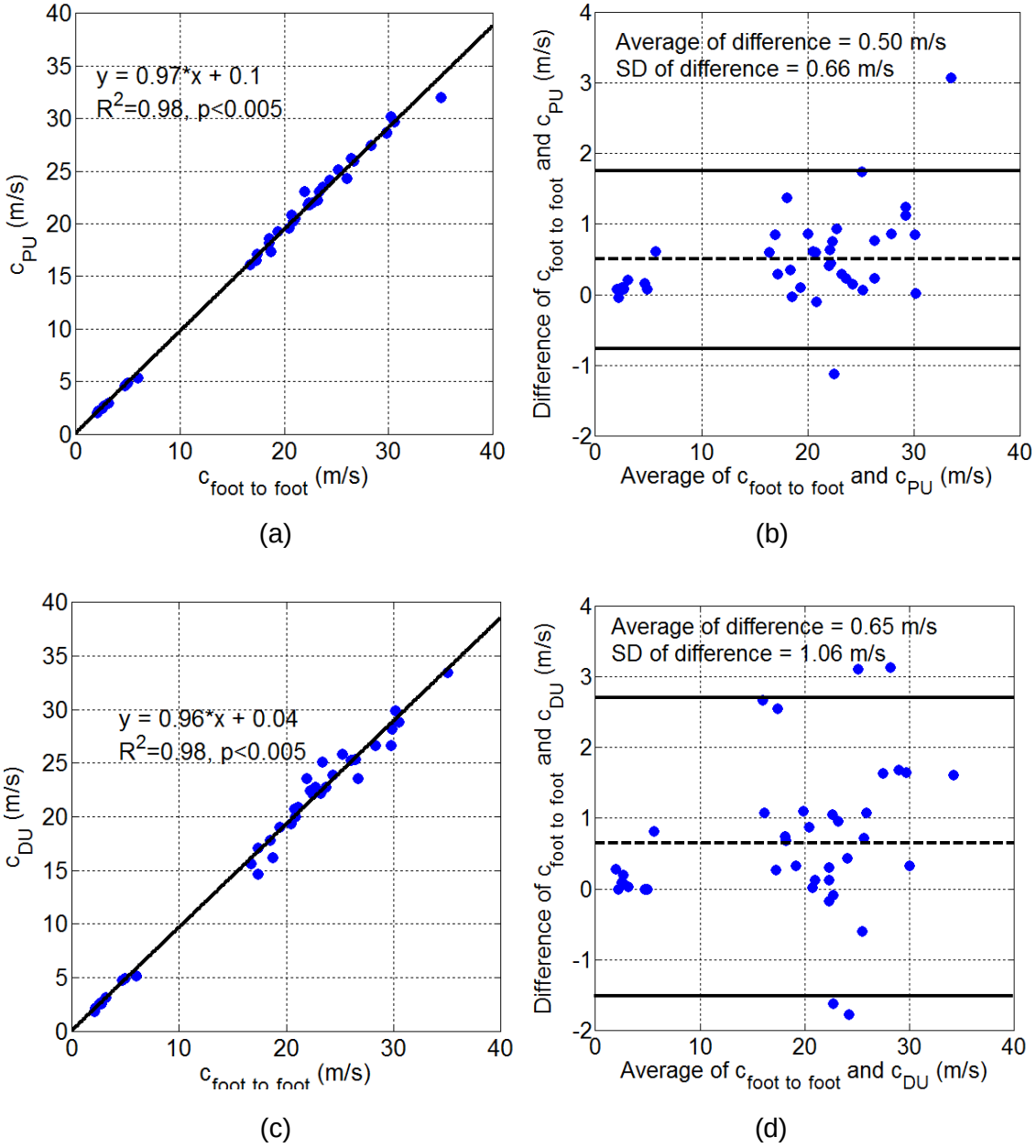

Figure 3.4: Correlation of $C_{foot\text{-}to\text{-}foot}$ with C_{PU} (a), and $C_{foot\text{-}to\text{-}foot}$ with C_{DU} (c). (b): The agreements between $C_{foot\text{-}to\text{-}foot}$ and C_{PU} (b), $C_{foot\text{-}to\text{-}foot}$ and C_{DU} (d) are assessed by Bland-Altman method. The middle horizontal line (dashed) indicates the mean of difference. The upper and lower horizontal lines (solid) indicate twice the standard deviation (2SD). Note that most of the data points fell within ±2SD range, and the zero line fell within the acceptable confidence limits of the average, indicating no statistically significant difference between different methods.

In order to compare the $C_{foot\text{-}to\text{-}foot}$ with C_{DU} and C_{PU}, mean values of C_{DU} and C_{PU} calculated as average value of measurements along each tube. The regression lines and Student's t-test show that mean values of $C_{foot\text{-}to\text{-}foot}$ and C_{PU}, $C_{foot\text{-}to\text{-}foot}$ and C_{DU} in all of the tubes, locations and fluid densities highly correlated (R^2=0.98, p<0.005), **Figure 3.4a, c**.

The agreement of wave speed determined by the foot-to-foot, *ln*DU-loop and PU-loop methods are also assessed using Bland-Altman method. The results show that mean of difference between foot-to-foot and PU-loop methods is 0.50 m/s, which indicated that wave speeds determined by PU-loop are slightly smaller than those determined by foot-to-foot method. The results show that mean of difference between foot-to-foot and *ln*DU-loop methods is 0.65 m/s, which indicated that wave speed determined by lnDU-loop is smaller than that determined by foot-to-foot method. The difference between $C_{foot\text{-}to\text{-}foot}$ and C_{PU}, $C_{foot\text{-}to\text{-}foot}$ and C_{PU} are within the acceptable range of mean±2SD, **Figure 3.4b, d**.

3.3.3 The effect of fluid density on wave speed

The main purpose of this section is to investigate the effect of varying fluid densities on the determination of wave speed by *ln*DU-loop. In this study, water, 50% and 75% glycerine-water solution were used in volume to change the fluid density from 1000 kg/m^3 to 1126.3 kg/m^3 and 1194.9 kg/m^3. Wave speed in all flexible tubes with these three types of fluid will be compared.

Wave speed in water is the biggest, followed by the wave speed in 50% glycerine-water solution, and wave speed in 75% glycerine-water solution is the smallest; this order is consistent in all sized tubes. For example, in the 16.7 mm diameter, 1.5mm wall thickness rubber tube, we measured C_{DU} using 75% and 50% glycerin-water solution of 21.88m/s and 22.59 m/s, which shows 9.3% and 6.4% reduction of wave speed as compared with that measured in water, 24.13 m/s (**Figure 3.5**). Fluid densities of 75% (ρ=1194.9 kg/m^3) and 50% (ρ=1126.3 kg/m^3) of glycerine-water solution are approximately 19.5% and 12.6% respectively greater than that of water (ρ=1000 kg/m^3). It is expected that wave speed in 75% and 50% glycerine-water solution to be 8.5% and 6% respectively smaller than that of water. The small differences between the theoretical and experimental results are acceptable within the experimental noise.

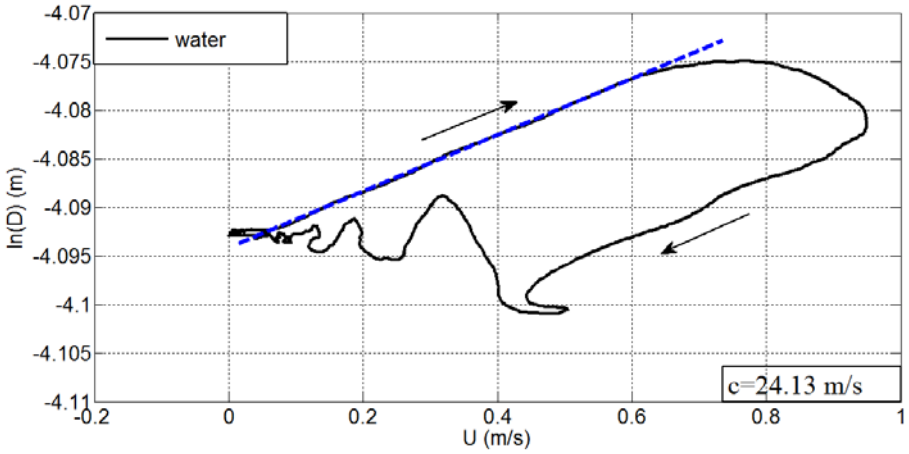

(a)

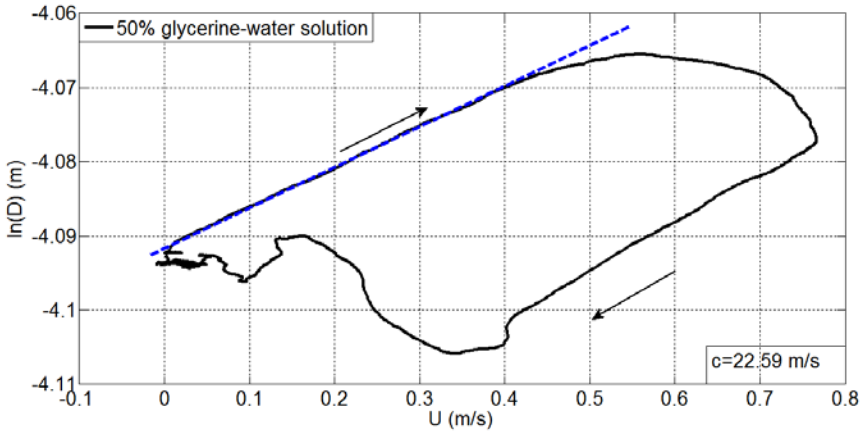

(b)

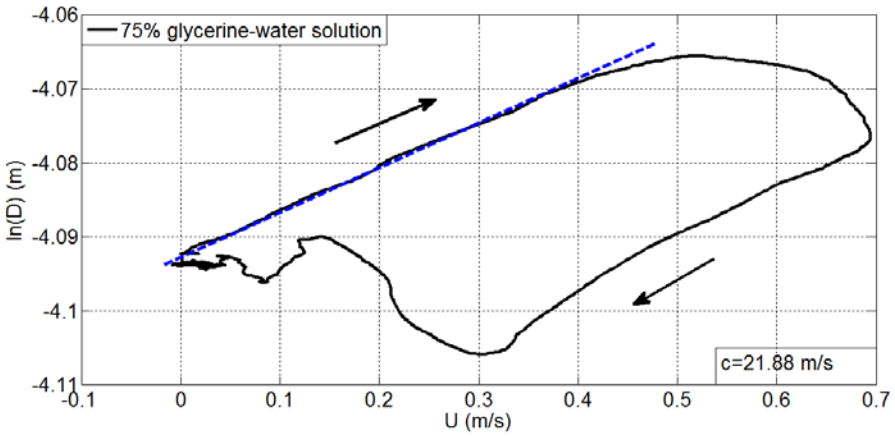

(c)

Figure 3.5: At 50 cm away from inlet of the 16.7 mm diameter rubber tube, wave speed was determined by *ln*DU-loop in water (a), 50% glycerine-water solution (b) and 75% glycerine-water solution (c). All the dash lines indicate the linear relationship between velocity and the natural logarithm of diameter at the early part of the pulse. Arrows indicate the direction of the loops.

The effect of the fluid density on wave speed determined by *ln*DU-loop is also plotted in **Figure 3.6**. From the Moens-Korteweg equation, equation (1.2), it is known that wave speed is related to the properties of the vessel. In order to show the direct relation between wave speed and properties of vessel, the figure is plotted as wave speed against square root of h/D, and the relation between them is linear, shown in the figure; if plot wave speed against h/D, the relation would be logarithmic. From this figure, it is found out that C_{DU} is slower with increased fluid density independently from h/D, for the same material tube, wave speed is different only when the ratio of thickness over internal diameter is not the same.

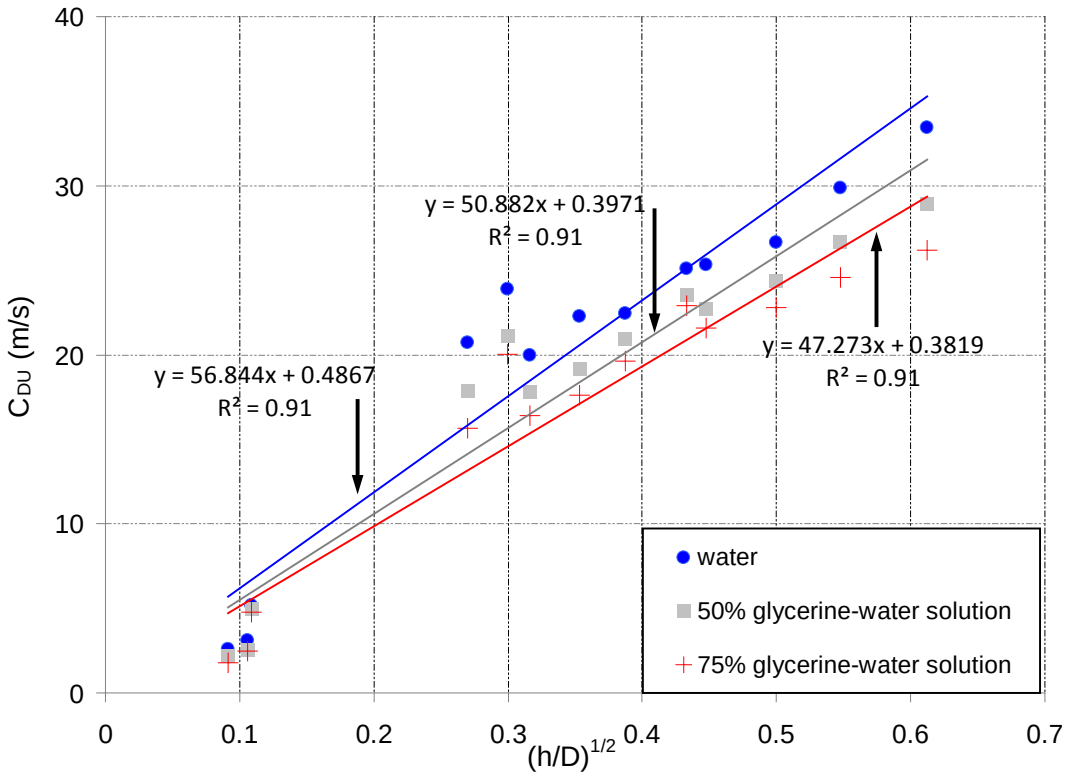

Figure 3.6: Average wave speed for each tube determined using the *ln*DU-loop method (C_{DU}) is plotted against the square root of the normalisation ratio of wall thickness to diameter (h/D). Although the method is independent of fluid density, C_{DU} changes as expected; increases with increased h/D and also with decreased fluid density for each tube.

3.3.4 The effect of pumping frequency on wave speed

The effect of pumping speed of piston on wave speed determined by *In*DU-loop was also investigated. This experiment aims to simulate the effect of increased heart rate on wave speed. The varied pumping speed of piston was controlled by varying the voltage of power driving the DC motor, with a range of 5.5 V to 8 V. The corresponding range of piston speed was approximately 2.2 cm/s to 4 cm/s, respectively (piston speed was calculated as pulse length divide the stroke of the piston). The duration of pulse corresponding to the piston speed was 0.5 s to 0.91 s, which represent the normal human heart rate 60-100 bpm (Healthy heart rate).

In this study of the effect of pumping speed on wave speed on every tube, one silicone tube (10 mm diameter, 1 mm wall thickness), one rubber tube (20.6 mm diameter, 1.5 mm wall thickness) and one latex tube (24.2 mm diameter, 0.27 mm wall thickness) were chosen to represent all the tubes used in the experiment.

With the unchanged experimental conditions, the greater diameter and velocity pulse occurs when the pumping speed of piston is faster. For example, at 50 cm away from inlet in 10 mm diameter, 1 mm wall thickness silicone tube the amplitude of the diameter when the pumping speed is 4 cm/s (voltage of power is set as 8 V) is approximately 15.4% greater than that when the pumping speed is 2.2 cm/s (voltage of power is set as 5.5 V), **Figure 3.7a**. Meanwhile, the amplitude of the velocity when the pumping speed is 4 cm/s (voltage of power is set as 8 V) is approximately 18.2% greater than that when the pumping speed is 2.2 cm/s (voltage of power is set as 5.5 V), **Figure 3.7b**.

The wave speeds determined at 5.5 V and 8 V are very similar, see **Table 3.3**. This means that wave speed is not affected by the pumping speed of the piston, we plotted wave speed determined at 8 V against wave speed determined at 5.5 V, **Figure 3.8**, the regression line also show that wave speeds are very similar for at 5.5 V and 8 V.

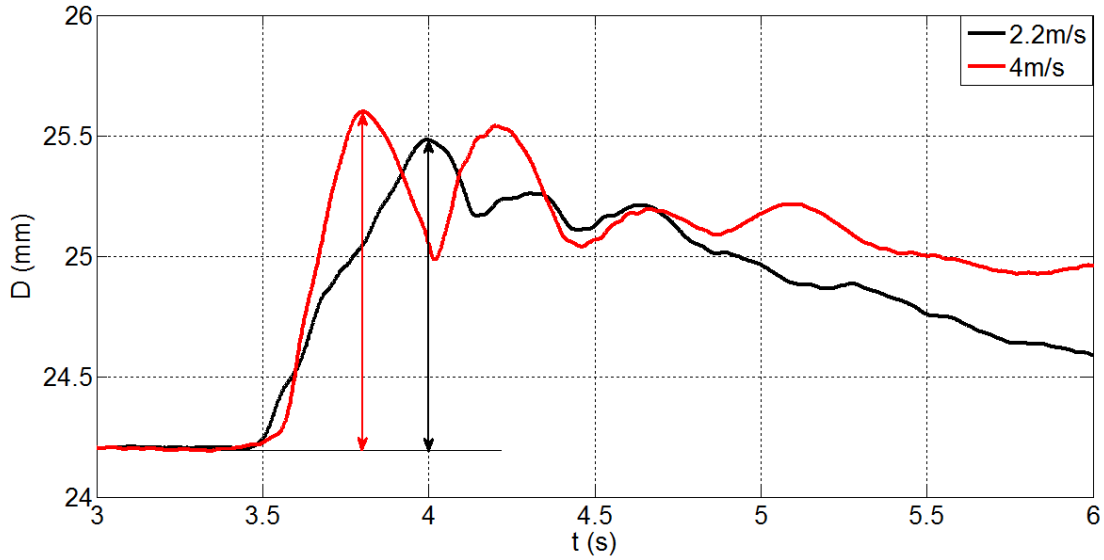

(a)

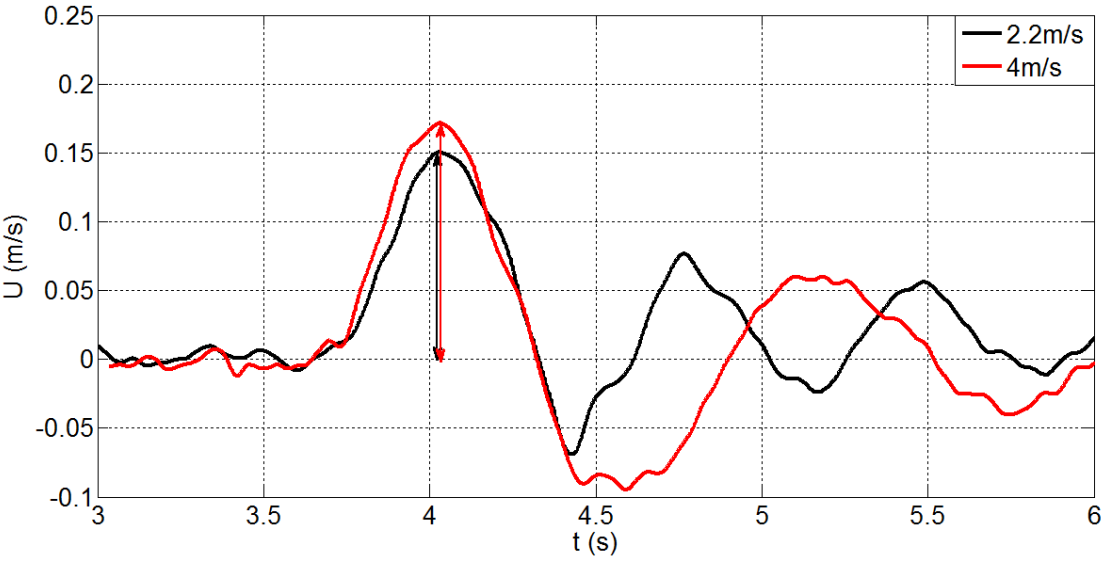

(b)

Figure 3.7: The diameter (a) and velocity (b) waveforms at 50 cm away from inlet of a 24.2 mm diameter, 0.27 mm wall thickness latex tube. The diameter and velocity were generated when the pumping speed of piston is 2.2 m/s and 4 m/s (voltage at 5.5 V and 8 V), respectively. The bigger amplitude of pulse occurs when the piston is going fast, compared to that when the piston is going slow.

Table 3.3 Wave speed determined by *In*DU-loop when the voltage is 5.5 V and 8 V respectively. D_{in} is the internal diameter, h is the wall thickness; Position is the distance the measurement was taken from the inlet; Mean* is the average wave speed along the length of the tube; Diff is the percentage of difference of wave speed determined at 5.5 V and 8 V. $Diff\,(\%) = \frac{c_{8V} - c_{5.5V}}{c_{5.5V}} \times 100\%$

Material	D_{in} (mm)	h (mm)	Position (cm)	c_{DU} (m/s)		Diff (%)
				5.5 V	8 V	
Silicone	10	1	25	19.65	20.32	3.41
			50	19.25	19.70	2.34
			75	20.99	19.68	-6.24
			Mean*	19.96	19.90	-0.30
Latex	24.2	0.27	25	2.79	2.90	3.94
			50	3.26	3.40	4.29
			75	3.28	3.11	-5.18
			Mean*	3.11	3.14	0.96
Rubber	20.6	1.5	25	18.36	18.50	0.76
			50	20.26	19.96	-1.50
			75	23.57	23.84	1.15
			Mean*	20.73	20.77	0.19

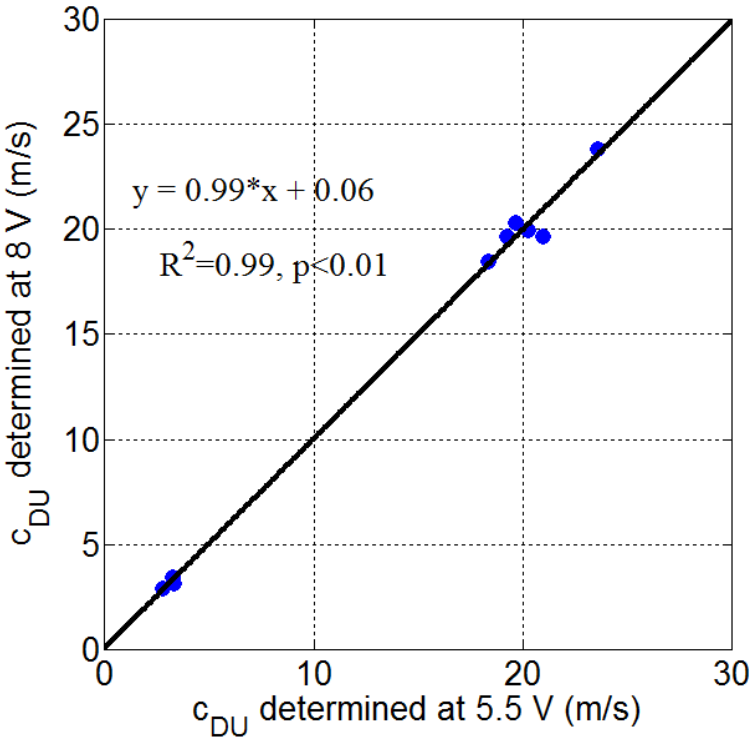

Figure 3.8: Correlation of wave speed determined at 5.5 V and at 8 V. The correlation coefficient R^2=0.99.

3.3.5 Wave Separation

The measured, forward and backward pressure waveforms (P, P_+, P_-) are very similar in shape to the corresponding (D, D_+, D_-), **Figure 3.9a**, **b**. Similarly, the shape of the forward and backward velocity (U_+, U_-) as determined by both techniques is almost identical, **Figure 3.9c**, **d**. Also the shape of dI_{PU} and dI_{DU} in the forward and backward directions is very similar, **Figure 3.9e**, **f**. All backward waveforms in **Figure 3.9**, (P_-, D_-, U_-, dI_{PU-} and dI_{DU-}) indicate the same Trw of 0.2 s.

Before the arriving of the reflected wave, the forward pressure (P_+) is expected to be superimposed to the measured pressure waveform (P), and likewise the forward diameter (D_+) is also superimposed to the measured diameter (D) only during incident wave occurring. The arrival time of reflected wave, Trw determined by the backward pressure (P_-) is very close to that determined by the backward diameter (D_-). The measured pressure and diameter increase sharply with the arrival of reflected wave (indicated with the black vertical

arrows). Similar to the forward and backward wave intensity determined by the pressure and velocity, dI_{PU}, the forward and backward diameter wave intensity determined by the diameter and velocity, dI_{DU}, also has two peaks; first one represents the compression wave and the second one represents expansion wave. Furthermore, the forward and backward velocity determined by the measured pressure and velocity are almost identical in shape to those determined by the measured diameter and velocity.

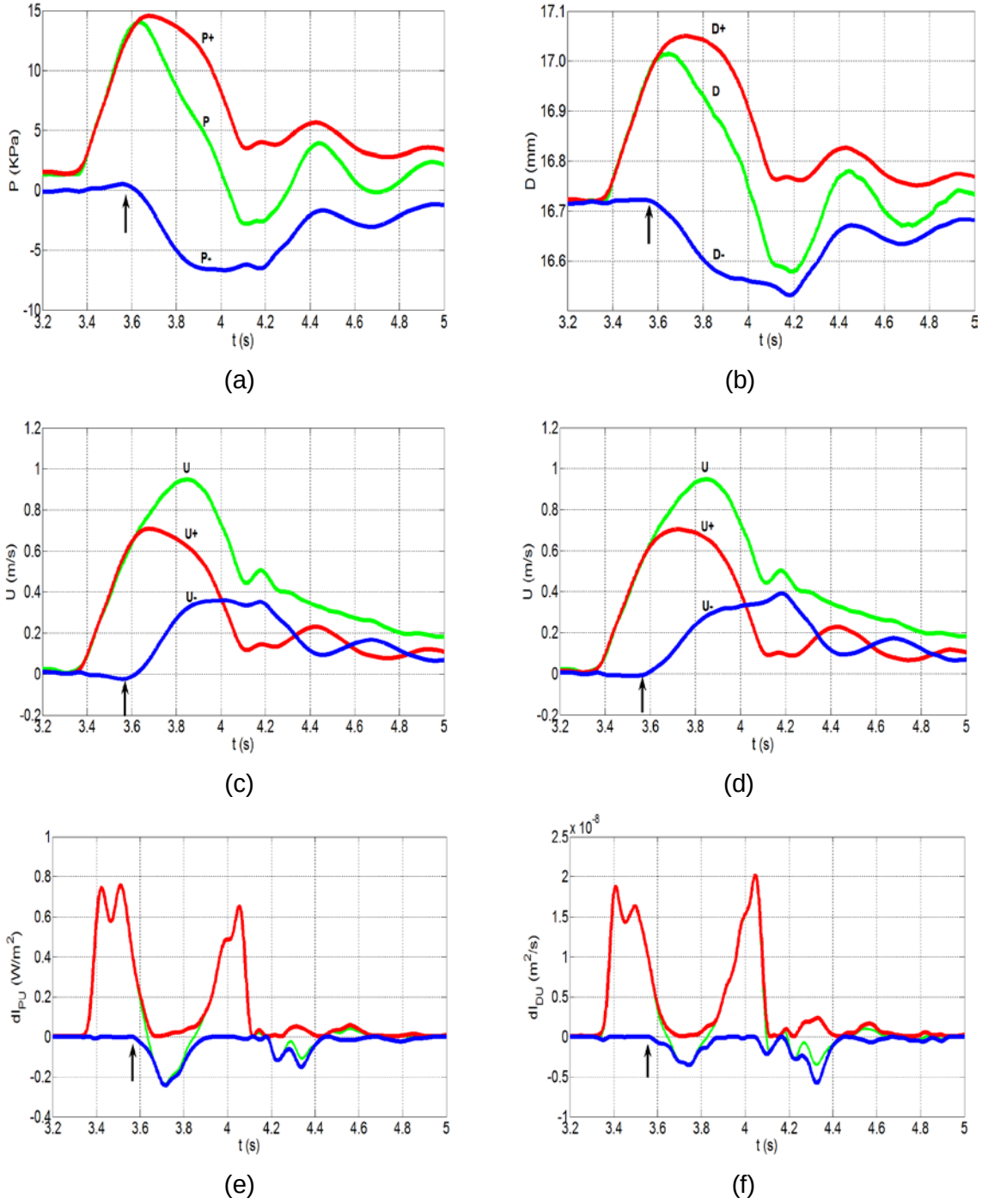

Figure 3.9: The measured, calculated forward (+) and backward (-) pressure (a), velocity (c) and wave intensity (e) using the PU equations are plotted against time. The measured, calculated forward and backward diameter (b), velocity (d) and non-invasive wave intensity (f) using the DU equations.The green lines show the measured parameters, red lines show the forward waveforms and blue lines show the backward waveforms. The arrival time of the reflected waves (Trw) detected by the onset of dI_{PU-} and ${}_{n}dI_{DU-}$ correspond to the onset of the backward pressure, diameter and velocity waves as indicated by the vertical arrows.

3.3.6 Arrival time of reflected waves

Arrival time of reflected waves could be determined by the onset of the backward wave intensity, also could be determined by the onset of the backward pressure, diameter and velocity waves. In this study, Trw is determined by the onset of the backward wave intensity dI_{PU-}, as Trw_{PU} and the backward non-invasive wave intensity ${}_{n}dI_{DU-}$, as Trw_{DU} judged by eye.

Values of Trw_{PU} and Trw_{DU} highly correlated (R^2=0.98, p<0.02) shown by the regression line (**Figure 3.10a**) and the agreement between these two methods determining Trw is assessed by Bland-Altman method. The result shows that average of difference between Trw_{PU} and Trw_{DU} is -0.001s±0.008, and the agreement limit (mean±2SD) of -0.015s to 0.013s is small and provides confidence that the two methods are in agreement without bias (**Figure 3.10b**).

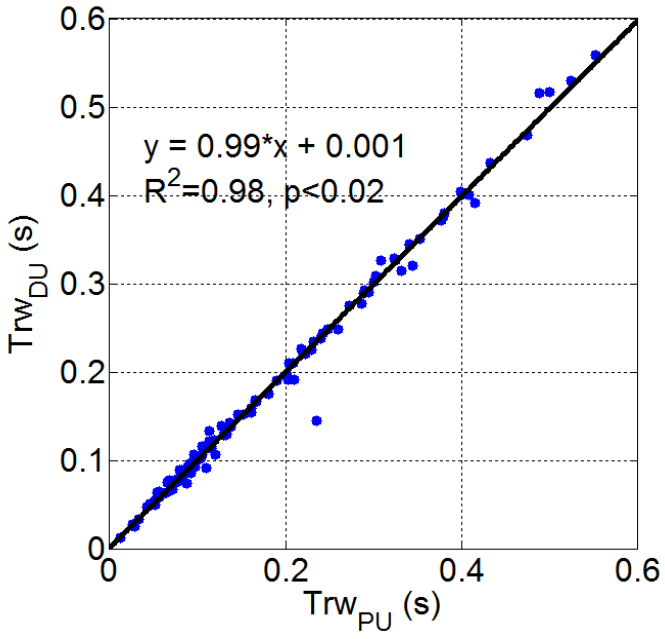

(a)

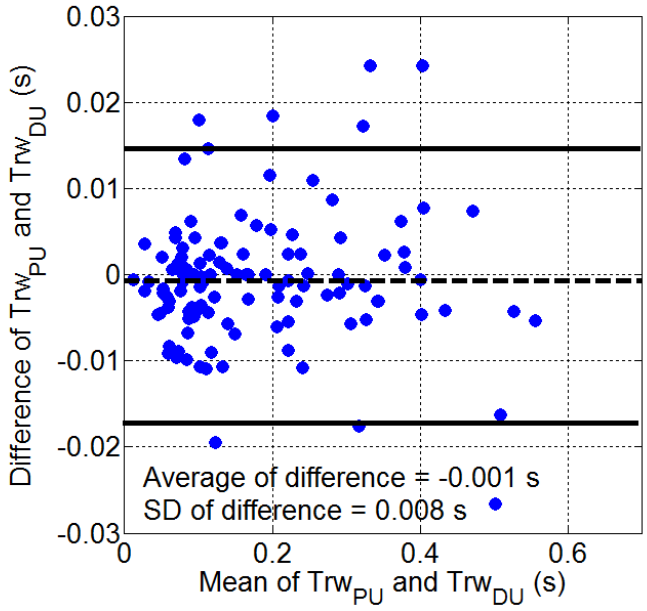

(b)

Figure 3.10: (a) Trw_{DU} and Trw_{PU} correlate well (R^2 = 0.98, p<0.02) and the trend line appears to fall on the identity line (not shown). (b) The Bland–Altman plot shows the agreement between the two results. The middle horizontal (dashed) line indicates the mean difference between the two methods. The upper and lower horizontal lines (solid) indicate twice the standard deviation (2SD) of the mean difference. Note that most of the data points fell within ±2SD range, and the zero line fell within the acceptable confidence limits of the average, indicating no statistical significant difference between Trw_{DU} and Trw_{PU}.

The difference of determining Trw by P- (Trw_P) and D- (Trw_D) in the tube of 10 mm diameter 1mm wall thickness silicone tube, 20.6 mm diameter 1.5 mm wall thickness rubber tube and 24.2 mm diameter 0.27 mm wall thickness latex tube were also compared. All the determined Trw in these three tubes are listed in **Table 3.4**. The results show that there is a small difference between Trw_{D-} and Trw_{P-}. The greatest percentage difference of Trw between the two methods is 5.45%, and the average percentage difference is 0.48±2.70.

The correlations of determining Trw by D- and P- in these three tubes (**Figure 3.11**) were also compared. From the regression line, we know that Trw determined by D- and P- are almost the same.

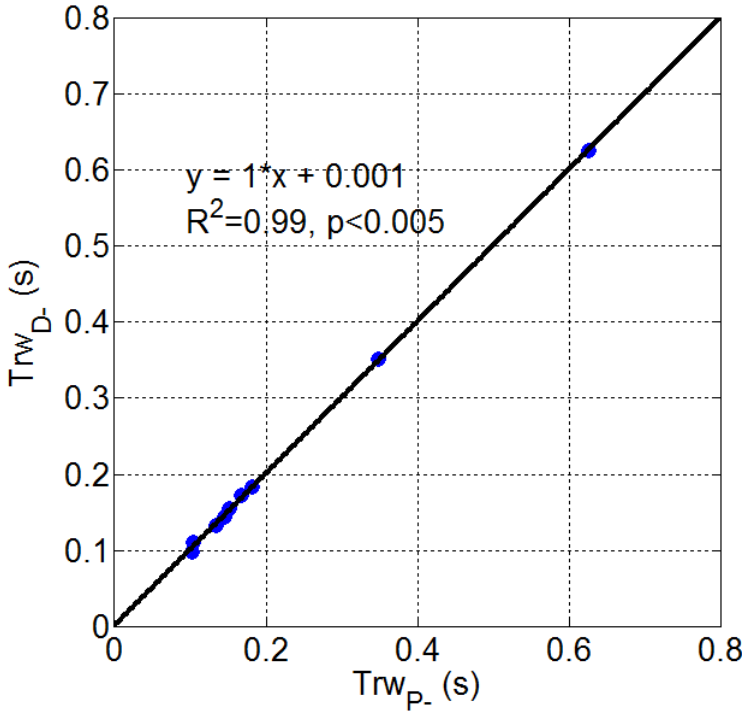

Figure 3.11: Trw_{D-} and Trw_{P-} correlate well (R^2 = 0.99) and the trend line appears to fall on the identity line (not shown).

Table 3.4 Arrival time of reflected wave determined by P- and D-. D_{in} is the internal diameter; h is the wall thickness; Position is the measurement site away from the inlet of the tube; Mean is the average of arrival time of reflected waves determined by P- and D-; Diff is the difference of Trw_{D-} and Trw_{P-}; Diff (%) is the percentage of difference between the arrival time of reflected waves determined by P- and D-

$$Diff\,(\%) = \frac{T_{rwD} - T_{rwP}}{Trw_D} \times 100\%$$

D_{in} (mm)	h (mm)	Position (cm)	Trw_{D-} (s)	Trw_{P-} (s)	Diff (s)	Diff (%)
10	1	25	0.172	0.168	0.004	2.33
		50	0.144	0.146	-0.002	-1.39
		75	0.110	0.104	0.006	5.45
20.6	1.5	25	0.184	0.182	0.002	1.09
		50	0.132	0.134	-0.002	-1.52
		75	0.098	0.102	-0.004	-4.08
24.2	0.27	25	0.626	0.626	0	0
		50	0.352	0.348	0.004	1.14
		75	0.154	0.152	0.002	1.30

3.4 Discussion

In this chapter, foot-to-foot, PU-loop methods and a new technique *ln*DU-loop for the determination of wave speed are tested and compared. The arrival time of reflected wave, separation of forward and backward waves using wave intensity based on pressure and velocity and non-invasive wave intensity based on diameter and velocity are experimentally tested and compared. Mean wave speeds determined by *ln*DU-loop and PU-loop methods are compared to those determined by foot-to-foot method. The results of the three methods are in good agreement and foot-to-foot method calculates the biggest wave speed. Local wave speeds determined by *ln*DU-loop method are compared to those determined by PU-loop method. The results of the two methods agree well and the small differences between the results of the two methods could not be attributed to any specific cause.

Flexible tube waves involve exchange between the kinetic energy of the fluid within the tube and the potential energy of the distending tube walls. Therefore, changes in P, U and D in flexible tubes are inextricably linked and a change in any of these parameters will induce a change to the other two. The distension of the tube wall is associated with a change in pressure and therefore the waves can be described either as pressure-velocity waves or as diameter-velocity waves. In the study of previous investigators, waves were described in terms of P and U, and in this chapter we present the waves in terms of D and U for the useful non-invasive benefits. Further, the term “Intensity” does not have natural fundamental units, and evidently there are two methods using P and U giving wave intensity in different units; (W/m^2) as described by Parker and Jones (1990) and (W/m^2s^2) as described by Ramsey and Sugawara (1997). Therefore, quite apart from the shape similarity between the curves produced by the previously and currently introduced WIA, describing the waves using D and U as intensity with units of m^2/s is a natural approach that does not contradict any of the other methods.

In the current study, it is defined the elemental waves by the changes in diameter (dD) and velocity (dU). It is also defined the direction of the waves as positive in the direction of the mean flow. In line with the well establish notations in gas dynamics, waves for which dP>0 and dD>0 (wall extension) are termed

‘compression waves’ and waves for which dP<0 and dD<0 (wall contraction) are termed ‘decompression’ waves. The effect of these waves on velocity depends upon their direction; both forward compression and backward decompression waves cause acceleration dU>0 while both forward decompression and backward compression waves cause deceleration, dU<0. The inter-relations between fluid and diameter waves are defined in **Table 2.1**.

Significance of *ln*DU-loop determining wave speed

It is well known that the wall properties and dimensions of the ascending aorta are not similar to those of the peripheral arteries (Nichols and O’Rourke 2005). Wave speed is directly related to the properties of the arterial wall. Hence, determination of wave speed using the measurements at one point is significant to hemodynamic study as it provides direct information about arterial distensibility. PU-loop method allows for determination of wave speed using measurements of pressure and velocity at one point. However, because of the invasive nature of the pressure measurement, PU-loop method is not convenient for the clinical routine examination.

Determination of wave speed and arrival time of reflected wave noninvasively has recently attracted the interest of several researchers. Harada et al. (2002) presented an on-line one-point measurement method to determine wave speed noninvasively; the principle of the method is based on Hoeks and his colleagues’ work (Hoeks et al., 1985; 1990), which the relative change in diameter during the cardiac cycle is obtained by taking the ratio of the distension and the diameter of the artery as observed along the ultrasound beam. In Harada’s work, they measured the diameter-change of the carotid artery, calibrated the maximal and minimal values of the diameter waveform using systolic and diastolic blood pressure measured with a cuff-type manometer at the upper arm, and then substituted the calibrated diameter waveform for the pressure waveform. Hence, the stiffness parameter can be obtained simultaneously. Also, Meinders et al. (2001) introduced a multiple M-line system to assess local pulse wave velocity, which was determined as the ratio of the temporal and spatial gradient of adjacent distension velocity waveforms that were determined simultaneously along a short arterial segment using a single 2D-vessel wall tracking. The advantage of this approach is that the segment length is set by the characteristics of the ultrasound probe and

does not vary over measurements. Further, Rabben et al. (2004) presented a method for estimating wave speed from ultrasound measurements; the flow-area loop method, in which wave speed is estimated as the ratio between the change in flow to the change in cross-sectional area during the reflection-free period of the cardiac cycle. This method is similar to the method examined in this paper (*ln*DU-loop) as wave speed is determined from the linear portion of the loop during the reflection-free period of the cardiac cycle. It is worth noting that although the range of *ln*D is small, **Figure 3.1**, the number of data points making the initial linear part of the *ln*DU-loop (n=116) are approximately the same as those making the initial linear part of the PU-loop (n=115). This evidently did not affect the relative accuracy between the *ln*DU-loop and the PU-loop methods for calculating wave speed, as shown in **Figure 3.2**.

Whilst using the PU-loop method and WIA for the determination of wave speed and arrival time of reflected wave requires an estimation of ρ, the new techniques for their determination are independent of ρ as shown in **Table 3.1.** In this study the experiments were repeated using three fluids with different densities to examine the relative accuracy of the *ln*DU-loop method to determine wave speed. The densities used in this study were chosen in order to simulate a range of blood density; in human blood density is approximately 1060 kg/m^3 (Cutnell and Johnson, 1998), the density of blood plasma is approximately 1025 kg/m^3 and the density of blood cells circulating in the blood is approximately 1125 kg/m^3 (Benson and Katherine, 1999). Fluid densities of 75% (ρ=1194.9 kg/ m^3) and 50% (ρ=1126.3 kg/ m^3) of glycerine-water solution are approximately 19.5% and 12.6% respectively greater than that of water (ρ=1000 kg/ m^3). The calculations show in **Section 3.3.3** show that although there is no density term in the equation, *ln*DU-loop is sensitive to the change of fluid density. The small differences between the theoretical and experimental results are acceptable within the experimental noise.

The results shown in **Figure 3.2a**, **3.10a** also indicate a good agreement between the P, U and D, U based techniques for the determination of wave speed and arrival time of reflected wave. In assessing the relationship between both methods, the results for both C_{PU} and C_{DU}, and Trw_{PU} and Trw_{DU} are highly correlated with the trend lines falling almost on top of the identity line. **Figure 3.2b**, **3.10b** show clearly that most of the data points fell between the

acceptable range of difference and were well distributed, with no bias, around the mean difference, which is close to the zero line; all indicating no significant difference between the results of the two techniques. The results of C_{DU} and Trw_{DU} are not only in agreement with those of C_{PU}, and Trw_{PU}, but also in agreement with earlier work. For example, Khir and Parker (2002) reported C_{PU} in a 1" (25.4 mm) diameter, 0.25 mm wall thickness latex tube using the PU-loop method to be 3.4±0.8 m/s. In this study, C_{DU} measured in a 24.2 mm diameter, 0.27 mm wall thickness latex is 3.1±0.9 m/s. Furthermore, Wang et al. (2009), using the foot-to-foot method reported C in a D_o=19.0 mm and h=3.18 mm elastic tube is 25.3±0.2 m/s. In our experiment, C_{DU}=29.86 m/s in a D_o=16.0 mm and h=3.0 mm silicone tube. Given the differences in D and h the, results of this study are considered comparable to those obtained by other investigators using different methods.

Table 3.2 shows that tubes of different material and different h/D ratios yielded very similar wave speed. For example C_{DU} measured in a 16.7 mm diameter rubber tube with h/D of 0.09 was very similar to that measured in a 16 mm diameter silicone tube with h/D of 0.15. This can be understood through the Moens-Korteweg equation; $C^2 = \frac{Eh}{\rho D}$, where E is Young's Modulus. Bessems et al. (2008) presented an experimentally study in viscoelastic tubes where they changed the wall thickness along the length of a tapered flexible tube to obtain constant C which is similar to that measured in a straight tube of the same material. The results presented in the present paper further confirm that the *ln*DU-loop is sensitive to changes of tubes dimensions and fluid density.

WIA provides a novel perspective on wave propagation along the ventricular-arterial system. The separation of instantaneous P and U, or D and U into their forward and backward travelling components allows for the quantitative assessment of the contribution of the ejecting left ventricle and of reflected waves from peripheral arteries. Accurate prediction of Trw is of clinical significance as it gives an indication to the mechanical properties of the arterial bed. However, almost all methods used for the determination of Trw require the invasive measurement of P, which is not practical in the clinical setting and may not be accurate enough if obtained noninvasively (the transfer function method could allow noninvasive measurement of pressure at superficial, large arteries

and derive the pressure to the central aortic pressure, but the complexity of the method and the requirement of establish the transfer function model cause it could not provide accurate pressure waveform). The new techniques using D, U based measurements offers a way for the determination of C and Trw noninvasively.

3.4.1 Limitations

The strong agreement between the results of the PU-loop and the *ln*DU-loop methods for determining C and between dI_{PU} and dI_{DU} for determining Trw are probably due to the properties of the tubes tested in this study. The relationship between P and D in the tubes we tested is linear indicating the walls are elastic over the range of pressures involved. However, the arterial wall is known to be viscoelastic and therefore further in vivo validation is required to establish the relative accuracy of the new techniques for clinical measurements.

The measurements of wall thickness were carried out with digital calliper. The tubes used in this work are flexible tubes, the best way to measure the wall thickness of soft materials is to put the material between two pieces of hard materials, measure the distances between the outer layer of the two pieces at several locations, averaged and minus the thickness of the two hard pieces, the wall thickness of the soft material will be obtained.

3.5 Conclusion

The *ln*DU-loop method for determining wave speed (C) provided comparable and consistent results to those provided by the PU-loop and foot-to-foot methods, over a range of different diameters and wall thicknesses of flexible tubes. Also, the results of non-invasive wave intensities (dI_{DU}) for the determination of arrival time of reflected wave (Trw) are very close to those calculated by wave intensities (dI_{PU}). The *ln*DU-loop and the dI_{DU} methods used for the determination of C and Trw respectively appear insensitive to the absence of a density term in their respective equations. The new techniques are able to separate the forward and backward diameter (D) and velocity (U) waveforms that appear typical to that traditionally used by impedance techniques or wave intensity analysis (WIA) for the separation of pressure (P) and U waveforms. The new techniques based on D and U provide an

integrated noninvasive system for studying waves traversing flexible tubes, requiring noninvasive measurements and hence may have an advantage in the clinical setting, for which further in vivo validation is required.

Chapter 4
Variation of Wave Speed Determined by PU-loop with Proximity to a Reflection Site

4.1 Introduction

Wave speed (C) is an important property of an artery and is directly related to its compliance (Merillon et al., 1982), which has been long used as a surrogate marker for aortic stiffness. Wave speed has also recently been shown to be an independent predictor of stroke (Laurent et al., 2003) and cardiovascular mortality (Laurent et al., 2001) in hypertensive patients.

In order to use wave speed as a diagnostic tool, researchers have proposed several methods for its evaluation. The most common method is the foot-to-foot method, which depends upon the transit time of the pressure wave and the distance between two sites of pressure measurement. Many researchers have been used this method (McDonald, 1968b; Latham et al., 1985; Mitchell et al., 1997b). The definition of the 'foot' and the distance travelled in a tortuous arterial path are major challenges to this technique, and the measured wave speed is an average over the distance. Local determination of wave speed in time domain are developed in recent years, PU-loop which relies on the simultaneous measurements of pressure and velocity (Khir et al., 2001a); sum of squares which also based on the simultaneous measurements of pressure and velocity (Davies et al., 2006a); *ln*DU-loop which using the measurements of velocity and diameter noninvasively (Feng and Khir, 2010); flow-area loop by Rabben et al. (2004) which determine the wave speed from the ultrasound measurements of flow rate and luminal area; and D^2P-loop, which estimates wave speed from simultaneous pressure and diameter measurements in late diastole (Alastruey, 2011).

Frequency domain methods for the determination of wave speed have also been developed (O'Rourke and Taylor, 1967; Milnor and Bertram, 1978; Stergiopulos et al., 1999). However, Aguado-Sierra et al. (2006) applied them in the human carotid arteries in normal conditions, they showed greater variation than the PU-loop and sum of squares methods.

In a previous paper the PU-loop method for determining local wave speed was introduced (Khir et al., 2001a). During the early part of systole, it is most probable that only forward waves are present, so that the relationship between pressure and velocity is linear and the initial slope of the PU-loop is directly related to wave speed. The PU-loop method has the advantage of measuring local wave speed, but in the coronary arteries, the PU-loop method fails because both backward and forward waves are generated during early systole. The coronary arteries are vitally important for supplying blood to the heart muscle, and allowing the heart to work continuously. As the measure of the arterial stiffness, wave speed in coronary artery plays an very important role in the diagnose and prevention of the coronary artery diseases. Kolyva et al. (2008) questioned its validity in the coronary circulation. They stated that due to the short length of the coronary artery, and the generation of concurrent coronary waves by proximal and distal sources conflicts, PU-loop method for determination of local wave speed is not suitable for the coronary circulation; PU-loop method requires unidirectional waves during at least part of the cycle.

Determination of the wave speed using the PU-loop relies on the existence of a reflection-free period during which there is a linear relationship between the change in pressure and the change in velocity given by the water hammer equation for forward travelling waves. The existence of a linear segment of the PU-loop during early systole has been taken as evidence of the absence of reflected waves. However, for the effect of a reflection site close to the measurement site suggests that there may be a linear relation between pressure and velocity in the presence of the reflected wave, but that the slope of the line will vary depending on the strength of the reflection. This implies that the measurement of wave speed close to a reflection site would result in an erroneous value of the wave speed.

The main purpose of this study is to investigate the effect of proximity to reflection site on wave speed determined using the PU-loop method. Also an

algorithm to correct the measured wave speed which is affected by the reflection is considered and discussed.

4.2 Materials and methods

4.2.1 Determination of wave speed by PU-loop

The theoretical basis of the PU-loop method for determining wave speed (c) has been described in previous study (Khir et al., 2001a). Briefly, the water hammer equation for forward and backward wave is

$$dP_{\pm} = \pm \rho c dU_{\pm} \quad (4.1)$$

Where dP and dU are the pressure and velocity differences across the wavefront, ρ is the density of the fluid. The water hammer equation can be used to determine the wave speed when the waves passing by the measurement site are in one direction only, which is most probably the case during the earliest part of systole. During this time, it is probable that only forward waves are present because it is too early for the arrival of any reflected waves.

When the measurement site is very close to the reflection site, the reflected wave will come back and intersect with the forward wave (**Figure 4.1**). This will shorten the part which only forward wave present. In this condition, the linear part of the PU-loop will change, and wave speed determined by PU-loop will be varied.

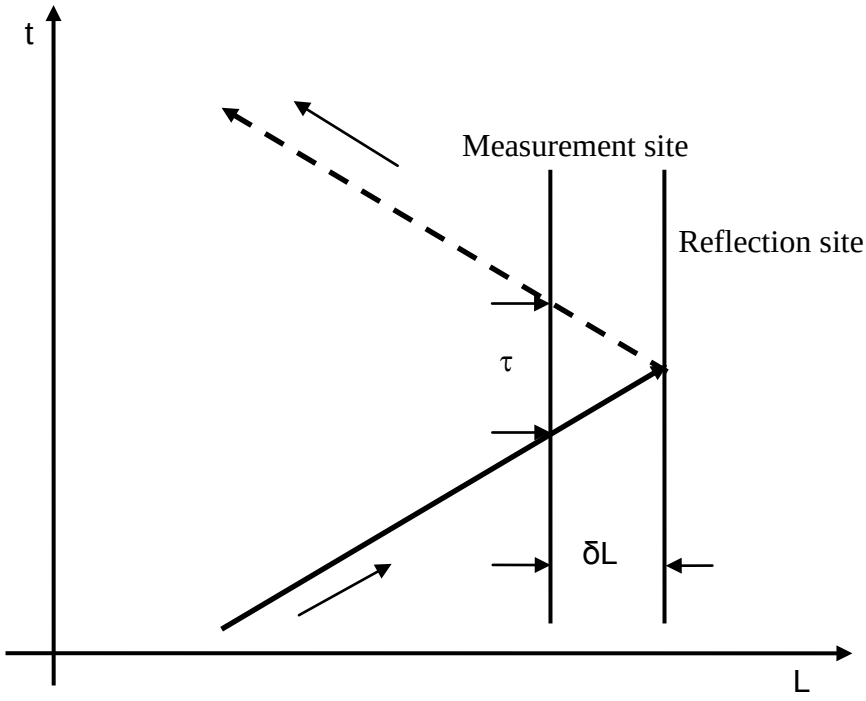

Figure 4.1: A schematic diagram of the wave propagation. The solid line shows the incident wave, the dash line shows the reflected wave. The time between the incident wave passing the measurement site and reflected wave passing the measurement site is τ. The distance between the measurement site and the reflection site is δL.

4.2.2 Correction of wave speed determined by PU-loop

Assuming that the forward and backward waves interact linearly

$$dP = dP_+ + dP_- \quad \text{and} \quad dU = dU_+ + dU_- \tag{4.2}$$

The slope of the PU-loop can be written

$$\frac{dP}{dU} = \frac{dP_+ + dP_-}{dU_+ + dU_-} \tag{4.3}$$

Using the water hammer equations (4.1)

$$\frac{dP}{dU} = \frac{dP_+ + dP_-}{dP_+ - dP_-}. \tag{4.4}$$

If the measurements site is close to a reflection site with reflection coefficient R_{dP}, the backward wave will be the reflection of the forward wave

$$dP_-(t) = R_{dP} dP_+(t-\tau) \tag{4.5}$$

Where τ is the time it takes for the wave to travel from the measurement site to the reflection site and come back. R_{dP} is the reflection coefficient calculated as the ratio of the peak values of forward and backward pressure.

$$R_{dP} = \frac{dP_-}{dP_+} \tag{4.6}$$

If τ is small, $dP_+(t-\tau)$ can be expanded in a Taylor series,

$$dP_+(t-\tau) = dP_+(t) - \tau\frac{d(dP_+(t))}{dt} + \frac{1}{2}\tau^2\frac{d^2(dP_+(t))}{dt^2} + \cdots \tag{4.7}$$

where the prime indicates the derivative of τ.

Substituting equation (4.7) into equation (4.4), this can be written

$$\frac{dP}{dU} = \rho c\left(\frac{1+R_{dP}}{1-R_{dP}}\right)\frac{(1-\frac{\tau R_{dP}d(dP_+(t))}{(1+R_{dP})dP_+}+\cdots)}{(1+\frac{\tau R_{dP}d(dP_+(t))}{(1+R_{dP})dP_+}+\cdots)} \tag{4.8}$$

Where the higher orders of τ have been neglected. If the first order of τ also be neglected, then

$$\frac{dP}{dU} = \rho c\left(\frac{1+R_{dP}}{1-R_{dP}}\right) \tag{4.9}$$

Comparing the expressions with and without the presence of a reflection site, it is seen that the wave speed c_m determined in the presence of a reflection is related to the true wave speed c determined in the absence of a reflection

$$c = \left(\frac{1-R_{dP}}{1+R_{dP}}\right)c_m \tag{4.10}$$

Where $E_c = (1-R_{dP})/(1+R_{dP})$ is the correction factor which used to correct the measurement made in the presence of a reflection site.

In the equations above, the orders of τ have been neglected. In order to see the difference between corrected wave speeds by using different orders of τ, first and second orders of τ also have been kept in the Taylor expansion, shown below.

Taylor's theorem is shown in equation (4.7), if first order of τ is considered,

$$dP_+(t-\tau) = dP_+(t) - \tau\frac{d(dP_+(t))}{dt} \tag{4.11}$$

Substiting equation (4.11) into equation (4.5), gives

$$dP_- \approx R_{dP}dP_+(t) - R_{dP}\tau\frac{d(dP_+(t))}{dt} \tag{4.12}$$

Substiting equation (4.12) into equation (4.4), gives

$$c = \frac{1}{\rho}\frac{dP}{dU}\frac{(1-R_{dP})+R_{dP}\tau\dfrac{d(dP_+(t))}{dP_+(t)}}{(1+R_{dP})-R_{dP}\tau\dfrac{d(dP_+(t))}{dP_+(t)}} \tag{4.13}$$

where $E_c = \dfrac{(1-R_{dP})+R_{dP}\tau\dfrac{d(dP_+(t))}{dP_+(t)}}{(1+R_{dP})-R_{dP}\tau\dfrac{d(dP_+(t))}{dP_+(t)}}$ (4.14)

If two order of τ kept, substiting equation (4.7) into equation (4.5), gives

$$dP_- \approx R_{dP}dP_+(t) - R_{dP}\tau\frac{d(dP_+(t))}{dt} + \frac{1}{2}R_{dP}\tau^2\frac{d^2(dP_+(t))}{dt^2} \tag{4.15}$$

Substiting equation (4.15) into equation (4.4), gives

$$c = \frac{1}{\rho}\frac{dP}{dU}\frac{(1-R_{dP})+R_{dP}\tau\dfrac{d(dP_+(t))}{dP_+(t)}-0.5R_{dP}\tau^2\dfrac{d^2(dP_+(t))}{dP_+(t)}}{(1+R_{dP})-R_{dP}\tau\dfrac{d(dP_+(t))}{dP_+(t)}+0.5R_{dP}\tau^2\dfrac{d^2(dP_+(t))}{dP_+(t)}} \tag{4.16}$$

Where $E_c = \dfrac{(1-R_{dP})+R_{dP}\tau\dfrac{d(dP_+(t))}{dP_+(t)}-0.5R_{dP}\tau^2\dfrac{d^2(dP_+(t))}{dP_+(t)}}{(1+R_{dP})-R_{dP}\tau\dfrac{d(dP_+(t))}{dP_+(t)}+0.5R_{dP}\tau^2\dfrac{d^2(dP_+(t))}{dP_+(t)}}$ (4.17)

When first and second terms of τ kept, τ is calculated as $\tau=2L/c$, L is the distance between the measurement site and reflection site.

To correct the affected wave speed, an iteration process has been shown in **Figure 4.2**. The process is, first to obtain the initial estimate of c_m from the slope of the PU-loop and use c_m to separate the measured pressure into dP_+ and dP_-. Using equation (4.6), the reflection coefficient R_{dp} can be obtained. This reflection coefficient has been substituted into equation (4.10) to obtain the next iteration of the wave speed c_2. This process is continued until the iteration converges, which means the corrected wave speed is within ±10% of the true wave speed.

In this study, measurements far from the reflection site were taken where it is assumed that the wave speed measured from the PU-loop is the true wave speed for the tube. This enables to compare the results obtained from measurements close to the reflection site after the iterative correction. Also

simultaneous pressure measurements at inlet and just upstream from reflection site in mother tube were taken several times to calculate the wave speed along the tube using foot-to-foot method; this also used to compare the results obtained from PU-loop method.

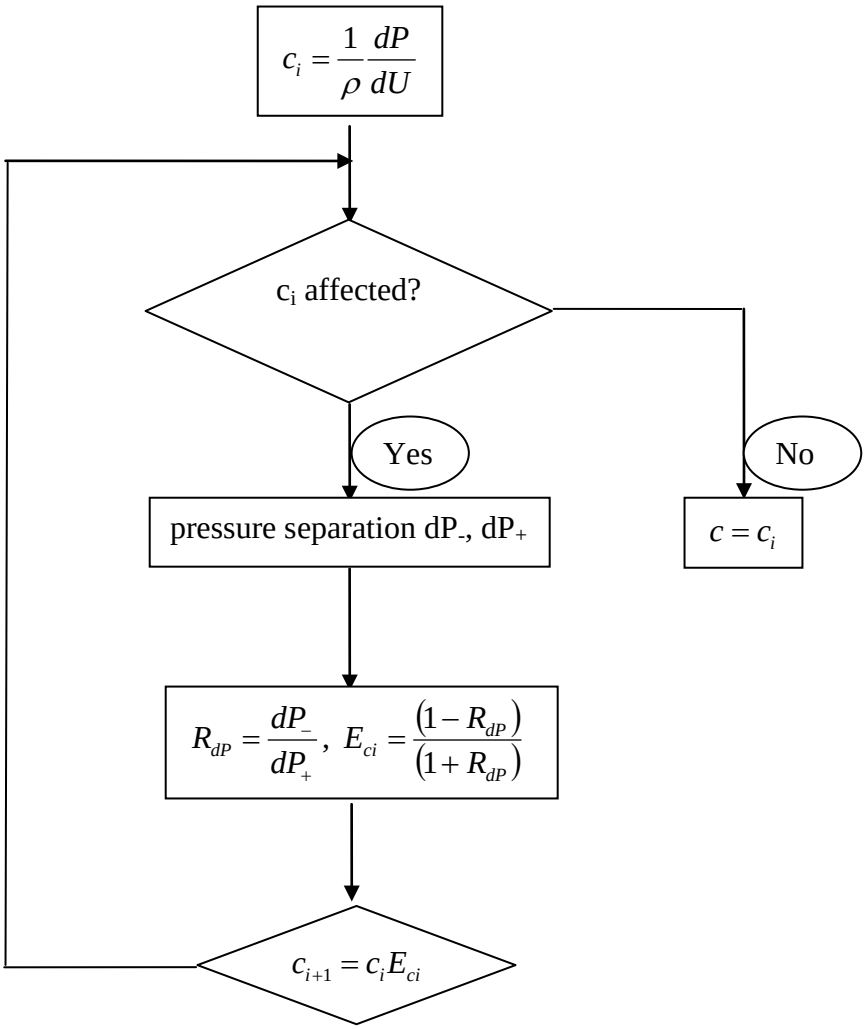

Figure 4.2: Flow chart for correction of the measured wave speed.

4.2.3 Experimental setup

The general experimental setup of this study is shown in **Figure 4.3** and a description of the individual elements follow.

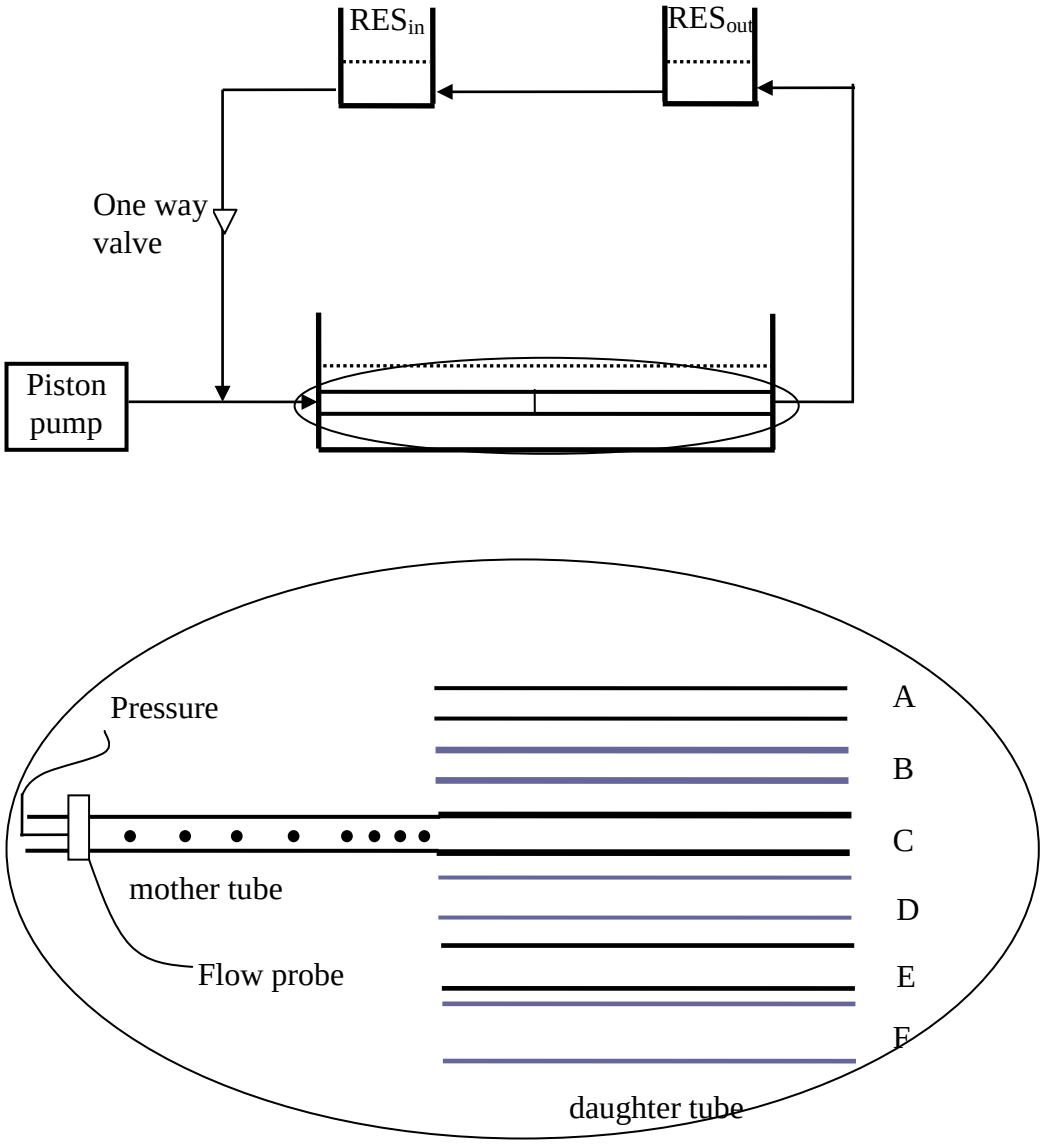

Figure 4.3: A schematic diagram of the experimental setup. RES$_{in}$ and RES$_{out}$ are the inlet and outlet reservoirs which provided the initial pressure to the system, and kept the tube free of air. Pressure and flow were measured using a transducer tipped catheter, and an ultrasonic flow meter and probes, respectively. All elements of the experiment are placed on the horizontal plane so that the heights of the inlet and outlet reservoirs were equal. The daughter tube was very long to delay reflection from the outlet.

Tubes: In this study one “mother” tube, which is 3 m long, 10 mm diameter and 1 mm wall thickness, made of silicone, and 6 “daughter” tubes of different sizes and materials, each 14 m long were used. This length was needed to ensure that the reflected wave from the end of the daughter tube arrives to the inlet of the tube after the incident wave has passed through the mother tube. Each daughter tube was connected with the mother tube to provide a different reflection coefficient; 3 positive and 3 negative reflection coefficients. The details of these tubes are given in **Table 4.1** and also **Table 3.2**. All of the tubes are uniform in both dimension and mechanical properties along their length. The mother tube was fully immersed in a water tank, where the water level was approximately 1 cm above the tubes. The various reflections were generated by the connection of the mother tube with each different daughter tubes, and these different connections were numbered by daughter tubes. For example, Set A shows the connection of mother tube with daughter tube A. Daughter tubes A, B, C, and D were connected directly to the mother tube by overlapping the inlet of each tube over the outlet of the mother tube. Daughter tubes E, F were connected to the mother tube by overlapping the inlet of each over a short connecting tube, which in turn was connected to the mother, also through overlapping. All tubes were kept in the horizontal position.

Table 4.1 Daughter tubes each used with the mother tube of 10 mm diameter 1 mm thickness 3 m length silicone tube. The properties of daughter tubes and reflection coefficients are shown. D_{in}: Internal diameter, h: Wall thickness, A: cross-sectional area and R_t: theoretical reflection coefficient

Set	D_{in} (mm)	h (mm)	A (mm^2)	Material	R_t
A	8	2	64	Silicone	+0.36
B	8	1	64	Silicone	+0.28
C	10	2	100	Silicone	+0.12
D	12	1	144	Silicone	-0.12
E	16.7	1.5	278.89	Rubber	-0.39
F	21	1.5	441	Rubber	-0.60

Measurements: Simultaneous pressure and flow waveforms were measured sequentially at different distances from the reflection site at the end of the mother tube. One pressure sensor was placed just upstream the reflection site in order to use the foot-to-foot method for measuring the wave speed. In the first 20 cm away from the reflection site, measurements were taken every 5 cm and the other measurements were taken every 10 cm. Due to the limited length of the pressure catheter, measurements could not be taken in the middle third of the mother tube. One measurement of pressure and flow was also taken in the daughter tube 10 cm downstream of the reflection site to measure the transmission coefficient in order to check the internal consistency and confirm the type and value of the reflection site. Theoretical reflection coefficients of all the sets of tubes have been calculated using equation (2.45), and presented in **Table 4.1**.

In this study (chapter 4) and chapter 5, 'L' distance is referred as the distance from the measurement site to the reflection site, for example, L=0 refers to the reflection site. This definition is different from those referred distances from the measurement site to the inlet of the tube in chapter 3 and 6, because the focus of studies of chapter 4 and 5 is related to the reflection.

Pressure and flow were measured using 6F tipped catheter pressure transducer (Millar Instruments Inc., Houston, Texas, USA) and an ultrasonic flow probe (Transonic System, Inc, Ithaca, NY, USA). All the data were acquired at a sampling rate of 500 Hz using Sonolab (Sonometrics Corporation, London, Ontario, Canada). External diameter and wall thicknesses of the tubes were measured by a digital calliper. The analysis procedure was carried out using programs written in Matlab (The Mathworks, Natick, MA, USA). In this study, all the measurements were taken twice, and the results shown in this study is the mean values of the two measurements.

4.2.4 Analysis

In this study, some of the measurements were taken two times, so the results are presented as mean±SD.

In order to validate the legitimate of the pooling of the measurements in the last metre of the mother tube from the reflection site to calculate the 'true' wave speed, a statistic analysis (the unequal sample sizes, unequal variance t-test)

has been performed in this work. The t-tests between true wave speed (calculated as the average of all the measured wave speed in the last metre from the reflection site) and the average wave speed in the last metre from the reflection site of each set (A, B, C, etc) were done to show the legitimation.

4.3 Results

4.3.1 Wave speed determined by the PU-loop

Figure 4.4 shows a typical example of the PU-loop measured near the inlet of the mother tube, 50 cm away from the inlet of the mother tube. The initial part of the PU-loop is very linear. Using the water hammer equation for forward wave, the slope of the loop equals ρc, where ρ is the density of water (1000 kg/m^3) and the wave speed c calculated from the slope is 20.98 m/s. This result is quite close to the foot-to-foot result which is 21.16±0.77 m/s, with a difference of only approximately 0.1%.

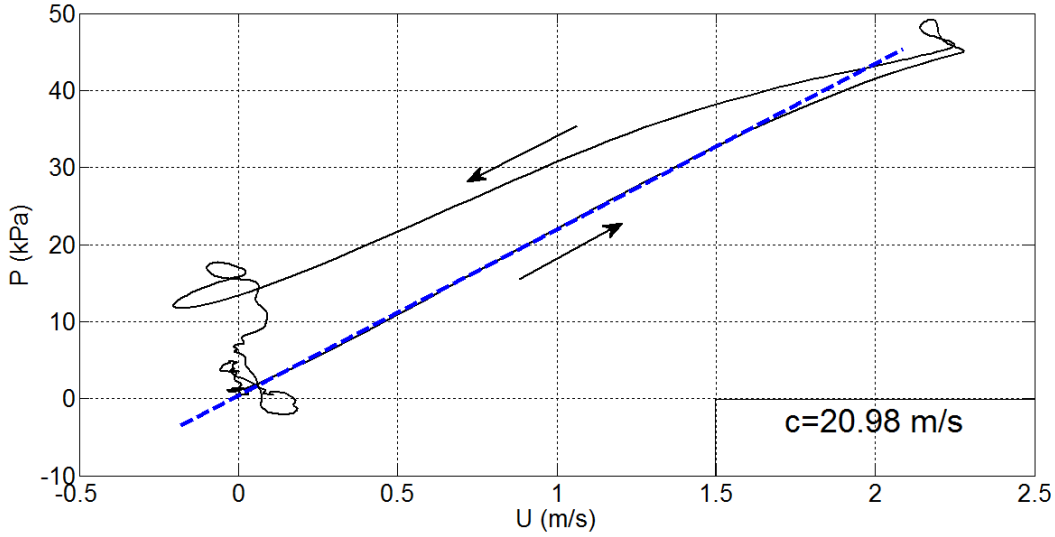

Figure 4.4: PU-loop measured at 50 cm away from the inlet of the mother tube (10 mm diameter, 1 mm thickness). The dashed line show the linear part of the PU-loop which indicated wave speed is 20.98 m/s. Arrows show the direction of the loop.

4.3.2 Effect of reflection on wave speed

Wave speed determined from the initial slope of the PU-loop was calculated at all of the measurement sites and the results are shown in **Figure 4.5** for all 6 different sets of tubes. The measured wave speeds determined from measurements in the last metre from the reflection site in mother tube were very similar, with not statistically significant differences between the measurements made with different daughter tubes (**Table 4.2**). Pooling all of these measurements, the average wave speed is 20.23±1.84 m/s, and this was taken as the true wave speed of the mother tube. At the last meter of the mother tube, the measured wave speed increased or decreased sharply depending on the sign and magnitude of the reflection coefficient.

Table 4.2 P values for the pooling of the true wave speed

	Mother tube	Daughter tube					
		A	B	C	D	E	F
Mean (m/s)	20.23	20.4	20.2	21.1	20.6	19.6	19.5
SD (m/s)	1.84	1.9	2.3	1.9	1.6	1.2	1.9
P		0.81	0.97	0.23	0.54	0.20	0.31

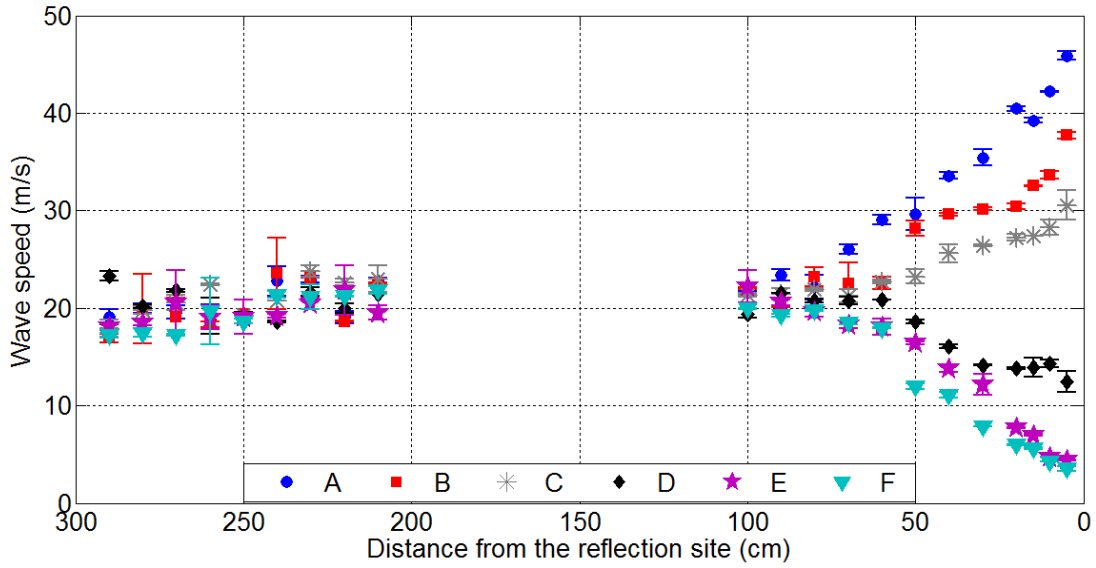

Figure 4.5: Measured wave speeds for all six different sets of tubes. No data presented at middle part of the mother tube due to the limited length of the pressure catheter.

As seen in **Figure 4.4**, far away from the reflection site, the initial portion of the PU-loop is very linear and the wave speed determined from the measurement of the slope of this line is very close to the true wave speed of the mother tube. When the measurement site is close to the reflection site, the reflected wave arrives earlier as shown in **Figure 4.6**. However, after the arrival of the reflected wave the PU-loop remains linear but with a different slope, which leads to an erroneous determination of the wave speed. When the measurement site is 80 cm away from reflection site, taking wave speed as 22.14 m/s, the reflected wave should arrive at 0.08 s, which corresponds to 40 sampling points at 500 Hz. The slope of the first 40 points is shown as the red line in **Figure 4.6**. When the measurement site is at 60 cm, the reflected wave arrives at 0.06 s and the linear part of the slope becomes shorter than in the previous case. When the measurement site is at 30 cm, the reflected wave arrives at 0.03 s. When the measurement site is only 5 cm from the reflection site the reflected wave will arrive after only 5 ms (less than 3 sampling times). After the arrival of the reflected wave, the PU-loop remains linear although with a significantly increased slope. From this, it is concluded that the arrival of the reflected wave

does not necessarily mean that the PU-loop becomes nonlinear, as had been assumed previously.

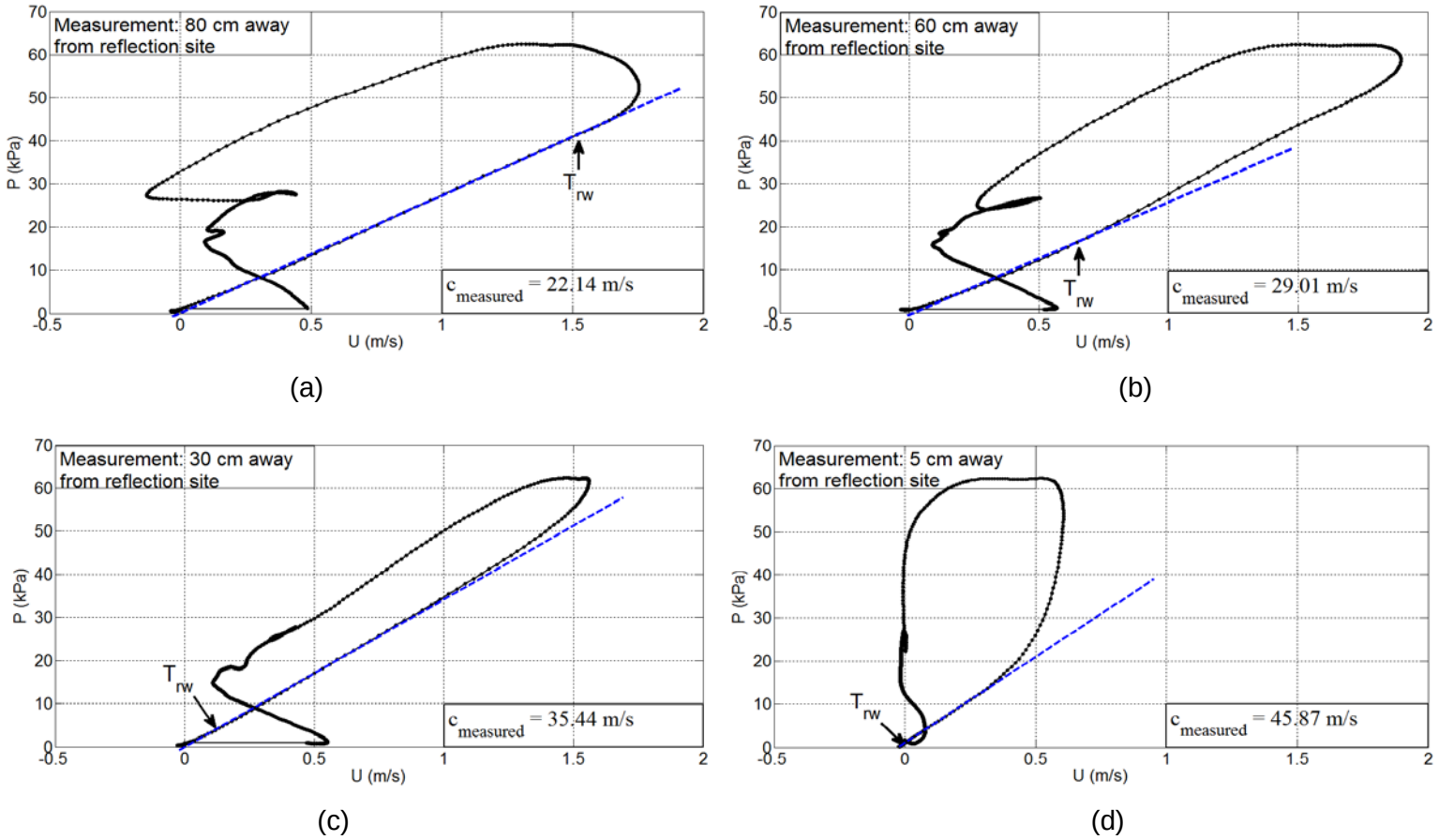

Figure 4.6: PU-loops measured at different sites, 80 (a), 60 (b), 30 (c) and 5 (d) cm away from the reflection site. Dash lines show the linear part of the PU-loop that was used to calculate the slope which was used to calculate the wave speed. The linear part of the slope was determined by fitting with the straight line by hand. Black arrows indicate the calculated arrival time of reflected waves. Note that in some of the cases the linear portion of the curve includes periods when both forward and backward waves are present.

4.3.3 Correction of measured wave speed

As shown in **Figure 4.6d**, when the measurement site is very close to the reflection site, there is still linear portion of the slope of PU-loop could be obtained. Wave speed could be determined from the linear portionof the slope, but it had been affected by the reflection. In order to correct the affected wave speed, a correction factor, which is calculated by the local reflection coefficient, the value of the ratio of the peaks of the reflected and forward pressure waveforms is applied to the affected wave speed. Correction of wave speed needed several iterations depending on the degree of the affection. The closer to the reflection site, the more times needed for the correction.

Figure 4.7 show the correction of measured wave speeds for all six different reflections. Because of the measured wave speeds at the first meter of the mother tube are not affected by the reflection. **Figure 4.7** only show the results of the last meter of the mother tube. The black points in **Figure 4.7** show the measured wave speed in the last metre of the mother tube, it is shown that the first two or three points of measured wave speeds are still not affected. The blue squares show the corrected wave speeds using the correction factor determined by the ratio of the local separated pressure, it is shown that the corrected wave speeds tend to the value of the true wave speed. The red stars show the corrected wave speeds using the theoretical correction factor as determined by the theoretical reflection coefficient (Equation 2.45). Unlike the local reflection coefficient, there is only one value for the theoretical reflection coefficient for the reflection, it is seen that the correction by the theoretical correction factor is not working well.

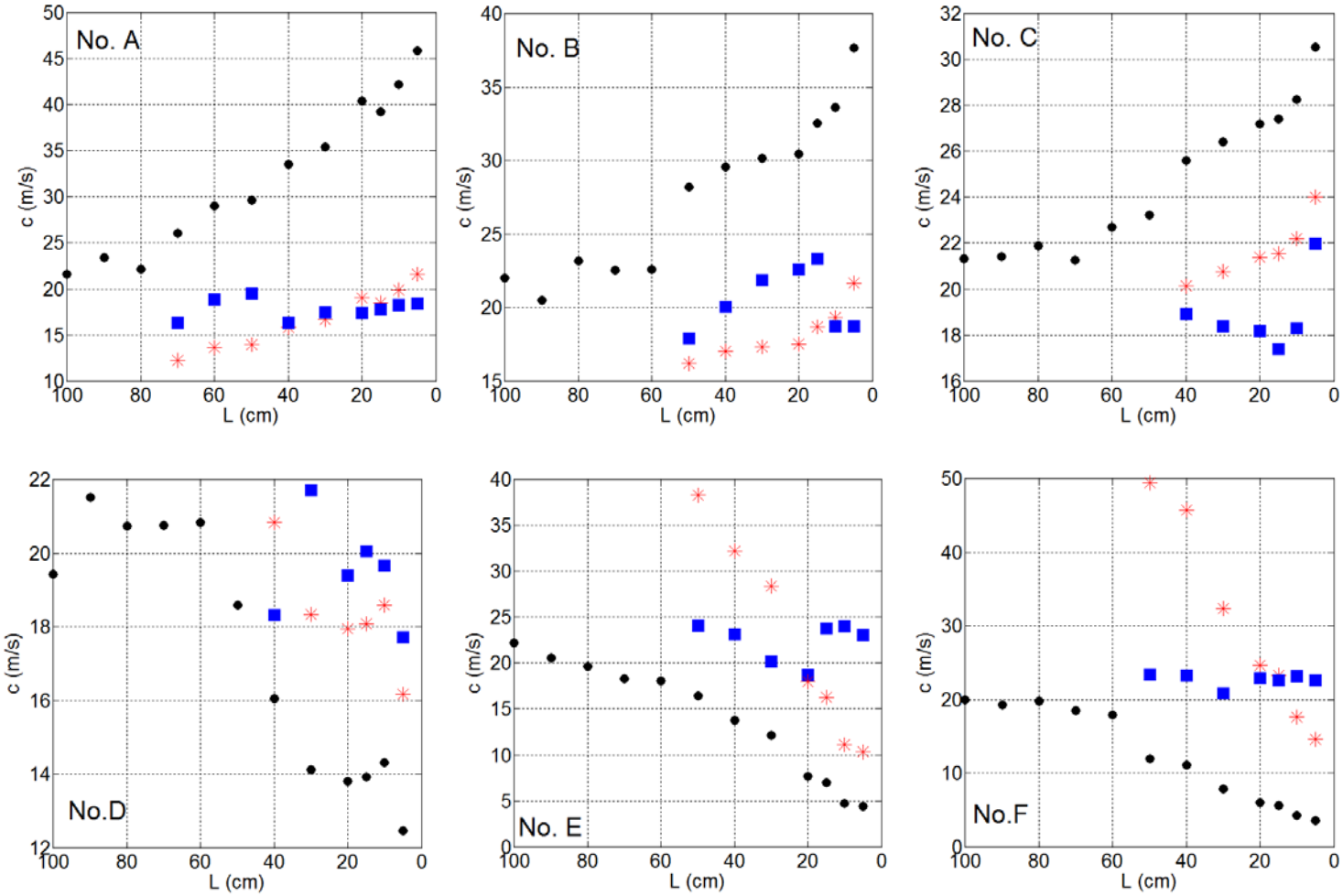

Figure 4.7: Measured and corrected wave speeds of all sets of daughter tubes. Top: reflections are positive. Bottom: Reflections are negative. Black dots show the measured c, blue squares show the corrected c, red stars show the corrected c using theoretical R_t.

In order to see the difference between the affected wave speed and the corrected wave speed, the mean values of the affected and the corrected wave speed, and the difference between them of each set of tubes are shown in **Table 4.3**. Also **Table 4.3** shows the true wave speed in each set of tubes.

Table 4.3 Affected and corrected wave speed. The wave speeds measured from the slope of the PU-loop for the different experimental conditions, the wave speed after iterative correction using the measured reflection coefficient and the difference between the two. The mean value of the true wave speed in all 6 sets of tubes is 20.23±1.84 m/s. Difference (%) is the percentage of difference of corrected and true wave speeds. $Difference(\%) = \frac{c_{corrected} - c_{unaffected}}{c_{unaffected}} \times 100\%$

Set	C_{true} (m/s)	$C_{affected}$ (m/s)	$C_{corrected}$ (m/s)	Difference (%)
A	20.4±1.9	35.7±6.7	17.8±1.1	-12.75
B	20.2±2.3	31.8±3.2	20.5±2.1	1.49
C	21.1±1.9	27.6±1.7	18.9±1.6	-10.43
D	20.6±1.6	14.1±1.2	19.5±1.4	-5.34
E	19.6±1.2	9.5±4.7	22.4±2.1	14.29
F	19.5±1.9	7.2±3.3	22.7±0.9	16.41

4.3.4 Effect of orders of τ on correction of wave speed

Two sets of Tubes of one positive reflection (No. A) and one negative reflection (No. D) are chosen to compare the effect of orders of τ on correction of wave speed. In order to distinguish the correction factor and wave speed determined by the different terms of order of τ, E_{c1}, E_{c2}, E_{c3} and c_1, c_2, c_3 will represent the correction factor and corrected wave speed using no order of τ, first order and second orders of τ in Taylor's expansion, respectively. The correction factor and wave speed determined by the different terms of order of τ are given in **Table 4.4** and **Table 4.5**. It is found that using different terms of order of τ, correction factor and wave speed have very small difference.

Table 4.4 Correction factors determined by different terms of order of τ. D_{in}: internal diameter; h: wall thickness; $Diff\,(\%) = \frac{E_{c2} - E_{c1}}{E_{c1}} \times 100\%$; $Diff\,(\%)^{*} = \frac{E_{c3} - E_{c1}}{E_{c1}} \times 100\%$

D_{in} (h) (mm)	Position (cm)	E_{c1}	E_{c2}	Diff (%)	E_{c3}	Diff (%)*
8 (2)	60	0.6515	0.6526	0.1594	0.6525	0.1574
	50	0.6570	0.6577	0.0972	0.6576	0.0932
	40	0.6513	0.6520	0.1072	0.6520	0.1040
	30	0.6384	0.6391	0.1112	0.6391	0.1031
	20	0.4295	0.4302	0.1642	0.4350	1.2951
	15	0.4523	0.4532	0.2077	0.4531	0.1952
	10	0.4328	0.4331	0.0407	0.4330	0.0362
	5	0.6219	0.6220	0.0090	0.6220	0.0070
12(1)	40	1.1415	1.1395	-0.1742	1.1408	-0.05682
	30	1.4110	1.4063	-0.3394	1.4067	-0.3106
	20	1.4037	1.3967	-0.4972	1.3994	-0.3047
	15	1.4377	1.4341	-0.2418	1.4354	-0.1529
	10	1.3723	1.3637	-0.6260	1.3687	-0.2604
	5	1.4274	1.4193	-0.5958	1.4195	-0.5799

Table 4.5 Corrected wave speed determined by different terms of order of τ. D_{in}: internal diameter; h: wall thickness; $Diff\,(\%) = \frac{c_2 - c_1}{c_1} \times 100\%$; $Diff\,(\%)^* = \frac{c_3 - c_1}{c_1} \times 100\%$

D_{in} (h) (mm)	Position (cm)	c_1	c_2	Diff (%)	c_3	Diff (%)*
8 (2)	60	18.9058	18.936	0.1598	18.9356	0.1577
	50	19.5001	19.5188	0.0960	19.5180	0.0921
	40	16.3091	16.3136	0.0276	16.3131	0.0245
	30	17.4513	17.4984	0.2700	17.5073	0.3206
	20	17.3641	17.3926	0.1643	17.5900	1.3008
	15	17.7488	17.7856	0.2076	17.7834	0.1951
	10	18.2682	18.2756	0.0407	18.2748	0.0362
	5	18.5256	18.5836	0.3126	18.5827	0.3081
12(1)	40	18.3194	18.2877	-0.1742	18.3092	-0.0568
	30	20.2120	19.8563	-1.7673	19.8621	-1.7387
	20	19.3936	19.2969	-0.4972	19.3344	-0.3047
	15	20.0479	19.9969	-0.2419	20.0155	-0.1530
	10	10.6599	19.5169	-0.7267	19.5887	-0.3615
	5	17.7191	17.6133	-0.5956	17.6161	-0.5798

4.4 Discussion

In this chapter, the effect of a reflection on the wave speed determined by the PU-loop was experimentally tested and the measured wave speed was corrected using the correction factor in an iterative way. It is found when the measurement site is close to the reflection site, measured wave speed increased or decreased sharply depending on the sign and magnitude of the reflection. By using the correction factor which is determined by the local ratio of peak of backward pressure and forward pressure, measured wave speeds have been corrected.

Measurement of wave speed is a useful parameter to assess arterial stiffness. Arterial stiffness is an important factor in cardiovascular physiology. It represents the ability of the arterial system to deal with the systolic ejection volume. It also means that the compliant arterial system's major function is to transmit cardiac contraction during diastole (Boutouyrie et al., 2009). Wave speed as a measure of arterial stiffness, has been proven that as a predictive value on risk evaluation in many cardiovascular studies in various geographical locations and population (Cruickshank et al., 2002; Sutton- Tyrrell et al., 2005; Shokawa et al., 2005; Mattace- Raso et al., 2006; Choi et al., 2007). Different techniques have been suggested to assess the wave speed, based either on pressure, distension or Doppler waveforms.

The PU-loop has been used to determine the wave speed in the ascending aorta of patients with cardiovascular disease (Khir et al., 2001b), but is unsuitable for wave speed analysis in the coronary arteries, because coronary arteries are subject to influences from the aortic and microcirculatory ends (Sun et al., 2000). This work suggests that when the appropriate correction factor is applied to the measured wave speed determined by the PU-loop, the measured wave speed could be corrected; the PU-loop method may therefore be able to determine the local wave speed even in short arterial segments.

Pooling all of the measurements taken in the first meter of the inlet of the mother tube, the wave speed measured for the mother tube was 20.23±1.84 m/s. In a previous experiment using tubing identical to the mother tube in a different setup without a fixed reflection site (Li and Khir, 2011), the wave speed was measured to be 20.0±5.3 m/s. It is therefore concluded that the wave

speeds measured in the entrance of the mother tube were not affected by the reflection and that the standard deviation is a measure of the error in our measurements.

At the end of the mother tube, 6 different tubes were connected in turn to generate six different reflection coefficients. We chose 3 tubes which were smaller or thicker than the mother tubes in order to generate positive reflections and 3 bigger or thinner tubes to obtain negative reflections. From **Table 4.1** and **Figure 4.5**, it is seen that the positive reflections increase the measured wave speed when the measurement site is close to the reflection site; whereas negative reflections induced a decrease in the measured wave speed. It is seen that the magnitude of the change increased with the magnitude of the reflection coefficient. It is also seen that the magnitude of the changes increased with decreasing distance to the reflection site for both positive and negative reflections.

4.4.1 Limitation

In this study, the effect of a reflection site on the wave speed determined by the PU-loop in elastic tubes was investigated, and the affected wave speed was corrected. The investigation was taken in a single tube formed by joining two tubes together end to end. But the artery system is much more complex so that experiments with bifurcations or tapered tubes will be necessary to understand and validate the method of correction more fully in arteries.

In the experiment, no measurements were taken in the middle part of the mother tube because of the limited length of the pressure catheter (effective length 1.2 m). This is not expected to influence the interpretations of the results as the first a few measurement sites downstream from this region also give results indicating that the wave speed was not affected.

In this study, the correction of the measured wave speed was based on that the true wave speed was known in advance. In each step of iteration of correction, the corrected wave speed was compared with the true wave speed to find out whether it is corrected. If apply this correction iteration into *in vivo* measurements, the true wave speed will not known, it will be difficult to decide when to stop the iteration and when it will get the corrected wave speed. It is assumed that there is a threshold when the corrected wave speed is close to

the true wave speed. Several different iteration methods have been tried to find the end point for the iteration.

Firstly, $c_i = c_{i-1} * E_{c(i-1)}$, is the method used to correct the measured wave speed in this study. $E_c=(1-R_{dP})/(1+R_{dP})$, R_{dP} is the ratio of the peak values of backward pressure and forward pressure. The percentage change calculated as $diff = \frac{c_i - c_{i-1}}{c_i} \times 100\%$. Two sets of tubes were chosen to test.

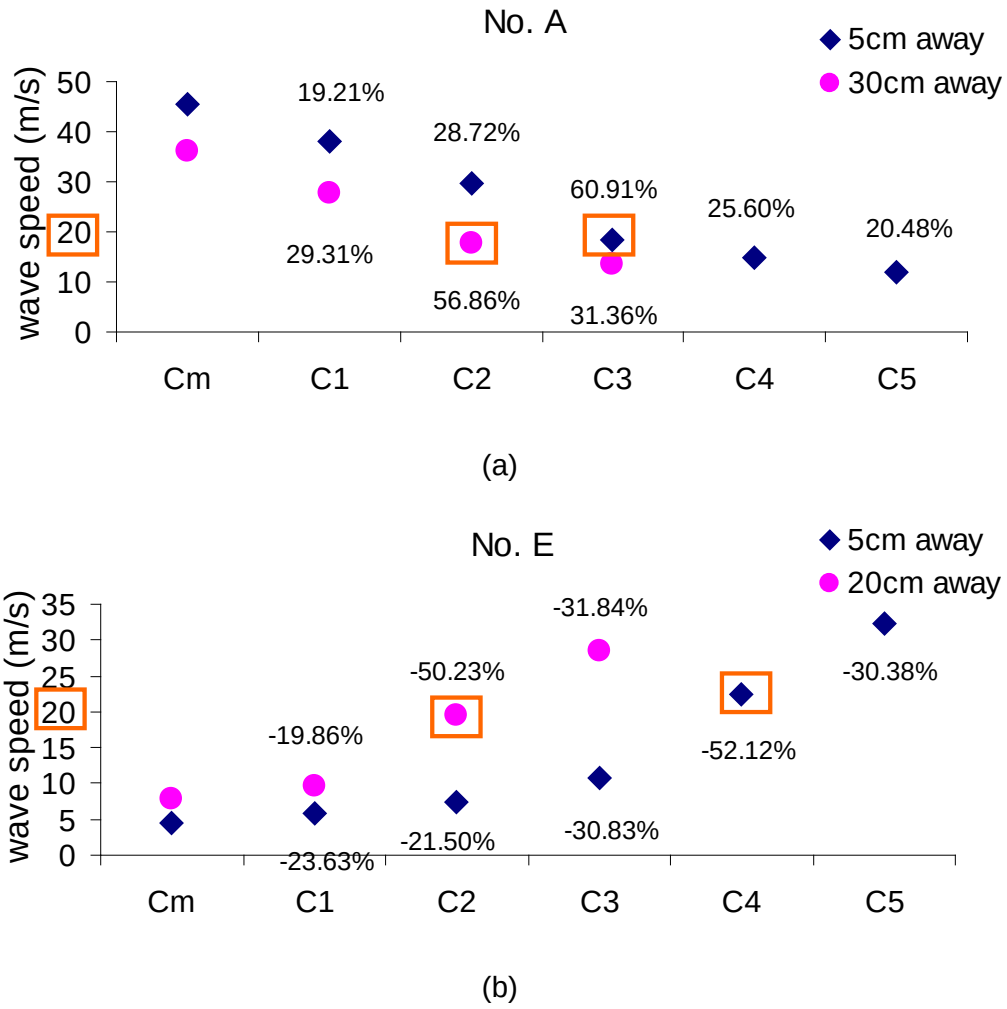

Figure 4.8: Correction of wave speeds in set A (a) and set E (b) tubes using the first method. The percentage values shown in figure indicate the difference changes of the iteration. The values surrounded by orange squares show the true wave speed.

Secondly, $c_i = c_m * E_{c(i-1)}$, correction factor E is always calculated by $c_{(i-1)}$. $E_c=(1-R_{dP})/(1+R_{dP})$, R_{dP} is the ratio of the peak values of backward pressure and forward pressure (**Figure 4.9**).

Last, $c_i = c_{i-1} * E_{c(i-1)}$, but this time the correction factor $E_c=(1-R_{dP})/(1+R_{dP})$, R_{dP} is the ratio of the peak values of backward pressure and forward pressure related to the initial linear part of the PU-loop (**Figure 4.10**).

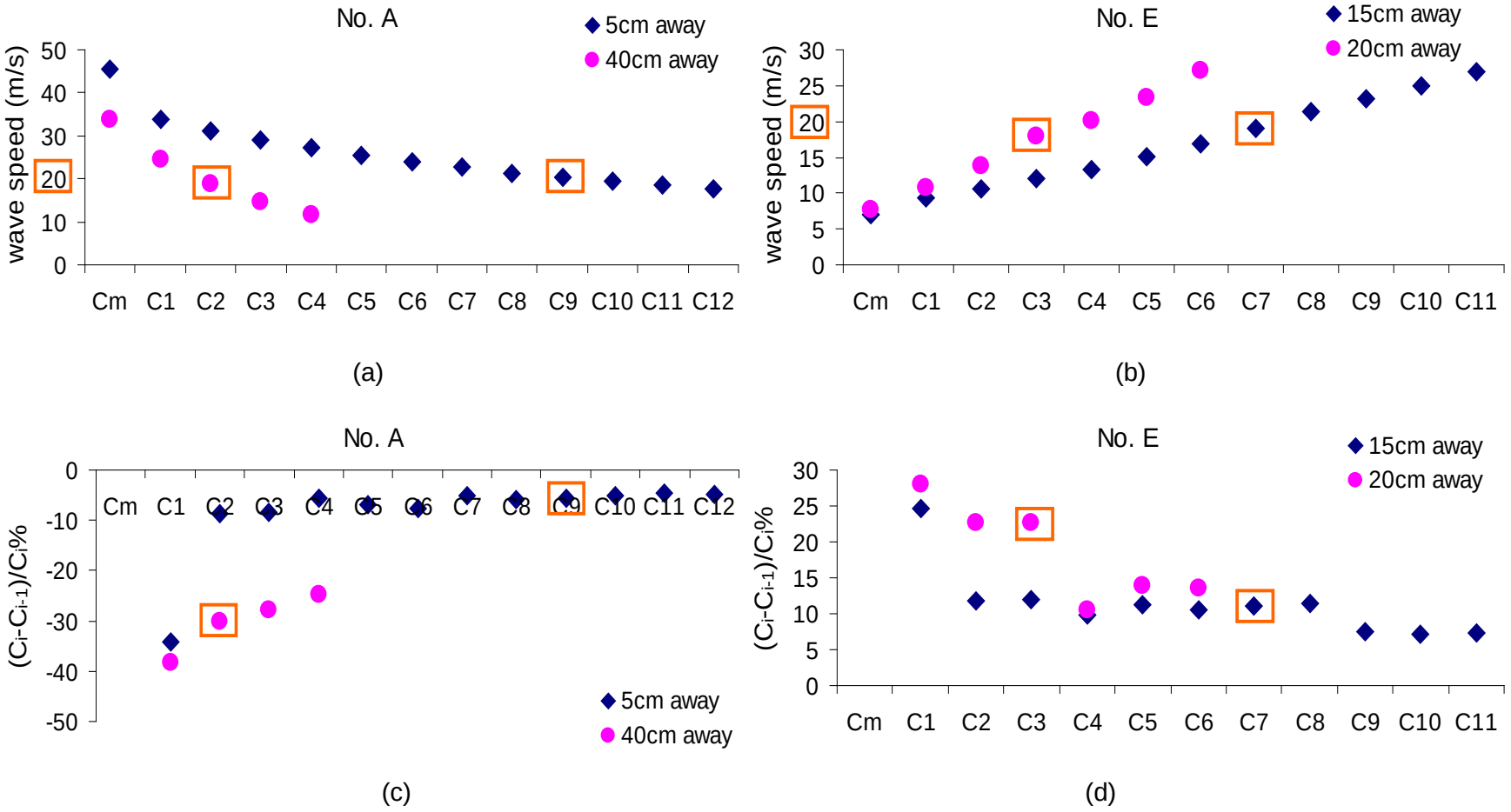

Figure 4.9: Correction of wave speeds in No. A (a) and No. E (b) tubes using the second method. The difference change of correction for No. A (c) and No. E (d) are also shown. The values surrounded by orange squares show the true wave speed.

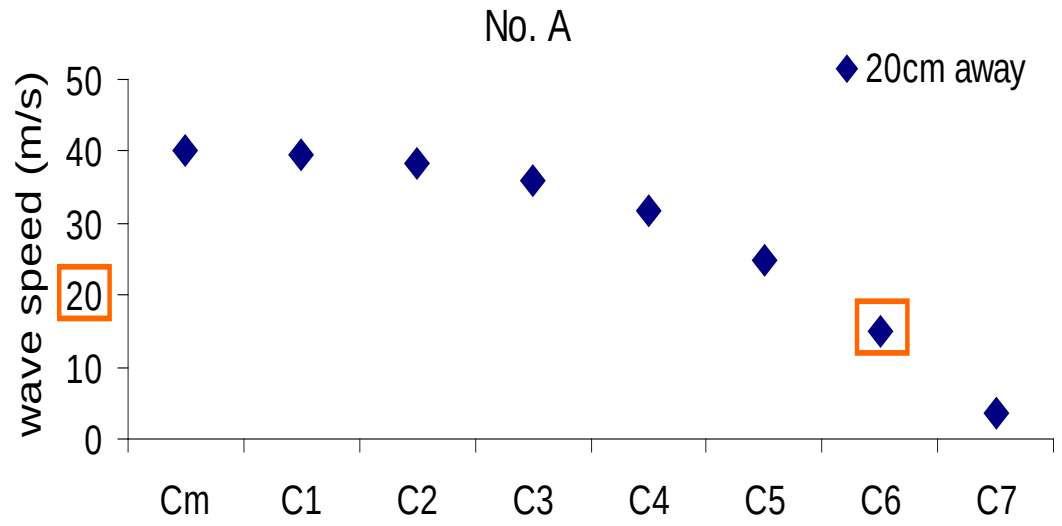

(a)

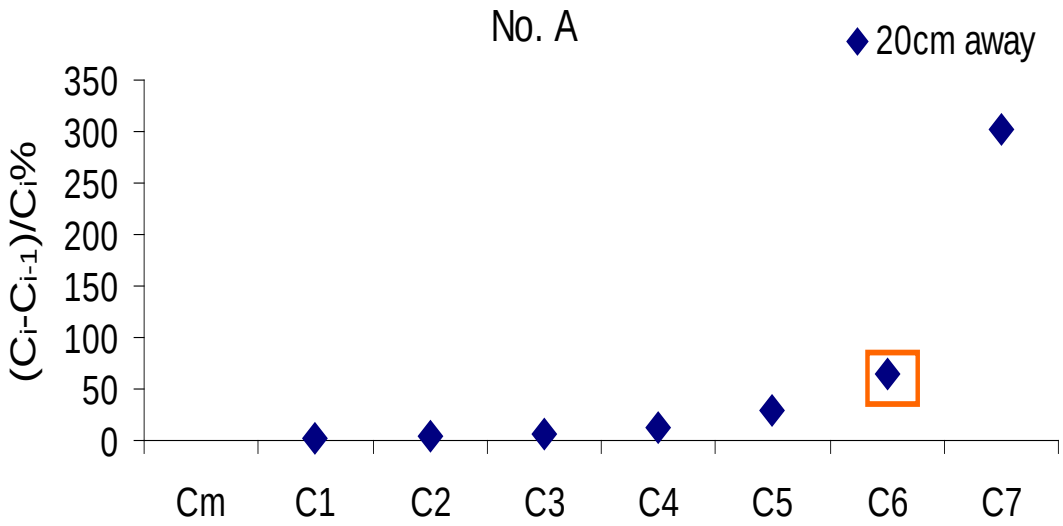

(b)

Figure 4.10: Correction of wave speeds in No. A (a) uses the last method. The difference change of correction for No. A (b) is also shown. The values surrounded by orange squares show the true wave speed.

From the figures above, it is shown that when the iteration of correcting wave speed reaches the true wave speed, there is still no sign to converge or stop the iteration.

4.5 Conclusion

When the measurement site is close to the reflection site, with the presence of reflected wave, the early part of PU-loop is still linear; Local measured wave speed determined by PU-loop has been affected. Measured wave speed increased with positive reflection; measured wave speed decreased with negative reflection. The bigger the reflection, the greater is the change of the measured wave speed. To resolve this phenomenon, an iteration has been considered to apply to correct the measured wave speed. This correction iteration improves PU-loop to determine local wave speed in short arterial segments. Further *in vivo* investigation and improvement should follow.

Chapter 5
Using WIA to Determine Local Reflection Coefficient in Flexible Tubes

5.1 Introduction

Pulse waves travelling along the arterial system will be partly reflected and partly transmitted if they meet any discontinuity in the properties of the artery, such as: changes in the cross sectional area, or local changes in the mechanical properties of the arterial wall. It is well known that arterial pressure wave reflection contributes to the increase in systolic and pulse pressure as seen with ageing and in patients with hypertension (Westerhof and O'Rourke, 1995; O'Rourke and Mancia, 1999). Timing and magnitude of wave reflection is related to coronary artery disease (Lekakis et al., 2006), left ventricular relaxation (Yano et al., 2001) and vascular stiffness (McEniery et al., 2005).

Quantification of wave reflection in the arterial system is important because it is responsible for the altered contour and amplitude of pressure waveform as it travels towards the periphery. The coefficient of wave reflection, is used when wave propagation is in a medium containing discontinuities. The reflection coefficient describes the amplitude or the energy of a reflected wave relative to an incident wave (Li et al., 1984; Alexander et al., 1989; Kelly et al., 1989a). Newman et al. (1983) studied the reflection from the elastic mismatching by an impulse technique, which enabled the magnitude and phase change of the reflection at the elastic discontinuity to be obtained. In this work, several tube combinations are examined and results are in good agreement between the measured reflection coefficient and the theoretical value.

The analysis of reflections at a discontinuity in 1-D has been discussed by Caro et al. (1978). The pulse wave is partially reflected at the discontinuity and returned to the inlet of the mother tube and the transmitted wave continues to

travel downstream in the daughter tubes. Murgo (1980) introduced the "augmentation index" (AIx), AIx is a parameter based on analysis of the pressure waveform and expresses the ratio of augmented pressure (attributed to wave reflection) to pulse pressure. However, because its value is influenced by several factors, aortic pulse wave velocity, the site and extent of wave reflection (Westerhof et al., 2006; Lemogoum et al., 2004; McEniery et al., 2005; Segers et al., 2007), AIx might not be the most appropriate parameter for an accurate quantification of the magnitude of wave reflection (Kips et al., 2009). To truly quantify the magnitude of wave reflection, both the pressure and flow wave should be recorded simultaneously at the same site then allows separation of the measured pressure waveform into its forward and backward components, as first demonstrated by Westerhof et al. (1972). Wave separation analysis is considered as a gold standard method to assess wave reflection (Nichols and O'Rourke, 2005; Westerhof et al., 2004). Wave Intensity Analysis (WIA) was introduced in 1990 by Parker and Jones (Parker and Jones, 1990). WIA is a 1-dimensional time-domain based method for the analysis of arterial waves that is based on the method of characteristics and considers pressure and velocity waveforms as successive wavefronts rather than a summation of simusoidal wavetrains. This approach has advantages in the clinical setting as it is a time domain analysis which can be easily related to physiological events. Using terminology derived from gas dynamics waves are considered to be either 'compression' waves associated with an increase in pressure or 'expansion' waves associated with a decrease in pressure.

The overall aim of this study is, therefore, to investigate using WIA methods to determine the local reflection coefficient experimentally.

5.2 Methods

5.2.1 Theoretical reflection coefficient

The value of the reflection coefficient R depends upon the area and wave speed upstream and downstream of the discontinuity. For arteries where the velocity is generally much lower than the wave speed the equation for R is valid (Pedley, 1980)

$$R_t = \frac{Y_0 - Y_1 - Y_2}{Y_0 + Y_1 + Y_2} \tag{5.1}$$

with the characteristic admittamce of the vessel defined as

$$Y = \frac{1}{Z} = \frac{A}{\rho c} \tag{5.2}$$

where Z is characteristic impedance, ρ is fluid density, A is initial cross-sectional area and c is wave speed upstream of the reflection site is 0, downstream are 1 and 2.

In this study, reflection coefficient is calculated in single vessel without bifurcation, equation (5.1) could be simplified as

$$R_t = \frac{\frac{A_0}{c_0} - \frac{A_1}{c_1}}{\frac{A_0}{c_0} + \frac{A_1}{c_1}} \tag{5.3}$$

For complete positive reflection (closed end), A_1=0 for which R_t = 1

For complete negative reflection (open end), A_1=∞ for which R_t = -1

5.2.2 Wave intensity analysis

Wave intensity analysis (WIA) views any wave as being composed of small incremental waves or wavefronts and that the intensity of a wave is a measure of energy flux density carried by the wave (Parker et al., 1988; Parker and Jones, 1990). The magnitude of wave intensity is calculated by multiplying the change in pressure by the change in velocity.

$$dI = dPdU \tag{5.4}$$

dI can be separated into forward wave intensity $dI_+ = dP_+ dU_+$ and backward wave intensity $dI_- = dP_- dU_-$, which can be obtained from measurement of P and U, and knowledge of wave speed:

$$dI_{\pm} = \pm \frac{1}{4\rho c}(dP \pm \rho c dU)^2 \tag{5.5}$$

Equation (5.5) shows that forward wave intensity is always positive and backward wave intensity is always negative. Furthermore, the forward and backward wave energy can be obtained by integration of $dI_{\pm}$ with respect to time.

$$I_{\pm} = \int_0^T dI_{\pm} dt \tag{5.6}$$

5.2.3 Calculation of reflection coefficients

Three approaches have been established to calculate R using WIA. The first uses the ratio of changes in pressure related to the forward (dP_+) and backward (dP_-) waves,

$$R_{dP} = \frac{dP_-}{dP_+} \tag{5.7}$$

The second approach, R has been obtained as the ratio of minimum backward wave intensity (dI_-) to peak forward wave intensity (dI_+) as follows:

$$R_{dI} = \pm \frac{|dI_-|}{dI_+} \tag{5.8}$$

The third approach, R has been calculated as the ratio of the area under the first peak of forward wave intensity, forward wave energy (I_+) to the area under the backward wave intensity, backward wave energy (I_-),

$$R_I = \pm \frac{|I_-|}{I_+} \tag{5.9}$$

The sign of both R_{dI} and R_I is positive (+) if the reflected wave is the same type as the incident wave and negative (-) if they are different.

The square roots of R_{dI} and R_I are also presented,

$$R_{dI}^{0.5} = \pm \sqrt{\frac{|dI_-|}{dI_+}} \tag{5.10}$$

$$R_I^{0.5} = \pm \sqrt{\frac{|I_-|}{I_+}} \tag{5.11}$$

5.2.4 Transmission coefficient

The transmission coefficient T is simply related to the reflection coefficient

$$T = 1 + R \tag{5.12}$$

5.2.5 Experimental setup

The general experimental setup of this study is the same as shown in **Figure 4.3**, the individual elements and the measurements are all described in section 4.2.3.

5.3 Results

5.3.1 Mean values of reflection coefficients

In **Figure 5.1**, the mean values of the local reflection coefficients R_{dP}, $R_{dI}^{0.5}$, $R_{I}^{0.5}$, R_{dI}, and R_{I} along each tube were plotted when R_t is varied between -0.60 and 0.36. It is found out that the results of mean values of three different methods R_{dP}, $R_{dI}^{0.5}$ and $R_{I}^{0.5}$ are very close to each other, and close to the theoretical reflection coefficient R_t. The mean values of the other two methods R_{dI}, and R_{I} are very close to each other, but not close to R_t.

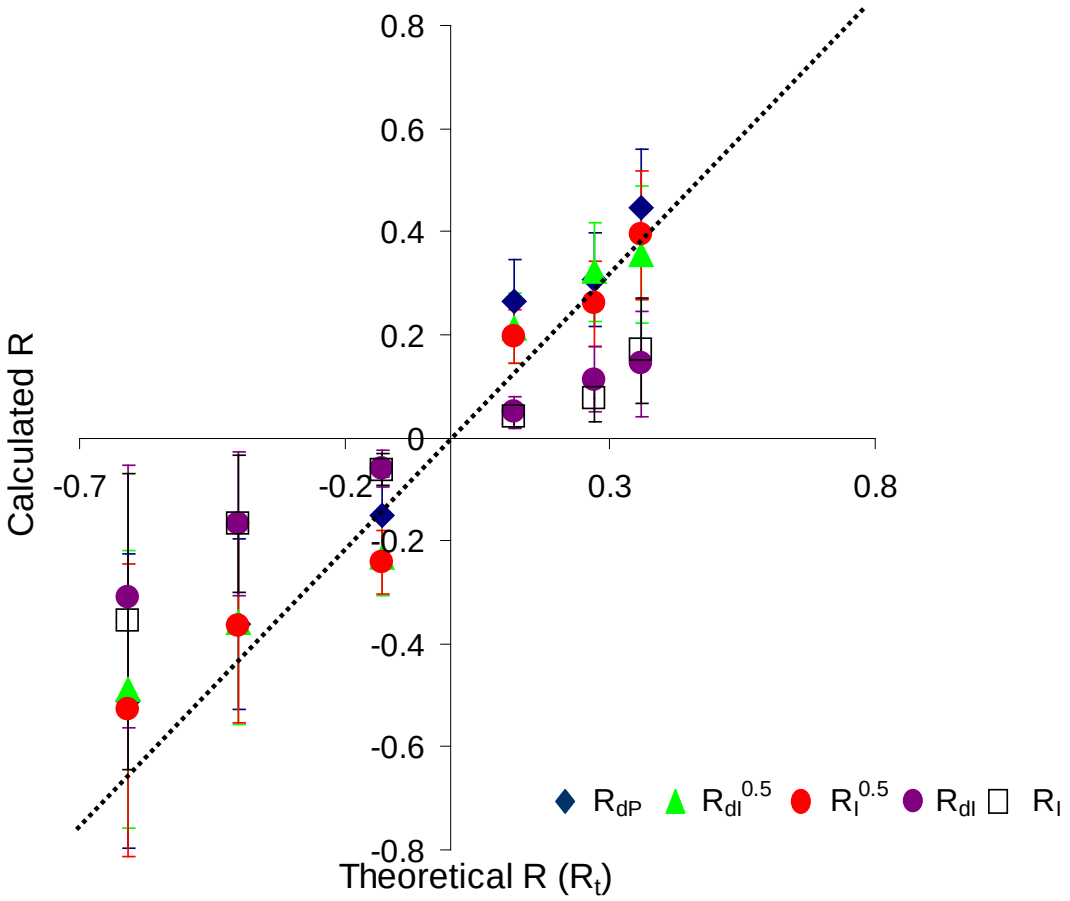

Figure 5.1: The mean values of local reflection coefficients in all sets compare to the theoretical reflection coefficient. The black dash line is the identity line. The values of Rt are -0.60, -0.39, -0.12, 0.12, 0.28 and 0.36, respectively shown in x axis.

5.3.2 Local reflection coefficient

Figure 5.2 to **Figure 5.4** show the local reflection coefficients of all the sets. It is seen that the values of the local reflection coefficient are increasing when the measurement site is close to the reflection site with the positive reflection, and decreasing with the negative reflection. The values of the three methods R_{dP}, $R_{dI}^{0.5}$ and $R_{I}^{0.5}$ are very close to each other at each measurement site in each set. The values of R_{dI}, and R_{I} are close to each other, and the values of R_{dI}, and R_{I} close to the reflection site are very close to R_t (the black solid horizontal lines show the values of R_t for each set). The mean values of these five methods for all 6 sets were calculated (**Table 5.1**), the results indicate that methods R_{dP}, $R_{dI}^{0.5}$ and $R_{I}^{0.5}$ are very close to each other, values of R_{dI}, and R_{I} are close to each other.

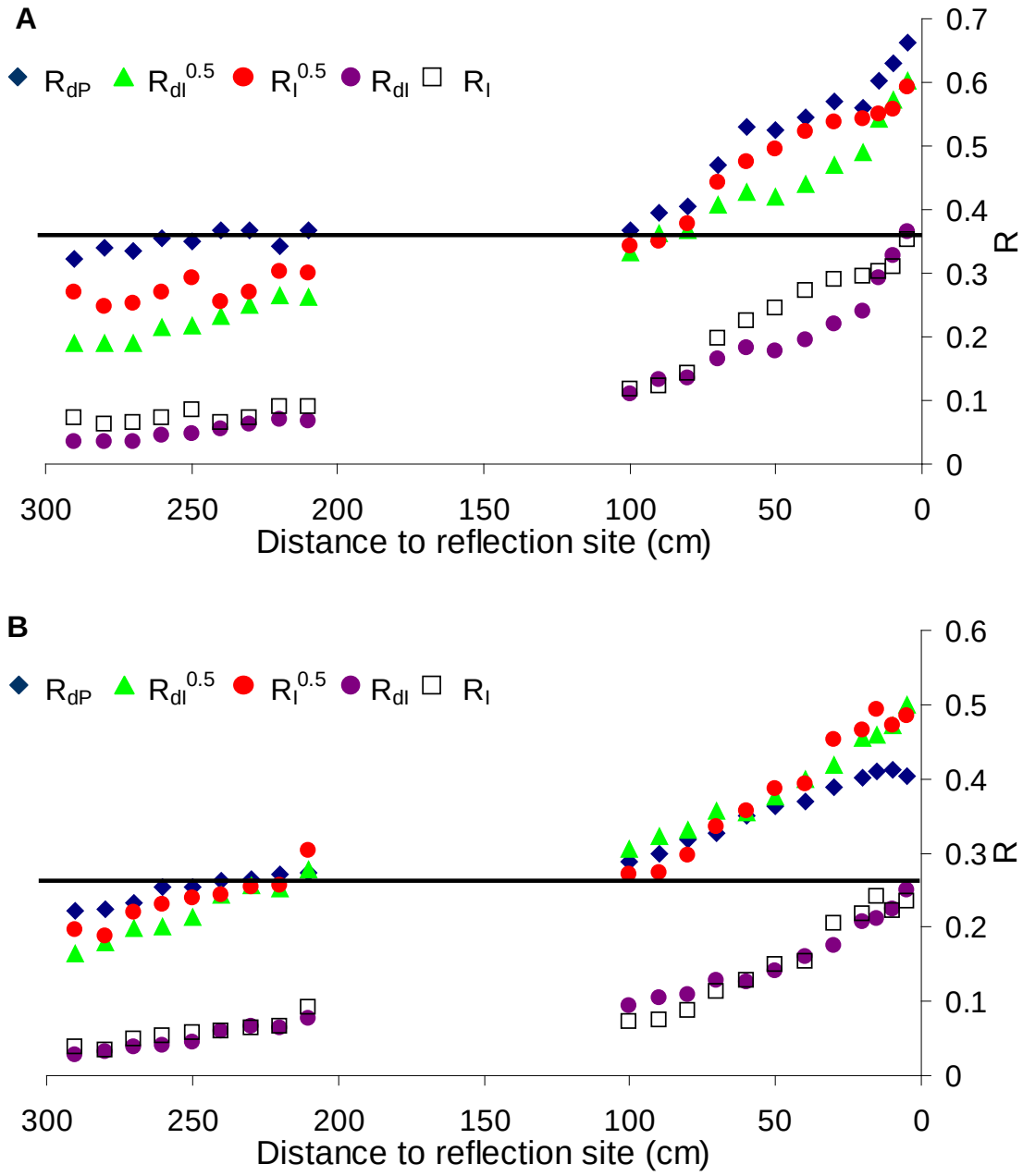

Figure 5.2: Local reflections determined by R_{dP}, $R_{dI}^{0.5}$, $R_I^{0.5}$, R_{dI}, and R_I for Sets A and B. The values of R_t are 0.36 and 0.28, respectively. The solid horizontal lines show the values of R_t.

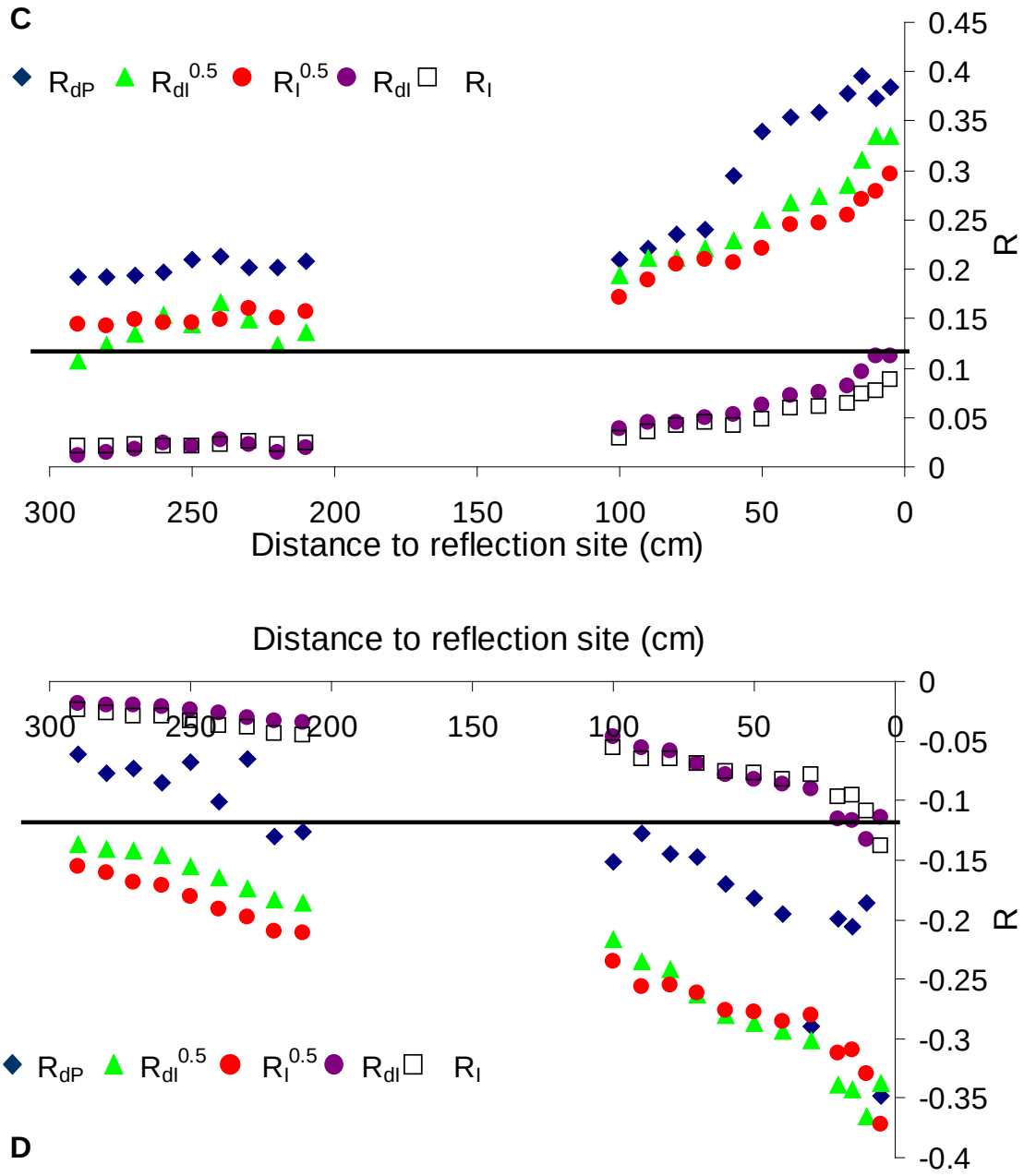

Figure 5.3: Local reflections determined by R_{dP}, $R_{dI}^{0.5}$, $R_I^{0.5}$, R_{dI}, and R_I for Sets C and D. The values of R_t are 0.12 and -0.12, respectively. The solid horizontal lines show the values of R_t.

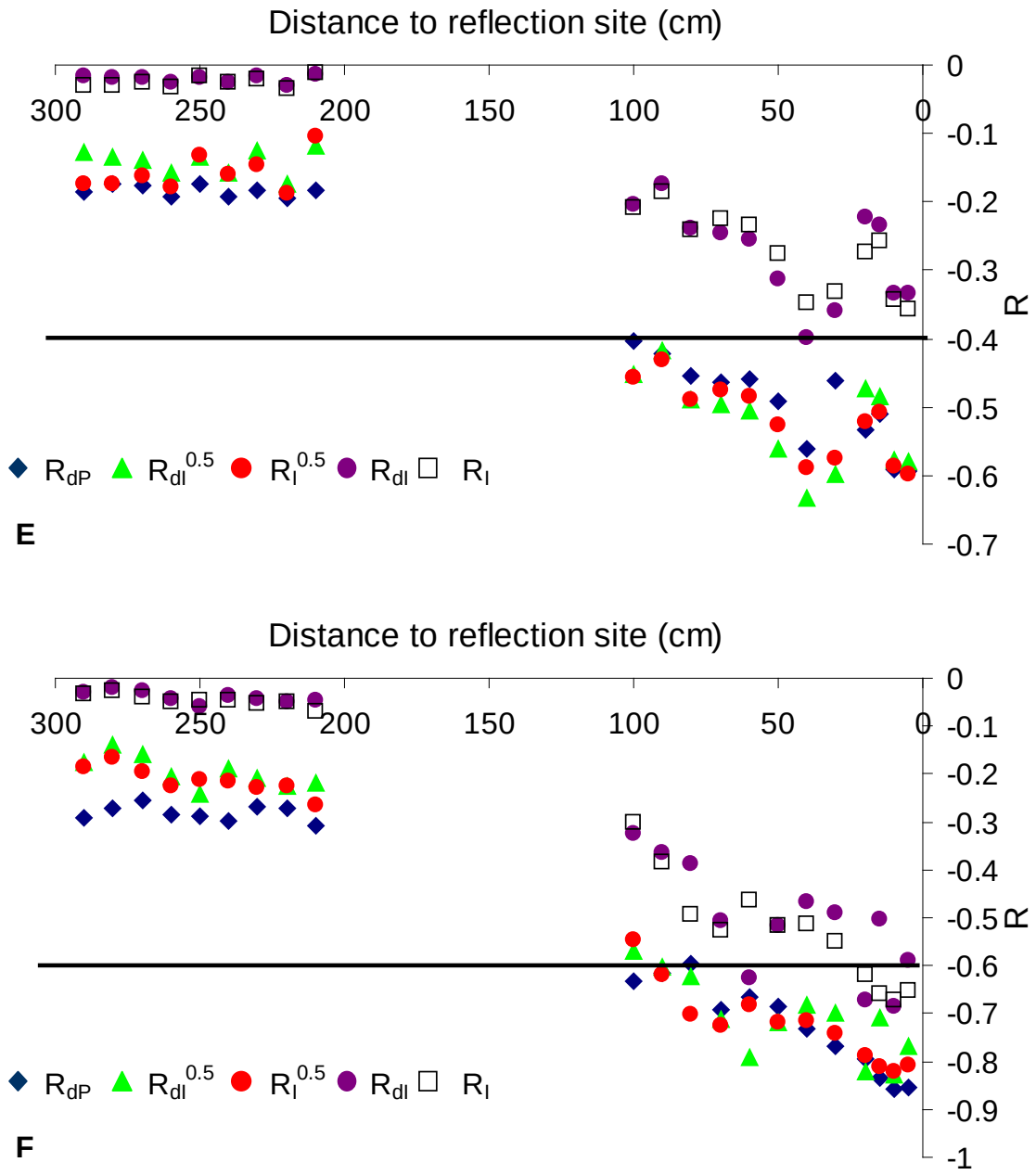

Figure 5.4: Local reflections determined by R_{dP}, $R_{dl}^{0.5}$, $R_{l}^{0.5}$, R_{dl}, and R_{l} for Sets E and F. The values of R_t are -0.39 and -0.60, respectively. The solid horizontal lines show the values of R_t.

Table 5.1 Local reflection coefficients determined for all sets of tubes (No. A and B)

Site (cm)	R (Set No. A)					R (Set No. B)				
	R_{dP}	$R_{dI}^{0.5}$	$R_{I}^{0.5}$	R_{dI}	R_{I}	R_{dP}	$R_{dI}^{0.5}$	$R_{I}^{0.5}$	R_{dI}	R_{I}
290	0.32	0.19	0.27	0.04	0.07	0.22	0.17	0.20	0.03	0.04
280	0.34	0.19	0.25	0.04	0.06	0.22	0.18	0.19	0.03	0.03
270	0.34	0.19	0.25	0.04	0.06	0.23	0.20	0.22	0.04	0.05
260	0.36	0.21	0.27	0.05	0.07	0.25	0.20	0.23	0.04	0.05
250	0.35	0.22	0.29	0.05	0.09	0.25	0.21	0.24	0.05	0.06
240	0.37	0.23	0.26	0.05	0.07	0.26	0.24	0.24	0.06	0.06
230	0.37	0.25	0.27	0.06	0.07	0.26	0.26	0.25	0.07	0.06
220	0.34	0.26	0.30	0.07	0.09	0.27	0.25	0.26	0.06	0.07
210	0.37	0.26	0.30	0.07	0.09	0.27	0.28	0.30	0.08	0.09
100	0.37	0.33	0.34	0.11	0.12	0.29	0.31	0.27	0.09	0.07
90	0.39	0.36	0.35	0.13	0.12	0.30	0.32	0.27	0.10	0.08
80	0.40	0.37	0.38	0.14	0.14	0.32	0.33	0.30	0.11	0.09
70	0.47	0.41	0.44	0.17	0.20	0.33	0.36	0.34	0.13	0.11
60	0.53	0.43	0.47	0.18	0.23	0.35	0.35	0.36	0.13	0.13
50	0.52	0.42	0.49	0.18	0.24	0.36	0.38	0.39	0.14	0.15
40	0.54	0.44	0.52	0.19	0.27	0.37	0.40	0.39	0.16	0.15
30	0.57	0.47	0.54	0.22	0.29	0.39	0.42	0.45	0.18	0.20
20	0.56	0.49	0.54	0.24	0.30	0.40	0.45	0.47	0.21	0.22
15	0.60	0.54	0.55	0.29	0.30	0.41	0.46	0.49	0.21	0.24
10	0.63	0.57	0.56	0.33	0.31	0.41	0.47	0.47	0.22	0.22
5	0.66	0.60	0.59	0.36	0.35	0.40	0.50	0.49	0.25	0.24
Mean	0.45	0.35	0.39	0.14	0.17	0.31	0.32	0.32	0.11	0.12
SD	0.11	0.13	0.12	0.10	0.10	0.07	0.10	0.10	0.07	0.07

Table 5.1 Local reflection coefficients determined for all sets of tubes (No. C and D)

Site (cm)	R (Set No.C)					R (Set No. D)				
	R_{dP}	$R_{dI}^{0.5}$	$R_{I}^{0.5}$	R_{dI}	R_{I}	R_{dP}	$R_{dI}^{0.5}$	$R_{I}^{0.5}$	R_{dI}	R_{I}
290	0.19	0.11	0.14	0.01	0.02	-0.06	-0.14	-0.16	-0.02	-0.02
280	0.19	0.12	0.14	0.02	0.02	-0.08	-0.14	-0.16	-0.02	-0.03
270	0.19	0.13	0.15	0.02	0.02	-0.07	-0.14	-0.17	-0.02	-0.03
260	0.20	0.15	0.15	0.02	0.02	-0.08	-0.15	-0.17	-0.02	-0.03
250	0.21	0.14	0.15	0.02	0.02	-0.07	-0.16	-0.18	-0.02	-0.03
240	0.21	0.17	0.15	0.03	0.02	-0.10	-0.16	-0.19	-0.03	-0.04
230	0.20	0.15	0.16	0.02	0.03	-0.07	-0.17	-0.20	-0.03	-0.04
220	0.20	0.12	0.15	0.02	0.02	-0.13	-0.18	-0.21	-0.03	-0.04
210	0.21	0.14	0.16	0.02	0.02	-0.13	-0.19	-0.21	-0.03	-0.04
100	0.21	0.19	0.17	0.04	0.03	-0.15	-0.22	-0.24	-0.05	-0.06
90	0.22	0.21	0.19	0.04	0.04	-0.13	-0.24	-0.26	-0.06	-0.07
80	0.24	0.21	0.21	0.04	0.04	-0.15	-0.24	-0.26	-0.06	-0.07
70	0.24	0.22	0.21	0.05	0.04	-0.15	-0.26	-0.26	-0.07	-0.07
60	0.30	0.23	0.21	0.05	0.04	-0.17	-0.28	-0.28	-0.08	-0.08
50	0.34	0.25	0.22	0.06	0.05	-0.18	-0.29	-0.28	-0.08	-0.08
40	0.35	0.27	0.24	0.07	0.06	-0.19	-0.29	-0.29	-0.09	-0.08
30	0.36	0.27	0.25	0.07	0.06	-0.29	-0.30	-0.28	-0.09	-0.08
20	0.38	0.28	0.25	0.08	0.06	-0.20	-0.34	-0.31	-0.12	-0.10
15	0.40	0.31	0.27	0.10	0.07	-0.21	-0.34	-0.31	-0.12	-0.10
10	0.37	0.34	0.28	0.11	0.08	-0.19	-0.36	-0.33	-0.13	-0.11
5	0.38	0.33	0.30	0.11	0.09	-0.35	-0.34	-0.37	-0.11	-0.14
Mean	0.27	0.21	0.20	0.05	0.04	-0.15	-0.23	-0.24	-0.06	-0.06
SD	0.08	0.07	0.05	0.03	0.02	0.07	0.08	0.06	0.04	0.03

Table 5.1 Local reflection coefficients determined for all sets of tubes (No. E and F)

Site (cm)	R (Set No. E)					R (Set No. F)				
	R_{dP}	$R_{dI}^{0.5}$	$R_{I}^{0.5}$	R_{dI}	R_{I}	R_{dP}	$R_{dI}^{0.5}$	$R_{I}^{0.5}$	R_{dI}	R_{I}
290	-0.19	-0.13	-0.17	-0.02	-0.03	-0.29	-0.18	-0.19	-0.03	-0.03
280	-0.17	-0.13	-0.17	-0.02	-0.03	-0.27	-0.14	-0.17	-0.02	-0.03
270	-0.18	-0.14	-0.16	-0.02	-0.03	-0.26	-0.16	-0.20	-0.03	-0.04
260	-0.19	-0.16	-0.18	-0.02	-0.03	-0.28	-0.20	-0.23	-0.04	-0.05
250	-0.17	-0.14	-0.13	-0.02	-0.02	-0.29	-0.24	-0.21	-0.06	-0.05
240	-0.19	-0.16	-0.16	-0.02	-0.03	-0.30	-0.19	-0.22	-0.04	-0.05
230	-0.18	-0.12	-0.15	-0.02	-0.02	-0.27	-0.21	-0.23	-0.04	-0.05
220	-0.19	-0.17	-0.19	-0.03	-0.04	-0.27	-0.23	-0.23	-0.05	-0.05
210	-0.18	-0.12	-0.10	-0.01	-0.01	-0.31	-0.22	-0.27	-0.05	-0.07
100	-0.40	-0.45	-0.46	-0.20	-0.21	-0.63	-0.57	-0.55	-0.32	-0.30
90	-0.42	-0.42	-0.43	-0.17	-0.19	-0.61	-0.60	-0.62	-0.36	-0.38
80	-0.45	-0.49	-0.49	-0.24	-0.24	-0.60	-0.62	-0.70	-0.39	-0.49
70	-0.46	-0.50	-0.48	-0.25	-0.23	-0.69	-0.71	-0.72	-0.51	-0.53
60	-0.46	-0.50	-0.48	-0.25	-0.23	-0.66	-0.79	-0.68	-0.63	-0.46
50	-0.49	-0.56	-0.53	-0.31	-0.28	-0.69	-0.72	-0.72	-0.52	-0.51
40	-0.56	-0.63	-0.59	-0.40	-0.35	-0.73	-0.68	-0.72	-0.47	-0.51
30	-0.46	-0.60	-0.58	-0.36	-0.33	-0.77	-0.70	-0.74	-0.49	-0.55
20	-0.53	-0.47	-0.52	-0.22	-0.27	-0.79	-0.82	-0.79	-0.67	-0.62
15	-0.51	-0.48	-0.51	-0.24	-0.26	-0.83	-0.71	-0.81	-0.50	-0.66
10	-0.59	-0.58	-0.59	-0.33	-0.34	-0.86	-0.83	-0.82	-0.68	-0.67
5	-0.59	-0.58	-0.60	-0.33	-0.36	-0.85	-0.77	-0.81	-0.59	-0.65
Mean	-0.36	-0.36	-0.36	-0.17	-0.17	-0.53	-0.49	-0.50	-0.31	-0.32
SD	0.17	0.20	0.19	0.14	0.13	0.24	0.27	0.27	0.25	0.26

5.3.3 Wave separation

Figure 5.5 show the peaks of separated forward and backward pressure for all six sets. From the figure, it is found out that due to the wave dissipation, the forward pressure decreases when the pulse wave travels ahead to the reflection site. When the pulse wave passes the reflection site and travel back to the inlet of the tube, the backward pressure (reflected pressure) also decreases due to the dissipation. The forward and backward wave intensity and wave energy also follow this rule shown in **Figure 5.6** and **Figure 5.7**.

Also from **Figure 5.5**, it is seen that the peaks of the forward pressure wave are almost the same in all six sets, the exponential decrease and the equation for the exponential decrease are similar. This is because the forward pressure wave is related to the pump which generates the pulse wave and the mechanical properties of the mother tube, but not affected by the reflection. **Figure 5.6** and **Figure 5.7** also shown that the forward wave intensity and wave energy are similar in all six sets.

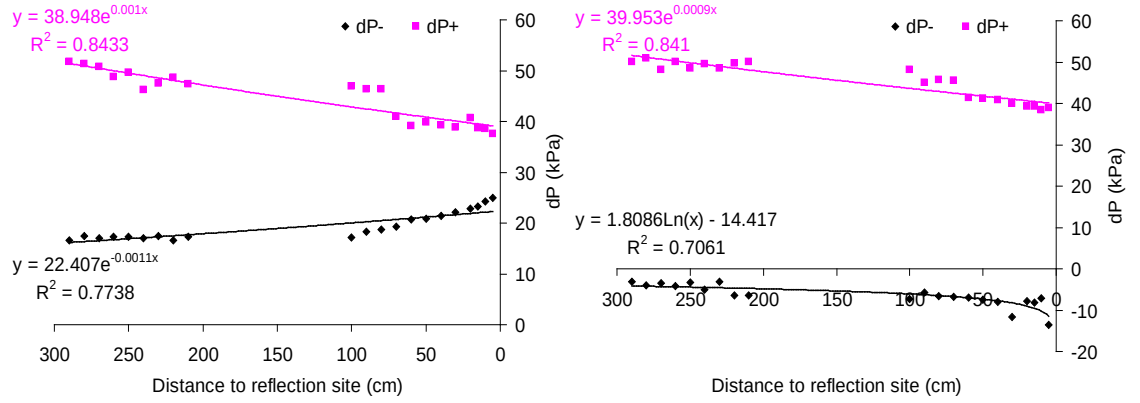

(a) R_t=0.36

(b) R_t=-0.12

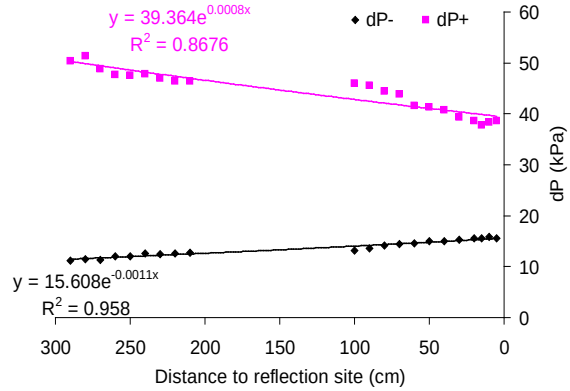

(c) R_t=0.28

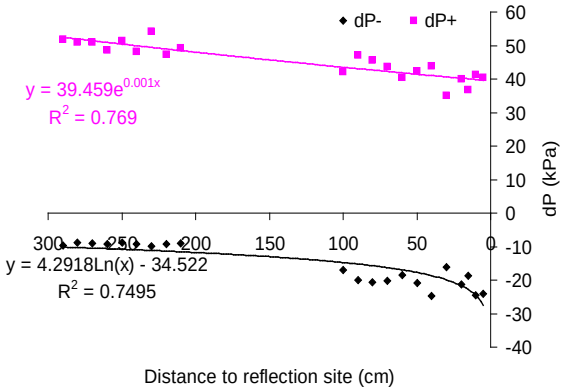

(d) R_t=-0.39

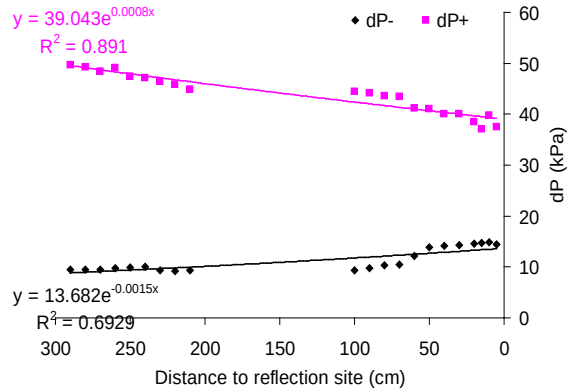

(e) R_t=0.12

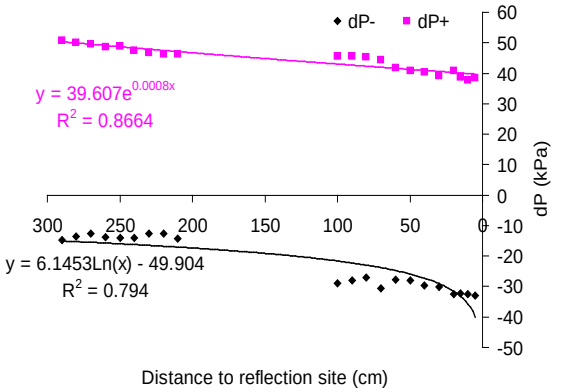

(f) R_t=-0.60

Figure 5.5: The peaks of separated forward and backward pressure waves are plotted against the distance to reflection site for all six sets. The forward and backward pressures are dissipating exponentially (pink and blue exponential lines) along the mother tube, respectively.

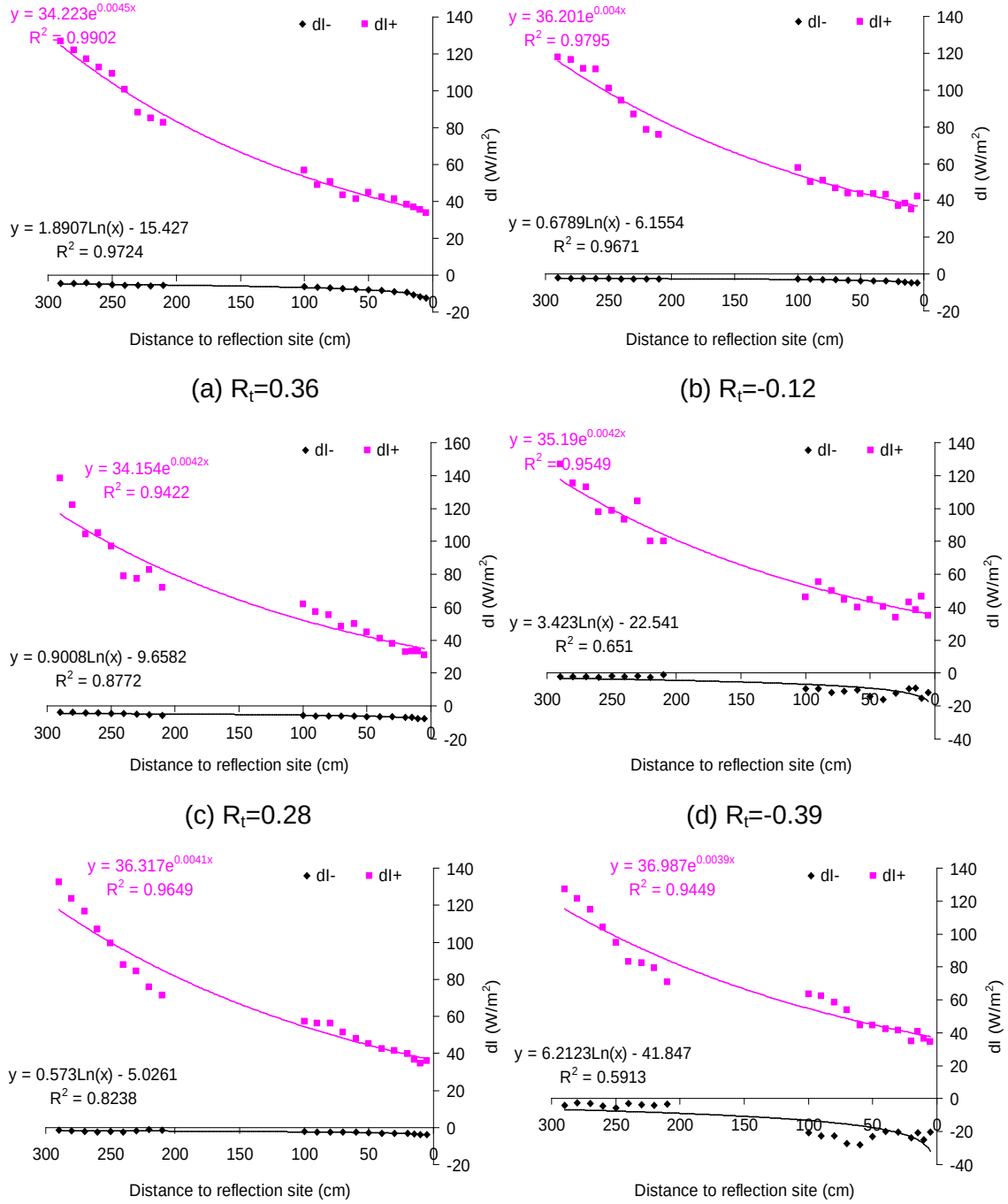

Figure 5.6: The peaks of separated forward and backward wave intensities are plotted against the distance to reflection site for all six sets. The forward and backward wave intensities are dissipating exponentially (pink and blue exponential lines) along the mother tube, respectively.

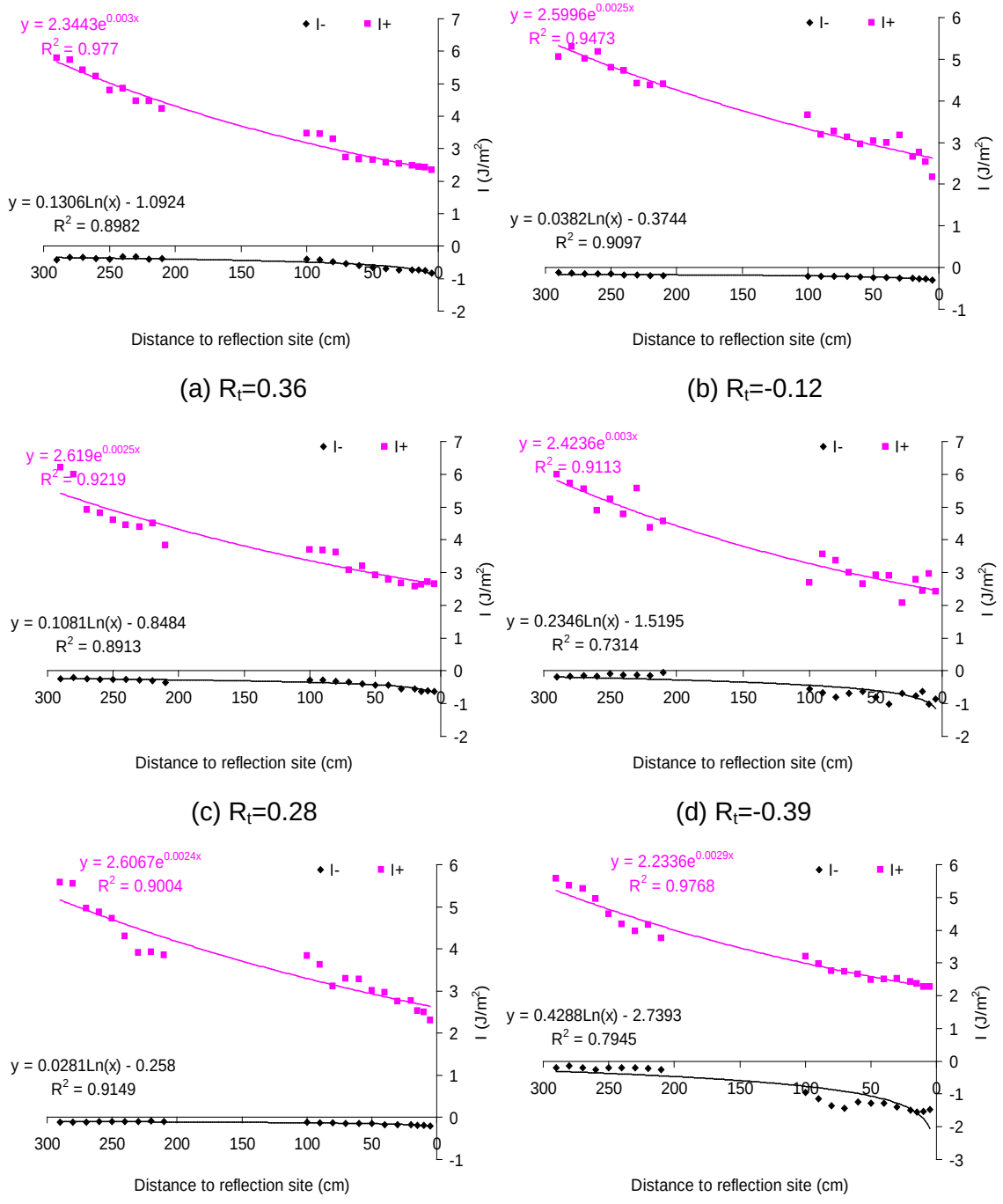

Figure 5.7: The separated forward and backward wave energies are plotted against the distance to reflection site for all six sets. The forward and backward wave energies are dissipating exponentially (pink and blue exponential lines) along the mother tube, respectively.

The backward pressure, wave intensity and wave energy are different in different sets according to the different reflection. For the positive reflection coefficient, the backward pressure is also positive, and negative backward pressure is related to negative reflection. Due to the value of the reflection coefficient, the magnitude of the backward pressure is also different. The same applied to the wave intensity and wave energy in **Figure 5.6** and **Figure 5.7**. In order to see the differences of backward wave between these tubes, the normalised backward pressures (**Figure 5.8**), backward wave intensities (**Figure 5.9**) and backward wave energies (**Figure 5.10**) are plotted. All the normalised wave dissipation equations are shown in **Table 5.2**.

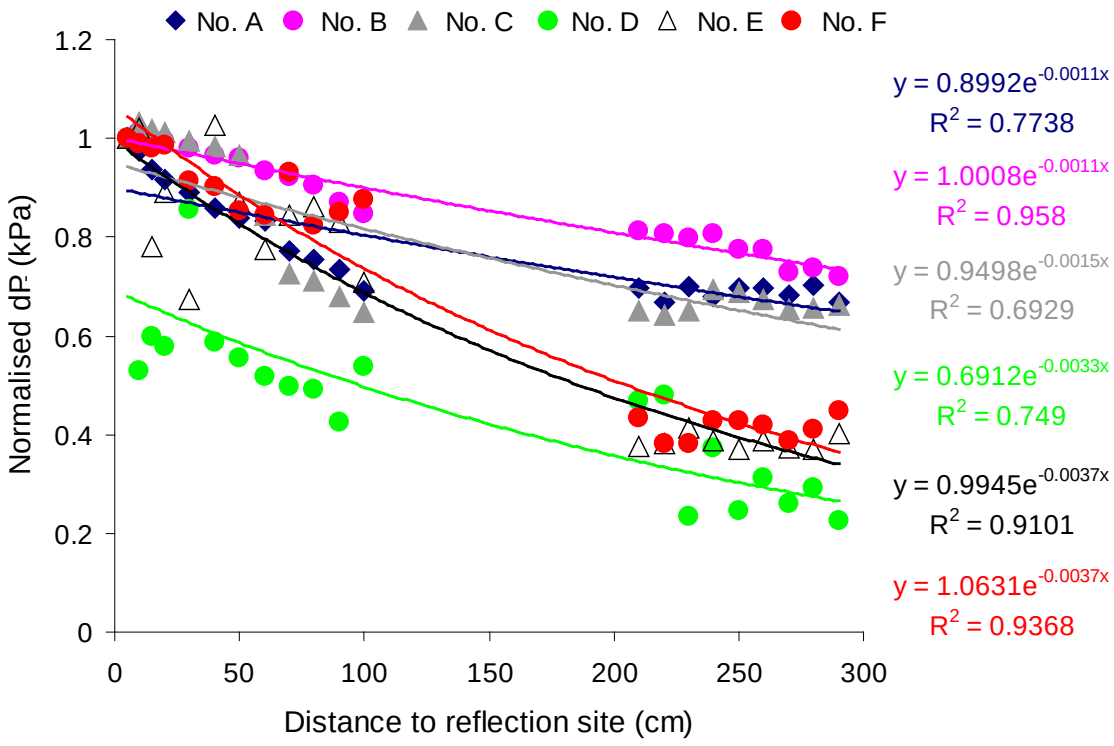

Figure 5.8: Normalised backward pressures against distance to reflection site in all sets.

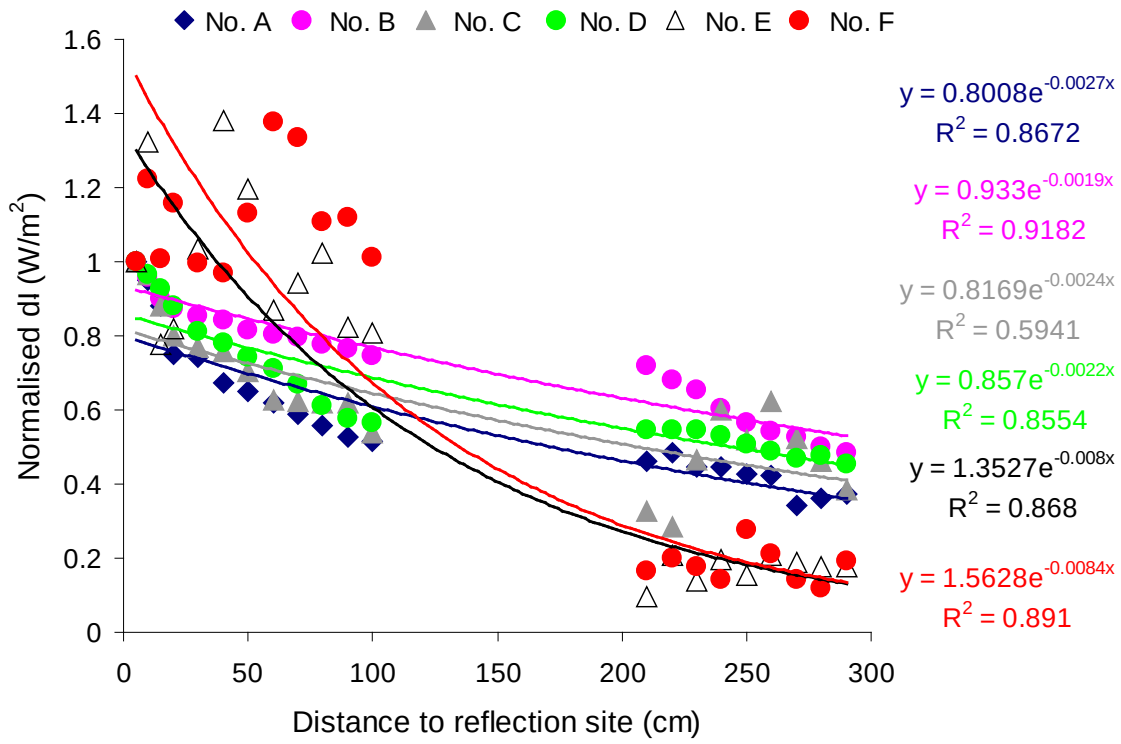

Figure 5.9: Normalised backward wave intensities against distance to reflection site in all sets.

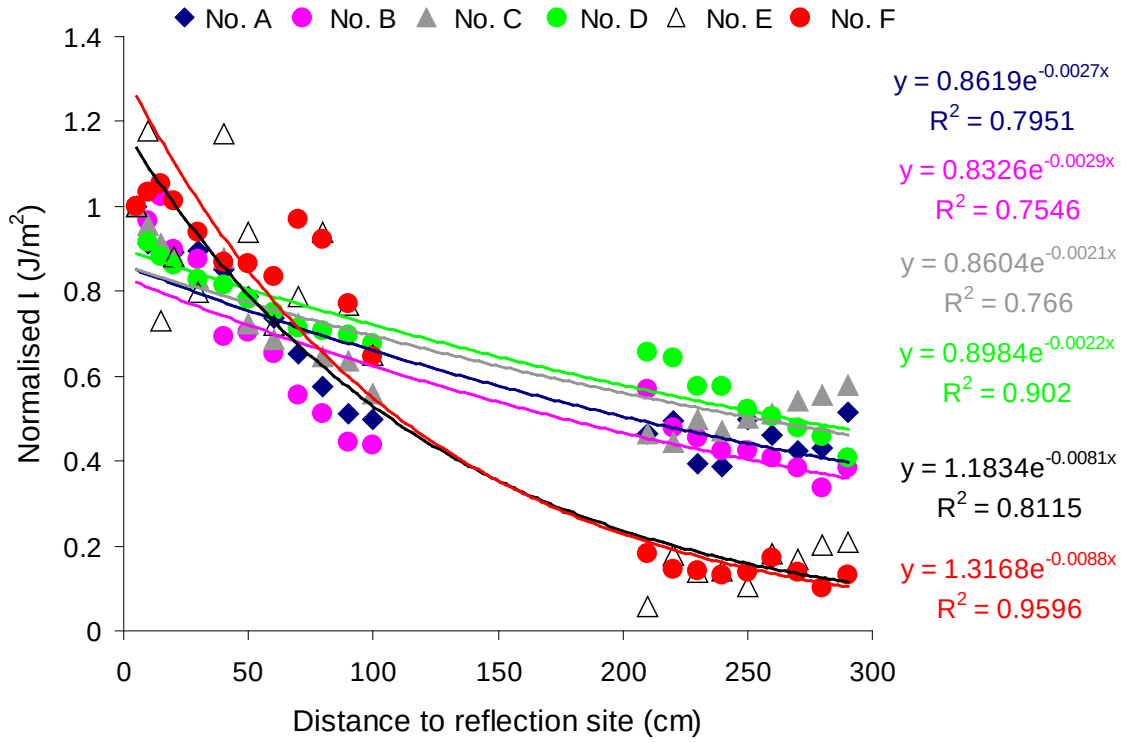

Figure 5.10: Normalised backward wave energies against distance to reflection site in all sets.

Table 5.2 Normalised wave dissipation equations for all six sets.

Set	Normalised wave dissipation equation					
	P		dI		I	
	P_+	P_-	dI_+	dI_-	I_+	I_-
A	$0.75e^{0.001x}$	$0.90e^{-0.0011x}$	$0.27e^{0.0045x}$	$0.80e^{-0.0027x}$	$0.40e^{0.003x}$	$0.86e^{-0.0027x}$
B	$0.78e^{0.0008x}$	$1.00e^{-0.0011x}$	$0.25e^{0.0042x}$	$0.93e^{-0.0019x}$	$0.42e^{0.0025x}$	$0.83e^{-0.0029x}$
C	$0.79e^{0.0008x}$	$0.95e^{-0.0015x}$	$0.27e^{0.0041x}$	$0.82e^{-0.0024x}$	$0.47e^{0.0024x}$	$0.86e^{-0.0021x}$
D	$0.80e^{0.0009x}$	$0.69e^{-0.0033x}$	$0.31e^{0.004x}$	$0.86e^{-0.0022x}$	$0.51e^{0.0025x}$	$0.90e^{-0.0022x}$
E	$0.76e^{0.001x}$	$0.99e^{-0.0037x}$	$0.28e^{0.0042x}$	$1.35e^{-0.008x}$	$0.40e^{0.003x}$	$1.18e^{-0.0081x}$
F	$0.78e^{0.0008x}$	$1.06e^{-0.0037x}$	$0.29e^{0.0039x}$	$1.56e^{-0.0084x}$	$0.40e^{0.0029x}$	$1.32e^{-0.0088x}$

5.3.4 Transmission coefficient

It is known that transmission coefficient equal to one plus the reflection coefficient, equation (5.12). In order to examine the internal consistency of the experiments, the transmission coefficient was calculated. **Table 5.3** shows the measured, forward and backward pressure in the mother tube for all the sets. For set A, the forward pressure is 46.90 kPa, backward pressure is 17.90 kPa, so the reflection coefficient calculated by the ratio of the forward pressure over backward pressure is 0.38. **Table 5.3** shows that measured pressure is 65.87 kPa in daughter tube in set A, neglect the experimental error, the measured pressure in the daughter tube is equal to the summation of the forward and backward pressures in the mother tube, and indicate that transmission coefficient equal to reflection coefficient plus one.

Table 5.3 Measured pressure and separated pressure in mother tube at 100 cm away from the reflection site, and calculated transmission coefficient in daughter tube. P: measured pressure in mother tube, P_+: forward pressure, P_-: backward pressure, R_{dP}: local reflection coefficient calculated as P_-/P_+, P_d: measured pressure in daughter tube, T: transmission coefficient.

Set	Mother tube				Daughter tube		
	P (kPa)	P_+ (kPa)	P_- (kPa)	R_{dP}	P_d (kPa)	T=1+R	$T=(P_d/P_+)$
A	61.75	46.90	17.90	0.38	65.87	1.38	1.40
B	58.87	45.99	13.12	0.29	56.30	1.29	1.22
C	54.58	44.81	9.05	0.20	56.01	1.20	1.25
D	45.53	48.38	-7.14	-0.15	45.11	0.93	0.85
E	39.05	42.25	-15.83	-0.37	24.21	0.63	0.49
F	32.16	45.37	-27.57	-0.61	21.35	0.39	0.47

5.3.5 Contribution of elastic mismatch on wave reflection

The reflection depends on the wave speed and cross-sectional area of the upstream and downstream of the discontinuity according to equation (5.3). Any change in wave speed or area will cause the change of the reflection. Wave speed is related to the properties of the vessel wall according to equation (1.2); The elastic mismatch was formed in this work by connecting two tubes with different internal diameter, wall thickness or material. From **Table 5.4**, **Figure 5.11** and **Figure 5.12**, it is found that a) when the materials of the mother tube and the daughter tube are the same (silicone material), and the cross-sectional area of the daughter tube (Area: 64 mm^2) is smaller than that of the mother tube (Area: 100 mm^2), wave speed in the daughter tube (A: c=26.7±2.8 m/s, B: c=22.3±1.5 m/s) is bigger than that in the mother tube (c=20.0±5.3 m/s), it generates positive reflection (A: R_t=0.36, B: R_t=0.28). When the cross-sectional area of the daughter tube (Area: 144 mm^2) is bigger than that of the mother tube, wave speed in the daughter tube (c=18.89±2.1 m/s) is smaller than that in the mother tube, it generates negative reflection (D: R_t=-0.12); b) when the areas of the mother tube and the daughter tube are the same (Area: 100 mm^2), and the wave speed of the daughter tube (c=25.3±1.5 m/s) is bigger than that of the mother tube, it will generate positive reflection (C: R_t=0.12); c) when the wave speeds in the daughter tube (c=20.7±6.2 m/s) and mother tube are smilar, the reflection will depend on the cross-sectional area of the daughter tube (Area: 441 mm^2) and the mother tube. Bigger cross-sectional area of the daughter tube generates negative reflection (F: R_t=-0.60).

Table 5.4 Area, wave speed (c) and Young's modulus (E) of all the tubes.

	Mother tube	Daughter tube					
No.		A	B	C	D	E	F
Area (mm^2)	100	64	64	100	144	278.89	441
c (m/s)	20.0±5.3	26.7±2.8	22.3±1.5	25.3±1.5	18.89±2.1	23.9±5.0	20.7±6.2
E (MPa)	3.84±0.05	2.90±0.06	3.26±0.06	3.28±0.06	3.10±0.10	4.77±0.20	3.76±0.01
R_t		0.36	0.28	0.12	-0.12	-0.39	-0.60

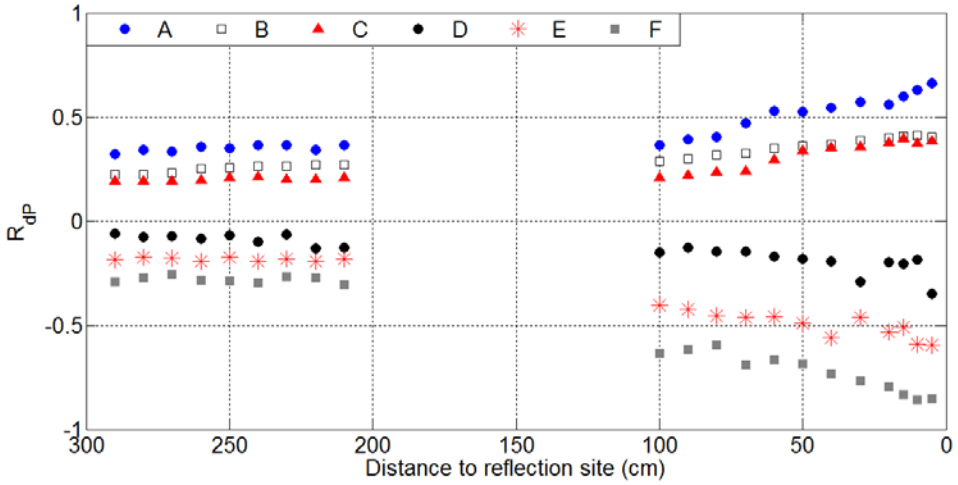

(a)

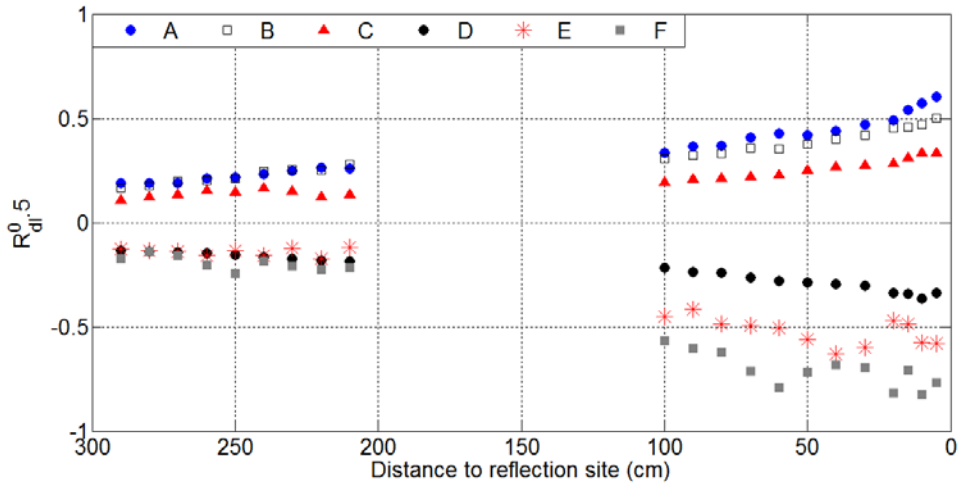

(b)

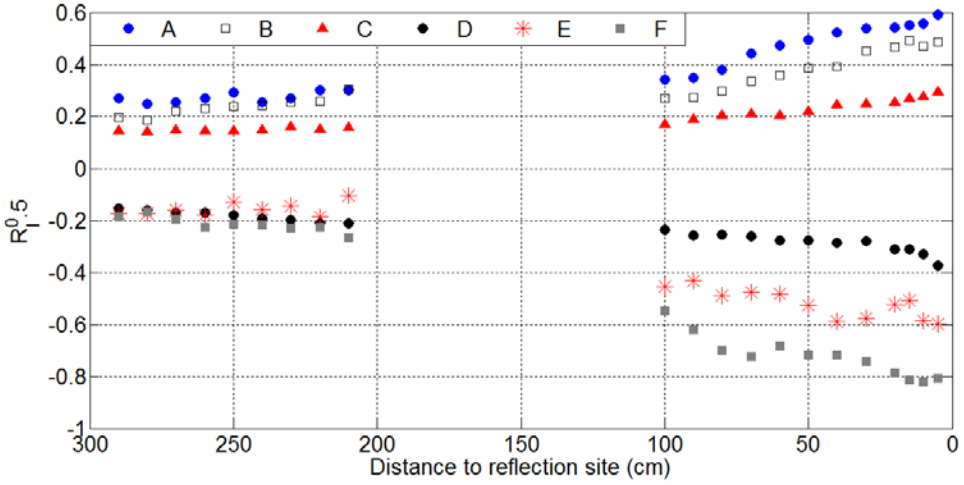

(c)

Figure 5.11: Local reflection coefficients determined as R_{dP} (a), $R_{dI}^{0.5}$ (b) and $R_{I}^{0.5}$ (c) for all sets of tubes.

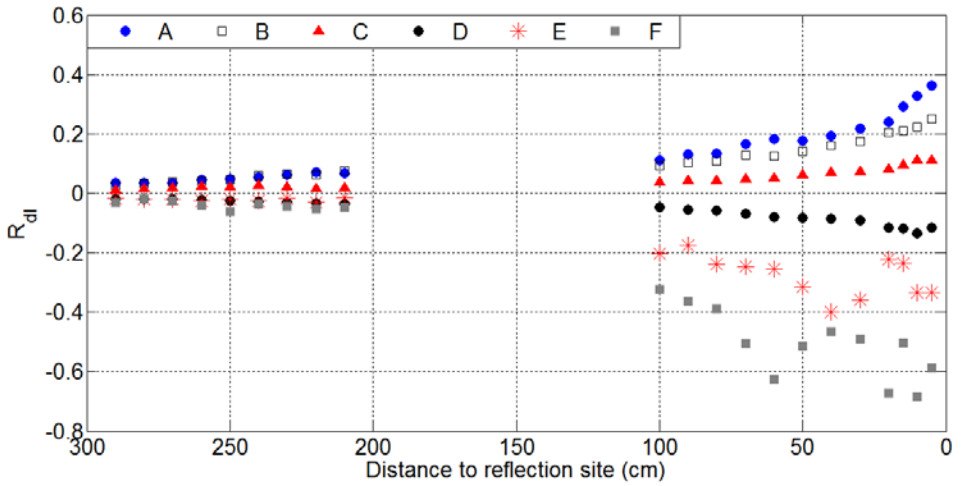

(a)

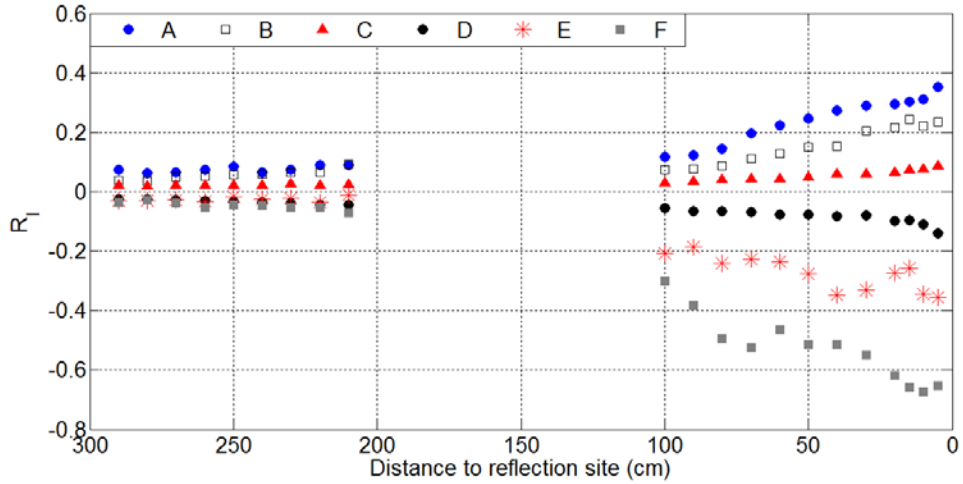

(b)

Figure 5.12: Local reflection coefficients determined as R_{dl} (a) and R_l (b) for all sets of tubes.

5.4 Discussion

In this study, it is experimentally investigated the WIA methods to determine the local reflection coefficient. R_{dP}, $R_{dI}^{0.5}$, $R_I^{0.5}$, R_{dI}, and R_I are the five methods used in this study to calculate the local reflection coefficient, and their results are compared with the theoretical reflection coefficient. From the results, it is known that all the reflection coefficients determined by different methods increased or decreased (depend on the type of the reflection site) towards the reflection site. Values of R_{dI} and R_I close to the reflection site are similar to the theoretical values, values of R_{dP}, $R_{dI}^{0.5}$, and $R_I^{0.5}$ overestimate the local reflection coefficient.

The reflection generated in this work is done by joint two tubes together which have different dimensions and materials. This is similar to the work of Newman et al. (1983). In their work, the elastic mismatching were formed by connecting two tubes of the same internal diameter but different wall thickness; the second tubes used in their experiment were sufficiently long, is agreed with this work. In this work, the daughter tubes (second tubes) are 14 m in length, which could delay the wave transmission in the daughter tube.

The mean values of R_{dP}, $R_{dI}^{0.5}$ and $R_I^{0.5}$ are close to R_t, R_{dI} and R_I are smaller than R_t (**Figure 5.1**). In previous computational work (Mynard et al., 2008), they reported under linear flow conditions, the square root of the magnitude of the WI derived coefficients $R_{dI}^{0.5}$ and $R_I^{0.5}$ are equal to the pressure-derived coefficient R_{dP}, they all equal to the theoretical coefficient R_t.

R_{dI} and R_I are calculated from the wave intensity and wave energy, they are considered as the ‘power-type’ coefficients; R_{dP} is calculated from the pressure separation and considered as the ‘pressure-type’ coefficient (Mynard et al., 2008). When apply the square root to R_{dI} and R_I, $R_{dI}^{0.5}$ and $R_I^{0.5}$ could also be considered as the ‘pressure-type’ coefficients. This explains why the values of R_{dI} and R_I are not comparable to R_{dP}, but values of $R_{dI}^{0.5}$ and $R_I^{0.5}$ are similar to those of R_{dP}.

Figure 5.2 and **Figure 5.3 top** show that the local reflection coefficient increases for the positive reflection, and **Figure 5.3 bottom** and **Figure 5.4** show that local reflection coefficient decreases for the negative reflection. The values of local reflection coefficients determined by wave intensity and wave

energy close to the reflection site reached the theoretical reflection coefficients, within 5% difference. These results show that the local reflection coefficient is not the same along the tube, the local reflection coefficient is smaller far away from the reflection site, and the local reflection coefficient at or close to the reflection site gives the best results matched the theoretical value. This result confirmed by the wave dissipation. The peak of the separated forward pressure waveform decrease exponentially along the tube, wave intensity and energy also dissipated exponentially along the tube. The backward pressure, wave intensity and wave energy also decrease in the backward direction in a similar way (Feng et al., 2007). As the plots in **Figure 5.5** to **Figure 5.7**, separated pressure, wave intensity and energy are decreasing exponentially along the wave travel direction, so the biggest magnitude of the local reflection coefficients shown at the nearest measurement site to the reflection site, and the smallest magnitude of the local reflection coefficients shown at the most far away measurement site to the reflection site. This is quite different from the previous computational work (Mynard et al., 2008). In their work, under non-linear flow conditions compression waves amplify as they propagate, so the R_{dI} and R_I are greater than R_t with compression reflection, and the error becomes greater when the measurement site is further from the reflection site.

In **Figure 5.8** to **Figure 5.10**, the backward pressure, backward wave intensity and backward wave energy of all the sets of tubes are plotted. The exponential dissipation of three positive reflections are similar, and the exponential dissipation of three negative reflections are also similar, respectively. The exponential dissipation of the negative reflections are bigger than those of the positive reflections. This finding agrees with Feng and Khir's work (2008). In their work, they found out that the dissipation of the expansion wave was greater than that of the compression wave.

In this study, WIA was used to determine the local reflection coefficient in flexible tubes. WIA has been tested *in vitro* (Khir and Parker, 2002), and proved to be useful in studying waves in the aorta (Koh et al., 1998; Khir and Parker, 2005), in the coronary arteries (Sun et al., 2003; Davies et al., 2006b) and in the carotid artery (Niki et al., 2002). WIA benefits this research in several respects: (a) WIA is a time domain method allowing for determining the local reflection coefficient in the flexible tubes to be studied and the results presented as a

function of time and space; (b) There is no assumptions made in WIA about the tube's wall nonlinearity, although the solution of one-dimensional equations along the characteristic directions involving the water hammer equation is linearised expression. Also, WAI takes into account the effects of the viscoelastic properties of vessel's wall, convective, frictional effects and fluid viscosity; (c) WIA provides the separation of pressure and velocity waveforms travelling in the forward and backward directions from the measured pressure and velocity waves. Thus, WIA provides a new technique to study the local reflection coefficient. (d) The physical meaning of the wave intensity is the flux of energy carried by the wave per unit cross-sectional area. This offers a convenient method to study the local reflection coefficient of energy carried by the waves along flexible tubes.

5.4.1 Limitation

In this study, the local reflection coefficient using these five different methods in elastic tubes was investigated. The investigations were done in a single tube formed by joining two tubes together end to end. In order to isolate other reflections from the reflection generated from the connection of two tubes, the mother and daughter tubes are very long, these were not physiologic. The arterial system is very complex, with tapering and tethering of the arteries, and presence of side branches, so that this experiment is just to test the concept. Experiments with bifurcations, tapered tubes or in vivo test will be necessary to further understand and validate the method.

In this study, no measurements were taken in the middle part of the mother tube because of the limited length of the pressure catheter (effective length 1.2 m). This is not expected to influence the interpretations of the results as the first a few measurement sites downstream from this region also give consistent results.

5.5 Conclusion

In conclusion, this study has shown that the local reflection coefficient determined by wave intensity and wave energy which close to the reflection site are very smilar to the theoretical reflection coefficient. So wave intensity, wave energy could be used to determine the local reflection coefficient when the measurement site is close to the reflection site. The local reflection

coefficients determined by these methods show that reflection coefficients along the tube are not the same. When the measurement site is far away from the reflection site, the local reflection coefficient is small; when the measurement site is close to the reflection site, the local reflection coefficient is big and reaches the theoretical value.

Chapter 6
In-vitro Non-invasive Determination of Mechanical Properties of Vessels

6.1 Introduction

There is an extensively increasing interest in the assessment of mechanical properties of the aortic wall and their relation to cardiovascular disease. Arterial hypertension (Dzau and Safar, 1988; Heintz, 1993), aging (Avolio et al., 1983; Gillensen et al., 1995; Salomma et al., 1995), diabetes (Liu and Fung, 1992; Salomma et al., 1995), and atherosclerosis (Dart et al., 1991) are associated with marked changes in structure and mechanical properties of large arteries (Safar and London, 1994). For example, Vaccarino et al. (Vaccarino et al., 2000) found a 10 mmHg increase in pulse pressure, a parameter as a measure of arterial stiffness (generic term to describe the resistance to deformation of an artery), was correlated with a 12% increased risk of coronary heart disease, a 14% increased risk of congestive heart failure, and a 6% increase in overall mortality. Furthermore, arterial stiffness has been shown to be an independent risk factor for cardiovascular events such as primary coronary events, stroke, and mortality (Boutouyrie et al., 2002; Laurent et al., 2003). Therefore, the evaluation of aortic mechanical properties is important in understanding the mechanisms of cardiovascular disease.

A considerable part of knowledge of the general mechanical behavior of arterial walls comes from Cox (Cox, 1974;1975;1978;1982) and Dobrin (Dobrin and Rovick, 1969; Dobrin, 1973; 1978; Dobrin and Canfield, 1984) in the 1970s and 1980s. These pioneering works have influenced subsequent experiments in the following years by many other researchers.

Humphrey and colleagues in 1987 presented a technique which quantifying the strain field in the central region of biaxially tested planar soft tissues. Their

method was based on tracking small particles affixed to the central region of the specimen surface using a video system, digitizer and computer (Humphrey et al., 1987). More recently, Humphrey has conducted a comparative study of a small number of constitutive models to describe the mechanical response of arteries (Humphrey, 1999). One important motivation for such studies is the belief that mechanical factors may be important in triggering the onset of atherosclerosis, the major cause of human mortality in the western world. In order to fully understand these mechanical influences it is necessary to have reliable constitutive models for the artery.

The first study that tried to quantify the nonlinear mechanics of the arterial wall by considering its layered structure was performed by Von Maltzahn and coworkers (Von Maltzahn et al., 1981). They performed multiaxial tests, pressure-diameter for different axial stretches, whose values were kept constant in bovine carotid arteries, both intact and free from the adventitia in a later work (Von Maltzahn et al., 1984). They concluded that both layers are anisotropic, with a stiffer media that support higher stresses than previously thought, and both layers were stiffer in the axial direction.

There are several studies investigating the non-invasive assessment of aortic mechanical properties. Ultrasound can be easily used to measure arterial mechanical properties (distensibility and compliance), but its use is limited to the larger and more accessible arteries. Thus this technique has been used mainly on the brachial, femoral and carotid arteries and the abdominal aorta (Hoeks et al., 1999; Shau et al.,1999; Aggoun et al., 2000). Limitations of using ultrasound to assess arterial mechanical properties include the limited resolution, which is difficult to detect the very small changes in vessel diameter. The technique also relies heavily on the ability of the operator to image the walls of the vessel being studied accurately.

There are also several research on mathematically model of the mechanical behaviour of the artery wall includes the investigation of stress distribution. The early attempt was made by Apter (Apter, 1964). In Apter's work, a mathematical model which the visco-leastic properties of aorta could be approximated by arrangement of two elastic rods and one viscous rod. Rachev and coworkers did lots of theoretical work on the mechanical properties of arteries in the 1990s. They assumed that the geometry of the arterial cross section and the

mechanical properties of arterial tissue change in a manner to restore the normal baseline values of the flow-induced shear stress at the intima, thenormal stress distribution across the arterial wall and the normal arterial compliance (Rachev et al., 1996;1998). In 1999, Rachev and Hayashi suggested that the vascular smooth muscle tone affects the stress distribution through the arterial wall and consequently, its geometrical and structural adaptation. Recent years the stress distribution still attracted investigation (Gasser et al., 2002; Zulliger et al., 2004). Different approaches are related to different model assumptions about the structure (1, 2 or 3 wall layers), the composition (relative proportion of elastin and collagen in each layer), the mechanical properties and the geometry of the arterial wall.

The aim of this chapter consists of the following parts. First, the non-invasive wave speeds determined by *In*DU-loop in flexible tubes will be presented. Second, wave speeds determined in flexible tubes will be used to obtain the mechanical properties of the flexible tubes including distensibility and Young's modulus noninvasively. These results will be compared with those determined by the tensile test. Third, wave speeds determined noninvasively in calf's aortas will be described, and the results will be compared with those determined by the PU-loop and foot-to-foot methods. Finally, non-invasive mechanical properties of calf's aorta including distensibility and Young's modulus will be presented and compared with results of static and dynamic determination of distensibility, and Young's modulus from tensile test, respectively.

6.2 Materials and Methods

The study in this chapter is to determine the mechanical properties of vessels noninvasively; the studies were done with flexible tubes and calf aortas respectively. In order to show the steps of the experimental procedure, flow charts are shown in **Figure 6.1** to explain the studies.

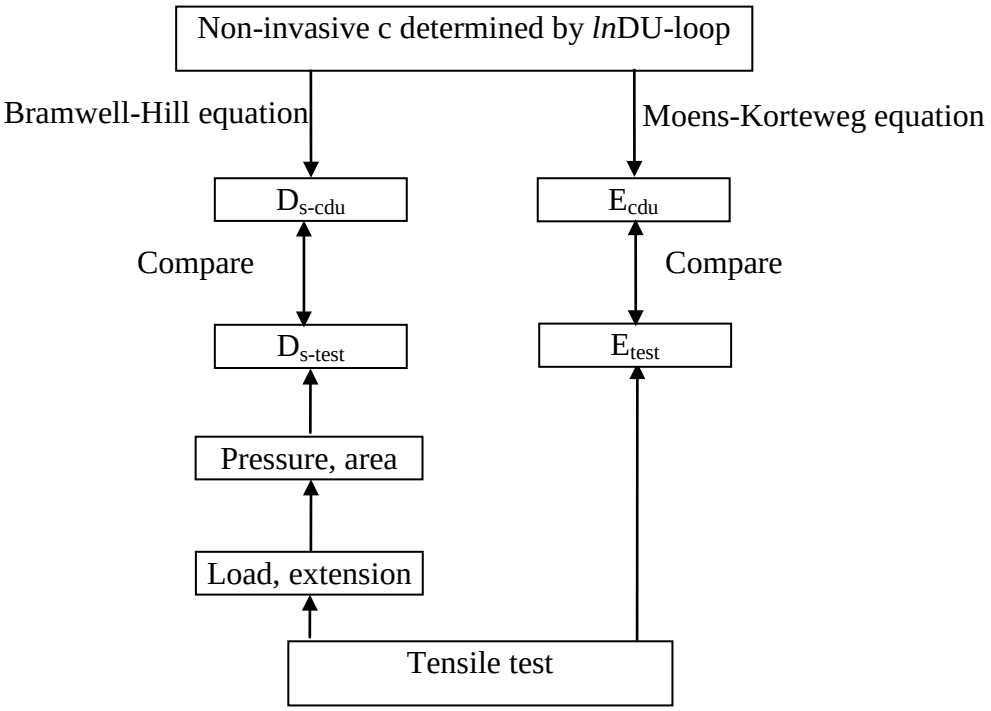

(a)

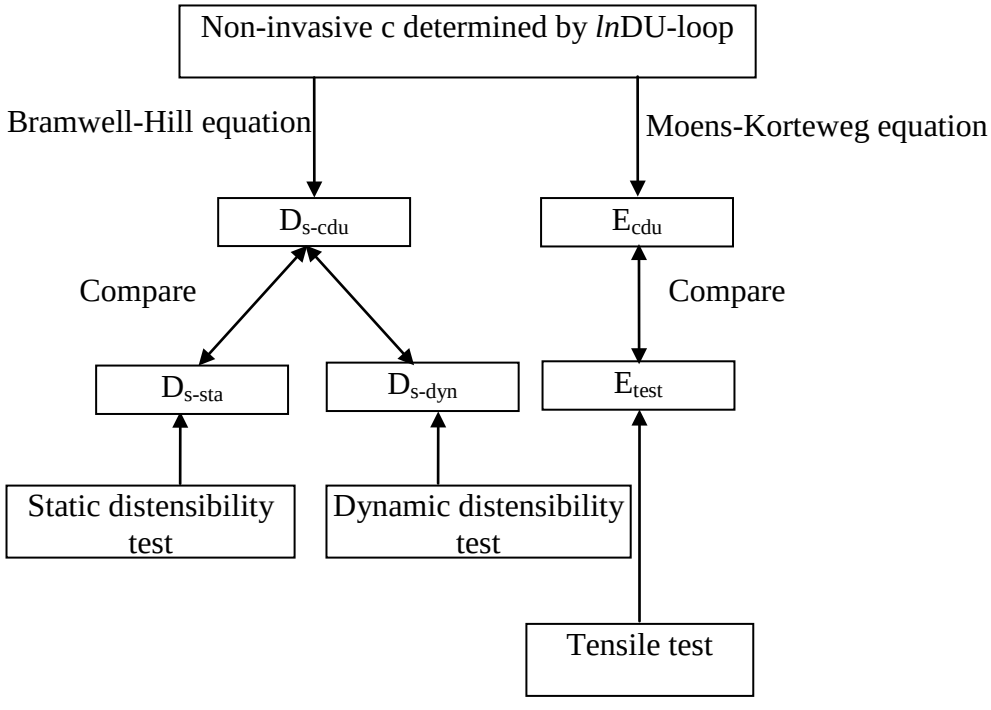

(b)

Figure 6.1: (a) tube experiments (b*)* aorta experiments procedures.

6.2.1 Determination of wave speed by *ln*DU-loop

The theoretical basis of the *ln*DU-loop method for determining wave speed (c) has been described in previous work (Feng and Khir, 2010) and Chapter 2 Section 2.1.7. Briefly, wave speed determined by *ln*DU-loop,

$$c = \pm \frac{1}{2} \frac{dU_{\pm}}{d \ln D_{\pm}} \tag{6.1}$$

Equation (6.1) describes a linear relationship between U and *ln*D for unidirectional waves. Therefore, plotting *ln*D against U gives an *ln*DU-loop, and a linear portion during the early part of systole should exist when it is most probable that reflected waves do no exist. In this study, the linear part of the loop is determined by fitting a straight line to the appropriate portion of the data by eye. The slope of the initial linear portion of the loop equals ½ c.

6.2.2 Non-invasive determination of distensibility

The distensibility of the arterial vessel wall, D_s, can be defined as the ratio of cross sectional area to the change of the pressure, compared to initial area:

$$D_s = \frac{1}{A} \frac{dA}{dP} \tag{6.2}$$

It is also known that the local pulse wave velocity c, in a thin-walled, uniform, elastic vessel containing an incompressible fluid, is related directly to the distensibility D_s via the Bramwell-Hill expression (Bramwell et al., 1923):

$$c^2 = \frac{1}{\rho D_s} \tag{6.3}$$

Rearrange the equation (6.3),

$$D_s = \frac{1}{\rho c^2} \tag{6.4}$$

Once the wave speed determined by *ln*DU-loop, it could be applied to determine the non-invasive distensibility.

6.2.3 Non-invasive determination of Young's modulus

Young's modulus, defined as the ratio of stress to strain, is a property of the material of the vessel. Moens (1878) and Korteweg (1878) arrived independently in the same year to the equation that is named after them, which

is a special form of equation (6.3), and only valid for thin walled vessels with homogeneous elastic properties,

$$c = \sqrt{\frac{Eh}{\rho d}} \tag{6.5}$$

Where E is the Young's modulus, h is wall thickness and d is internal diameter of the vessel.

Rearrange equation (6.5),

$$E = \frac{\rho c^2 d}{h} \tag{6.6}$$

6.2.4 Mechanical test

The tensile test machine has been detailed introduced in Chapter 2, Section 2.2.3.

Tensile tests have been carried out following a protocol created to guarantee the repeatability and reproducibility of each test, and the accuracy of the measurements.

The mechanical tests were planned to perform on flexible tubes and calf aortas. Different procedures were used according to the different specimens.

Mechanical test on flexible tubes

The samples from the flexible tubes were cut into standardized specimens (**Figure 6.2**), so that each specimen was 40 mm long. Each specimen had two ends of 10 mm length each. The effective length for each specimen was 20 mm long and 4 mm wide. The thickness of each specimen was measured at three different sites using a digital calliper and the mean of these measures was calculated. The ends of each specimen were mounted into the grips shown in **Figure 2.11b**.

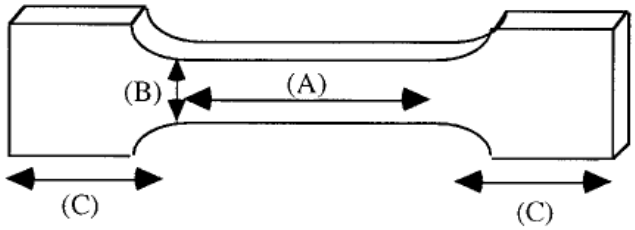

Figure 6.2: Example of the cut tube sample. Total length of the sample, 40 mm. (A) Initial effective length, 20 mm. (B) Sample width at the effective height, 4 mm. (C) Sample ends to be mounted into the grips of the machine, 10 mm.

Then the test started until the specimen was broken. Raw data was exported and used to derive the distensibility $D_{s\text{-}test}$.

$$P = \frac{F}{wr} \tag{6.7}$$

Where, F is the load on the specimen, w is the width of the specimen, r is the radius of the specimen, r=L/2π, L is the length of the specimen, P is the pressure in the radial direction.

$$D_{s-test} = \frac{1}{A}\frac{dA}{dP} \tag{6.8}$$

Where A is the cross sectional area of the specimen.

Mechanical test on calf aorta

The mechanical test for calf aorta is more complex than that for flexible tubes, the protocol for aorta test is shown below, all the preparation and test are performed under room temperature:

1. Preparation

- Cut symmetrical ring, free of arterial branches or irregular sections.
- Measure width at several points with digital calliper at five random locations and then averaged.
- Measure internal half circumference several times using digital calliper at five random locations and then averaged, radius then calculated.
- Measure thickness at several points with calliper.
- Zero load on Instron tensile test machine.
- Mount loose in grips.
- Sample should be kept wet by spraying with phosphate buffered saline.

- Increase length until very beginning of load being taken up, measure length with calliper.

2. Testing sequence

- Preload: Increase length until load equals 0.005N, which allows for automatic data collection after the negative load has been removed.
- Cycle 3 times between 0 and 60 mmHg at a rate of 10 mm/min, hold at 60 mmHg for 30 seconds.
- Cycle 3 times between 60 mmHg and 160 mmHg at the rate of 10 mm/min, and decrease load to 30 mmHg, hold at 30 mmHg for 30 seconds.
- Cycle 3 times between 30 mmHg and 200 mmHg at the rate of 10 mm/min.
- Decrease load to zero and hold for 30 seconds.

The test sequence is shown in **Figure 6.3**, all the samples of aortas were cut at the sites which took the measurements during the wave speed experiment. Because of the softness of the tissue of the aorta sample, aorta samples were cut into ring sample and using the grips shown in **Figure 2.11c** to do the test.

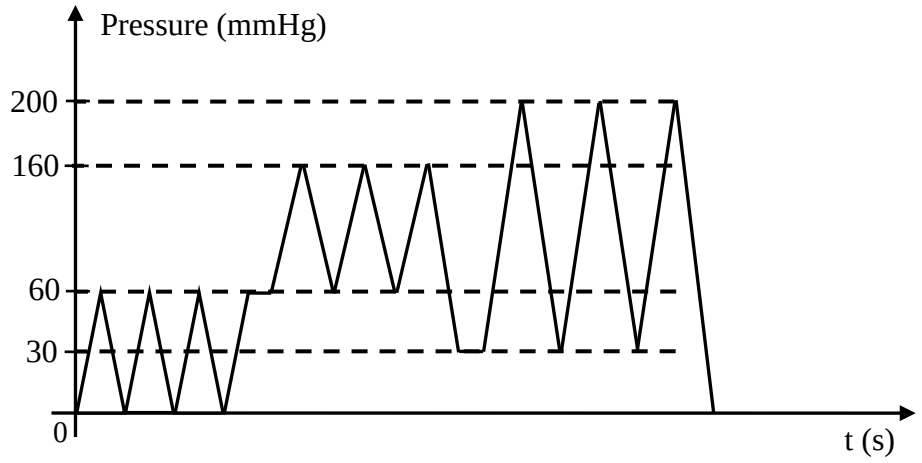

Figure 6.3: Test sequence for the tensile test of calf aortas.

6.2.5 Experiments of calf aortas

6.2.5.1 Subject

Fourteen ascending aortas from the matured calf (average 18 months, gender not known) were obtained from an abattoir, and excess adipose tissue was removed from the adventitial surface. The aortas were stored at a freezing temperature of -20 ^{o}C, each aorta was allowed to thaw at room temperature for 3 hours before testing without pre-conditioned. All the branches of small arteries were kept and closed at the root of the branches using the cable ties in order to avoid the leakage and the reflection from the small branches; the holes on the aortas were closed with PTFE water tape and 3M vetbond tissue adhensive. The length of the aorta was measured by a ruler, and the average is 37.52±3.38 cm. In order to implant the ultrasound crystals, on the surface of the measurement site on the aorta, two 5×5-mm area were cut with depth of 3 mm. Before the experiment, crystals were implanted with 3M vetbond tissue adhensive.

6.2.5.2 Wave speed experiment

The general setup of the experiment is shown in **Figure 6.4** and a description of the individual elements follow.

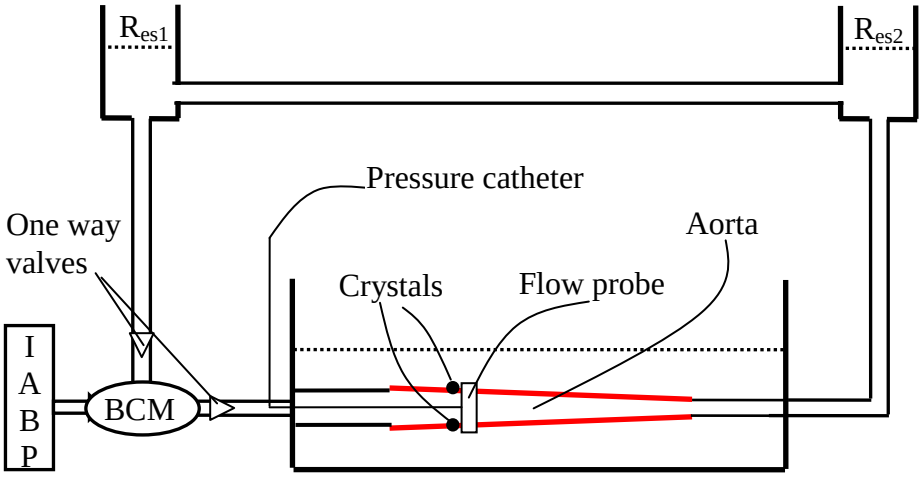

(a)

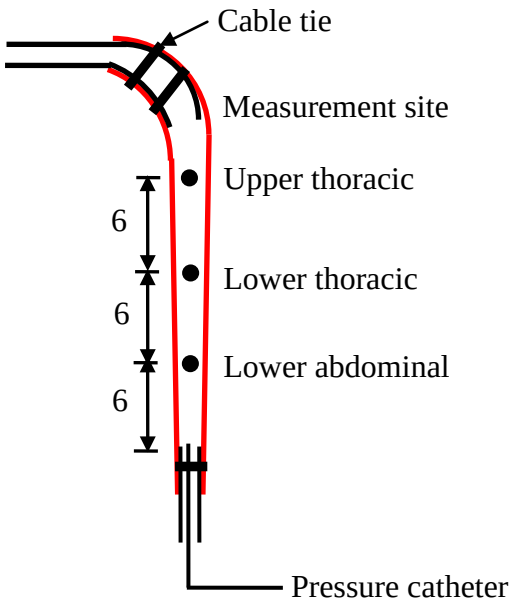

(b)

Figure 6.4: (a) A schematic diagram of the experimental setup. R_{es1} and R_{es2} are the inlet and outlet reservoirs which provide the initial pressure to the system, and keep the system free of air. Pressure and flow were measured using transducer tipped catheters, and ultrasonic flow meter and probes, respectively. Diameter was measured using a pair of ultrasound crystals. (b) The detailed diagram of the aorta and the measurement site. Two flexible tubes were inserted into the aorta to connect the aorta to the water tank, and tied with the cable ties. Distance was measured in the preparation (cm).

BCM (Cardialcare, Minneapolis, MN, USA) is a flexible diaphragm pulsatile left ventricular assist device (LVAD), which can be operated using an Intra Aortic Balloon Pump (IABP). As shown in **Figure 6.4a**, the inlet of BCM was connected with the left reservoir and the outlet of BCM was connected with inlet of the aorta. There were two one-way valves placed in the inlet and outlet of the BCM, respectively, to ensure that the water in the system flowed in one direction. In this work, the BCM was operated by IABP and generates a pulsatile wave. Heart rate was set to 80bpm and augmentation of scale , which indicates the strength by which the BCM pumped, was set at the highest level, level 10.

Reservoirs: The inlet and outlet reservoirs were interconnected, and the height of the fluid in the reservoirs was adjusted to 100 cm above the longitudinal axis of the aorta; producing an initial hydrostatic pressure of 10 kPa (physiological diastolic pressure 75mmHg). The experimental aortas were connected to the reservoirs using rigid polyurethane tubing.

Measurements: External diameter was measured using a pair of ultrasonic crystals (Sonometrics Corporation, Ontario, Canada), and wall thickness was measured using a digital caliper after the wave speed experiment. Simultaneous waveforms of pressure (P), outer diameter (D_o) and flow rate (Q), from which U were determined, were measured sequentially in time every 6 cm from the inlet of each aorta. P and Q were measured using a 6F tipped catheter pressure transducer (Millar Instruments, Texas, USA) and ultrasonic flow probe (Transonic System, Inc, NY, USA), respectively. All data were sampled at 500Hz using Sonolab (Sonometrics Corporation) and analysed using Matlab (The Mathworks, MA, USA).

6.2.5.3 Static and dynamic distensibility

Figure 6.5 shows the experimental setup for the static distensibility test. It consists mainly of a graduated syringe a displaceable volume of 50 ml with an precision of 2 ml and, one plastic three-way valve where the syringe was plugged, two rubber caps used to plug the sample, a Y-connector, a pressure catheter transducer and a pair of crystals used to measure the diameter change of the vessel. This setup was created to be the simplest possible in order not to

introduce any component which could have increased the compliance of the system and also to easily take the air bubbles out from the system.

Compliance experiments have been carried out following a protocol created to guarantee the repeatability and reproducibility of each test, and the correctness of the measurements.

Once the sample was fixed to the connectors, it was filled with a volume of water comparable to its internal volume; before to start the measurement the setup was put horizontally in order to allow the excessive water to come out; this operation was used to ensure a transmural pressure just above zero. Eventually, once the setup was also bubble free, the three-way valve was closed.

When all the preliminary operations were terminated, the compliance experiment itself was ready to be started; the pressure=volume relationship was then determined by infusing water in ΔV=10 ml increments until all the volume was displaced. The whole volume which infused into the sample was around 70 ml, which was similar to the input volume of the BCM (Khir et al., 2006). For every sample, three measurements have been taken at three different sites (the same site which take the wave speed experiment). For each ΔV which was inflated, the increment of volume was maintained constant for approximately 5 seconds in order for the pressure catheter and the ultrasound crystals to acquire the equilibrium value of pressure and diameter, respectively.

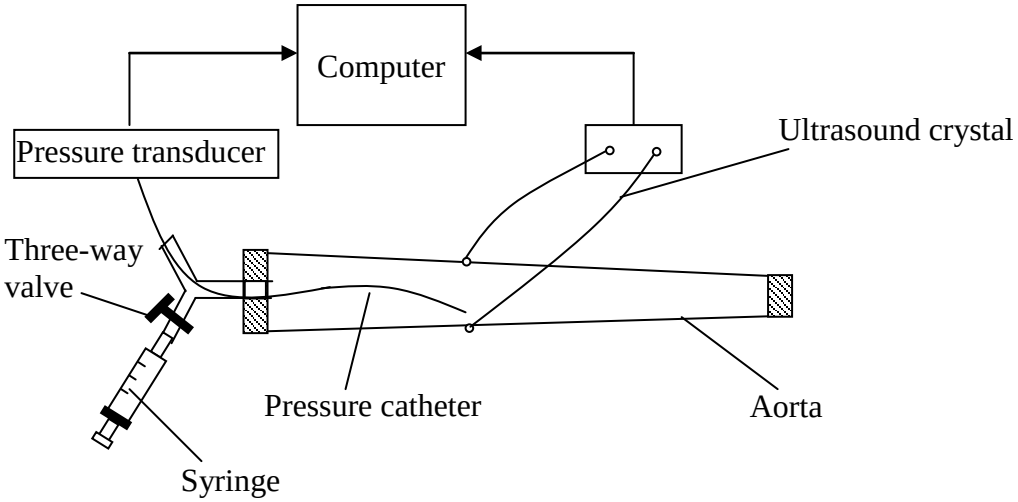

Figure 6.5: The experimental setup for the static distensibility test. The pressure catheter and the Syringe were connected to the inlet of the aorta by the 'Y' connection; the end of the aorta was closed by the rubber cap. In order to measure diameter change, a pair of crystals were attached on the aorta, and placed in a water tank with the aorta to make sure the normal working of the crystals.

6.2.6 Analysis

Regression and paired t-test analysis were performed to identify the correlation between $D_{s\text{-}test}$ and $D_{s\text{-}cdu}$, and between E_{test} and E_{cdu} to indicate the relative accuracy. In this study, some of the measurements were taken two times, so the results are presented as mean±SD and values of $p<0.05$ were considered significant. The Bland-Altman technique (Bland and Altman, 1986) is also used to establish the agreement between different techniques, and the acceptable range for the mean difference was taken as ±2SD.

6.3 Results

6.3.1 Results of flexible tubes

6.3.1.1 Wave speed determined by *In*DU-loop

The wave speeds used to determine the non-invasive distensibility and Young's modulus of the flexible tubes were calculated as in **Chapter 3**, here **Table 6.1** shows the details of dimensions of the flexible tubes and the wave speeds determined by *In*DU-loop and foot-to-foot methods.

Table 6.1 Materials and dimensions of the flexible tubes. Also shown are the average wave speeds measured in each tube with water (ρ = 1000 kg/m^3) by *In*DU-loop and foot-to-foot methods, and results of distensibility and Young's modulus.D_{in}: internal diameter, h: wall thickness, C_{DU}: wave speed determined by *In*DU-loop, $D_{s\text{-}test}$: distensibility calculated from the tensile test, $D_{s\text{-}cdu}$:distensibility calculated from C_{DU}, E_{test}: Young's modulus from the tensile test, E_{cdu}:Young's modulus calculated from C_{DU}.

Material	D_{in} (mm)	h (mm)	$C_{foot\text{-}to\text{-}foot}$ m/s	C_{DU} m/s	$D_{s\text{-}test}$ (10^{-6} Pa^{-1})	$D_{s\text{-}cdu}$ (10^{-6} Pa^{-1})	E_{test} (MPa)	E_{cdu} (MPa)
Silicone	8	1	22.4±0.6	22.3±1.5	2.46±0.10	2.04±0.28	3.26±0.06	3.97±0.55
		2	29.8±1.2	26.7±2.8	1.38±0.08	1.44±0.29	2.90±0.06	2.85±0.59
		3	35.1±1.4	33.5±3.3	0.93±0.06	0.91±0.18	2.88±0.07	2.99±0.59
	10	1	20.8±0.6	20.0±5.3	2.60±0.05	2.88±1.46	3.84±0.05	3.98±0.57
		2	26.0±0.9	25.3±1.5	1.53±0.04	1.57±0.18	3.28±0.06	3.20±0.39
		3	30.2±0.3	29.9±3.3	1.18±0.07	1.15±0.24	2.82±0.08	2.97±0.66
	16	2.4	22.3±1.1	22.4±2.8	1.90±0.35	2.31±1.31	3.50±0.30	3.35±1.07
		3	23.3±0.5	25.1±4.5	1.57±0.02	1.89±1.09	3.39±0.01	3.37±1.04
Rubber	16.7	1.5	24.3±0.3	23.9±5.0	2.34±0.18	1.90±0.69	4.77±0.20	6.35±2.79
	20.6	1.5	20.7±0.4	20.7±6.2	3.65±0.03	2.75±1.46	3.76±0.01	5.90±2.74
Latex	8.5	0.1	6.0±0.4	5.2±0.5	57.7±0.1	38.3±8.0	1.47±0.03	2.28±0.47
	24.2	0.27	3.1±0.3	3.1±0.9	106.8±0.2	105.1±19.8	0.84±0.04	0.87±0.15
	32.3	0.27	2.7±0.2	2.6±0.7	151.8±0.2	170.0±83.1	0.79±0.06	0.85±0.46

6.3.1.2 Non-invasive distensibility

Distensibility was calculated from the wave speed determined by *In*DU-loop by equation (6.3). The distensibility from the load and area which were determined by the tensile test was also calculated. In **Table 6.1**, all the distensibility results are shown. In **Figure 6.6**, the agreement of distensibility determined by these two methods was shown and compared.

The regression line and Student's t-test show that $D_{s\text{-}test}$ and $D_{s\text{-}cdu}$ of all of the tubes is significantly correlated (R^2=0.98, $p < 0.05$), shown in **Figure 6.6a**.

The agreement of distensibility determined by the *In*DU-loop and tensile test methods is also assessed using Bland-Altman method. The results show that mean of difference between these two methods is 2.29×10^{-6} Pa^{-1}, which indicated that distensibility determined by *In*DU-loop is slightly smaller than that determined by tensile test. The difference between $D_{s\text{-}test}$ and $D_{s\text{-}cdu}$ is within the acceptable range of mean±2SD ($2.29 \times10^{-6} \pm1.10 \times10^{-5}$ Pa^{-1}), **Figure 6.6 b**.

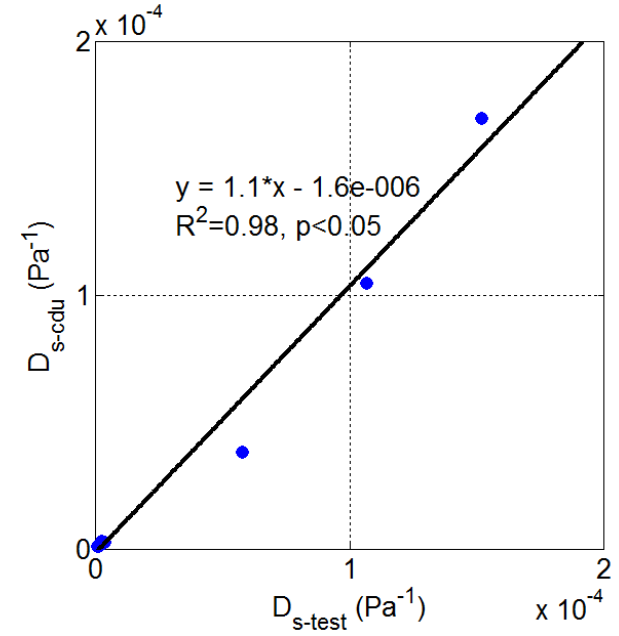

(a)

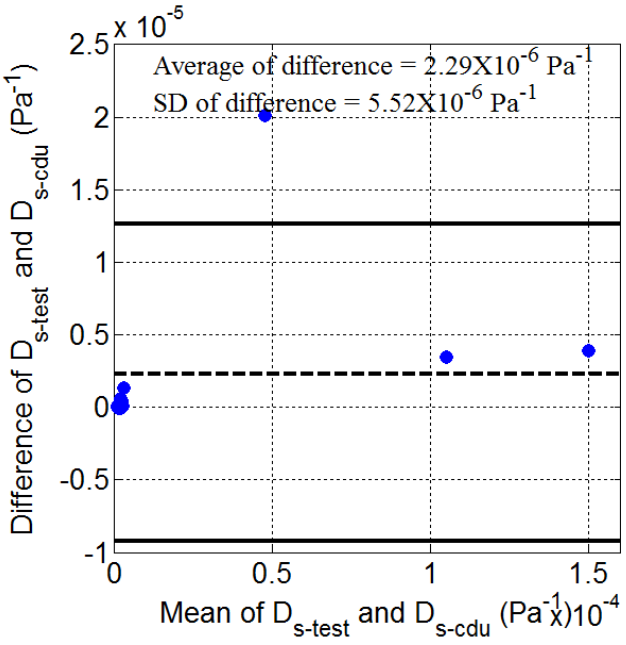

(b)

Figure 6.6: (a) Correlation of distensibility determined by *In*DU-loop and tensile test of the flexible tubes. The correlation coefficient R^2=0.98, p<0.05. (b) The agreement between distensibility determined by the *In*DU-loop and tensile test is assessed by Bland-Altman method. The middle horizontal line (dashed) indicates the mean of difference of wave speed determined by two methods. The upper and lower horizontal lines (solid) indicate twice the standard deviation (2SD). Note that most of the data points fell within ±2SD range, and the zero line fell within the acceptable confidence limits of the average, indicating no statistically significant difference between these two methods.

6.3.1.3 Non-invasive Young's modulus

Young's modulus was calculated from the wave speed determined by *In*DU-loop by equation (6.5). Young's modulus was also obtained from the tensile test. In **Table 6.1**, all the Young's modulus results are shown.

In **Figure 6.7**, the load versus extension curve and the stress strain curve for silicone tube which diameter is 8 mm, wall thickness is 2 mm are plotted.

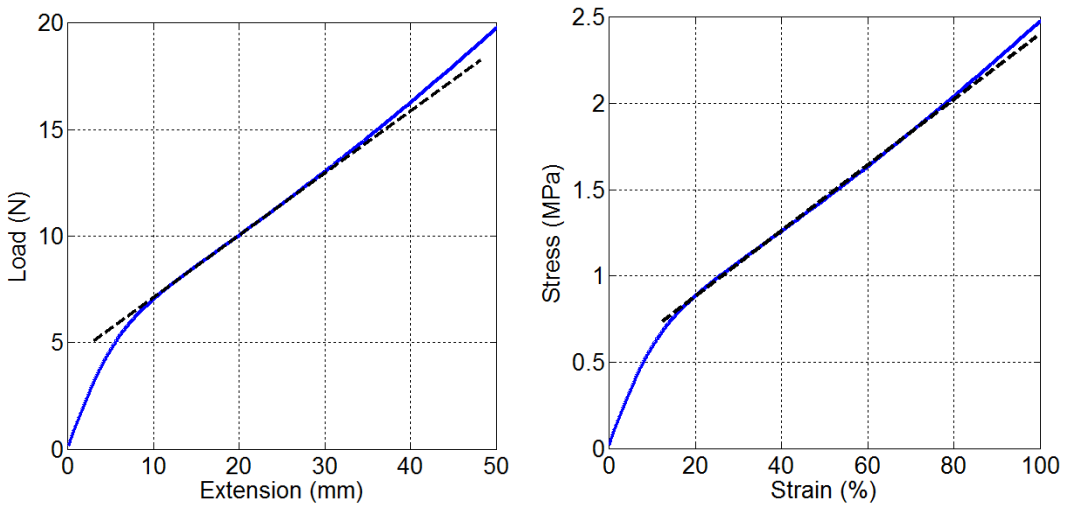

Figure 6.7: Tensile test for silicone tube diameter 8 mm, wall thickness 2 mm. (a) Test force versus displacement, (b) Stress versus strain. The black dash lines show the determination of Young's modulus in the range of pressure 80-200 mmHg.

The regression line and Student's t-test show that values of E_{test} and E_{cdu} of all of the tubes are highly correlated (R^2=0.82, $p < 0.03$), **Figure 6.8a**.

The agreement of Young's modulus determined by the *In*DU-loop and tensile test methods is also assessed using Bland-Altman method. The results show that mean of difference between these two methods is 0.41 MPa, which indicated that Young's modulus determined by *In*DU-loop is slightly smaller than that determined by tensile test. The difference between these two methods is within the acceptable range of mean±2SD (0.41 ±1.42 MPa), **Figure 6.8b**.

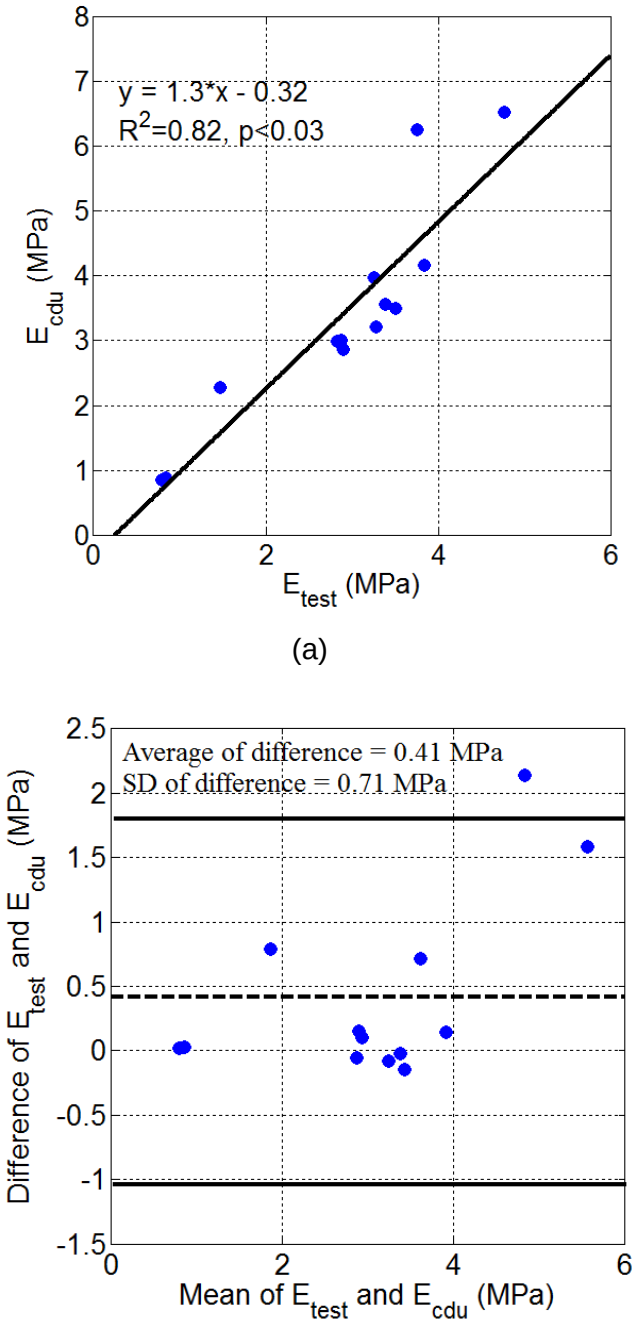

Figure 6.8: (a) Correlation of Young's modulus determined by *In*DU-loop and test. The correlation coefficient R^2=0.82, p<0.03. (b) The agreement between Young's modulus determined by the *In*DU-loop and test is assessed by Bland-Altman method. The middle horizontal line (dashed) indicates the mean of difference of wave speed determined by the two methods. The upper and lower horizontal lines (solid) indicate twice the standard deviation (2SD). Note that most of the data points fell within ±2SD range, and the zero line fell within the acceptable confidence limits of the average, indicating no statistically significant difference between these two methods.

6.3.2 Results of calf aortas

6.3.2.1 Dimension of the specimens

The measurement of dimension of the aorta was carried out during the preparation of the tensile test, in **Table 6.2** the dimensions of the aortas are shown.

Table 6.2 Dimension of the aortas (mean±SD) and the wave speeds.

Aorta measurement site	Internal diameter (mm)	Wall thickness (mm)	c_{DU} (m/s)	c_{PU} (m/s)	$c_{foot\text{-}to\text{-}foot}$ (m/s)
Upper thoracic	24.73±2.11	5.42±0.52	3.90±0.47	4.06±0.58	4.31±0.82
Lower thoracic	21.68±2.22	4.39±0.53	4.02±0.47	4.28±0.59	4.63±0.49
Lower abdominal	19.79±1.52	3.30±0.42	4.16±0.39	4.31±0.44	4.76±0.50

The internal diameter ranged from 22.05 to 29.13 mm in the upper thoracic, 18.18 to 24.33 mm in the lower thoracic, and 17.83 to 22.23 mm in the lower abdominal aortas. Thickness ranged from 4.45 to 6.4 mm in the upper thoracic, 3.50 to 5.31 mm in the lower thoracic, and 2.77 to 4.20 mm in the lower abdominal aortas. The internal diameter (D), wall thickness (h) and the ratio of h/D of all the aortas are plotted in **Figure 6.9**. From this figure, it is found out that the $D_{Upper\ thoracic} > D_{Lower\ thoracic} > D_{Lower\ abdominal}$, and the wall thickness follow the same pattern.

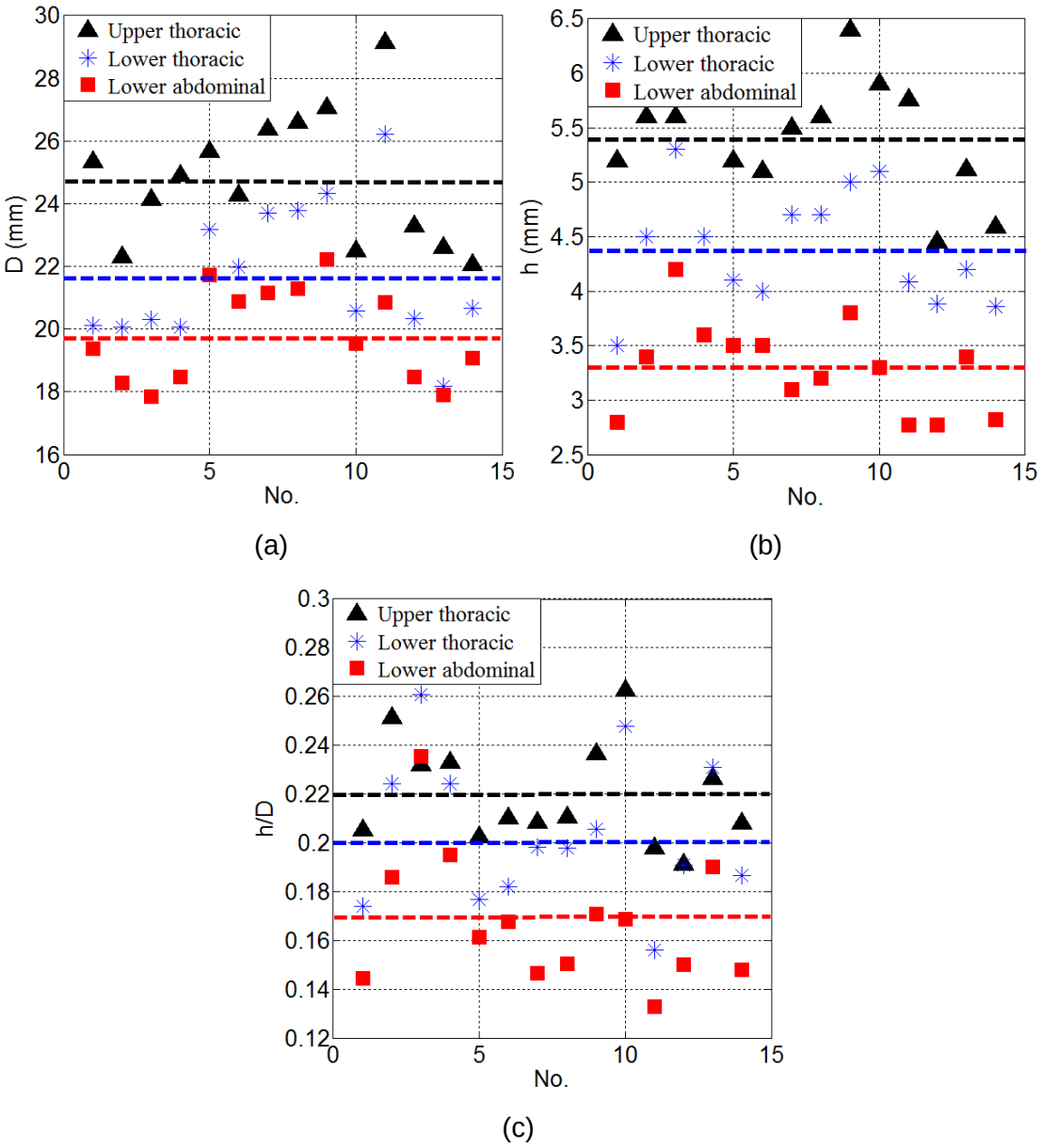

Figure 6.9: Dimensions of all the aortas (a) internal diameter (b) wall thickness (c) h/D. The black, blue and red dash lines show the mean values of the upper thoracic, lower thoracic and lower abdominal, respectively.

6.3.2.2 Wave speed

Wave speeds were determined by *In*DU-loop, PU-loop and foot-to-foot methods, separately in order to compare the results. **Figure 6.10** shows the determination of wave speed by *In*DU-loop (a), PU-loop (b), and foot-to-foot method (c) at the upper thoracic of an aorta. The wave speeds determined by these three methods are 4.58, 4.72 and 4.8 m/s, respectively for *In*DU-loop, PU-loop and foot-to-foot methods. The average values of wave speeds determined by these three methods along upper thoracic, lower thoracic and lower abdominal have been shown in **Table 6.2**. From the table, it is found out that $c_{DU} < c_{PU} < c_{foot\text{-}to\text{-}foot}$, but the difference is not very big.

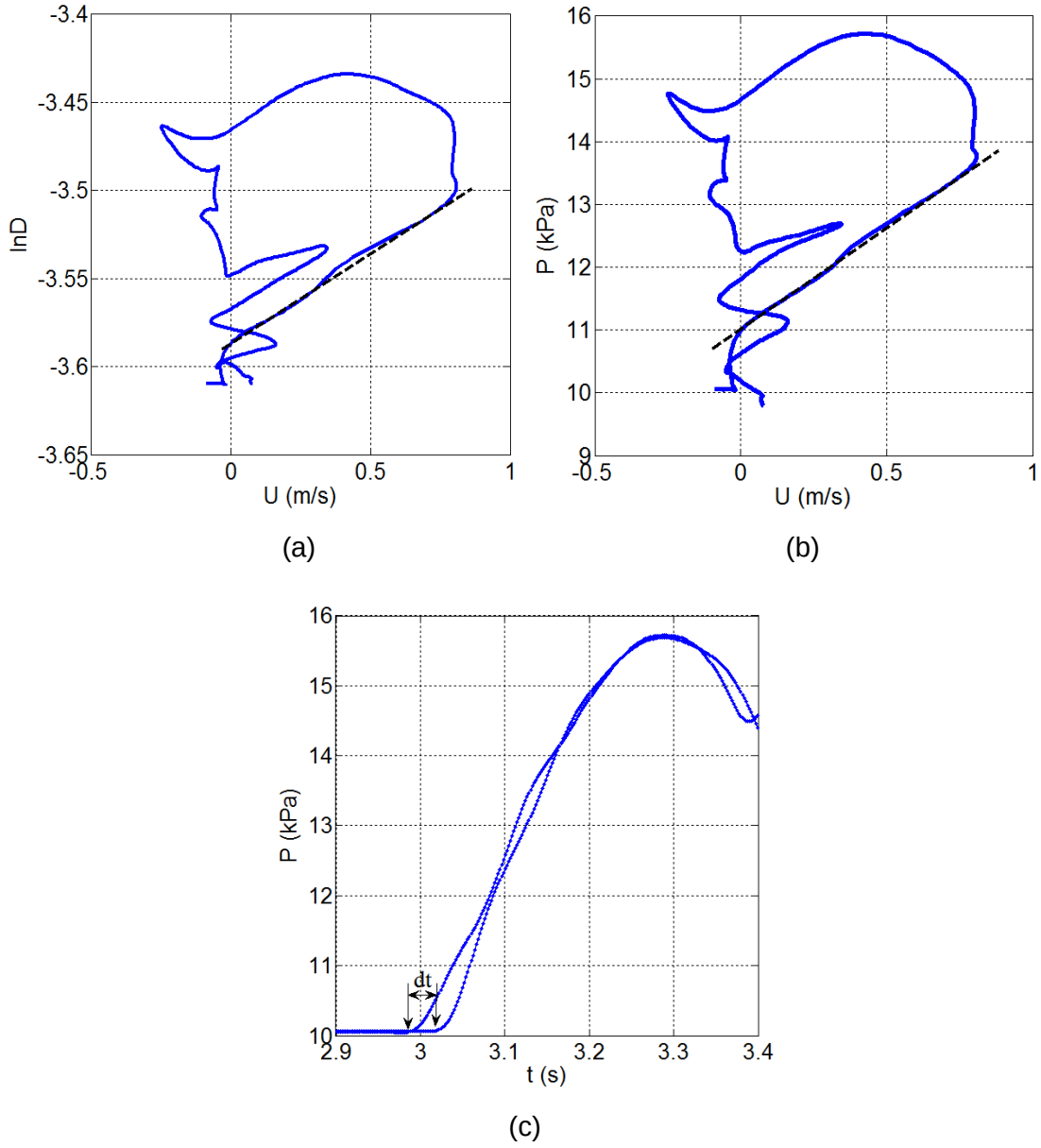

Figure 6.10: Wave speed measured at the upper thoracic of an aorta by (a) *ln*DU-loop method. The wave speed determined is 4.58 m/s. (b) PU-loop method. The slope of the initial part of the PU-loop indicates wave speed of 4.72 m/s. (c) foot-to-foot method. The time that takes the wave to run from one site to the other, Δt, is 0.05 m as indicated by the arrows which point at the foot of the wave at each site. The distance between the two sites is 0.24 m and the calculated wave speed is 4.8 m/s.

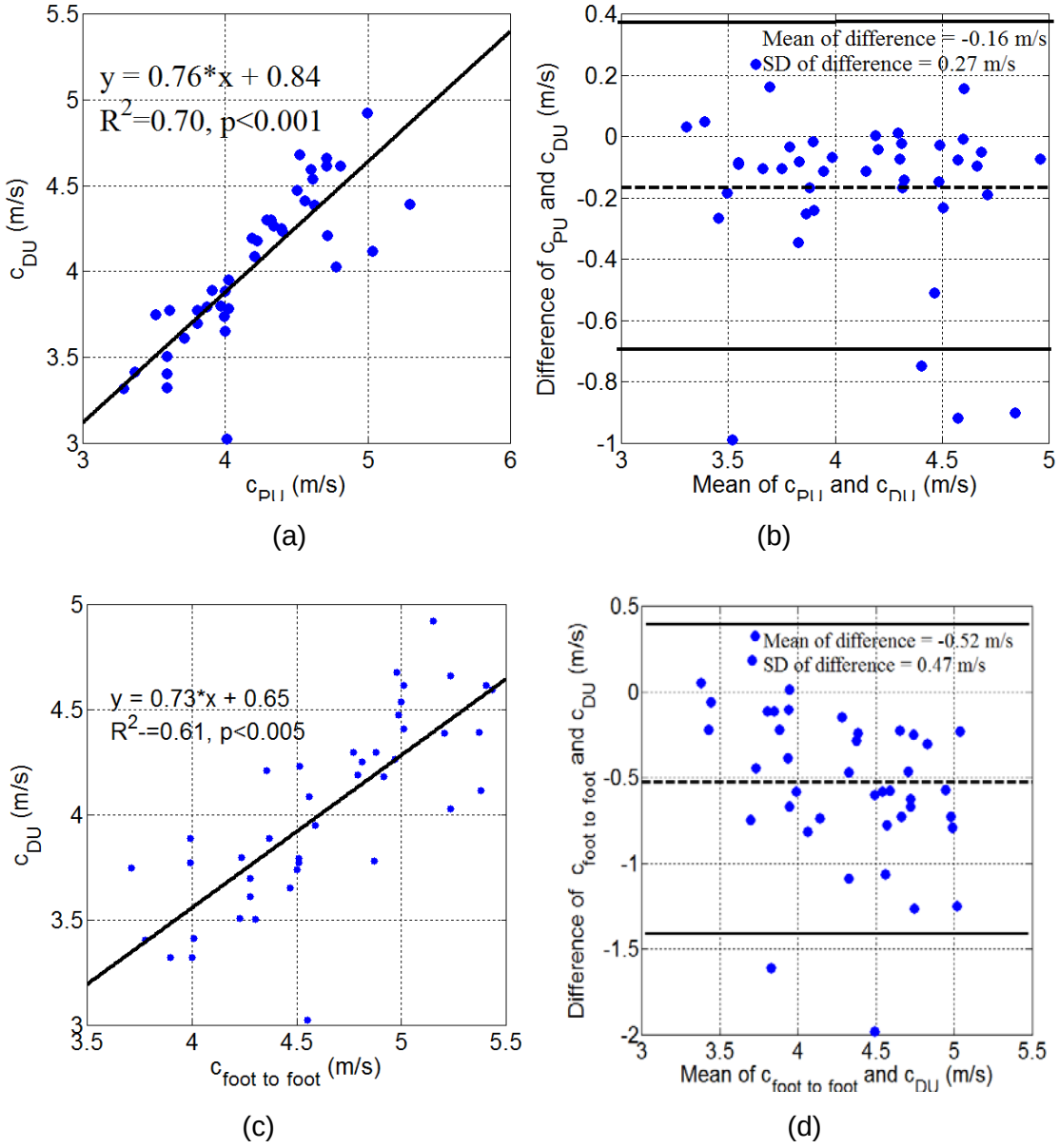

Figure 6.11: Correlation of c_{DU} with c_{PU} (a), and c_{DU} with $c_{foot\text{-}to\text{-}foot}$ (c). The black solid lines indicate the correlation between c_{DU} with c_{PU}, and c_{DU} with $c_{foot\text{-}to\text{-}foot}$. The agreements between c_{DU} and c_{PU} (b), c_{DU} and $c_{foot\text{-}to\text{-}foot}$ (d) are assessed by Bland-Altman method. The middle horizontal line (dashed) indicates the mean difference. The upper and lower horizontal lines (solid) indicate twice the standard deviation (2SD). Note that most of the data points fell within ±2SD range, and the zero line fell within the acceptable confidence limits of the average, indicating no statistically significant difference between different methods.

The agreements of these different methods are also assessed using the Bland-Altman method, **Figure 6.11** right. The results show that the means of difference between these methods are all very small, close to the zero line, it means that the difference between these methods are very small, and the ±2SD lines show that most of the results are in the acceptable range.

Wave speeds determined by *In*DU-loop at different measurement site individually are also plotted in **Figure 6.12**, and it is found that wave speed at the lower abdominal is the biggest, 4.16±0.39 m/s, and the wave speed at the Upper thoracic is the smallest, 3.90±0.47 m/s.

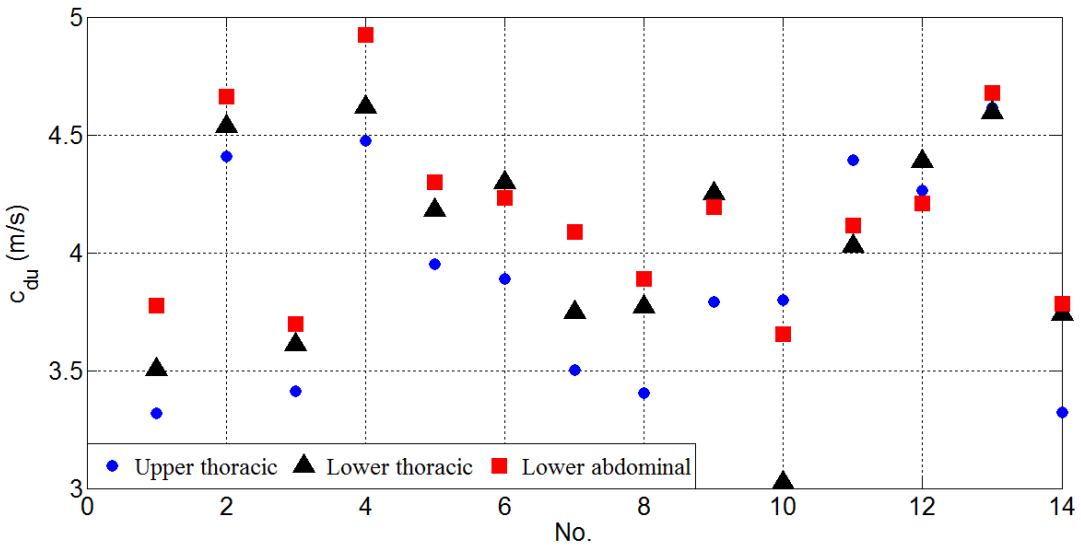

Figure 6.12: Wave speeds determined by *In*DU-loop. It indicates that the wave speeds measured at the upper thoracic is the smallest, followed by the wave speeds measured at the lower thoracic, and the wave speeds at the lower abdominal is the biggest.

6.3.2.3 Non-invasive determination of distensibility

The non-invasive distensibility of the aorta was calculated by wave speed determined by *In*DU-loop with equation (6.3). The average value of the non-invasive distensibility is 6.61 ± 1.52 10^{-5} Pa^{-1}, the average value of the static distensibility is 6.46 ± 1.55 10^{-5} Pa^{-1}, the average value of the dynamic distensibility is 6.39 ± 1.24 10^{-5} Pa^{-1}. The non-invasive distensibility is 2.32% bigger than the static distensibility, and 3.44% bigger than the dynamic distensibility. The individual distensibility against measurement site reported in **Figure 6.15**.

The methods to determine the static and dynamic distensibility had been introduced in Section 6.5.2.3, the static distensibility is done by increasing the distending pressure inside the vessel and measuring the change in radius (or in volume); the dynamic distensibility is determined by measuring arterial pulse-related changes in vessel diameter and arterial pressure (**Figure 6.13**).

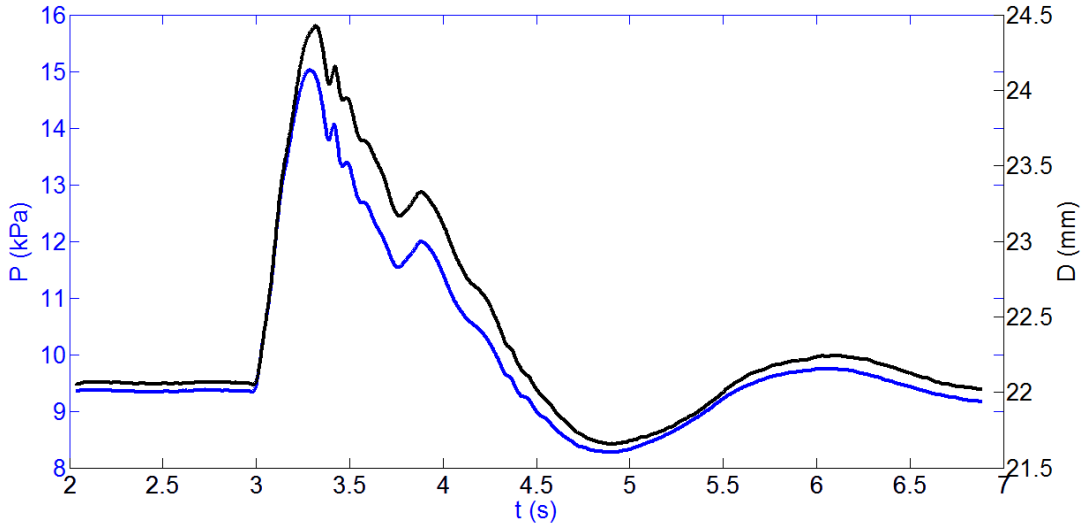

(a)

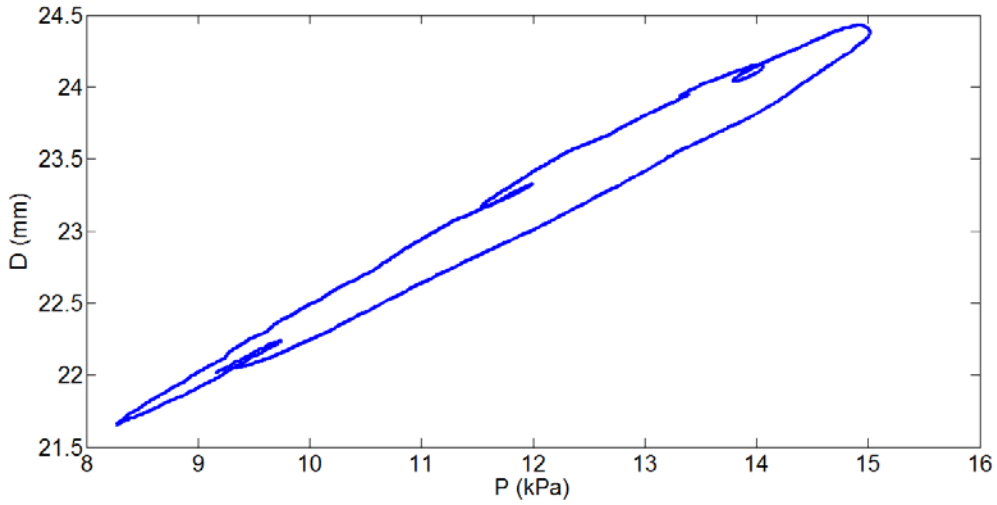

(b)

Figure 6.13: (a) Time courses of one pair of corresponding pressure and diameter pulses recorded from the beginning site of one calf aorta. (b) Hysteresis loop formed by the pressure and diameter pulse shown in (a).

The artery diameter pulse measured at the beginning site (upper thoracic) was related to the pressure pulse measured simultaneously at the same site. **Figure 6.13a** illustrates corresponding pressure and diameter pulse from a representative calf aorta. The pressure and diameter pulse contours were almost identical during the rising part, whereas diameter was lagging behind pressure during the falling part, i.e. from peak to end. This delay in the pressure-diameter relation resulted in a hysteresis loop, i.e. at identical pressure the diameter was greater for falling than for rising pressures (**Figure 6.13b**). The extent of hysteresis was quantified by measuring the loop area, normalized by both pressure and diameter amplitudes, thus giving a measure of vessel wall viscosity.

The average value of the static and dynamic distensibilities are $6.46 \pm 1.53\ 10^{-5}$ Pa^{-1} and $6.39 \pm 1.22\ 10^{-5}$ Pa^{-1}, respectively.

The agreements of these different methods are also assessed using the Bland-Altman method, **Figure 6.14** right. The results show that the means of difference between these methods are all very small, close to the zero line, this means that the difference between these methods are very small, and the ±2SD lines show that most of the results are in the acceptable range.

Distensibility against position is also plotted, and it is found out that the aorta was more rigid in the lower abdominal than in the upper thoracic (distensibility is smallest at the lower abdominal, and biggest at the upper thoracic), **Figure 6.15**.

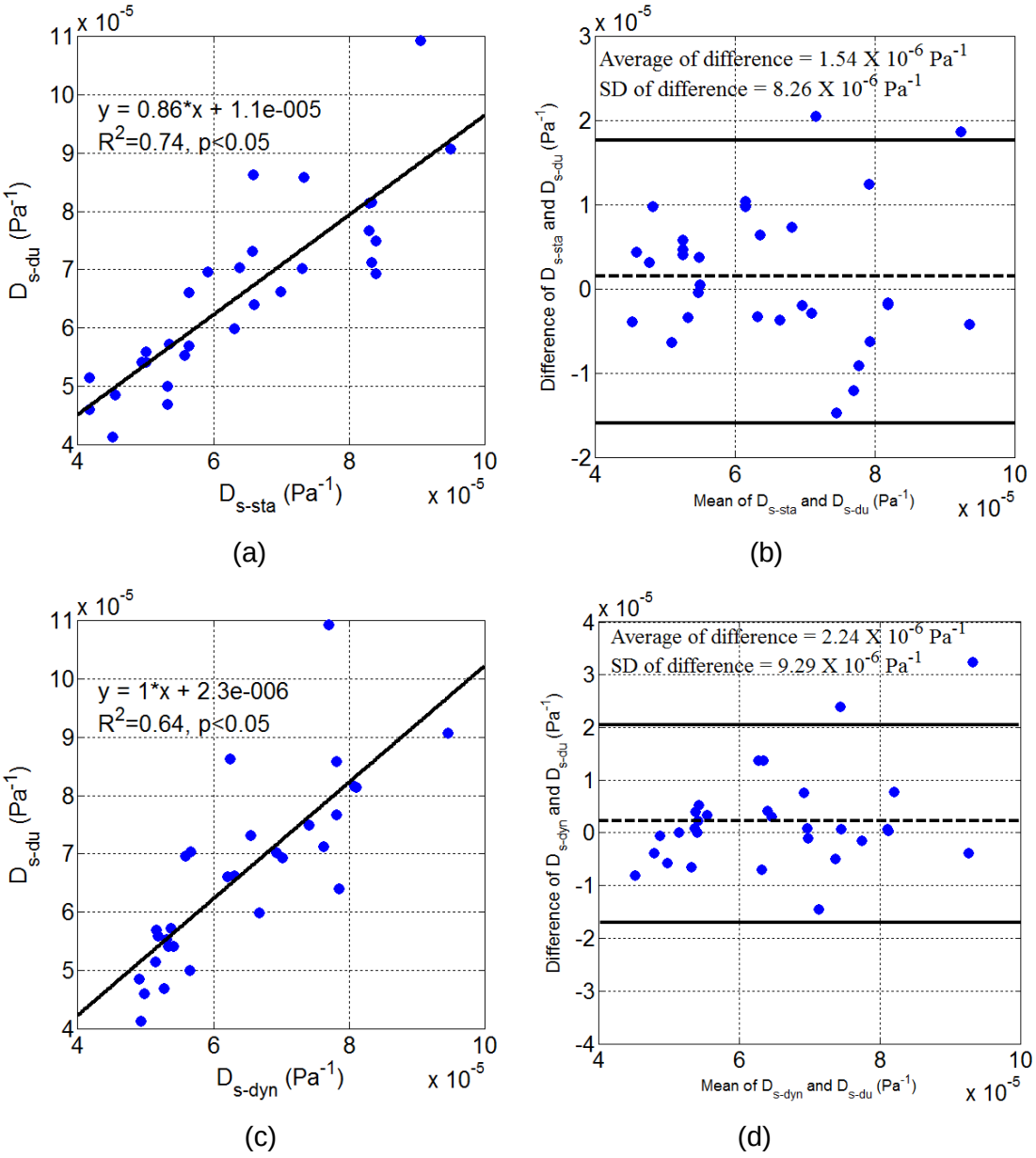

Figure 6.14: Correlation of $D_{s\text{-}du}$ with $D_{s\text{-}sta}$ (a), and $D_{s\text{-}du}$ with $D_{s\text{-}dyn}$ (c). The agreements between $D_{s\text{-}du}$ and $D_{s\text{-}sta}$ (b), $D_{s\text{-}du}$ and $D_{s\text{-}dyn}$ (d) are assessed by Bland-Altman method. The middle horizontal line (dashed) indicates the mean of difference. The upper and lower horizontal lines (solid) indicate twice the standard deviation (2SD). Note that most of the data points fell within ±2SD range, and the zero line fell within the acceptable confidence limits of the average, indicating no statistically significant difference between different methods.

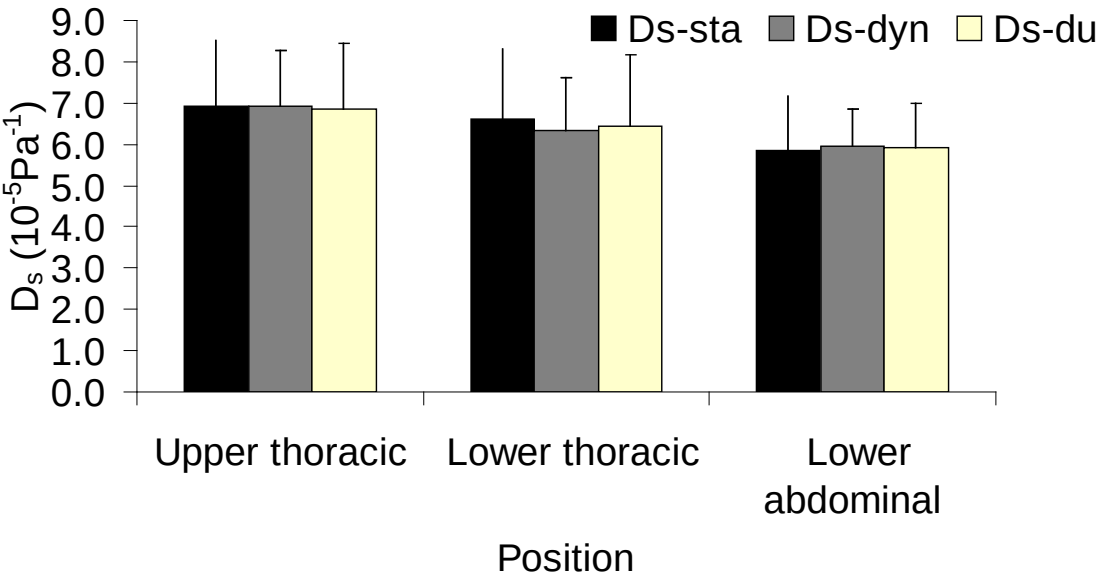

Figure 6.15: Distensibility against position (column with error bar). The distensibility become smaller when the measurement site is close to the lower abdominal, it means the lower abdominal part of the aorta is more rigid than the upper thoracic part of the aorta.

6.3.2.4 Non-invasive determination of Young's modulus

The non-invasive Young's modulus of the aorta was calculated by wave speed determined by *In*DU-loop with equation (6.5). The average value of the non-invasive Young's modulus is 0.086 ± 0.023 MPa.

The method to determine the Young's modulus by tensile test had been introduced in Section 6.2.4. The results of the Young's modulus (30 mmHg, 60 mmHg, 160 mmHg, 200 mmHg and 80-120 mmHg) were taken from the last cycle (the rising part) of the test, **Figure 6.16**.

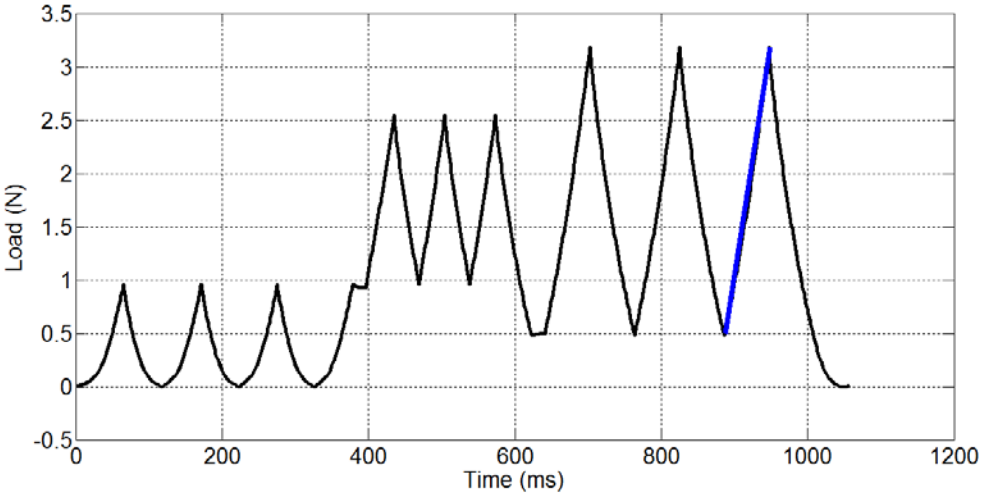

Figure 6.16: Test procedure of the tensile test of one of the aorta. All the Young's modulus results were taken from the last cycle, the rising part, shown in blue.

The regression line and Student's t-test show that values of E_{test} and E_{cdu} of all of the aortas are highly correlated (R^2=0.70, $p < 0.001$), **Figure 6.17a**.

The agreement of Young's modulus determined by the *In*DU-loop and tensile test methods is also assessed using Bland-Altman method. The results show that mean of difference between these two methods is -0.006 MPa, which indicate that Young's modulus determined by *In*DU-loop is slightly smaller that determined by tensile test. The difference between these two methods is within the acceptable range of mean±2SD (-0.006 ±0.0264 MPa), **Figure 6.17b**.

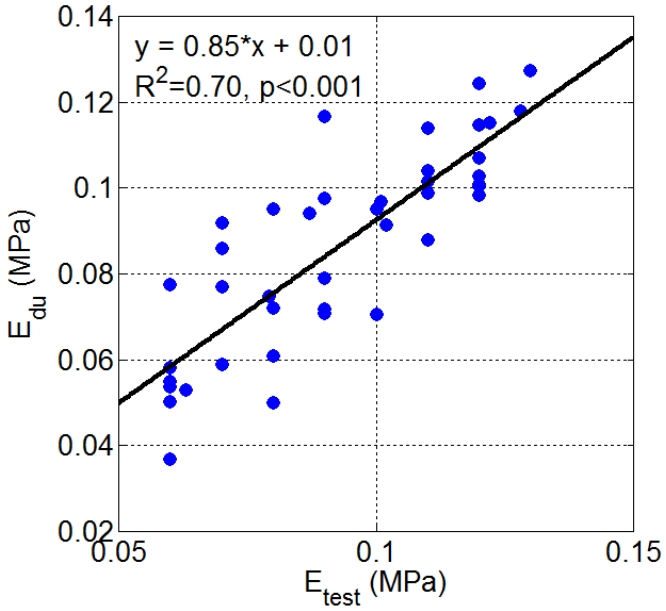

(a)

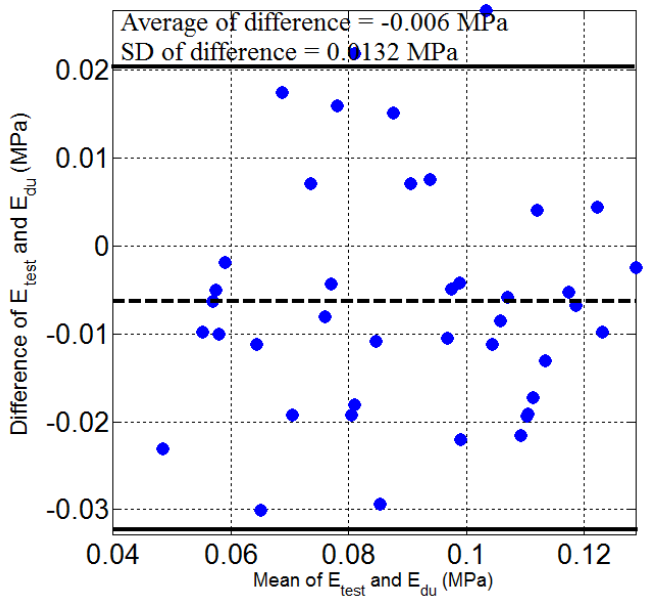

(b)

Figure 6.17: (a) Correlation of Young's modulus determined by *In*DU-loop and test. The correlation coefficient R^2=0.70, p<0.001. (b) The agreement between Young's modulus determined by the *In*DU-loop and test is assessed by Bland-Altman method. The middle horizontal line (dashed) indicates the mean of difference of wave speed determined by the two methods. The upper and lower horizontal lines (solid) indicate twice the standard deviation (2SD). Note that most of the data points fell within ±2SD range, and the zero line fell within the acceptable confidence limits of the average, indicating no statistically significant difference between these two methods.

Young's modulus against position is also plotted, it is found that the aorta becomes more rigid progressing along its length; Young's modulus is biggest at the lower abdominal, and smallest at the upper thoracic, **Figure 6.18**.

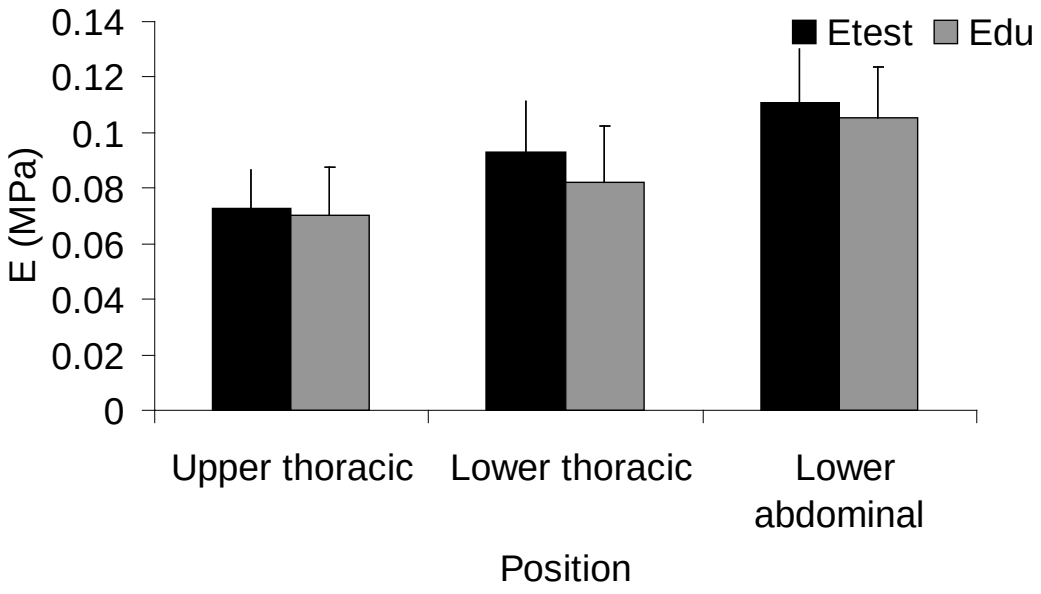

Figure 6.18: Young's modulus results from test (80-120 mmHg) and Young's modulus calculated using equation (6.5) and c_{DU} (column with error bar). Young's modulus become bigger as the measurement site moves distally, indicating the end of the aorta closer to the lower abdominal is more rigid than its inlet at the upper thoracic.

Young's modulus against pressure calculated in the tensile test for all the aortas is also plotted. It is found out that with bigger pressure on the aorta, the Young's modulus becomes bigger, the aorta is more rigid or stiffer, **Figure 6.19**.

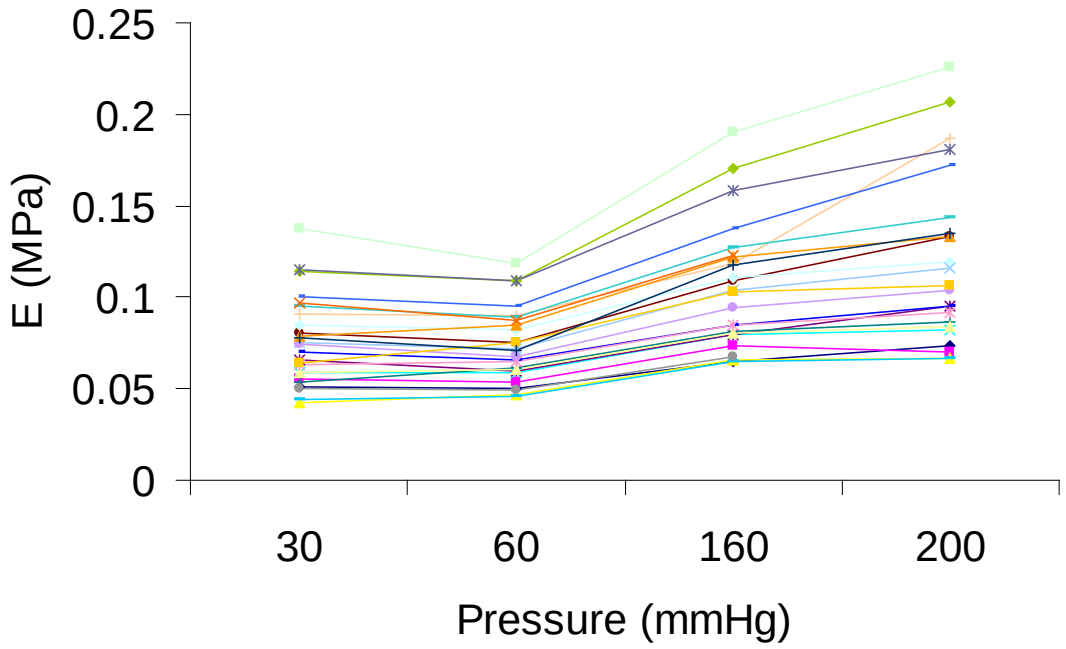

Figure 6.19: Young's modulus from the tensile test versus pressure. Different coloured lines show the individual aortas. Young's modulus increases with increased pressure.

6.4 Discussion

Mechanical properties are important to the understanding of the physiology of the arteries. The present study aimed to develop and test a new algorithm to determine the mechanical properties of vessels noninvasively. The algorithm is based on the non-invasive determination of local wave speed by the measurements of diameter and velocity. The algorithm is used to determine the distensibility and Young's modulus of flexible tubes and calf aortas. The distensibility and Young's modulus results show the agreements with static and dynamic distensibility tests, and tensile test, respectively.

Bergel (Bergel 1961a, b) developed an apparatus to determine the pressure-radius relationship of arterial specimens, both static and dynamic behaviour were measured using this technique. The vessels he used for the experiments included big arteries; thoracic, abdominal aorta, and also small arteries; femoral and carotid arteries. It was shown that the pressure-radius curve in an aorta that is under static distension does not follow the same path over an inflation and deflation cycle and a hysteresis loop is obtained. This implies that the energy put into the system during inflation is not fully recovered during deflation.

Patel (1969) studied the static anisotropic elasticity in the middle descending thoracic aorta of 14 living dogs. He used a displacement sensing device and a force gauge to measure radius and longitudinal stress respectively at several pressures in an isolated vessel segment *in situ*. He modified the standard technique to minimize hysteresis effects. Prior to his experiment, to determine elastic coefficients, the vessel was inflated and deflated for three cycles over the physiological range of pressure. He found out that the elastic modulus in the radial, circumferential and longitudinal directions increased with the increase in intravascular pressure, and the longitudinal modulus decreased when the vessel was studies in vitro.

Dobrin (1978) reported that the vascular stiffness was greatly influenced by the extracellular matrix, elastin is also considered an important determinant of arterial wall mechanical properties, and essential for vascular structural integrity and function. Elastin fibres have a modulus of elasticity of 0.6 MPa, and can stretch in excess of 250% of its original length. Collagen fibres are much stiffer

with a modulus of elasticity of 500 MPa, which is almost 1000 times larger than elastin.

Von Maltzahn et al. (1984) experimentally measured the elastic properties of media and adventitia of bovine carotid arteries. They found out that the media and the adventitia are anisotropic; the media is stiffer, more non-linear, and subjected to higher stresses than commonly assumed; and that both layers are stiffer in the axial direction than in the tangential direction.

Large arteries have a high degree of elasticity because elastin plays a major role in determination of mechanical properties of the vascular wall (O'Rourke, 1982). This property is essential for cardiovascular function. By reducing pressure variations during the cardiac cycle, this allows a relatively constant blood flow and correct organ irrigation (Safar and London, 1994).

The static and dynamic distensibility behaviour of various arteries has been studied extensively. It has been established that, the dynamic distensibility shows lower value than the corresponding static distensibility (Glaser et al., 1995; Lichtenstein et al., 1998). And the results in this study show that the distensibility calculated from the local wave speed is $6.61X10^{-5}$ Pa^{-1}, the static and dynamic distensibilities are 6.46 $X10^{-5}$ Pa^{-1} and 6.39 $X10^{-5}$ Pa^{-1}. The results in this study also show that the distensibility is decreasing from the upper thoracic to the lower abdominal along the aorta (**Figure 6.15**).

In this study, Young's modulus determined by *In*DU-loop and tensile test are all increased from the upper thoracic to the lower abdominal of the aorta. It means the mechanical properties of the arterial wall are different from site to site, and it is confirmed with other researchers' work (Harkness et al., 1957; Guo and Kassab, 2003; Lillie and Gosline, 2007). In Lillie and Gosline's work, they investigated the mechanical properties of the thoracic aorta in the pig, they reported that the circumferential secant modulus increased from that at aortic arch to that near diaphragm, indicated that the stiffness of the elastin increased with position along the aorta. In Guo and Kassab's work, they reported similar results in mice; the circumferential modulus is greatest (most rigid) near the diaphragm, and the majority of volume compliance (85%) is in the thoracic compared with the abdominal aorta.

The second objective of the present study was to validate the non-invasive determination of local wave speed by measurements of diameter and velocity *in*

situ. This method was developed by Feng and Khir (Feng and Khir, 2010), validated in flexible tubes *in vitro* (Li and Khir, 2011). In this study, it has been used to determine the local wave speed in calf aortas, the results were compared with those determined by PU-loop and foot-to-foot methods. The results shown in **Table 6.2** and **Figure 6.11** indicate that wave speed determined by *ln*DU-loop is comparable to those of the PU-loop and foot-to-foot methods. The wave speed determined by *ln*DU-loop is 4.15% and 13.11% smaller than those of PU-loop and foot-to-foot methods, respectively.

It is also found out that the internal diameter and wall thickness at the lower abdominal aorta is smaller than those at upper thoracic and lower thoracic aorta, **Table 6.2** and **Figure 6.9**, the shape of the internal of the aorta is like a tapered tube, the wave speed supposed to be bigger when the measurement site is close to the end of the aorta, and this is confirmed by the results (**Figure 6.12)**. The results show that all wave speeds at the lower abdominal for all the aortas are bigger than those at the lower thoracic, and all the wave speeds at the lower thoracic are bigger than those at the upper thoracic of the aorta.

All experiments in the present study were performed within the physiological range. The determination of the local wave speed was performed in the pressure range of 10 to 16 kPa, which is 75 to 120 mmHg. The tensile test was carried out between 30-200 mmHg which cover the pressure range of the wave speed experiment. The volume of the pump which used to generate the pulse was 70 ml, and the volume which inserted for the static distensibility was also 70 ml.

Importance of non-invasive determination of mechanical properties

The importance of assessing arterial wall properties has been shown by studies demonstrating that a decrease of the pulsatile function of large arteries represents an independent risk factor for future cardiovascular events (Madhavan et al., 1994; Benetos et al., 1998; Franklin et al., 1999; de Simone et al., 1999). Several *in vivo* and *ex vivo* techniques have been developed to assess the mechanical properties of vessels. *In vivo* approaches, for example, magnetic resonance imaging, have shown correlation of disease and mortality with arterial elasticity in population studies. Because of the expense and limited availability of these approaches, they are not widely used as a clinical tool for the diagnosis and follow up of patients. Most *ex vivo* techniques have focused

their study on the mechanical properties of the arterial tissue in different axes. These techniques are usually destructive which can not be applied in an *in vivo* setting. The mechanical properties measurements are assessed by numerous methods and devices. These methods are different according to their physical basis, simplicity to use and nature of the measured parameter. The non-invasive method which could directly measure the parameter, provide accurate results, easily performed in routine and low expense should be pay attention and applied.

6.4.1 Limitation

In this work, the mechanical properties of flexible tubes and calf aortas were determined. The experiments were performed with flexible tubes and calf aortas in limited numbers. Although the materials of the flexible tubes are isotropic, the tensile tests conducted in this study for the flexible tubes were limited to tests in the longitudinal direction because of the size of the tubes. Test specimens that could be obtained from the tubes in the circumferential direction were very small and consequently very difficult to grip and test.

The tensile test was performed with ring aorta specimens at load speed (10mm/min). This test can only show the stress-strain relation in the circumference direction at one time. The aorta specimen could not be physiologically loaded with an axial prestretch corresponding to the in situ length of the vessel. During the extension test, the width of the specimen would decrease due to the increase of the length.

In the static distensibility test, the end of the aorta was closed with caps, the pressure catheter was inserted into the inlet of the aorta by a Y-connection, the branches on the aorta were closed by the cable ties. The volume ejected into aorta is comparable to the stroke volume, 70 ml. However, the static test was not start at the physiological pressure (75mmHg), and this could overestimate the distensibility results. The static distensibility test preserves the native collagen/elastin structure and provides for a more physiological representation of the in vivo loading conditions. Both the tests were performed to represent the in vivo conditions. However, the average thoracic diameter increased 1.7 mm during systole (Mao et al., 2008), so the diameter change of the thoracic aorta is 3.4 mm/sec (heart beat 60 bpm); the 10 mm/min (0.17 mm/sec) load speed of

the ring test is very slow, and could not represent the diameter change of the aorta during the heart beat. The static test is performed step by step, also could not represent the dynamic behaviour of the hear beat.

The new technique was also tested in calf descending aortas in a limited numbers. The function of elastin in small arteries is not as important as in large aortas, it is not a major contributor to the mechanical properties of the small arteries, so tests on small arteries such as the femoral, arteries should be applied in the future work.

The applicability of the animal data presented here to normal vessels *in vivo* has certain limitations: for example the mechanical properties of blood vessels *in vivo* are strongly influenced by the tethering to surrounding tissues and by the tone in the smooth muscles in the vessel wall, which in turn depend on the humoral and neural factors.

6.5 Conclusion

In this work, the non-invasive determination of local wave speed by measurements of diameter and velocity was validated by the experiments performed in calf aortas. The results show an agreement with those determined by PU-loop and foot-to-foot methods. Followed up, a non-invasive algorithm was developed using the non-invasive wave speed to determine the mechanical properties including distensibility and Young's modulus of vessels. The new algorithm was tested with flexible tubes and calf aortas. The distensibility and Young's modulus results using the new technique agree well with those determined by the static and dynamic distensibility tests, and tensile test, respectively. The results also show that the internal shape of the calf aortas is like a taper tube with decreasing diameter and thickness from proximal to distal; Distensibility decreasing from proximal to distal along the aortas and Young's modulus increasing, in contrast. It is suggested that it is worth to do further investigation in order to prove the application in vivo, such as the non-invasive distensibility measurements in coronary arteries.

Chapter 7
Conclusions and Future Works

The biomechanical relevance of this thesis lies in its potential application to better understand the cardiovascular system in health and disease. Also in particular, this thesis provides information on measurement of arterial stiffness and non-invasive diagnosis of cardiovascular diseases such as hypertension, stroke and other conditions.

In this study, it is found that the wave speed determined by a non-invasive technique *ln*DU-loop is very close to those determined by PU-loop and foot-to-foot methods (chapter 3). Although the density term is not part of the equation of *ln*DU-loop determining wave speed, *ln*DU-loop is still sensitive to changes in the fluid density for the determination of local wave speed. Wave speed determined by *ln*DU-loop is used to determine the mechanical properties of flexible tubes and calf aortas (chapter 6). Moens-Korteweg equation and Bramwell-Hill equations allow the determination of Young's modulus and distensibility by wave speed. The *ln*DU-loop method of determining wave speed in this research using the measured diameter and velocity provides a potential non-invasive technique for the determination of mechanical properties of vessel wall.

Effect of wave speed determined by PU-loop with proximity to the reflection site was observed (chapter 4), and it is found that when the measurement site is close to the reflection site, wave speed determined by PU-loop will increase or decrease depending on whether the reflection is positive or negative, respectively. The effect of change on the measured wave speed increased as the measurement site become close to the reflection site.

In chapter 3 I compared the foot-to-foot, PU-loop and *ln*DU-loop methods for the determination of wave speed, which was measured in 1 m long tube, at 25 cm, 50 cm, and 75 cm away from the inlet of the tube. These results should not be involved by the observation in chapter 4, regarding the increase or decrease

in wave speed determined by PU-loop, when measures in close proximity to the reflection site. The observation in chapter 3 doesn't show any significant change of wave speed determined by PU-loop, and the correlation between PU-loop and foot-to-foot method is very good. This is because the experimental setup of chapter 3 is different from that of chapter 4, the first reflection site in the setup of chapter 3 is the reservoir connected to the outlet of the tube, which is 1.75 m away from the last measurement site, the wave speed should not be affected by the reflection site. In chapter 4, in order to separate the reservoir reflection from the reflection which is generated by the connection of the mother and daughter tubes, a 13 m long connection tube was used to connect the daughter tube and the reservoir.

Wave intensity analysis allows the determination of local reflection coefficient using the wave intensity and wave energy when the measurement site is close to the reflection site. The local reflection coefficients determined by wave intensity and wave energy which are very close to the reflection site are in good agreements with the theoretical reflection coefficients. Local reflection coefficients determined by wave intensity and wave energy are not comparable to those determined by pressure, however, the square roots of local reflection coefficients determined by wave intensity and wave energy are similar to those determined by pressure, although with a degree of overestimation. Local reflection coefficients determined by wave intensity, wave energy and pressure all increased or decreased along the tube toward the reflection site due to wave dissipation. Forward and backward wave intensities, wave energies and pressures are dissipating exponentially. For the backward wave intensity, wave energy and pressure, the dissipation of expansion waves are greater than the compression waves, this is in agreement with earlier work (Feng and Khir, 2008). In their previous work (Feng et al., 2007), they also concluded that the dissipations of the forward and backward compression wave (pressure, wave intensity and wave energy) are the same, but in this study, the dissipations of backward compression wave intensity and wave energy are smaller than the dissipations of forward compression wave.

7.1 Conclusions

This thesis has met the objectives set out in Section 1.3.

The main findings drawn from this study are:

1) The algorithm derived from the previous study for determining wave speed and wave intensity non-invasively using measurement of diameter and velocity at same site has been validated and compared in flexible tubes and calf aortas. Wave speed determined by *ln*DU-loop is generally slightly smaller than that determined by PU-loop. The shapes of the separated forward and backward wave intensities based on diameter and velocity are very similar to the shapes of those based on pressure and velocity technique, respectively. The timing of arrival time of reflected wave based on diameter and velocity highly agreed with the corresponding timing based on pressure and velocity technique. Although the density term is not part of the equation, the *ln*DU-loop method for determining local wave speed is sensitive to the fluid density; increasing fluid density causes a decrease in wave speed determined by *ln*DU-loop. Therefore, it is concluded that *ln*DU-loop method can be used to determine local wave speed and wave intensity using measurement of diameter instead of pressure.

2) PU-loop method used to determine local wave speed is affected by the reflection. It is found: (a) measured wave speed is affected as the measurement site closer to the reflection site; (b) measured wave speed increased with the positive reflections, and decreased with the negative reflections; (c) the larger the reflection coefficient, the greater is the change of the wave speed.

3) An algorithm has been used in this thesis to correct the measured wave speed with proximity to the reflection site. In this technique, a correction factor is applied to the measured wave speed, then, after several iterations, the corrected wave speed is within 10% difference of the wave speed not affected.

4) The amplitude of the local reflection coefficient measured by pressure, square root of and wave intensity and wave energy increase or decrease (for positive or negative reflection) with proximity to the reflection site. It is found: (a) the closer the measurement site to the reflection site, of the greater the value of the local reflection coefficient; (b) an increase in local reflection coefficient related to the positive reflection, a decrease in local reflection coefficient related to the negative reflection.

5) Wave intensity and wave energy are used to determine the local reflection coefficient. Due to wave dissipation, the closer the measurement site to the reflection site, the greater the value of the local reflection coefficient; the local reflection coefficient determined by wave intensity and wave energy near the reflection site is the closest to the theoretical value of the reflection coefficient. Therefore, wave intensity analysis could be used to determine the local reflection coefficient only if measurement and reflection sites are in close proximity.

6) The technique utilising the *ln*DU-loop for determining mechanical properties of the arterial wall using measurement of diameter and velocity at one point, could potentially be non-invasive. Distensibility determined by this new technique is very close to the static and dynamic distensibilities in calf aortas. Young's modulus determined by the new technique is also very close to that determined by the tensile test in both flexible tubes and bovine aortas. Therefore, it is concluded that the new technique can be used to determine mechanical properties non-invasively.

7.2 Future work

1) From the previous and current study, it is shown that the wave speed determined by *ln*DU-loop is always smaller than the wave speed determined by PU-loop. Instead of measuring pressure and velocity, diameter and velocity measurements are required for the *ln*DU-loop technique. The pressure, diameter relationship, which is probably related to the wall properties could be investigated, to resolve this inconsistency.

2) Wave speed determined by PU-loop is affected when the measurement site is close to the reflection site. An algorithm is used in chapter 4 to correct the affected wave speed. But in clinical application, the real wave speed is not known in the vessel, so it is not possible to judge whether the measured wave speed is affected or not. It would be useful to improve the algorithm used in this thesis, so that the iteration could converge or stopped with a threshold when the corrected wave speed becomes closer to the real wave speed.

3) Due to wave dissipation, the local reflection coefficient increased along the tube towards to the reflection site. It is shown the dissipation of the backward compression wave is smaller than that of the forward compression wave; the

dissipation of the backward expansion wave is bigger than that of the forward compression wave. It would be useful to investigate the dissipation of the forward and backward compression and expansion waves and to quantify the difference between them in flexible tubes with different materials.

4) The structural components of the vessel wall change with various conditions, for example, ageing, diabetes, and hypertension. These raise a risk factor for arteriosclerosis due to the mechanical or metabolic abnormality through various mechanisms. One of the implications of the structural changes is the change in mechanical properties of the blood vessel, for example, the compliance or modulus. In this thesis, distensibility and Young's modulus have been determined noninvasively. The application of this new non-invasive determination in clinically, is to determine their suitability for the diagnoses of these disease would be good.

Glossary

A	Area
c	Wave speed
$C_{foot\text{-}to\text{-}foot}$	Wave speed determined by foot-to-foot
C_{PU}	Wave speed determined by PU-loop
C_{DU}	Wave speed determined by *In*DU-loop
c_m	Measured wave speed
D	Diameter
D_0	Undisturbed diameter
D_{in}	Internal diameter
dA	The first derivative of area
dD	The first derivative of diameter
dI_{PU}	Wave intensity determined by pressure and velocity
dI_{DU}	Wave intensity determined by diameter and velocity (non-invasive wave intensity)
dP	The first derivative of pressure
d(dP)	The second derivative of pressure
dU	The first derivative of velocity
D_s	Distensibility
$D_{s\text{-}cdu}$	Distensibility determined by C_{DU}
$D_{s\text{-}dyn}$	Dynamic distensibility
$D_{s\text{-}test}$	Distensibility determined by pressure and extension in the tensile test
$D_{s\text{-}sta}$	Static distensibility
E	Young's modulus
E_c	Correction factor
E_{cdu}	Young's modulus calculated by C_{DU}
E_{test}	Young's modulus from the tensile test
h	Wall thickness
I_{DU}	Wave energy determined by diameter and velocity

I_{PU}	Wave energy determined by pressure and velocity
L	Length/distance
*ln*DU-loop	Diameter-Velocity loop
P	Pressure
p	p value
PU-loop	Pressure-Velocity loop
Q	Flow
R	Reflection coefficient
R^2	Square of the correlation coefficient
r	Radius
ρ	Density
R_{dP}	Reflection coefficient determined by ratio of peak backward and forward pressures
R_{dI}	Reflection coefficient determined by ratio of peak backward and forward wave intensity determined by pressure and velocity
R_I	Reflection coefficient determined by square root of ratio of backward and forward wave energy determined by pressure and velocity
$R_{dI}^{0.5}$	Reflection coefficient determined by square root of ratio of peak backward and forward wave intensity determined by pressure and velocity
$R_I^{0.5}$	Reflection coefficient determined by ratio of backward and forward wave energy determined by pressure and velocity
R_t	Theoretical reflection coefficient
SD	Standard deviation
T	Transmission coefficient
t	Time
τ	Time it takes for the wave to travel from the measurement site to the reflection site and come back
Trw	Arrival time of reflected wave

$Trw_{D\_}$	Arrival time of reflected wave using D_-
Trw_{DU}	Arrival time of reflected wave using dI_{DU-}
$Trw_{P\_}$	Arrival time of reflected wave using P_-
Trw_{PU}	Arrival time of reflected wave using dI_{PU-}
U	Velocity
WIA	Wave intensity analysis

Appendix

List of Publications

1. Journal Publications

1. **Li Y, Khir AW**. Experimental validation of non-invasive and fluid density independent methods for the determination of local wave speed and arrival time of reflected wave. *Journal of Biomechanics* 44 (7): 1393-1399. 2011.

2. Conference Proceedings

1. **Li Y, Borlotti A, Parker K, Khir AW**. Variation of wave speed determined by the PU-loop with proximity to a reflection site. *33rd Annual international Conference of the IEEE Engineering in Medicine and Biology Society* (In press). 2011.

2. **Li Y, Borlotti A, Hickson SS, McEniery CM, Wilkinson IB, Khir AW**. Using magnetic resonance imaging measurements for the determination of local wave speed and arrival time of reflected waves in human ascending aorta. *32nd Annual international Conference of the IEEE Engineering in Medicine and Biology Society*, pp. 5153-5156. 2010.

3. **Li Y, Khir AW**. Determination of mechanical properties of flexible tubes using diameter and velocity. *17th Congress of the European Society of Biomechanics*. 2010.

4. **Li Y, Khir AW**. Determination of wave speed and distensibility of flexible tubes using diameter and velocity. *31st Annual international Conference of the IEEE Engineering in Medicine and Biology Society*, pp. 1796-1799. 2009.

References

Aakhus S, Torp H, Haugland T, Hatle L. Non-invasive estimates of aortic root pressures: external subclavian arterial pulse tracing calibrated by oscillometrically determined brachial arterial pressures. Clinical Physiology and Functional Imaging 13(6): 573-586. 1993.

Aggoun Y, Sidi D, Levy BI, Lyonnet S, Kachaner J, Bonnet D. Mechanical properties of the common carotid artery in Williams syndrome. *Heart* 84: 290-293. 2000

Aguado-Sierra J, Parker KH, Davies J, Francis D, Hughes A, Mayet J. Arterial pulse wave velocity in coronary arteries. *28th Annual International Conference of the IEEE Engineering in Medicine and Biology Society* 1: 867-870. 2006

Alastruey J. Numerical assessment of time-domain methods for the estimation of local arterial pulse wave speed. *Journal of Biomechanics* 44, 885-891. 2011.

Alexander J, Burkhoff D, Schipke J, Sagawa K. Influence of mean pressure on aortic impedance and reflections in the arterial system. *AJP-Heart and Circulatory Physiology* 257: H969-H978. 1989.

Alleyne R. Heart disease beats breast cancer as the biggest killer. http://www.telegraph.co.uk/health/healthnews/8585195/Heart-disease-beats-breast-cancer-as-the-biggest-killer.html. 2011

Apter JT. Mathematical development of a physical model of some visco-elastic properties of the aorta. *Bulletin of Mathematical Biology* 26(4): 367-388. 1964.

Arnett DK, Evans GW, Riley WA. Artery stiffness: a new cardiovascular risk factor? *American Journal of Epidemiology* 140(8): 669-682. 1994.

Arterial stiffness index. Online sheet. http://www.fukuda.co.jp/english/products/special_features/vasera/cavi.html. last access on 15/05/2012.

Asmar R, Benetos A, Topouchian J, Laurent P, Pannier B, Brisac AM, Target R, Levy BI. Assessment of arterial distensibility by automatic pulse wave velocity measurement. *Hypertension* 26: 485-490. 1995.

Avolio AP, Chen SG, Wang RP, Zhang CL, Li MF, O'Rourke MF. Effects of aging on changing arterial compliance and left ventricular load in a northern Chinese urban community. *Circulation* 68: 50-58. 1983.

Avolio AP, Deng FQ, Li WQ, et al. Effects of aging on arterial distensibility in populations with high and low prevalence of hypertension: comparison between urban and rural communities in China. *Circulation* 71: 202-210. 1985.

Avolio AP. Aging and wave reflection. *Journal of Hypertension* 10(6): S83-86. 1992.

Bank AJ, Kaiser DR, Rajala S, Cheng A. *In vivo* human brachial artery elastic mechanics: effects of smooth muscle relaxation. *Circulation* 100: 41-47. 1999.

Benetos A, Safar M, Rudnichi A, Smulyan H, Richard JL, Ducimetiere P, Guize L. Pulse pressure: a predictor of long-term cardiovascular mortality in a French male population. *Hypertension* 30: 1410-1415. 1997.

Benetos A, Rudnichi A, Safar M, Guize L. Pulse pressure and cardiovascular mortality in normotensive and hypertensive subjects. *Hypertension* 32: 560-564. 1998.

Benson, Katherine. MCAT Review, Emory University pp. 61.1999.

Bergel DH. The static elastic properties of the arterial wall. *Journal of Physiology* 156:445-457. 1961a.

Bergel DH. The dynamic elastic properties of the arterial wall. *Journal of Physiology* 156:458-469. 1961b.

Bessems D, Giannopapa CG, Rutten MCM, van de Vosse FN. Experimental validation of a time-domain-based wave propagation model of blood flow in viscoelastic vessels. *Journal of Biomechanics* 41, 284-291. 2008.

Blacher J, Asmar R, Djane S, London GM, Safar ME. Aortic pulse wave velocity as a marker of cardiovascular risk in hypertensive patients. *Hypertension* 33(5): 1111-1117. 1999a.

Blacher J, Guerin AP, Pannier B, Marchais SJ, Safar ME, London GM. Impact of aortic stiffness on survival in end-stage renal disease. *Circulation* 99(18): 2434-2439. 1999b.

Bland JM, Altman DG. Statistical methods for assessing agreement between two methods of clinical measurement. *Lancet* 327, 307-310. 1986.

Bleasdale RA, Parker KH, Jones CJH. Chasing the wave. Unfashionable but important new concepts in arterial wave travel. *AJP-Heart and Circulatory Physiology* 284: H1879-1885. 2003.

Boutouyrie P, Bussy C, Hayoz D, Hengstler J, Dartois N, Laloux B, Brunner H, Laurent S. Local pulse pressure and regression of arterial wall hypertrophy during long-term antihypertensive treatment. *Circulation* 101: 2601-2606. 2000.

Boutouyrie P, Tropeano AI, Asmar R, Gautier I, Benetos A, Lacolley P, Laurent S. Aortic stiffness is an independent predictor of primary coronary events in hypertensive patients: a longitudinal study. *Hypertension* 39: 10-15. 2002.

Boutouyrie P, Briet M, Collin C, Vermeersch S, Pannier B. Assessment of pulse wave velocity. *Artery Research* 3(1): 3-8. 2009.

Bramwell JC, Hill AV. The velocity of the pulse wave in man. *Proceedings of the royal society of London Series B*: 298-306. 1922.

Bramwell JC, Hill AV, McSwiney BA. The velocity of the pulse wave in man in relation to age as measured by the hot-wire sphygmograph. *Heart* 10: 233-255. 1923.

Brin KP, Yin FC. Effect of nitroprusside on wave reflections in patients with heart failure. *Annals of Biomedical Engineering* 12(2): 135-150. 1984.

British Heart Foundation, BHF Facts. Online sheet. http://www.bhf.org.uk/media/news-from-the-bhf/bhf-facts.aspx. 2011.

Cameron JD, Jennings GL, Dart AM. The relationship between arterial compliance, age, blood pressure and serum lipid levels. *Journal of Hypertension* 13: 1718-1723. 1995.

Cameron JD, Dart AM. Exercise training increases total systemic arterial compliance in humans. *American Journal of Physiology* 266: H693-701. 1994.

Caro CG, Pedley TJ, Schroter RC, Seed WA. The Mechanics of the Circulation. Oxford University Press, Oxford, UK. 1978.

Chen CH, Nevo E, Fetics B, Pak PH, Yin FCP, Maughan WL, Kass DA. Estimation of central aortic pressure waveform by mathematical transformation of radial tonometry pressure. Validation of generalized transfer function. *Circulation* 95: 1827-1836. 1997.

Choi CU, Park EB, Suh SY, Kim JW, Kim EJ, Rha SW, et al. Impact of aortic stiffness on cardiovascular disease in patients with chest pain: assessment with direct intra-arterial measurement. *American Journal of Hypertension* 20(11): 1163-1169. 2007.

Cox RH. Three-dimensional mechanics of arterial segments in vitro: methods. *Journal of Applied Physiology* 36: 381-384. 1974.

Cox RH. Arterial wall mechanics and composition and the effects of smooth muscle activation. *American Journal of Physiology* 229: 807-812. 1975.

Cox RH. Passive mechanics and connective tissue composition of canine arteries. *American Journal of Physiology* 234: H533-H541. 1978.

Cox RH. Changes in arterial wall properties during development and maintenance of renal hypertension. *American Journal of Physiology* 242: H477-H484. 1982.

Cruickshank K, Riste L, Anderson SG, Wright JS, Dunn G, Gosling RG. Aortic pulse-wave velocity and its relationship to mortality in diabetes and glucose intolerance: an integrated index of vascular function? *Circulation* 106 (16): 2085-2090. 2002.

Cutnell JD, Johnson K. Physics. 4th ED. Wiley, New York pp.308. 1998.

Dart AM, Lacombe F, Yeoh JK, Cameron JD, Jenning GL, Laufer E, Esmore DS. Aortic distensibility in patients with isolated hypercholesterinemia, ocornary artery disease or cardiac transplant. *Lancet* 338: 270-273. 1991.

Davies JE, Whinnett ZI, Francis DP, Willson K, Foale RA, Malik IS, Hughes AD, Parker KH, Mayet J. Use of simultaneous pressure and velocity measurements to estimate arterial wave speed at a single site in human. *AJP-Heart and Circulatory Physiology* 290: H878-885. 2006a.

Davies JE, Whinnett ZI, Francis DP, Manisty CH, Aguado-Sierra J, Willson K, Foale RA, Malik IS, Hughes AD, Parker KH, Mayet J. Evidence of a dominant backward-propagating "suction" wave responsible for diastolic coronary filling in humans, attenuated in left ventricular hypertrophy. *Circulation* 113(14): 1768-1778. 2006b.

Davies JE, Hadjiloizou N, Leibovich D, Malaweera A, Alastruey J, Whinnett ZI, Manisty CH, Francis DP, Aguado J, Foale RA, Malik IS, Parker KH, Mayet J, Hughes AD. Importance of the aortic reservoir in determining the shape of the arterial pressure waveform-the forgotten lessons of Frank. *Artery Research* 1 (2): 40-45. 2007.

Davis RF. Clinical comparison of automated auscultatory and oscilometric and catheter-transducer measurements of arterial pressure. *Journal of Clinical Monitoring and Computing 1*(2): 114-119. 1985.

Debes JC, Fung YC. Biaxial mechanics of excised canine pulmonary arteries. *AJP-Heart and Circulatory Physiology* 269: H433-442. 1995.

De Simone G, Roman MJ, Koren MJ, Mensah GA, Ganau A, Devereux RB. Stroke volume/pulse pressure ratio and cardiovascular risk in arterial hypertension. *Hypertension* 33: 800-805. 1999.

Dobrin PB, Rovick AA. Influence of vascular smooth muscle on contractile mechanics and elasticity of arteries. *American Journal of Physiology* 217: 1644-1651. 1969.

Dobrin PB. Isometric and isobaric contraction of carotid arterial smooth muscle. *American Journal of Physiology* 225: 659-663. 1973.

Dobrin PB. Mechanical properties of arteries. *Physiological Reviews* 58(2): 397-460. 1978.

Dobrin PB, Canfield TR. Elastase, collagenase, and the biaxial elastic properties of dog carotid artery. *AJP-Heart and Circulatory Physiology* 247(1): H124-131. 1984.

Duan B, Zamir M. Pressure peaking in pulsatile flow through arterial tree structures. *Annals of Biomedical Engineering* 23(6): 794-803. 1995.

Dzau VJ, Safar ME. Large conduit arteries in hypertension: role of the vascular enin-angiothnsin system. *Circulation* 77(5): 947-954. 1988.

Euler L. Principia pro motu sanguinis per arterias determinando. *Opera posthuma mathematica et physica anno 1844 detecta*, 2: 814-823, 1775. Ediderunt P.H. Fuss et N. Fuss Petropoli; Apund Eggers et Socios.

Feng J, Long Q, Khir AW. Wave dissipation in flexible tubes in the time domain: In vitro model of arterial waves. *Journal of Biomechanics* 40: 2130-2138. 2007.

Feng J, Khir AW. The compression and expansion waves of the forward and backward flows: an in-vitro arterial model. *Proceedings of the Institution of Mechanical Engineers. Part H, Journal of engineering in medicine* 222(4): 531-542. 2008

Feng J, Khir AW. Determination of wave speed and wave separation in the arteries using diameter and velocity. *Journal of Biomechanics* 43: 455-462. 2010.

Fox SI. Human physiology. 4th Ed. McGraw-Hill Education.1992.

Frank O. Die grundform des arteriellen pulses. *Z. Biol* 37: 483-526. 1899.

Frank O. Der puls inden arterien. *Z Biol* 46: 441-553. 1905

Franklin K, Muir P, Scott T, Wilcocks L, Yates P. Introduction to biological physics for the health and life sciences. John Wiley and Sons Ltd, 2010: 142.

Franklin SS, Khan SA, Wong ND, Larson MG, Levy D. Is pulse pressure useful in predicting risk for coronary heart disease? The Framingham Heart Study. *Circulation* 100: 354-360. 1999.

Frequency Response. http://www.transonic.com/data/RL-20a-ds.pdf, last accessed on 07/12/2011

Fujimoto S, Mizuno R, Saito Y, Nakamura S. Clinical application of wave intensity for the treatment of essential hypertension. *Heart and Vessels* 19(1): 19-22. 2004.

Gasser TC, Schulze-Bauer CAJ, Holzapfel GA. A three dimensional finite element model for arterial clamping. *Journal of Biomechanical Engineering* 124(4): 355-363. 2002.

Gatzka CD, Cameron JD, Kingwell BA, Dart AM. Relation between coronary artery disease, aortic stiffness, and left ventricular structure in a population sample. *Hypertension* 32: 575-578. 1998.

Gillensen T, Gillensen F, Sieberth H, Hanrath P, Heintz B. Age-related changes in the elastic properties of the aortic tree in normotensive patients: investigation by intravascular ultrasound. *European Journal of Medical Research* 1(3): 144-148. 1995.

Glaser E, Lacolley P, Boutouyrie P, Sacunha R, Lucet B, Safar ME, Laurent S. Dynamic versus static compliance of the carotid artery in living Wistar-Kyoto rats. *Journal of Vascular Research* 32: 254-265. 1995.

Goodfellow J, Ramsey MW, Luddington LA, Jones CJH, Coates PA, Dunstan F, Lewis MJ, Owens DR, Henderson AH. Endothelium and inelastic arteries: an early marker of vascular dysfunction in non-insulin dependent diabetes. *BMJ* 312: 744-745. 1996.

Gravlee G, Bauer S, O'Rourke M et al. A comparison of brachial, femoral and aortic intraarterial pressures before and after cardiopulmonary bypass. *Anaesthesia and Intensive Care* 17(3): 305-311. 1989.

Greenwald SE, Carter AC, Berry CL. Effect of age on the in vitro reflection coefficient of the aortoiliac bifurcation in humans. *Circulation* 82(1): 114-123. 1990.

Gregg D. The physiological basis of medical practice, chapter Dynamics of blood and lymph flow, Williams and Wilkins, New York, 8th edition. 1966.

Guinea GV, Atienza JM, Elices M, Aragoncillo P, Hayashi K. Thermomechanical behavior of human carotid arteries in the passive state. *AJP-Heart and Circulatory Physiology* 288: H2940-2945. 2005.

Guo XM, **Kassab GS**. Variation of mechanical properties along the length of the aorta in C57bl/6 mice. *AJP-Heart and Circulatory Physiology* 285: H2614-H2622. 2003.

Hales S. Statistical Essays: Containing Haemastaticks. New York: Hafner, Reprinted in 1964. 1733.

Harada A, Okada T, Sugawara M, Niki K. Development of a non-invasive measurement system of wave intensity. *IEEE Ultrasonics symposium* 2: 1517-1520. 2000.

Harada A, Okada T, Niki K, Chang D, Sugawara M. Online noninvasive one-point measurements of pulse wave velocity. *Heart and vessels* 17: 61-68. 2002.

Harkness MLR, Harkness RD, McDonald DA. The collagen and elastin content of the arterial wall in the dog. *Proceedings of the royal society B Biological Science* 146(925): 541-551. 1957.

Hayoz D, Rutschmann B, Perret F et al. Conduit artery compliance and distensibility are not necessarily reduced in hypertension. *Hypertension* 20: 1-6. 1992.

Healthy Heart Rate. http://www.healthyheartrate.org/.

Heitz B, Gillessen T, Walkenhorst F, vom Dahl J, Dorr R, Krebs W, Hanrath P, Sieberth HG. Evaluation of segmental elastic properties of the aorta in normotensive and medically treated hypertensive patients by intravascular ultrasound. *Journal of Hypertension* 11: 1253-1258. 1993.

Hobson TN, Flewitt JA, Belenkie I, Tyberg JV. Wave intensity analysis of left atrial mechanics and energetics in anesthetized dogs. *AJP-Heart and Circulatory Physiology* 292(3): H1533-1540. 2007.

Hodes RJ, Lakatta EG, McNeil CT. Another modifiable risk factor for cardiovascular disease? Some evidence points to arterial stiffness. *Journal of the American Geriatrics Society* 43: 581-582. 1995.

Hoeks AP, Ruissen CJ, Hick P, Reneman RS. Transcutaneous detection of relative changes in artery diameter. *Ultrasound in Medicine and Biology* 11: 51-59. 1985.

Hoeks AP, Brands PJ, Smeets FA, Reneman RS. Assessment of the distensibility of superficial arteries. *Ultrasound in Medicine and Biology* 16: 121-128. 1990.

Hoeks APG, Brands PJ, Willigers JM, Reneman RS. Non-invasive measurement of mechanical properties of arteries in health and disease. *Proceedings of the Institution of Mechanical Engineers* 213 Part H: 195-202. 1999.

Hollander EH, Wang JJ, Dobson GM, Parker KH, Tyberg JV. Negative wave reflections in pulmonary arteries. *AJP-Heart and Circulatory Physiology* 281(2): H895-902. 2001

Holzapfel GA, Sommer G, Regitnig P. Anisotropic mechanical properties of tissue components in human atherosclerotic plaques. *Journal of Biomechanical Engineering* 126: 657-665. 2004.

Horvath IG, Nemeth A, Lenkey Z, Alessandri N, Tufano F, Kis P, Gaszner B, Cziraki A. Invasive validation of a new oscillometric device (Arteriograph) for measuring augmentation index, central blood pressure and aortic pulse wave velocity. *Journal of Hypertension* 28: 2068-2075. 2010.

Humphrey JD, Vawter DL, Vito RP. Quantification of strains in biaxially tested soft tissues. *Journal of Biomechanics* 20(1): 59-65. 1987.

Humphrey JD. An evaluation of pseudoelastic descriptors used in arterial mechanics. *Journal of Biomechanical Engineering* 121(2): 259-262. 1999.

Jones CJH, Parker KH, Hughes R, Sheridan DJ. Nonlinearity of human arterial pulse wave transmission. *Journal of Biomechanical Engineering* 114(1): 10-14. 1992.

Jones CJH, Parker KH. Arterial wave intensity: physical meaning and physiological significance. *Recent progress in cardiovascular mechanics*. Harwood academic publisher, pp. 129-148. 1994.

Jones CJH, Sugawara M, Kondoh Y, Uchida K, Parker KH. Compression and expansion wavefront travel in the canine ascending aortic flow: wave intensity analysis. *Heart and Vessels* 16: 91-98. 2002.

Kelly R, Daley J, Avolio A, O'Rourke M. Arterial dilatation and reduced wave reflection benefit of dilevelol in hypertension. *Hypertension* 14: 14-21. 1989a.

Kelly R, Hayward C, Avolio A, O'Rourke M. Noninvasive determination of age-related changes in the human arterial pulse. *Circulation* 80: 1652-1659. 1989b.

Kelly RP, Tunin R, Kass DA. Effect of reduced aortic compliance on cardiac efficiency and contractile function of in situ canine left ventricle. *Circulation Research* 71: 490-502. 1992.

Khan Z, Millard RW, Gabel M, Walsh RA, Hoit BD. Effect of congestive heart failure on in vivo canine aortic elastic properties. *Journal of American College of Cardiology* 33(1): 267-272. 1999.

Khir AW, O'brien A, Gibbs JSR, Parker KH. Determination of wave speed and wave separation in the arteries. *Journal of Biomechanics* 34(9): 1145-1155. 2001a.

Khir AW, Henein MY, Koh T, Das SK, Parker KH, Gibson DG. Arterial waves in humans during peripheral vascular surgery. *Clinical Science* 101(6): 749-757. 2001b.

Khir AW, Parker KH. Measurements of wave speed and reflected waves in elastic tubes and bifurcations. *Journal of Biomechanics* 35(6): 775-783. 2002.

Khir AW, Zambanini A, Parker KH. Local and regional wave speed in the aorta: effects of arterial occlusion. *Medical Engineering & Physics* 26(1): 23-29. 2004.

Khir AW, Parker KH. Wave intensity in the ascending aorta: effects of arterial occlusion. *Journal of Biomechanics* 38(4): 647-655. 2005.

Khir AW, Swalen MJ, Segers P, Verdonck P, Pepper JR. Hemodynamics of a pulsatile left ventricular assist device driven by a counterpulsation pump in a mock circulation. *Artificial Organs* 30(4): 308-312. 2006.

Kips JG, Rietzschel ER, De Buyzere ML, Westerhof BE, Gillebert TC, Van Bortel LM, Segers P. Evaluation of noninvasive methods to assess wave reflection and pulse transit time from the pressure waveform alone. *Hypertension* 53: 142-149. 2009.

Kirkpatrick RD, Campbell KB, Bell DL, Taheri H. Method for studying arterial wave transmission effects on left ventricular function. *American Journal of Physiology* 260: H1003-1012. 1991.

Koh TW, Pepper JR, DeSouza AC, Parker KH. Analysis of wave reflections in the arterial system using wave intensity: a novel method for predicting the timing and amplitude of reflected waves. *Heart and Vessels* 13: 103-113. 1998.

Kolyva C, Spaan JAE, Piek JJ, Siebes M. Windkesselness of coronary arteries hampers assessment of human coronary wave speed by single-point technique. *AJP-Heart and Circulatory Physiology* 295(2), H482-H490. 2008.

Korteweg DJ. Uber die Fortpflanzungsgeschwindigkeit des schalles in elastischen Rohern. *Annals of Physics and Chemistry* (NS) 5: 525-527. 1878.

Lanir Y, Fung YC. Two – dimensional mechanical properties of rabbit skin. I. Experimental system. *Journal of Biomechanics* 7(1): 29-34. 1974.

Latham RD, Westerhof N, Sipkema P, Rubal BJ, Reuderink P, Murgo JP. Regional wave travel and reflections along the human aorta: a study with six simultaneous micromanometric pressure. *Circulation* 72: 1257-1269. 1985.

Latham RD. Pulse propagation in the systemic arterial tree. In: Westerhof N, Gross DR (Eds), Vascular Dynamics. Plenum Press, London. (Chapter 4). 1988.

Laurent S, Boutouyrie P, Asmar R, Gautier I, Laloux B, Guize L, Ducimetiere P, Benetos A. Aortic stiffness is an independent predictor of all-cause and cardiovascular mortality in hypertensive patients. *Hypertension* 37: 1236-1241. 2001.

Laurent S, Katsahian S, Fassot C, Tropeano AI, Gautier I, Laloux B, Boutouyrie P. Aortic stiffness is an independent predictor of fatal stroke in essential hypertension. *Stroke* 34: 1203-1206. 2003.

Laurent S, Cockcroft J, Van Bortel L, Boutouyrie P, Giannattasio C, Hayoz D, Pannier B, Vlachopoulos C, Wilkinson I, Boudier HS. Expert consensus document on arterial stiffness: methodological issues and clinical applications. *European heart journal* 27(21): 2588-2605. 2006.

Lehmann ED, Watts GF, Gosling RG. Aortic distensibility and hypercholesterolaemia. *Lancet* 340: 1171-1172. 1992.

Lekakis JP, Ikonomidis I, Protogerou AD, Papaioannou TG, Stamatelopoulos K, Papamichael CM, Mavrikakis ME. Arterial wave reflection is associated with severity of extracoronary atherosclerosis in patients with coronary artery disease. *European Journal of Cardiovascular Prevention & Rehabilitation* 13 (2): 236-242. 2006.

Lemogoum D, Van Bortel L, Najem B, Dzudie A, Teutcha C, Madu E, Leeman M, Deqaute JP, van de Borne P. Arterial stiffness and wave reflections in patients with sickle cell disease. *Hypertension* 44(6): 924-929. 2004.

Levy BI. The mechanical properties of the arterial wall in hypertension. *Prostaglandins Leukot Essent Fatty Acids* 54(1): 39-43. 1996.

Li JK, Melbin J, Noordergraaf A. Directional disparity of pulse reflection in the dog. *AJP-Heart and Circulatory Physiology* 247(1): H95-H99. 1984.

Li Y, Khir AW. Experimental validation of non-invasive and fluid density independent methods for the determination of local wave speed and arrival time of reflected wave, *Journal of Biomechanics* 44(7): 1393-1399. 2011.

Lichtenstein O, Safar ME, Mathieu E, Poitevin P, Levy BI. Static and dynamic mechanical properties of the carotid artery from normotensive and hypertensive rats. *Hypertension* 32: 346-350. 1998.

Lighthill J. Waves in fluids. Cambridge: Cambridge University Press. 1978.

Lillie MA, Gosline JM. Mechanical properties of elastin along the thoracic aorta in the pig. *Journal of Biomechanics* 40(10): 2214-2221. 2007.

Liu SQ, Fung YC. Changes of rheological properties of the blood vessels due to tissue remodeling in the course of development of diabetes. *Biorheology* 29: 443-457. 1992.

Liu SQ, Fung YC. Changes in the structure and mechanical properties of pulmonary arteries of rats exposed to cigarette smoke. *The American Review of Respiratory Disease* 148: 768-777. 1993.

London GM, Pannier B, Vicaut E, Guerin A, Marchais S, Safar M, Cuche J. Antihypertensive effects and arterial haemodynamic alterations during angiotensin converting enzyme inhibition. *Journal of Hypertension* 14(9): 1139-1146. 1996.

London GM, Blacher J, Pannier B, Guerin AP, Marchais SJ, Safar ME. Arterial wave reflections and survival in end-stage renal failure. *Hypertension* 38 (3): 434-438. 2001.

Mackenzie IS, Wilkinson IB, Cockcroft JR. Assessment of arterial stiffness in clinical practice. *Q J Med* 95:67-74. 2002.

Madhavan S, Ooi WL, Cohen H, Alderman MH. Relation of pulse pressure and blood pressure reduction to the incidence of myocardial infarction. *Hypertension* 23(3): 395-401. 1994.

Mancia G, Backer GD, Dominiczak A, et al. 2007 guidelines for the management of arterial hypertension: the task force for the management of arterial hypertension of the European society of hypertension (ESH) and of the european society of cardiology (ESC). *Journal of Hypertension* 25(6): 1105-1187. 2007

Mao SS, Ahmadi N, Shah B, Bechmann D, Chen A, Ngo L, Flores FR, Gao YL, Budoff M. Normal thoracic aorta diameter on cardiac computed tomography in healthy asymptomatic adult; impact of age and gender. *Academic Radiology* 15(7): 827-834. 2008.

Mattace – Raso FUS, van der Cammen TJM, Hofman A, van Popele NM, Bos ML, Schalekamp MA, et al. Arterial stiffness and risk of coronary heart disease and stroke: the Rotterdam Study. *Circulation* 113(5): 657-663. 2006.

Matthys K and Verdonck P. Development and modelling of arterial applanation tonometry: A review. *Technology and Health Care* 10: 65-76. 2002.

McDonald DA. The relation of the pulsatile pressure to flow in the arteries. *Journal of Physiology* 127: 533-552. 1955.

McDonald DA. Wave attenuation in visco-elastic arteries. Hemorheology. Oxford: A.L.Copley, Pergamon Press. P.113-125. 1968a.

McDonald DA. Regional pulse wave velocity in the arterial tree. *Journal of Applied Physiology* 24, 73-78. 1968b.

McEniery CM, Yasmin, Hall IR, Qasem A, Wilkinson IB, Cockcroft JR. Normal vascular aging: Differential effects on wave reflection and aortic pulse wave velocity. *Journal of the American College of Cardiology* 46(9), 1753-1760. 2005.

McVeigh GE, Hamilton PK, Morgan DR. Evaluation of mechanical properties: clinical, experimental and therapeutic aspects. *Clinical Science* 102: 51-67. 2002.

Meaume S, Benetos A, Henry OF, Rudnichi A, Safar ME. Aortic pulse wave velocity predicts cardiovascular mortality in subjects > 70 years of age. *Arteriosclerosis Thrombosis and Vascular Biology* 21(12): 2046-2050. 2001

Meinders JM, Kornet L, Brands PJ, Hoeks APG. Assessment of local pulse wave velocity in arteries using 2D distension waveforms. *Ultrasound Imaging* 23: 199-215. 2001.

Merillon JP, Motte G, Masquet C, Azancot I, Guiomard A, Gourgon R. Relationship between physical properties of the arterial system and left

ventricular performance in the course of aging and arterial hypertension. *Eur Heart* 3 (supplement A), 95-102. 1982.

Milnor W, Bertram C. The relation between arterial viscoelasticity and wave propagation in the canine femoral artery in vivo. *Circulation Research* 6: 870-879. 1978.

Milnor WR. Hemodynamic. Baltimore: Williams & Wilkins, 1982: 11-48, 56-96, 192-239.

Mitchell GF, Moye LA, Braunwald E, Rouleau JL, Bernstein V, Geltman EM, Flaker GC, Pfeffer MA. Sphygmomanometrically determined pulse pressure is a powerful independent predictor of recurrent events after myocardial infarction in patients with impaired left ventricular function. SAVE investigators. Survival and Ventricular Enlargement. *Circulation* 96: 4254-4260. 1997a.

Mitchell GF, Pfeffer MA, Finn PV, Pfeffer JM. Comparison of techniques for measuring pulse wave velocity in the rat. *Journal of Applied Physiology* 82, 203-210. 1997b.

Mitchell GF, Pfeffer MA. Pulsatile hemodynamics in hypertension. *Current Opinion in Cardiology* 14 (5): 361-369. 1999.

Mitchell GF, Parise H, Benjamin EJ, Larson MG, Keyes MJ, Vita JA, Vasan RS, Levy D. Changes in arterial stiffness and wave reflection with advancing age in healthy men and women: the Framingham heart study. *Hypertension* 43: 1239-1245. 2004.

Mitchell GF, Conlin PR, Dunlap ME, Lacourciere Y, Arnold JM, Ogilvie RI, Neutel J, Izzo JL Jr, Pfeffer MA. Aortic diameter, wall stiffness, and wave reflection in systolic hypertension. *Hypertension* 51: 105-111. 2008.

Moens AI. Die Pulskurve, Leiden. 1878.

Murgo JP, Westerhof N, Giolma JP, Altobelli SA. Aortic input impedance in normal man: relationship to pressure wave forms. *Circulation* 62: 105-116. 1980.

Mynard J, Penny DJ, Smolich JJ. Wave intensity amplification and attenuation in non-linear flow: Implications for the calculation of local reflection coefficients. *Journal of Biomechanics* 41(16): 3314-3321. 2008.

Newman DL, Greenwald SE. Analysis of forward and backward pressure waves by a total –occlusion method. *Medical & Biological Engineering & Computing* 18(2): 241-245. 1980.

Newman DL, Greenwald SE, Moodie TB. Reflection from elastic discontinuities. *Medical & Biological Engineering & Computing* 21: 697-701. 1983.

Newman DL, Sipkema P, Greenwald SE, Westerhof N. High frequency characteristics of the arterial system. *Journal of Biomechanics* 19(10): 817-824. 1986.

Nichols W, O'Rourke M. McDonald's blood flow in arteries. Theoretical, Experimental and Clinical Principles. 5th ED. H Arnold. USA: Oxford University Press. 2005.

Nichols WW. Clinical measurement of arterial stiffness obtained from noninvasive pressure waveforms. *American Journal of Hypertension* 18: 3s-10s. 2005.

Niki K, Sugawara M, Chang D, Harada A, et al. A new non-invasive measurement system for wave intensity: evaluation of carotid arterial wave intensity and reproducibility. *Heart and Vessels* 17: 12-21. 2002.

O'Rourke MF, Taylor M. Inout impedance on the systemic circulation. *Circulation research* 20: 365-380. 1967.

O'Rourke MF. Arterial function in health and disease. Edinburgh; Churchill Livingstone, 1982. pp. 3-32, 53-93, 170-224.

O'Rourke MF, Kelly RP. Wave reflection in the systemic circulation and its implications in ventricular function. *Hypertension* 11(4): 327-337. 1993.

O'Rourke MF, Mancia G. Arterial stiffness. *Journal of Hypertension* 17(1): 1-4. 1999.

O'Rourke MF, Staessen JA, Vlachopoulos C, Duprez D, Plante GE. Clinical applications of arterial stiffness; definitions and reference values. *American Journal of Hypertension* 15 (5): 426-444. 2002

O'Rourke MF, Avolio A, Qasem A. Clinical assessment of wave reflection. *Hypertension* 42: e15- 16. 2003

Page CM. Evidence of left ventricular wall movement actively decelerating aortic blood flow. PhD thesis, Brunel University, London: 2009.

Parker KH, Jones CJH, Dawson JR, Gibson DG. What stops the flow of blood from the heart? *Heart and Vessels* 4(4): 241-245. 1988.

Parker KH, Jones CJH. Forward and backward running waves in the arteries: analysis using the method of characteristics. *Journal of Biomechanical Engineering* 112(3): 322-326. 1990.

Patel DJ, Janicki JS, Carew TE. Static anisotropic elastic properties of the aorta in living dogs. *Circulation Research* 25: 765-779. 1969.

Patel DJ, Vaishnav RN. The rheology of large blood vessels. In Cardiovascular Fluid Dynamics. (Edited by Bergel DH) 2 pp. 1-64. Academic Press: New York. 1972.

PCU2000. PMSINSTRUMENTS.co.uk/PDF/PCU2000.PDF, last accessed on 19/4/2011

Pedley TJ. The fluid mechanics of large blood vessels. Cambridge: Cambridge: C.U.P. 1980.

Penny DJ, Mynard JP, Smolich JJ. Aortic wave intensity analysis of ventricular-vascular interaction during incremental dobutamine infusion in adult sheep. *AJP-Heart and Circulatory Physiology* 294(1): H481-489. 2008.

Probe Validation. TRANSONIC.COM/CO_PROBE_VALIDATION.PDF, last accessed on 19/4/2011

Rabben SI, Stergiopulos N, Hellevik LR, Smiseth OA, Slordahl S, Urheim S, Angelsen B. An ultrasound-based method for determining pulse wave velocity in superficial arteries. *Journal of biomechanics* 37(10): 1615-1622. 2004.

Rachev A, Stergiopulos N, Meister JJ. Theoretical study of dynamics of arterial wall remodelling in response to changes in blood pressure. *Journal of Biomechanics* 29: 635-642. 1996.

Rachev A, Stergiopulos N, Meister JJ. A model for geometric and mechanical adaptation of arteries to sustained hypertension. *Journal of Biomechanical Engineering* 120: 9-17. 1998.

Rachev A, Hayashi K. Theoretical study of the effects of vascular smooth muscle contraction on strain and stress distribution in arteries. *Annals of Biomedical Engineering* 27(4): 459-468. 1999.

Ramsey MW, Goodfellow J, Jones CJH, Luddington LA, Lewis MJ, Henderson AH. Endothelial control of arterial distensibility is impaired in chronic heart failure. *Circulation* 92: 3212-3219. 1995.

Ramsey MW, Sugawara M. Arterial wave intensity and ventriculoarterial interaction. *Heart and Vessels* Suppl 12: 128-134. 1997.

Remington JW, O'Brien LJ. Construction of aortic flow pulse from pressure pulse. *American Journal of Physiology* 218(2): 437-447. 1970.

Riemann B. Gesammelte mathematische Werke un wissenschaftlicher Nachlass 1860.

Roach MR, Burton AC. The reason for the shape of the distensibility curves of arteries. Canadian *Journal of Biochemistry and Physiology* 35(8): 681-690. 1957.

Roy CS, Brown JG. The blood-pressure and its variations in the arterioles, capillaries and smaller veins. *The Journal of Physiology* 2: 323-446. 1880.

Roy S, Silacci P, and Stergiopulos N. Biomechanical properties of decellularized porcine common carotid arteries. *AJP-Heart and Circulatory Physiology* 289(4): H1567-1576. 2005.

Safar ME, Simon A. Hemodynamics in systolic hypertension. In Zanchetti A, Tarazi R.C., eds. Handbook of hypertension 7: Pathophysiology of hypertension, cardiovascular aspects. Amsterdam: Elsevier: 225-241. 1986.

Safar ME, London GM. Arterial and venous compliance in sustained essential hypertension. *Hypertension* 10: 133-139. 1987.

Safar ME, London GM. The arterial system in human hypertension. In Textbook of Hypertension, ed. Swales JD, pp. 85-102. Blackwell Scientific Publication, Oxford, UK. 1994.

Salomaa V, Riley W, Kark JD, Nardo C, Folsom AR. Non-insulin-dependent diabetes mellitus and fasting glucose and insulin concentrations are associated with arterial stiffness indexes. The ARIC study. Atherosclerosis Risk in Communities Study. *Circulation* 91(5): 1432-1443. 1995.

Schultz DJ, Tunstall-Pedoe DS, Lee FJ, Funning AJ, Belhouse BJ. Velocity distribution and transition in the arterial system. In Ciba symposium on Circulatory and Respiratory and Mass Transport. Chuchill, London: Wolstenholme GEW and Knight J Eds. 1969.

Schulze-Bauer CAJ, Regitnig P, Holzapfel GA. Mechanics of the human femoral adventitia including high-pressure response. *AJP-Heart and Circulatory Physiology* 282: H2427-H2440. 2002.

Schulze-Bauer CAJ, Morth C, Holzapfel GA. Passive biaxial mechanical response of aged human iliac arteries. *Journal of Biomechanical Engineering* 125: 395-406. 2003.

Segers P, Carlier S, Pasquet A, Rabben S, Hellevik L, Remme E, De Backer T, De Sutter J, Thomas J, Verdonck P. Individualizing the aorto-radial pressure transfer function: feasibility of a model-based approach. *AJP-Heart and Circulatory Physiology* 279: 542-549. 2000.

Segers P, De Backer J, Devos D, Rabben SI, Gillebert TC, Van Bortel LM, De Sutter J, De Paepe A, Verdonck PR. Aortic reflection coefficients and their association with global indexes of wave reflection in healthy controls and patients with Marfan's syndrome. *AJP-Heart and Circulatory Physiology* 290(6): H2385-H2392. 2006.

Segers P, Rietzschel ER, De Buyzere ML, De Bacquer D, Van Bortel LM, De Backer G, Gillebert TC, Verdonck PR. Assessment of pressure wave

reflection: getting the timing right. *Physiological Measurement* 28(9): 1045-1056. 2007.

Shau YW, Wang CL, Shieh JY, Hsu TC. Noninvasive assessment of the viscoelasticity of peripheral arteries. *Ultrasound in Medicine and Biology* 25(9): 1377-1388. 1999.

Shokawa T, Imazu M, Yamamoto H, Toyofuku M, Tasaki N, Okimoto T, et al. Pulse wave velocity predicts cardiovascular mortality: findings from the Hawaii – Los Angeles – Hiroshima study. *Circulation Journal* 69 (3): 259-264. 2005.

Sipkema P, Westerhof N. Effective length of the arterial system. *Annals of Biomedical Engineering* 3(3): 296-307. 1975.

Smolich JJ, Mynard JP, Penny DJ. Simultaneous pulmonary trunk and pulmonary arterial wave intensity analysis in fetal jambs: evidence for cyclical, midsystolic pulmonary vasoconstriction. *American Journal of Physiology-Regulatory, Integrative & Comparative Physiology* 294(5): R1554-1562. 2008.

Sommer G, Gasser TC, Regitnig P, Auer M, Holzapfel GA. Dissection properties of the human aortic media: an experimental study. *Journal of Biomechanical Engineering* 130: 021007-1-021007-12. 2008.

Stamler J, Vaccaro O, Neaton JD, Wentworth D, et al. Diabetes, other risk factors, and 12-yr cardiovascular mortality for men screened in the multiple risk factor intervention trial. *Diabetes Care* 16:434-444. 1993.

Stefanadis C, Tsiamis E, Vlachopoulos C, Stratos C, Toutouzas K, Pitsavos C, Marakas S, Boudoulas H, Toutouzas P. Unfavorable effect of smoking on the elastic properties of the human aorta. *Circulation* 95: 31-38. 1997.

Stergiopulos N, Westerhof B, Westerhof N. Total arterial inertance as the fourth element of the windkessel model. *American Journal of Physiology* 276: H81-H88. 1999.

Sugawara M, Niki K, Furuhata H, Ohnishi S, Suzuki S. Relationship between the pressure and diameter of the carotid artery in humans. *Heart and Vessels* 15(1): 49-51. 2000.

Sun YH, Anderson TJ, Parker KH, Tyberg JV. Wave intensity analysis: a new approach to coronary hemodynamics. *Journal of Applied Physiology* 89(4): 1636-1644. 2000.

Sun YH, Anderson TJ, Parker KH, Tyberg JV. Effects of left ventricular contractility and coronary vascular resistance on coronary dynamics. *AJP-Heart and Circulatory Physiology* 286(4): H1590-H1595. Epub 2003 Dec 18.

Sutton – Tyrrell K, Najjar SS, Boudreau RM, Venkitachalam L, Kupelian V, Simonsick EM, et al. Elevated aortic pulse wave velocity, a marker of arterial

stiffness, predicts cardiovascular events in well-functioning older adults. *Circulation* 111(25): 3384-3390. 2005.

Tanaka H, DeSouza CA, Seals DR. Absence of age-related increase in central arterial stiffness in physically active women. *Arteriosclerosis, Thrombosis, and Vascular Biology* 18: 127-132. 1998.

Tardy Y, Meister JJ, Perret F, Brunner HR, Arditi M. Non-invasive estimate of the mechanical properties of peripheral arteries from ultrasonic and photoplethysmographic measurements. *Clinical Physics and Physiological Measurement* 12(1):39-54. 1991.

Taylor MG. Wave travels in arteries. PhD edn. University of London: University of London. 1959.

Taylor MG. Wave transmission through an assembly of randomly branching elastic tubes. *Biophysical Journal* 6: 697-716. 1966.

The artery with plaque inside Image. http://www.biosbcc.net/doohan/sample/htm/vessels.htm

Tsatsaris A. Effect of temperature increase on the distensibility of porcine thoracic aorta. *International Journal of Artificial Organs* 29(11): 887-891. 2005.

Vaccarino V, Holford TR, Krumholz HM. Pulse pressure and risk for myocardial infarction and heart failure in the elderly. *Journal of American College of Cardiology* 36: 130-138. 2000.

Venkatasubramanian RT, Grassl ED, Barocas VH, Lafontaine D, Bischof JC. Effects of freezing and cryopreservation on the mechanical properties of arteries. *Annals of biomedical engineering* 34(5): 823-832. 2006.

Von Maltzahn WW, Besdo D, Wiemer W. Elastic properties of arteries: A nonlinear two-layer cylindrical model. *Journal of Biomechanics* 14(6): 389-397. 1981.

Von Maltzahn WW, Warriyar RG, Keitzer WF. Experimental measurements of elastic properties of media and adventitia of bovine carotid arteries. *Journal of Biomechanics* 17(11): 839-847. 1984.

Wang JJ, O'Brien AB, Shrive NG, Parker KH, Tyberg JV. Time-domain representation of ventricular-arterial coupling as a windkessel and wave system. *AJP-Heart and Circulatory Physiology* 284(4): H1358-1368. 2003.

Wang JJ, Parker KH. Wave propagation in a model of the arterial circulation. *Journal of Biomechanics* 37(4): 457-470. 2004.

Wang Z, Jalali F, Sun YH, Wang JJ, Parker KH, Tyberg JV. Assessment of left ventricular diastolic suction in dogs using wave-intensity analysis. *AJP-Heart and Circulatory Physiology* 288(4): H1641-H1651. 2005.

Wang JJ, Shrive NG, Parker KH, Tyberg JV. “Wave” as defined by wave intensity analysis. *Medical and Biological Engineering and Computing* 47, 189-195. 2009.

Westerhof N, Sipkema P, Van den Bos GC, Elzinga G. Forward and backward waves in the arterial system. *Cardiovascular Research* 6(6): 648-656. 1972.

Westerhof N, Huisman RM. Arterial haemodynamic in hypertension. *Clinical Science* 72: 391-398. 1987.

Westerhof N, O’Rourke MF. Haemodynamic basis for the development of left ventricular failure in systolic hypertension and for its logical therapy. *Journal of Hypertension* 13(9): 943-952. 1995.

Westerhof N, Stergiopulos N, Noble M. Snapshots of hemodynamics. An aid for clinical research and graduate education. New York: Springer. 2004.

Westerhof BE, Guelen I, Westerhof N, Karemaker JM, Avolio A. Quantification of wave reflection in the human aorta from pressure alone – a proof of principle. *Hypertension* 48: 595-601. 2006.

Westerhof N, Lankhaar JW, Westerhof BE. The arterial Windkessel. *Medical and Biological Enginerring and Computing* 47:131-141. 2009.

Wetterer E. Wetterer, Die wirkung der herztatigkeit auf die dynamic des arteriensystems. *Verhandlungen der duetchen gesellschaft fur krieslaufforschungen* 22, pp. 26-60. 1956.

Wolinsky H, Glagov S. Structural basis for the static mechanical properties of the aortic media. *Circulation Research* 14: 400-413. 1964.

Wolinsky H, Glagov S. A lamellar unit of aortic medial structure and function in mammals. *Circulation Research* 20: 99-111. 1967.

Womersley JR. Method for calculation of velocity, rate of flow and viscous drag in arteries when the pressure gradient is known. *Journal of Physiology* 127(3): 553-563. 1955.

World Health Organisation, Cardiovascular diseases. Online fact sheet. 2011. http://www.who.int/mediacentre/factsheets/fs317/en/index.html

Yano M, Kohno M, Kobayashi S, Obayashi M, Seki K, Ohkusa T, Miura T, Fujii T, Matsuzaki M. Influence of timing and magnitude of arterial wave reflection on left ventricular relaxation. *AJP-Heart and Circulatory Physiology* 280(4): H1846-H1852. 2001.

Zulliger MA, Fridez P, Hayashi K, Stergiopulos N. A strain energy function for arteries accounting for wall composition and structure. *Journal of Biomechanics* 37(7): 989-1000. 2004.